UNIVERSITY OF CALIFORNIA, SAN DIEGO

Mechanisms of Selective Autophagy of Peroxisomes

A dissertation submitted in partial satisfaction of the requirements for the degree

Doctor of Philosophy

in

Biology

by

Sarah Frances Burnett

Committee in Charge:

Professor Suresh Subramani, Chair
Professor Susan Ferro-Novick
Professor Kun-Liang Guan
Professor Amy Kiger
Professor Maho Niwa

2015

The Dissertation of Sarah Frances Burnett is approved, and it is acceptable in quality and form for publication on microfilm and electronically:

_____

_____

_____

_____

_____
Chair

University of California, San Diego

2015

DEDICATION

I dedicate my dissertation to my partner and wonderful friends that I have made in graduate school and my friends who are 3,000 miles away but always pick up when I call. I dedicate my dissertation to my grandmother, Franma, who has always encouraged me to be curious and creative; and to my parents, who maintain the highest integrity and ethics and make their life's work enjoyable.

TABLE OF CONTENTS

LIST OF FIGURES

LIST OF TABLES

ACKNOWLEDGEMENTS

I have been in the Subramani lab since February 2008 and entered graduate school in 2010. In this time I have collaborated and learned from every member, past and current. Most importantly, I thank my thesis advisor, Suresh, who has shared with me his personal keys to success and encouraged me to be independent and critical in my thinking. Also, thanks to my committee for their advice and encouragement.

Chapter 1, in full, is a reprint of material that has been published in *International Journal of Cell Biology*, 2012. Andreas Till, Ronak Lakhani, **Sarah F. Burnett**, Suresh Subramani. The thesis author was one of the authors of the review article.

Chapter 2, in full, is a reprint of material that has been published in *EMBO Molecular Medicine*, 2014. Ronak Lakhani, Kara Vogel, Andreas Till, **Sarah F. Burnett**, Michael Gibson, and Suresh Subramani. The thesis author was one of the investigators and authors of the paper.

Chapter 3, in full, is a reprint of material that has been published in the *EMBO Reports*, 2013. Jean-Claude Farre, Aaron Burkenroad, **Sarah F. Burnett** and Suresh Subramani. The thesis author was one of the investigators and authors of this paper.

Chapter 4, in full, is a reprint of material that has been published in the *Journal of Biological Sciences,* 2014. **Sarah F. Burnett**, Jean-Claude Farre, Taras T. Nazarko, and Suresh Subramani. The thesis author was the primary investigator and author of this paper.

VITA

2006	Bachelor of Arts, Biochemistry & Molecular Biology, Boston University
2006-2007	Staff Research Associate, Harvard Medical School
2008-2010	Staff Research Associate, University of California, San Diego
2010-2015	Graduate Researcher, University of California, San Diego
2015	Doctor of Philosophy, University of California, San Diego

PUBLICATIONS

Sarah F. Burnett, Jean-Claude Farre, Taras Y. Nazarko, Suresh Subramani. Peroxisomal Pex3 regulates the recruitment of Atg11 by affecting the phosphorylation of the pexophagy receptor, Atg30. *Journal of Biological Chemistry*. 2014. *In press.*

Ronak Lakhani, Kara Vogel, Andreas Till, Jingjing Liu, **Sarah F. Burnett**, Mike Gibson, Suresh Subramani. Defects in GABA metabolism affect selective autophagy pathways and are alleviated by Tor inhibition. *EMBO Molecular Medicine*. 2014.

Jean-Claude Farre, Aaron Burkenroad, **Sarah F. Burnett**. Molecular Mechanisms of Selective Autophagy Receptors. *EMBO Reports*. 2013.

Andreas Till, Ronak Lakhani, **Sarah F. Burnett**, Suresh Subramani. Pexophagy – the selective autophagic degradation of peroxisomes. *International Journal of Cell Biology*. 2012.

Paula G. Fraenkel, Yann Gibert, Jason L. Holzheimer, Victoria J. Lattanzi, **Sarah F. Burnett**, Kimberly A. Dooley, Rebecca A. Wingert, and Leonard I. Zon. Transferrin-a modulates hepcidin expression in zebrafish embryos. *Blood*. 2009.

FIELDS OF STUDY

Major Field of Study: Biology
Studies in Yeast Cell Biology, Ph.D. Thesis Work
Professor Suresh Subramani

Studies in Zebrafish Iron Homeostasis
Dr. Paula Fraenkel, post-graduate research, Harvard Medical School

Studies in Neuronal Calcium Flux in Mouse
Professor Changiz Geula, undergraduate research, Harvard Medical School

ABSTRACT OF THE DISSERTATION

Mechanisms of Selective Autophagy of Peroxisomes

by

Sarah Frances Burnett

Doctor of Philosophy in Biology

University of California, San Diego, 2015

Professor Suresh Subramani, Chair

The study of pexophagy (selective peroxisome degradation by autophagy) is relevant to other selective autophagy pathways that are implicated in human diseases. In this dissertation I explore the signaling of pexophagy by γ-aminobutyric acid (GABA), the protein-protein interactions of the pexophagy receptor and its regulation by phosphorylation and the putative role of a pexophagy receptor-associated protein in pexophagy. Yeast was used as a model organism to study the physiological effects of elevated levels of the inhibitory neurotransmitter, GABA, in

mammalian disorders, such as succinic acid-semialdehydyde dehydrogenease (SSADH) deficiency. GABA blocked pexophagy and mitophagy specifically in yeast, but not general, or other selective autophagy pathways and increased intracellular levels of reactive oxygen species (ROS). Mechanistically, the GABA effect was mediated by elevation of Tor1 activity and the effects of GABA could be alleviated by rapamycin, a Tor1 inhibitor. These results were extended to studies in SSADH mice, suggesting the possibility of using rapamycin and its analogues to alleviate disorders caused by elevated GABA levels. In studies involving the *Pichia pastoris* pexophagy receptor, Atg30, we found that this protein is regulated by phosphorylation: determining the ability of Atg30 to interact with two key proteins of the core autophagy machinery, Atg8 and Atg11, thereby activating pexophagy. We also found that the phosphorylation state of the receptor is affected by its interaction with a component, Pex3 (of the peroxisome biogenesis machinery). We describe a new domain on, and a function for, Pex3 that regulates the phosphorylation, and therefore activation, of Atg30. Finally, by examining the protein-protein interactions of the Atg30 network to better understand the pexophagy signaling process, we identified using mass spectrometry, a potential interacting protein, Rvs167, that could also be involved in pexophagy. In summary, these studies shed light on the signaling and regulation of the important selective autophagy pathway of pexophagy.

General Introduction to Dissertation

Autophagy: Bulk and Selective

Autophagy, or macroautophagy, refers to the highly conserved mechanism involving bulk degradation and recycling of cytosolic components and organelles depending on the needs and nutrient conditions of the eukaryotic cell (1,2). The organization of the membrane components is orchestrated by core Atg proteins, organized into a PAS (phagophore assembly site), which then extends into a phagophore or isolation membrane (IM). A transition to the autophagosome then occurs and facilitates fusion with the vacuole. The majority of the core autophagy machinery is conserved from yeast to mammals and can be simplified into four major groups: (a) Atg1/Ulk2-kinase complex (Atg1, Atg13, Atg11, Atg17, etc.) (b) class III phosphatydlinositol-3-kinase (PI3K) complex 1 (c) Atg9 trafficking complex and (d) ubiquitin-like conjugation system (including Atg8/LC3, etc.). The core autophagy proteins assemble in a hierarchical manner at the phagophore assembly site (PAS) to orchestrate destruction of the targeted cargo (3).

Selective cargos can also be enclosed by the membrane structure initially discovered for non-selective autophagy, the autophagosome, whose contents are degraded in the vacuole (in yeast) or lysosome (in mammals) following autophagosome/lysosome fusion (4). Selective autophagy-related pathways exist for mitochondria, lipid droplets, endoplasmic reticulum, ribosome, and the peroxisome. Selective autophagy is regulated by ubiquitination and phosphorylation of certain selective receptors, which act in concert with core Atg proteins that localize to the cargo and facilitate autophagosome formation and fusion with lysosomes. The process of selective autophagy will be discussed in this dissertation.

Pexophagy

The process of bulk autophagy is also called macroautophagy, which is defined as core autophagy machinery assembling at the PAS and elongating into a double membrane structure that fuses at the edge to form a vesicle called the autophagosome. The autophagosome then

fuses with the vacuole/lysosome to release its constituents into the vacuole lumen, where various hydrolases degrade and recycle the macromolecular constituents (2). Alternatively, microautophagy occurs when the vacuole massively rearranges and cups the cytosolic constituents. Here the PAS forms at the vacuole periphery and the vacuolar membranes elongate to form the isolation membrane (called vacuolar sequestering membrane, VSM) or phagophore (5). Peroxisomes can be degraded by either macro- or micropexophagy. Each peroxisome is individually surrounded by a pexophagosome (in macropexophagy) or is engulfed by the VSM (in micropexophagy) (6,7). In micropexophagy, the VSMs fuse with another double-membrane structure called the micropexophagic apparatus (MIPA) before engulfing the targeted peroxisomes. The VSMs and MIPA form a cup and lid structure that surrounds the engulfed peroxisomes. The process of pexophagy has mostly been elucidated in the yeasts *Saccharomyces cerevisiae (Sc)*, *Pichia pastoris (Pp)* and *Hansenula polymorpha* (*Hp*) (6). In addition to yeasts, mammalian cell culture as well as murine models are used in this dissertation.

Signaling Events in Pexophagy

In yeast, the PAS is first organized by a scaffold of proteins that are part of the Atg1 kinase complex (8). The binding of Atg13 stabilizes and activates Atg1 via phosphorylation (9). The Atg1-Atg13 complex, in turn, is the target of the nutrient-sensing, target of rapamycin, TOR complex 1 (TORC1). In nutrient rich conditions, Atg13 is phosphorylated by TORC1 and averts autophagy; however under starvation, TORC1 is inactive and Atg13 is hypo-phosphorylated thus inducing autophagy (10). The PAS is organized during starvation (typically for nitrogen) and depends on the interaction between Atg13 and Atg17, along with Atg1 (11). During selective autophagy, Atg11 is required, but it is not necessary in bulk autophagy (12); it does not interact with Atg13 but instead with Atg1 (13). The Atg11-Atg1 interaction is likely Tor-independent (14) and quickly being recognized as an essential part of the selective autophagy machinery as it is required for mitophagy, pexophagy and the Cvt pathway to date (15-17). Atg11 has been shown to interact with all the selective autophagy receptors in yeast (17,18). Many of the core autophagy

proteins are conserved from yeast to mammals. However, Atg11 and Atg17 are not conserved but maintain functional homology to mammalian RB1CC1/FIP2000 (19).

The phosphoregulation of the selective autophagy receptors, which will be described in detail later, serves to assemble components of the selective autophagy-specific PAS and to recruit the protein Atg8 to the PAS for phagophore membrane elongation. This regulation has been studied among yeast, especially the mitophagy receptor Atg32 (20), and applied to the other receptors for pexophagy such as *Pp*Atg30 and *Sc*Atg36 (16,18). The mitogen-activated protein kinase pathways (MAPK) regulate mitophagy and pexophagy specifically and likely are involved in phosphorylating the receptors, most likely indirectly; these include the cell wall integrity (CWI) pathway, MAPK kinase kinase (Bck1), MAPK kinase (Mkk1/Mkk2), MAPK (Slt2) and cell surface receptors, Wsc1 and Mid2 (21,22). As described later, it is likely that selective autophagy receptors are phosphoregulated by casein kinase 1 and 2 in yeast (23-26). How the MAPK pathways might activate the receptors is not understood currently.

In Chapter 2, we assign a new role to the inhibitory neurotransmitter GABA, or γ-aminobutyric acid, in selective autophagy pathways pexophagy and mitophagy in yeast (27). We found the effects of GABA can be overridden by treatment of the cells with the Tor1 inhibitor, rapamycin. GABA can activate the Ser/Thr kinase, Tor1, and this activation, which inhibits pexophagy and mitophagy, requires a downstream target of Tor1, the kinase Sch9 (28). The presence of high levels of GABA leads to oxidative stress in the mammalian model of succinic acid-semialdehyde dehydrogenease (SSADH) disorder. In this model, GABA directly inhibits mitophagy through mTor and affects S6 phosphorylation while rapamycin rescues the mitophagy inhibition (29). Here, we find when GABA accumulates in both the yeast and the murine model of SSADH, that rapamycin relieves selective autophagy. This result offers a potential therapeutic approach to human disorders caused by abrogated cellular GABA concentration.

Yeast Pexophagy Receptors Identified

Conservation of the pexophagy machinery across yeasts is seen at the PAS and downstream signaling; yet the receptors in pexophagy are functionally similar but are not homologs. Atg30 is the pexophagy receptor in *P. pastoris* (17), while Atg36 is the pexophagy receptor in *S. cerevisiae* (16). Both Atg30 and Atg36 interact with Pex3 at the peroxisome, and interact with Atg11 and Atg8 at the pexophagy-specific PAS (17,18). In addition, both Atg30 and Atg36 are phosphorylated proteins (16-18). Phospho-dependent protein-protein interactions (PPI) of Atg8 and Atg11 with Atg30 are the subject of both Chapters 3 and 4 of this dissertation, which focus on the phosphoregulation of selective autophagy receptors by kinases.

In Chapter 3, we show a phosphorylation-dependent interaction of Atg8 and Atg11 with known selective autophagy receptors for pexophagy and mitophagy in both *P. pastoris* and *S. cerevisiae*. In the case of Atg30, there is a cryptic Atg8-interacting motif (AIM) that requires Serine-71 on Atg30, immediately upstream of the AIM, to be phosphorylated in order to interact with Atg8 (18). The same general principle is required for Atg11 interaction with Atg30, however Serine-112 was found to be phosphorylated in a previous study (17). The mechanism of interaction with Atg30 for the two proteins Atg8 and Atg11 was found to be random yet sequential and irrefutably phosphorylation-dependent (18).

In Chapter 4, we show that a domain on Pex3 can affect the phosphorylation of Atg30. This was shown with a mutant, Pex3m, which, unlike wildtype Pex3, fails to interact with Atg30. This failure of Pex3m to interact with Atg30 leads to the improper hypo-phosphorylation of Atg30 and this, in turn, affects the Atg11-Atg30 interaction (30). In this chapter, we show that regulation of pexophagy at the level of the peroxisome with Pex3 is likely a key activator of Atg30 phosphorylation.

Atg30, Atg32 and Atg36 are hyperphosphorylated proteins with at least two known phosphorylation sites regulating the receptor's interaction with Atg8 and Atg11 (18,20). The casein kinase 1, Hrr25, promotes Atg11 interaction via phosphorylation of distinct Atg11-binding sites in Atg19, Atg34 and Atg36 (23-25). As of now, Hrr25 is the only pexophagy-related kinase

that phosphorylates Atg36; Hrr25 phosphorylation of Atg36 enhances the Atg36-Atg11 interaction and activates the signaling cascade for assembly of the pexophagy-specific PAS (25). The kinase that phosphorylates Atg30 at the onset of pexophagy likely is Hrr25 but this remains unproved. Other kinases could be implicated in future studies.

At the pexophagy-specific PAS, and at the peroxisome itself, Atg30 also interacts with Atg17, Pex14 (17) and Atg37 (31). Meanwhile, Atg36 additionally interacts with components of the peroxisome fission machinery, Dnm1 and Vps1 (32) (Table I-1). It is unknown if Atg30 also interacts with peroxisome fission machinery as in *S. cerevisiae* but this would be interesting to confirm. Another protein that potentially interacts with Atg30 is the BAR-domain protein, Rvs167, which is the topic of Chapter 5 of this dissertation. Using Atg30 as bait, we designed a study to compare Atg30-interacting proteins in WT *PEX3* versus *pex3m* cells, using mass spectrometry of all proteins co-immunoprecipitating with Atg30 during pexophagy conditions. Using both *S. cerevisiae* and *P. pastoris*, we have preliminary data suggesting a role for Rvs167 in pexophagy via its interaction with Atg30. However, the mechanism involved remains to be elucidated.

Peroxisomal biogenesis machinery involved in pexophagy

In the 1980's and 90's, much was learned about the peroxins (*PEX* genes) required for peroxisome biogenesis based on genetic screens, as well as the disease states of patients who are born with genetic defects in proteins required for peroxisome biogenesis (33). Peroxisomes are different from chloroplasts or mitochondria in that they have a nuclear-encoded genome and can post-translationally import fully folded proteins (34). The accepted model of peroxisomal matrix protein import is as follows: (i) Proteins with a peroxisomal targeting signaling tripeptide, SKL (PTS1) are recognized and directly interact with Pex5 in the cell cytosol; alternatively, the use another N-terminal targeting signal called PTS2, which interacts with the proteins Pex7 and Pex20 in the cytosol; (ii) the cargo protein/PTS receptor complex associates with the peroxisome membrane via the docking complex (Pex13/Pex14/Pex17); (iii) For the PTS1 import pathway, Pex5 and Pex14 then assemble a transient pore and (iv) PTS1-containing cargoes are then

transported across the peroxisome membrane and released into the peroxisomal matrix; (v) Pex5 is mono-ubiquitinated by E2 and E3 ubiquitin ligases (Pex4/22, Pex2/10/12, respectively); (vi) Ub-Pex5 is released from the peroxisome membrane by the receptor-recycling machinery comprised of Pex1/Pex6, which are anchored at the peroxisome membrane via PMP Pex15; (vii) in the event that receptor recycling is blocked, Pex5 is then poly-ubiquitinated and targeted for proteasomal degradation by the ubiquitin proteasome system (UPS) (35).

The peroxins that are responsible for peroxisome membrane protein (PMP) biogenesis were discovered by the study of mutants, *pex3* or *pex19,* in which mature, functional peroxisomes are absent (36,37). Similar observations were made about the requirement of Pex16 in mammals (38). Both Pex3 and Pex19 are required for the budding of pre-peroxisomal vesicles from the ER (39-41). Pex3 is essential for PMP biogenesis and has been proposed to be the peroxisome membrane-associated docking site for Pex19, which is believed to bind the mPTS on PMPs and bring them to the peroxisome membrane for insertion there (42). It has recently been suggested that when Pex3 loses binding affinity with Pex19, it changes conformation, fails to associate tightly with membranes (43) and becomes destabilized (44). Pex3 also has a role in anchoring the peroxisome inheritance machinery (Inp1 and Inp2) to the peroxisome by interacting with Inp1, which has a function in affixing peroxisomes to the cell periphery (45). Inp2, however, is the peroxisome-specific receptor for class V myosin2 (Myo2), that transports peroxisomes along actin cables from the mother to daughter cell in *S. cerevisiae* (46); Myo2 also interacts with Pex19 (47). Pex3 is also the receptor for Myo2 in another yeast, *Yarrowia lipolytica* (48).

The Pex3-Pex19 interaction has been studied extensively and the complex has been crystallized (49,50). Pex3 has dynamic biological activity assigned to different domains on the protein, with domains for biogenesis (with Pex19); domains for inheritance (51) and as described in Chapter 4, a new domain for pexophagy in *Pp*Pex3 (30).

The first pexophagy receptor to be identified, Atg30, is involved in the selective degradation of peroxisomes in *P. pastoris*. Atg30 interacts with the peroxisomal biogenesis machinery, Pex14 and Pex3 (17), which both already have roles in pexophagy in another

methylotrophic yeast, *H. polymorpha* (52,53). Interestingly, both Pex3 and Pex14 have also been designated unique roles in mammalian pexophagy (54,55). What is unclear though is how Pex3 and Pex14 in both *H. polymorpha* or in mammalian systems interact with the selective autophagy receptors. The accepted pexophagy receptor in mammals is NBR1, in concert with p62. Knockdown of *PEX14* affects NBR1-peroxisomal interaction but the coordination of these two proteins or this complex during pexophagy is unknown (56).

An interesting correlation between *H. polymorpha* and mammals is that Pex3 ubiquitination can induce pexophagy. In the case of *H. polymorpha*, the E3 ligases, Pex2 and Pex10, are also required for pexophagy along with ubiquitinated Pex3 (57). In mammals, Pex3 ubiquitination and overexpression induce pexophagy and recruit receptor NBR1 (55). *Hs*Pex3 has 3 predicted ubiquitin sites (K100, K208, K262) as well as 7 predicted phosphorylation sites (Phosphosite). In mammals, artificial ubiquitin fused to PEX3 on peroxisomes is enough to recruit NBR1 (58). PEX3 may act in the transduction of the signal for pexophagy, but likely is not the sole signal for pexophagy in mammals because when it is in a non-ubquitinatable form, pexophagy is still induced (55). In mammals it was also shown that PEX14 interacts with LC3-II, the mammalian homolog to yeast Atg8, that is conjugated to phosphatidylethanolamine (54). Pex14 can also be phosphorylated in yeasts (17,59) and is likely ubiquitinated (60).

Other examples of the pexophagic signals from the yeast peroxisome include studies showing that mutations in *PEX1*, *PEX6* or *PEX15* (the PTS receptor recycling machinery) can increase ubiquitination in *S. cerevisiae* and induce pexophagy (61). Certain peroxisome biogenesis proteins are key players in pexophagy (Pex3, Pex14, especially); and modification at the peroxisome membrane in the form of phosphorylation or ubiquitination drives pexophagy (Table I-2).

Pexophagy in mammals

Although pexophagy has been studied extensively in yeasts, the mechanistic studies in mammalian cells have been remarkably harder technically. As such, little is known about the physiological basis of pexophagy, except the lack of peroxisomes in human patients causes a variety of fatal disease states (62). One such physiological association of pexophagy is in endothelial cells where peroxisome homeostasis was altered from induced renal toxicity or sepsis (63). In another study hypoxia inducible factor, Hif2a, when activated, was able to induce pexophagy in mammalian cells (64). Thus two disease states show dysregulation of pexophagy is seen in models of sepsis (63), as well as in renal cell carcinoma (64). This is the first time pexophagy has been linked to disease states in mammals.

Many labs were looking for mechanisms of selective autophagy. NBR1 was found to be the mammalian pexophagy receptor (56) after it was shown that p62/SQSTM associated with ubiquitin-decorated peroxisomes (58). NBR1 was shown to be a ubiquitin-regulated autophagy receptor (65,66) dependent upon the co-receptor p62/SQSTM (67), that also interacts with autophagy core machinery LC3/Atg8 (68).

Although the PAS in mammalian cells has not been distinctly defined, a membrane structure called the omegasome might be a phagophore intermediate (69). Research in the field of bulk or selective autophagy continues to find functional homologs of proteins and adds depth to the specificity of the process. Fine tuning this level of detail and modeling autophagy in disease states is the next step as the field, as well as finding drugable candidates.

Table I-1: Peroxisome biogenesis machinery involved in pexophagy

Organism	Peroxin(s)	Pexophagy Machinery	Function	References
CHO cells	Pex14	LC3-II	Pex14 binds directly to LC3-II and Pex5 competively inhibits interaction	Fujiki 2008 and 2015 papers
CHO cells	Pex3	NBR1	Overexpression of Pex3 increases peroxisomal ubiquitin and recruits NBR1	Fujiki 2014
H. polymorpha	Pex3	N/A	Removing Pex3 stimulates pexophagy, Pex3 is ubiquitinated	Van der klei 2002 and 2013
H. polymorpha	Pex14	NBR1	Pex14 necessary and sufficient for pexopahgy; knockdown mislocalizes NBR1	Van der klei 2001 and 2008, Deosaran 2013
H. polymorpha	Pex2/Pex10	N/A	Involved in degradation of Pex3, which is required for pexophagy in this yeast	Van der Klei 2013
S. cerevisiae	Pex1/Pex6/Pex15	Atg36	*pex1*Δ affects Atg36 modification, exportomer deficiency enhances pexophagy via accumulated ubiquitin	Hettema 2014
S. cerevisiae	Pex3	Atg36	Pex3 is a docking factor for Atg36 at the peroxisome membrane	Hettema 2012
P. pastoris	Pex3, Pex14	Atg30	in *pex3*Δ or *pex14*Δ cells, Atg30 is mislocalized, Pex3 can affect the phosphorylation of Atg30	Farre 2008, Burnett 2015
P. pastoris	Pex19	Atg37	Involved in Atg37 trafficking to peroxisome	Nazarko et al., unpublished

Table I-2: Proteins associated with pexophagy receptors in yeast

Atg36:		
Interacting Proteins	**Function**	**Reference**
Dnm1, Vps1	Dnm1, Vps1 invovled in peroxisome division, required for pexophagy	Klionsky 2014
Pex3	Pex3 is a docking factor for Atg36 at the peroxisome membrane	Hettema 2012
Atg11, Atg8	Autophagy core machinery	Farre 2013
Hrr25	Kinase that phosphorylates Atg36	Nakatogawa 2014
Atg30:		
Interacting Proteins	**Function**	**Reference**
Pex3	involved in activation of Atg30; *pex3D* cells mislocalize Atg30 to nucleus	Farre 2008, Burnett 2015
Pex14	*pex14D*cells mislocalize Atg30	Farre 2008
Atg17, Atg11, Atg8	Autophagy core machinery	Farre 2008 and 2013
Atg37	recruited by Atg30 for phagophore formation	Nazarko 2014

References

1. Mizushima, N., Yoshimori, T., and Ohsumi, Y. (2010) The Role of Atg Proteins in Autophagosome Formation. *Annu Rev Cell Dev Biol* **27***,* 107-132

2. Suzuki, K., and Ohsumi, Y. (2007) Molecular machinery of autophagosome formation in yeast, *Saccharomyces cerevisiae*. *FEBS Letters* **581**, 2156-2161

3. Suzuki, K., Kubota, Y., Sekito, T., and Ohsumi, Y. (2007) Hierarchy of Atg proteins in pre-autophagosomal structure organization. *Genes Cells* **12**, 209-218

4. Klionsky, D. J., Cueva, R., and Yaver, D. S. (1992) Aminopeptidase I of *Saccharomyces cerevisiae* is localized to the vacuole independent of the secretory pathway. *J Cell Biol* **119**, 287-299

5. Sahu, R., Kaushik, S., Clement, C. C., Cannizzo, E. S., Scharf, B., Follenzi, A., Potolicchio, I., Nieves, E., Cuervo, A. M., and Santambrogio, L. (2011) Microautophagy of cytosolic proteins by late endosomes. *Dev Cell* **20**, 131-139

6. Till, A., Lakhani, R., Burnett, S. F., and Subramani, S. (2012) Pexophagy: the selective degradation of peroxisomes. *Int J Cell Biol* **2012**, 512721

7. Farré, J. C., and Subramani, S. (2004) Peroxisome turnover by micropexophagy: an autophagy-related process. *Trends Cell Biol* **14**, 515-523

8. Wong, P. M., Puente, C., Ganley, I. G., and Jiang, X. (2013) The ULK1 complex: sensing nutrient signals for autophagy activation. *Autophagy* **9**, 124-137

9. Raught, B., Gingras, A. C., and Sonenberg, N. (2001) The target of rapamycin (TOR) proteins. *Proc Natl Acad Sci U S A* **98**, 7037-7044

10. Hosokawa, N., Hara, T., Kaizuka, T., Kishi, C., Takamura, A., Miura, Y., Iemura, S., Natsume, T., Takehana, K., Yamada, N., Guan, J. L., Oshiro, N., and Mizushima, N. (2009) Nutrient-dependent mTORC1 association with the ULK1-Atg13-FIP200 complex required for autophagy. *Mol Biol Cell* **20**, 1981-1991

11. Kabeya, Y., Kamada, Y., Baba, M., Takikawa, H., Sasaki, M., and Ohsumi, Y. (2005) Atg17 functions in cooperation with Atg1 and Atg13 in yeast autophagy. *Mol Biol Cell* **16**, 2544-2553

12. Kim, J., Kamada, Y., Stromhaug, P. E., Guan, J., Hefner-Gravink, A., Baba, M., Scott, S. V., Ohsumi, Y., Dunn, W. A., and Klionsky, D. J. (2001) Cvt9/Gsa9 functions in sequestering selective cytosolic cargo destined for the vacuole. *J Cell Biol* **153**, 381-396

13. Kim, J., Huang, W. P., and Klionsky, D. J. (2001) Membrane recruitment of Aut7p in the autophagy and cytoplasm to vacuole targeting pathways requires Aut1p, Aut2p, and the autophagy conjugation complex. *J Cell Biol* **152**, 51-64

14. Kamada, Y., Funakoshi, T., Shintani, T., Nagano, K., Ohsumi, M., and Ohsumi, Y. (2000) Tor-mediated induction of autophagy via an Apg1 protein kinase complex. *J Cell Biol* **150**, 1507-1513

15. Monastyrska, I., Shintani, T., Klionsky, D. J., and Reggiori, F. (2006) Atg11 directs autophagosome cargoes to the PAS along actin cables. *Autophagy* **2**, 119-121

16. Motley, A. M., Nuttall, J. M., and Hettema, E. H. (2012) Pex3-anchored Atg36 tags peroxisomes for degradation in *Saccharomyces cerevisiae*. *EMBO J* **13**, 2852-2868

17. Farré, J. C., Manjithaya, R., Mathewson, R. D., and Subramani, S. (2008) *Pp*Atg30 tags peroxisomes for turnover by selective autophagy. *Dev Cell* **14**, 365-376

18. Farré, J. C., Burkenroad, A., Burnett, S. F., and Subramani, S. (2013) Phosphorylation of mitophagy and pexophagy receptors coordinates their interaction with Atg8 and Atg11. *EMBO Rep* **5**, 441-449

19. Hara, T., and Mizushima, N. (2009) Role of ULK-FIP200 complex in mammalian autophagy: FIP200, a counterpart of yeast Atg17? *Autophagy* **5**, 85-87

20. Aoki, Y., Kanki, T., Hirota, Y., Kurihara, Y., Saigusa, T., Uchiumi, T., and Kang, D. (2011) Phosphorylation of Ser114 on Atg32 mediates mitophagy. *Mol Biol Cell* **17**, 3206-3217

21. Manjithaya, R., Jain, S., Farre, J. C., and Subramani, S. (2010) A yeast MAPK cascade regulates pexophagy but not other autophagy pathways. *The Journal of Cell Biology* **189**, 303-310

22. Mao, K., Wang, K., Zhao, M., Xu, T., and Klionsky, D. J. (2011) Two MAPK-signaling pathways are required for mitophagy in *Saccharomyces cerevisiae*. *J Cell Biol* **193**, 755-767

23. Mochida, K., Ohsumi, Y., and Nakatogawa, H. (2014) Hrr25 phosphorylates the autophagic receptor Atg34 to promote vacuolar transport of α-mannosidase under nitrogen starvation conditions. *FEBS Lett* **588**, 3862-3869

24. Pfaffenwimmer, T., Reiter, W., Brach, T., Nogellova, V., Papinski, D., Schuschnig, M., Abert, C., Ammerer, G., Martens, S., and Kraft, C. (2014) Hrr25 kinase promotes selective autophagy by phosphorylating the cargo receptor Atg19. *EMBO Rep* **15**, 862-870

25. Tanaka, C., Tan, L. J., Mochida, K., Kirisako, H., Koizumi, M., Asai, E., Sakoh-Nakatogawa, M., Ohsumi, Y., and Nakatogawa, H. (2014) Hrr25 triggers selective autophagy-related pathways by phosphorylating receptor proteins. *J Cell Biol* **207**, 91-105

26. Kanki, T., Kurihara, Y., Jin, X., Goda, T., Ono, Y., Aihara, M., Hirota, Y., Saigusa, T., Aoki, Y., Uchiumi, T., and Kang, D. (2013) Casein kinase 2 is essential for mitophagy. *EMBO Rep* **14**, 788-794

27. Lakhani, R., Vogel, K. R., Till, A., Liu, J., Burnett, S. F., Gibson, K. M., and Subramani, S. (2014) Defects in GABA metabolism affect selective autophagy pathways and are alleviated by mTOR inhibition. *EMBO Mol Med* **6**, 551-566

28. Urban, J., Soulard, A., Huber, A., Lippman, S., Mukhopadhyay, D., Deloche, O., Wanke, V., Anrather, D., Ammerer, G., Riezman, H., Broach, J. R., De Virgilio, C., Hall, M. N., and Loewith, R. (2007) Sch9 is a major target of TORC1 in *Saccharomyces cerevisiae*. *Mol Cell* **26**, 663-674

29. Blommaart, E. F., Luiken, J. J., Blommaart, P. J., van Woerkom, G. M., and Meijer, A. J. (1995) Phosphorylation of ribosomal protein S6 is inhibitory for autophagy in isolated rat hepatocytes. *J Biol Chem* **270**, 2320-2326

30. Burnett, S. F., Farré, J. C., Nazarko, T. Y., and Subramani, S. (2015) Peroxisomal Pex3 activates selective autophagy of peroxisomes via interaction with pexophagy receptor, Atg30. *J Biol Chem.* In press.

31. Nazarko, T. Y., Ozeki, K., Till, A., Ramakrishnan, G., Lotfi, P., Yan, M., and Subramani, S. (2014) Peroxisomal Atg37 binds Atg30 or palmitoyl-CoA to regulate phagophore formation during pexophagy. *J Cell Biol* **204**, 541-557

32. Mao, K., Liu, X., Feng, Y., and Klionsky, D. J. (2014) The progression of peroxisomal degradation through autophagy requires peroxisomal division. *Autophagy* **10**, 652-661

33. Ebberink, M. S., Mooijer, P. A., Gootjes, J., Koster, J., Wanders, R. J., and Waterham, H. R. (2011) Genetic classification and mutational spectrum of more than 600 patients with a Zellweger syndrome spectrum disorder. *Human mutation* **32**, 59-69

34. Léon, S., Goodman, J. M., and Subramani, S. (2006) Uniqueness of the mechanism of protein import into the peroxisome matrix: transport of folded, co-factor-bound and oligomeric proteins by shuttling receptors. *Biochim Biophys Acta* **1763**, 1552-1564

35. Ma, C., Agrawal, G., and Subramani, S. (2011) Peroxisome assembly: matrix and membrane protein biogenesis. *J Cell Biol* **193**, 7-16

36. Hettema, E. H., Girzalsky, W., van Den Berg, M., Erdmann, R., and Distel, B. (2000) *Saccharomyces cerevisiae* Pex3p and Pex19p are required for proper localization and stability of peroxisomal membrane proteins. *EMBO J* **19**, 223-233

37. Pinto, M. P., Grou, C. P., Alencastre, I. S., Oliveira, M. E., Sá-Miranda, C., Fransen, M., and Azevedo, J. E. (2006) The import competence of a peroxisomal membrane protein is determined by Pex19p before the docking step. *J Biol Chem* **281**, 34492-34502

38. Yonekawa, S., Furuno, A., Baba, T., Fujiki, Y., Ogasawara, Y., Yamamoto, A., Tagaya, M., and Tani, K. (2011) Sec16B is involved in the endoplasmic reticulum export of the peroxisomal membrane biogenesis factor peroxin 16 (Pex16) in mammalian cells. *Proceedings of the National Academy of Sciences of the United States of America* **108**, 12746-12751

39. van der Zand, A., Braakman, I., and Tabak, H. F. (2010) Peroxisomal membrane proteins insert into the endoplasmic reticulum. *Mol Biol Cell* **21**, 2057-2065

40. van der Zand, A., Gent, J., Braakman, I., and Tabak, H. F. (2012) Biochemically distinct vesicles from the endoplasmic reticulum fuse to form peroxisomes. *Cell* **149**, 397-409

41. Agrawal, G., Joshi, S., and Subramani, S. (2011) Cell-free sorting of peroxisomal membrane proteins from the endoplasmic reticulum. *Proc Natl Acad Sci U S A* **108**, 9113-9118

42. Fujiki, Y., Matsuzono, Y., Matsuzaki, T., and Fransen, M. (2006) Import of peroxisomal membrane proteins: the interplay of Pex3p- and Pex19p-mediated interactions. *Biochimica et biophysica acta* **1763**, 1639-1646

43. Pinto, M. P., Grou, C. P., Fransen, M., Sa-Miranda, C., and Azevedo, J. E. (2009) The cytosolic domain of PEX3, a protein involved in the biogenesis of peroxisomes, binds membrane lipids. *Biochimica et biophysica acta* **1793**, 1669-1675

44. Schmidt, F., Dietrich, D., Eylenstein, R., Groemping, Y., Stehle, T., and Dodt, G. (2012) The role of conserved PEX3 regions in PEX19-binding and peroxisome biogenesis. *Traffic* **9**, 1244-1260

45. Munck, J. M., Motley, A. M., Nuttall, J. M., and Hettema, E. H. (2009) A dual function for Pex3p in peroxisome formation and inheritance. *J Cell Biol* **187**, 463-471

46. Fagarasanu, A., Fagarasanu, M., Eitzen, G. A., Aitchison, J. D., and Rachubinski, R. A. (2006) The peroxisomal membrane protein Inp2p is the peroxisome-specific receptor for the myosin V motor Myo2p of *Saccharomyces cerevisiae*. *Dev Cell* **10**, 587-600

47. Otzen, M., Rucktaschel, R., Thoms, S., Emmrich, K., Krikken, A. M., Erdmann, R., and van der Klei, I. J. (2012) Pex19p Contributes to Peroxisome Inheritance in the Association of Peroxisomes to Myo2p. *Traffic* **13**, 947-959

48. Chang, J., Mast, F. D., Fagarasanu, A., Rachubinski, D. A., Eitzen, G. A., Dacks, J. B., and Rachubinski, R. A. (2009) Pex3 peroxisome biogenesis proteins function in peroxisome inheritance as class V myosin receptors. *J Cell Biol* **187**, 233-246

49. Sato, Y., Shibata, H., Nakatsu, T., Nakano, H., Kashiwayama, Y., Imanaka, T., and Kato, H. (2010) Structural basis for docking of peroxisomal membrane protein carrier Pex19p onto its receptor Pex3p. *EMBO J* **29**, 4083-4093

50. Schmidt, F., Treiber, N., Zocher, G., Bjelic, S., Steinmetz, M. O., Kalbacher, H., Stehle, T., and Dodt, G. (2010) Insights into peroxisome function from the structure of PEX3 in complex with a soluble fragment of PEX19. *J Biol Chem* **285**, 25410-25417

51. Knoblach, B., Sun, X., Coquelle, N., Fagarasanu, A., Poirier, R. L., and Rachubinski, R. A. (2013) An ER-peroxisome tether exerts peroxisome population control in yeast. *EMBO J* **18**, 2439-2453

52. Bellu, A. R., Salomons, F. A., Kiel, J. A., Veenhuis, M., and Van Der Klei, I. J. (2002) Removal of Pex3p is an important initial stage in selective peroxisome degradation in *Hansenula polymorpha*. *J Biol Chem* **277**, 42875-42880

53. van Zutphen, T., Veenhuis, M., and van der Klei, I. J. (2008) Pex14 is the sole component of the peroxisomal translocon that is required for pexophagy. *Autophagy* **4**, 63-66

54. Hara-Kuge, S., and Fujiki, Y. (2008) The peroxin Pex14p is involved in LC3-dependent degradation of mammalian peroxisomes. *Exp Cell Res* **314**, 3531-3541

55. Yamashita, S. I., Abe, K., Tatemichi, Y., and Fujiki, Y. (2014) The membrane peroxin PEX3 induces peroxisome-ubiquitination-linked pexophagy. *Autophagy* **10**

56. Deosaran, E., Larsen, K. B., Hua, R., Sargent, G., Wang, Y., Kim, S., Lamark, T., Jauregui, M., Law, K., Lippincott-Schwartz, J., Brech, A., Johansen, T., and Kim, P. K. (2013) NBR1 acts as an autophagy receptor for peroxisomes. *J Cell Sci* **126**, 939-952

57. Williams, C., and van der Klei, I. J. (2013) Pexophagy-linked degradation of the peroxisomal membrane protein Pex3p involves the ubiquitin-proteasome system. *Biochem Biophys Res Commun* **438**, 395-401

58. Kim, P. K., Hailey, D. W., Mullen, R. T., and Lippincott-Schwartz, J. (2008) Ubiquitin signals autophagic degradation of cytosolic proteins and peroxisomes. *Proceedings of the National Academy of Sciences of the United States of America* **105**, 20567-20574

59. Tanaka, K., Soeda, M., Hashimoto, Y., Takenaka, S., and Komori, M. (2013) Identification of phosphorylation sites in *Hansenula polymorpha* Pex14p by mass spectrometry. *FEBS Open Bio* **3**, 6-10

60. Kim, W., Bennett, E. J., Huttlin, E. L., Guo, A., Li, J., Possemato, A., Sowa, M. E., Rad, R., Rush, J., Comb, M. J., Harper, J. W., and Gygi, S. P. (2011) Systematic and quantitative assessment of the ubiquitin-modified proteome. *Mol Cell* **44**, 325-340

61. Nuttall, J. M., Motley, A. M., and Hettema, E. H. (2014) Deficiency of the exportomer components Pex1, Pex6, and Pex15 causes enhanced pexophagy in *Saccharomyces cerevisiae*. *Autophagy* **10**, 835-845

62. Ribeiro, D., Castro, I., Fahimi, H. D., and Schrader, M. (2012) Peroxisome morphology in pathology. *Histol Histopathol* **27**, 661-676

63. Vasko, R., Ratliff, B. B., Bohr, S., Nadel, E., Chen, J., Xavier, S., Chander, P., and Goligorsky, M. S. (2013) Endothelial peroxisomal dysfunction and impaired pexophagy promotes oxidative damage in lipopolysaccharide-induced acute kidney injury. *Antioxid Redox Signal* **3**, 211-230

64. Walter, K. M., Schönenberger, M. J., Trötzmüller, M., Horn, M., Elsässer, H. P., Moser, A. B., Lucas, M. S., Schwarz, T., Gerber, P. A., Faust, P. L., Moch, H., Köfeler, H. C., Krek, W., and Kovacs, W. J. (2014) Hif-2α promotes degradation of mammalian peroxisomes by selective autophagy. *Cell Metab* **20**, 882-897

65. Kirkin, V., Lamark, T., Sou, Y. S., Bjørkøy, G., Nunn, J. L., Bruun, J. A., Shvets, E., McEwan, D. G., Clausen, T. H., Wild, P., Bilusic, I., Theurillat, J. P., Øvervatn, A., Ishii, T., Elazar, Z., Komatsu, M., Dikic, I., and Johansen, T. (2009) A role for NBR1 in autophagosomal degradation of ubiquitinated substrates. *Mol Cell* **33**, 505-516

66. Kirkin, V., McEwan, D. G., Novak, I., and Dikic, I. (2009) A role for ubiquitin in selective autophagy. *Mol Cell* **34**, 259-269

67. Lamark, T., Kirkin, V., Dikic, I., and Johansen, T. (2009) NBR1 and p62 as cargo receptors for selective autophagy of ubiquitinated targets. *Cell Cycle* **8**, 1986-1990

68. Pankiv, S., Clausen, T. H., Lamark, T., Brech, A., Bruun, J. A., Outzen, H., Øvervatn, A., Bjørkøy, G., and Johansen, T. (2007) p62/SQSTM1 binds directly to Atg8/LC3 to facilitate degradation of ubiquitinated protein aggregates by autophagy. *J Biol Chem* **282**, 24131-24145

69. Axe, E. L., Walker, S. A., Manifava, M., Chandra, P., Roderick, H. L., Habermann, A., Griffiths, G., and Ktistakis, N. T. (2008) Autophagosome formation from membrane compartments enriched in phosphatidylinositol 3-phosphate and dynamically connected to the endoplasmic reticulum. *The Journal of Cell Biology* **182**, 685-701

Chapter 1: Pexophagy - The selective degradation of peroxisomes

Abstract

Peroxisomes are single-membrane-bounded organelles present in the majority of eukaryotic cells. Despite the existence of great diversity among different species, cell types and under different environmental conditions, peroxisomes contain enzymes involved in β-oxidation of fatty acids and the generation, as well as detoxification, of hydrogen peroxide. The exigency of all eukaryotic cells to quickly adapt to different environmental factors requires the ability to precisely and efficiently control peroxisome number and functionality. Peroxisome homeostasis is achieved by the counterbalance between organelle biogenesis and degradation. The selective degradation of superfluous or damaged peroxisomes is facilitated by several tightly regulated pathways. The most prominent peroxisome degradation system uses components of the general autophagy core machinery and is therefore referred to as 'pexophagy'. In this review we focus on recent developments in pexophagy and provide an overview of current knowledge and future challenges in the field. We compare different modes of pexophagy and mention shared and distinct features of pexophagy in yeast model systems, mammalian cells and other organisms.

Introduction to peroxisome biology

Peroxisomes were initially described as 'microbodies' in a Ph.D. thesis on the cellular morphology of rodent kidneys (1) and were characterized as novel eukaryotic organelles by Christian de Duve and colleagues in the 1960s (2). Biochemical analysis of isolated peroxisomes from rat liver resulted in the identification of several enzymes involved in hydrogen peroxide generation and detoxification and thus led to the term 'peroxisome' for this new organelle. Almost 50 years later, despite significant insights regarding peroxisome function, several aspects of peroxisome biology still remain unresolved. This is partly based on the fact that peroxisomes display an unusually high variability in function, morphology and biochemical features. For example, the presence of enzymes involved in the glyoxylate cycle has resulted in the denotation

‘glyoxysomes’ for some plant peroxisomes (3), while the same organelle is dubbed ‘glycosome’ in trypanosomatids because it houses glycolytic enzymes (4,5). Exemplifying the remarkable specialization of peroxisomal enzymes is the protein luciferase and proteins required for synthesis of penicillin. Luciferase is responsible for the bioluminescent characteristic of the firefly *Photinus pyralis* (6,7) and the enzymatic cascade involved in penicillin production derives from the fungus *Penicillium chrysogenum* and its relatives (8,9). In vertebrates, peroxisomes harbor the enzymatic pathways for synthesis of specialized ether phospholipids vital for integrity of the central nervous system (10).

In contrast to these specializations, most peroxisomes share the enzymatic components for the β-oxidation of fatty-acyl-CoA derivatives, as well as for the production and degradation of hydrogen peroxide and other reactive oxygen species (ROS). The common evolutionary origin of all peroxisome subtypes is best illustrated by the ubiquitous presence of orthologs of a specific set of *PEX* genes, encoding peroxins, involved in peroxisome biogenesis, maintenance and division. Additional commonalities are that all peroxisomal proteins are encoded in the nucleus, translated in the cytosol and imported into the peroxisomes by a highly conserved set of localization signals (called peroxisomal targeting signals or PTSs) and corresponding receptors and transporters (11,12). Figure 1-1 summarizes shared and unique metabolic and enzymatic functions of peroxisomes.

The evolutionary origin of peroxisomes is still a matter of debate (13). Their presence in all main eukaryotic taxa and the mentioned similarities argue for a singular evolutionary origin in a common ancestor of eukaryotic cells, most likely as a consequence of an increase in oxygen levels in the archaic atmosphere. While it was initially hypothesized that peroxisomes evolved in the course of events related to endosymbiosis, similar to mitochondria and plastids (14-16), research in the past decade has provided conclusive evidence that peroxisomes are not remnants of endosymbiotic microorganisms but have evolved from specialization of distinct parts of the endoplasmatic reticulum (ER) (17,18). Peroxisomes (unlike mitochondria and chloroplasts) have a single membrane, do not possess their own genome, and require several peroxisomal

membrane proteins (PMPs) that transit via the ER before reaching their final destination in the peroxisomal membrane (19-22). In the light of these findings it is generally believed that peroxisomes represent organelles originating from a specialization of the endomembrane system, rather than examples of endosymbiotic events.

The vital importance of peroxisomes in higher eukaryotes is documented by the dramatic effects of peroxisome dysfunction on human health. Peroxisomal Disorders (PDs) are subdivided into two major groups: 'single Peroxisomal Enzyme/transporter Deficiencies' (PEDs) and 'Peroxisomal Biogenesis Disorders' (PBDs). PEDs are caused by a functional defect in one peroxisomal pathway and include metabolic syndromes such as acatalasia, Acyl-CoA deficiency and X-linked adrenoleukodystrophy (23). PBDs are caused by mutations affecting a set of at least 12 human genes, which function in peroxisome biogenesis and assembly (*PEX* genes), resulting in manifestation of numerous pathological conditions (24,25). PBDs involve autosomal recessive neurodevelopmental disorders that display numerous other symptoms including skeletal and craniofacial dysmorphism, liver dysfunction, and retinopathy. These diseases are caused by complete or partial loss of peroxisome functionality and include the Zellweger syndrome spectrum disorders (e.g. Zellweger syndrome, neonatal adrenoleukodystrophy, infantile Refsum's disease) as well as rhizomelic chondrodysplasia punctata (26,27).

The severity of these defects emphasizes the pivotal role of peroxisomal metabolism for cellular integrity, especially in neuronal cells. In line with these observations, peroxisomes serve an important function in the central nervous system for the formation and maintenance of the myelin sheath and for the preservation of long-term axonal integrity (10,28,29). In addition, recent reports point to a specific role of peroxisomal metabolism as a determinant of the cellular aging process, with peroxisome-derived ROS being triggers of anti-aging pathways (at low concentrations), but also being decisive accelerators of aging by damage accumulation (at high concentrations) (30,31). This is further underscored by the finding that aging human fibroblasts accumulate peroxisomes with impaired protein import capacity, leading to ROS accumulation and

exacerbation of the aging process (32). Homeostasis in peroxisome number and functionality not only plays a role in the described disease settings, but also for the physiological aging process.

Peroxisome homeostasis

Due to their importance for a variety of metabolic functions, peroxisome number is tightly controlled by environmental conditions. Yeasts (e.g. *Hansenula polymorpha, Pichia pastoris, and Saccharomyces cerevisiae*), are capable of utilizing different carbon sources and increasing peroxisome number and biomass when grown in these media requiring peroxisomal metabolism (Figure 1-2). Conversely, the shift of these cells from peroxisome induction conditions to carbon sources wherein peroxisomes are unnecessary triggers the degradation of superfluous peroxisomes by autophagy. These observations of peroxisome induction and removal have resulted in utilization of yeasts as model organisms to study peroxisome biogenesis and turnover, which have led to the identification of several genes and mechanisms controlling peroxisome homeostasis (11,33-47). In rodents, the administration of phthalate esters or hypolipidemic drugs such as fibrates results in upregulation of peroxisomal proteins and a concomitant increase in peroxisome number (48). This process is dependent on members of a special class of nuclear receptors, called 'peroxisome proliferator-activated receptors (PPARs)' (49,50). However, this effect does not represent a general conserved mechanism since PPAR agonists fail to induce peroxisome proliferation in human cells (51,52). In contrast, it has been demonstrated that drugs, such as 4-phenylbutyrate (4-PBA), that act as chemical chelators and/or affect histone deacetylase (HDAC) activity can act as non-classical peroxisome proliferators independent of PPAR activity in human cells (53,54).

Here we present model systems to study peroxisome turnover and outline mechanisms that contribute to peroxisome homeostasis by regulating the selective degradation of peroxisomes. The main focus will be on selective degradation of peroxisomes in the vacuolar/lysosomal compartment, a process mediated by components of the general autophagy core machinery and usually referred to as pexophagy.

Methylotrophic yeasts as model systems for pexophagy

The large peroxisome clusters of methylotrophic yeasts (e.g. *P. pastoris* and *H. polymorpha*), as well as the experimental ease of manipulation of peroxisome number, volume and content by media shifts in a genetically tractable organism have facilitated studies on pexophagy. These yeasts, when grown in media containing methanol as the sole carbon source, rapidly proliferate their peroxisomes, which can occupy up to 40% of the cell volume. This makes fluorescence imaging of tagged proteins involved in pexophagy, as well as biochemical analysis of peroxisomal markers, much easier to monitor than in mammalian or other yeast systems. The autophagic degradation of peroxisomes was first noted by De Duve & Baudhuin (2) when they observed the appearance of peroxisomes within the lysosomes of mammalian cells, thus documenting the earliest description of pexophagy. Since then, much has been learnt from studies on pexophagy conducted in methylotrophic yeasts.

Modes of pexophagy: micropexophagy and macropexophagy

All organisms from yeast to humans possess basal and inducible macroautophagy. During macroautophagy (referred to here as 'autophagy'), a double membrane originates from a site known as the phagophore assembly site (PAS) to engulf cargo into a double-membrane vesicle known as the autophagosome, which upon fusion with a lysosome (or vacuole in yeast cells), releases into the lysosomal/vacuolar lumen an autophagic body comprised of a single membrane surrounding the cytosolic cargo. Once in the lysosomal lumen, the membrane and other macromolecular contents of the autophagic body are degraded by hydrolases to their constituent building blocks for re-use by the cell. This entire process, from the assembly of the PAS, to the engulfment of cargo into autophagosomes, fusion of autophagosomes with the lysosome/vacuole and subsequent degradation of the cargo, is orchestrated by the hierarchical recruitment of autophagy-related (Atg) proteins (55). An alternative process called microautophagy also exists, in which the lysosome/vacuole membrane invaginates to engulf cytosolic cargo directly to degrade and recycle it (56,57).

In contrast to the non-selective nature of cargo engulfed by macroautophagy and microautophagy, other autophagy-related pathways capture cargo selectively from the cytosol. These include oligomeric proteins delivered to the vacuole by the cytosol-to-vacuole targeting (Cvt) pathway, ribosomes (ribophagy) and subcellular organelles such as peroxisomes (pexophagy), mitochondria (mitophagy), parts of the ER (ER-phagy) and segments of the nucleus (micronucleophagy) (38). In most of these selective processes, the phagophore membrane, originating from specific PAS structures required for each form of selective autophagy (e.g. Cvt- or pexophagy-specific PAS, Figure 1-3A and 1-3C), engulfs the specific cargo and delivers it to the lysosome/vacuole for degradation. The source of the phagophore membrane is a widely debated topic within the field of autophagy, with the focus primarily on how Atg9 (ATG9L1 in mammals), which is the only transmembrane protein of the core Atg machinery, is recruited to the PAS (58). Atg9 is thought to be involved directly or indirectly in trafficking membrane and/or lipid components during phagophore expansion from the PAS. However, this mechanistic concept remains a hypothesis (59-61).

To date, 37 autophagy-related (*ATG*) genes involved in several autophagy-related pathways have been discovered. Macropexophagy and micropexophagy (described next) are both used in *P. pastoris* for selective peroxisome degradation (62,63). As these represent specialized types of autophagy, it should not be surprising that they require many of the core genes also used for autophagy, as well as specific genes in addition (see Table 1-1) (38,64). Many yeast mutants with pexophagy defects provide insights into the mechanism of the two pexophagy modes (see Table 1-1).

Micropexophagy occurs when a cluster of peroxisomes is directly engulfed by vacuolar sequestering membranes (VSMs) that extend from a septated vacuole, and a double-membrane structure called the micropexophagy-specific membrane apparatus (MIPA) (65). The MIPA extends from the PAS to form a cup-shaped lid over the VSM-engulfed peroxisomes and fuses with the VSMs to completely sequester the targeted peroxisomes from the cytosol and to ultimately deliver the pexophagic body into the vacuole lumen to be degraded by resident

vacuolar enzymes (Figure 1-4A). During macropexophagy, an individual peroxisome is surrounded by the phagophore membrane originating from the pexophagy-specific PAS to form a double membrane-bounded pexophagosome (Figure 1-4A), before the outer membrane fuses with the vacuole membrane in a process resembling macroautophagy (41). In *P. pastoris*, the choice between induction of either micro- or macropexophagy is determined by ATP levels in the cell (66). High levels of ATP induce micropexophagy while lower levels activate macropexophagy. One explanation for this observation may be that the massive vacuolar re-arrangement during micropexophagy and formation of the MIPA may be a more energy-intensive process than formation of the pexophagosome and thus may demand more energy in the form of ATP from the cell.

Nutrient conditions that induce pexophagy

In *S. cerevisiae*, pexophagy is induced by transferring cells from growth media containing oleate as a carbon source to glucose-containing medium without a nitrogen source (67). In *P. pastoris*, peroxisomes can be induced when cells are grown in media containing methanol, oleate or amines. Transferring cells grown in methanol to ethanol or from oleate or methylamine to glucose without nitrogen induces macropexophagy (Figure 1-4B and C) (68). Shifting cells from methanol medium to glucose induces micropexophagy (Figure 1-4B and C) (69). Intriguingly, the two modes of pexophagy can be triggered by different experimental conditions in different yeasts. In *H. polymorpha*, macropexophagy, rather than micropexophagy, is induced when cells are shifted from methanol medium to glucose (47).

Interestingly, it was shown that simultaneous treatment of *H. polymorpha* with both nitrogen limitation and excess glucose conditions results in concomitant induction of both microautophagy and macropexophagy, thus exemplifying the fact that selective (i.e. pexophagy) and non-selective (autophagy) pathways can be initiated in parallel (70).

Regulation of yeast pexophagy

It has long been realized that not only surplus, but also damaged components or potentially toxic structures within the cytosol of eukaryotic cells can be selectively removed by autophagy. Using ectopic expression of a temperature-sensitive degron-Pex3 fusion, it was recently shown in *H. polymorpha* that damage to peroxisomes by abruptly removing the essential PMP, Pex3, causes pexophagy to occur (71). This conditional selective degradation was apparent even when cells were placed in conditions that would normally require peroxisome biogenesis for cell growth. In methanol-excess conditions the authors saw a transient increase of ROS in wild-type cells that corresponds with the degradation of the peroxisome matrix protein, alcohol oxidase, as well as PMPs, Pex3 and Pex14, suggesting the possible physiological significance of pexophagy. However, it is unclear at present if there is a similar requirement of Pex3 removal from the peroxisome membrane for pexophagy in other methylotrophic yeasts such as *P. pastoris*, where Pex3 is actually essential to recruit the pexophagy receptor, Atg30, to the peroxisome, before the organelle is targeted for pexophagy.

The signaling events that regulate the specific removal of cellular components are still poorly understood. The emerging role of intracellular signaling pathways controlling pexophagy was shown by our group and has since been replicated and refined further. Using the degradation of a peroxisomal marker to investigate the role protein kinases play in pexophagy in *S. cerevisiae*, the Slt2 mitogen-activated protein kinase (MAPK) and several other upstream components of this signaling pathway were shown to be required for pexophagy, but not for pexophagosome formation, suggesting a block at the step of pexophagosome targeting or pexophagosome-vacuole fusion (37).

This theme of the involvement of yeast MAPK in selective autophagy has been extended by the recent discovery that Slt2 also plays a role in mitophagy (72), along with another MAPK (Hog1) (72,73). Slt2 is crucial for recruiting mitochondria to the PAS, a step required for the specific packaging of cargo into autophagosomes. Interestingly, mitophagy in mammalian cells is

activated by ERK2, another MAPK (74). Thus, the differential involvement of MAPK pathways represents a central process in controlling diverse selective autophagy pathways (72).

Other signaling pathways have also been shown to have a direct role in pexophagy (35,75,76). The phosphoinositide, phosphatidylinositol-3-phosphate (PtdIns3P), as well as the sole phosphatidylinositol 3-kinase, Vps34, that generates PtdIns3P in yeast, are required for all autophagy-related pathways, including pexophagy (36,77). In addition, phosphatidylinositol-4-phosphate (PtdIns4P), as well as the kinase that is responsible for PtdIns4P generation (Pik1) and Atg26, a sterol-glucosyltransferase that binds PtdIns4P via its GRAM domain, are necessary for micropexophagy in *P. pastoris* (46).

General themes of selective autophagy pathways

Since all autophagy-related pathways share common components required for PAS assembly, elongation of the phagophore membrane around cargo, vesicle formation, fusion and vacuolar degradation, the key decision point in any selective autophagy pathway is the mechanism by which the core autophagy machinery is redirected to degrade primarily selective cargo. The study of these selectivity factors for pexophagy in yeast has revealed a set of key principles. Where applicable, we describe how these events are relevant to other selective autophagy pathways:

1. Every selective autophagy pathway studied to date requires a specific cargo receptor. Examples of these include Atg30 for pexophagy (34), Atg19 and Atg34 for the Cvt pathway (78-80) and Atg32 for mitophagy (81,82).
2. These cargo receptors typically have a tripartite role – (a) in cargo binding, (b) interaction with Atg11, a protein required by all selective yeast autophagy pathways to create the specific PAS structures from which the phagophore membrane will expand (78,81,82), and (c) interaction with Atg8, via an Atg8-interaction motif (AIM) (83), to allow phagophore expansion (78,81,82). The receptors Atg19 and Atg32, required for the Cvt

and mitophagy pathways in yeast, have all these properties, but as of now, only the first two roles have been attributed to Atg30 during pexophagy (34).

3. The selective autophagy receptors are often synthesized even under conditions wherein the cargoes are not degraded, but receptor activation often relies on protein modifications, such as phosphorylation or ubiquitination (34,73,84).
4. Some of the pexophagy-mediating factors, such as Atg11 and the sterol glucosyltransferase Atg26 that binds PtdIns4P (46), are required in an absolute fashion for the degradation of large cargoes, but are partially dispensable when the cargo size is small (85). We predict that since the phagophore membrane has to engulf cargoes of varying sizes from individual cytosolic proteins to organelles, bacteria and viruses, analogous factors will be required for selective autophagy of other large cargoes.
5. Specialized membrane structures, such as the MIPA, are needed for micropexophagy, and not for macropexophagy. Indeed, the protein Atg35 is needed for MIPA formation during micropexophagy, but not for pexophagosome formation during macropexophagy (43).
6. Generally the receptors are degraded in the vacuole along with the cargo.

The pexophagy-specific PAS

Like autophagy, pexophagy is also initiated at a specific PAS (Figure 1-3C) that is distinct from other types of PAS for selective autophagy (Figure 1-3A and 3B). The autophagy-specific PAS is organized by Atg11, Atg17, Atg29 and Atg31, but Atg11 is dispensable (86). The Cvt-specific PAS requires Atg11 and Atg19 for its organization (78-80) (Figure 1-3A), whereas the mitophagy-specific PAS uses Atg11 and Atg32 (81,82) (Figure 1-3B). The pexophagy-specific PAS is organized by Atg11, Atg17 and Atg30 (34,85).

For the onset of pexophagy in *P. pastoris*, Atg30 phosphorylation by a hitherto unknown kinase occurs and facilitates direct physical interaction with Atg11 (34). The two proteins co-localize at the PAS, and Atg30 also directly interacts with Atg17. The role of Atg11 and Atg17 are as scaffolds at the PAS that recruit other proteins, such as constituents of the core autophagy

machinery described next. Surprisingly, there is a size requirement of the scaffolding proteins. For degradation of small peroxisomes, Atg11 and Atg17 are only partially required, but are essential for degradation of large peroxisomes in nitrogen-starvation conditions (85).

The assembly of a specific PAS is followed by the recruitment of core proteins of the autophagic machinery to the PAS including, but not limited to Atg1, Atg2, Atg5, Atg8, Atg9, Atg12, Atg13, Atg16, Atg18, Atg23, Atg24, Atg25, Atg27, Atg28, Atg35 and the PtdIns3-kinase (PI3K) complex. These proteins typically assemble in a complex hierarchy (87), such as our demonstration that the recruitment of PtdIns-3-Kinase to the PAS precedes Atg8 recruitment (88)

Elongation of the phagophore membrane

The protein Atg35 is a micropexophagy-specific protein recruited by Atg28 and is required for efficient MIPA formation but not for pexophagosome formation, giving the first evidence that the formation of the MIPA could be genetically distinct from the formation of the pexophagosome in macropexophagy (43).

Atg26, a sterol glucosyltransferase that synthesizes sterol glucoside, is essential for pexophagy, but not autophagy in *P. pastoris*. The protein is associated with the MIPA during micropexophagy, and that a single amino acid substitution within the GRAM domain (domain found in glycosyltransferases, Rab-like GTPase activators and myotubularins) of the protein abolished this association (44). However, it was found that although Atg26 is required for utilization of decane in *Y. lipolytica,* it was unnecessary for pexophagy in this yeast, showing that sterol glucosyltransferases play different functional roles in the two yeasts (89).

In *P. pastoris*, phosphatidylinositol-4-phosphate (PtdIns4P) initiates *de novo* membrane synthesis that is required for pexophagy. PtdIns4P, generated primarily by the PtdIns-4-kinase, Pik1, recruits Atg26 via its GRAM domain (46), and the sterol glucosyltransferase activity of Atg26 at the nucleation complex is necessary for the elongation of the membrane.

In both *S. cerevisiae* and *P. pastoris*, the only integral membrane protein of the autophagy machinery, Atg9, cycles between a peripheral compartment comprising a reservoir of

Atg9 and the PAS, or PAS-like structures. The shuttling mechanism has been studied in both organisms but the process is better understood in *S. cerevisiae* and is therefore described next, before the role of this protein in pexophagy is described.

In *S. cerevisiae,* Atg9 colocalizes at the PAS but is not present on completed autophagosomes, suggesting it must be recycled during autophagosome formation. It cycles between a peripheral compartment and the PAS (60). The anterograde trafficking of Atg9 from the peripheral compartment to the PAS requires Atg11, Atg23 and Atg27 (61). Atg9 retrieval from the PAS is regulated by the Atg1-Atg13 signaling complex and requires Atg2, Atg18 and the PtdIns3P generated by the Atg14-containing PtdIns-3-kinase complex (90). However, only Atg2, Atg18 and PtdIns3P are necessary for Atg9 recycling, while the Atg1-Atg13 complex and Atg1 kinase activity, but not Atg2, Atg18 and PtdIns3P, are necessary for Atg23 cycling to and from the PAS (90).

The subcellular movement of Atg9 in *S. cerevisiae* requires interaction with the actin cytoskeleton as has been shown by the sensitivity of relocation of Atg9 to the inhibitor Latrunculin A, as well as by the phenotype displayed by conditional mutants of actin and the actin-related protein Arp2 (91,92).

The proteins Atg11 and/or Atg17 are necessary for Atg9 recruitment to the PAS (59,93). Also required at the PAS is PtdIns3P, generated by the Vps34 (PtdIns-3-kinase) complex, to recruit PtdIns3P-binding proteins (e.g. Atg18 and Atg24), which then recruit yet other proteins, such as Atg2, to the PAS (94).

P. pastoris Atg9 (*Pp*Atg9) is necessary for the formation of the VSM, assembly of the MIPA and for pexophagosome formation. As in *S. cerevisiae*, the *P. pastoris* Atg9 also shuttles to the PAS from a peripheral compartment, perhaps supplying the membrane to the PAS and elongating the phagophore membrane to form the VSM, MIPA and pexophagosome (95). *Pp*Atg9 shuttles from a peripheral compartment near the ER/mitochondria to unique perivacuolar structures (PVS; PAS-like structures) that contain Atg11, but not Atg2 or Atg8. Atg9 then traffics from the vacuole surface to the VSMs that engulf peroxisomes for degradation (95). Movement of

the PpAtg9 from the peripheral compartment to the PVS requires PpAtg11 and PpVps15 (a subunit of the PtdIns-3-kinase). PpAtg2 and PpAtg7 are essential for PpAtg9 trafficking from the PVS to the vacuole and sequestering membranes, whereas trafficking of PpAtg9 proceeds independent of PpAtg1, PpAtg18, and PpVac8. How exactly PpAtg9 contributes to the formation of the MIPA and pexophagosome formation is less clear.

In *P. pastoris*, expression of dominant-negative forms (Sar1-T34N and Sar1- H79G) of the ER protein Sar1, impairs Atg8 lipidation and MIPA formation, but not the formation of the VSMs or the trafficking of Atg11 and Atg9 to these VSMs during micropexophagy (96). During macropexophagy, the expression of Sar1-T34N inhibited the formation of the pexophagosome, whereas Sar1-H79G suppressed the delivery of the peroxisome from the pexophagosome to the vacuole. In this case, the pexophagosome contained Atg8 in wild-type cells, but in cells expressing Sar1-H79G these organelles contain both Atg8 and endoplasmic reticulum components, suggesting a defect in retrieval of components back to the ER, prior to pexophagosome/vacuole fusion.

The protein Atg25 has been described in *H. polymorpha* to be required for macropexophagy. It interacts with Atg11 and colocalizes with it at the PAS. In its absence, peroxisomes are constitutively degraded by nonselective microautophagy, a process that in wild-type *H. polymorpha* is only observed under nitrogen starvation conditions, suggesting that nonselective microautophagy is deregulated in *H. polymorpha atg25Δ* cells (39).

Requirement of specific proteins during the final stages of pexophagy

Atg24, a molecule with a PtdIns3P-binding module (PX domain) is required for micropexophagy and macropexophagy, but not for general autophagy in *P. pastoris* and *S. cerevisiae* (33). CFP-tagged PpAtg24 localizes to the vertex and boundary region of the pexophagosome-vacuole fusion complex during macropexophagy. Depletion of PpAtg24 blocked macropexophagy after pexophagosome formation and before its fusion to the vacuole. These results suggest that PpAtg24 is involved in the regulation of membrane fusion at the vacuolar

surface during pexophagy via binding to PtdIns3P and could potentially be involved in pexophagosome fusion with the vacuole (33). During micropexophagy, *Ppatg24Δ* cells form the MIPA and exhibit aberrantly septated vacuoles, reminiscent of other mutants defective in vacuolar fusion, but engulfment of peroxisomes is also impaired (33).

Pexophagy in mammalian cells

In contrast to yeast models, which have greatly contributed to the mechanistic understanding of pexophagy as outlined above, the molecular details of mammalian pexophagy are less well understood. This is partly based on fundamental differences between mammalian and yeast peroxisomes: While in yeasts the number of peroxisomes varies between 1-20 dependent on the species and growth conditions (see above), average mammalian cells contain between several hundred to thousands of peroxisomes (Figure 1-2A) (97). Induction of peroxisome proliferation in rodents by phthalate esters [e.g. di-(2-ethylhexyl)phthalate; DEHP)], hypolipidemic drugs (e.g. fibrates) or non-classical peroxisome proliferators (e.g. 4-PBA) results in a 2-3-fold increase of peroxisomal mass, which is a significantly smaller effect compared to the effects observed in yeasts. Consequently, quantitative analyses of peroxisome turnover in mammalian systems are limited by the detection method applied. Mammalian peroxisomes differ from those of yeast cells not only in number and induction mechanisms, but also by their modes of selective degradation. At least three independent degradation systems have been described: the Lon protease system, 15-lipoxygenase (15-LOX)-mediated autolysis and lysosomal degradation/pexophagy (Figure 1-6) (98). Based on studies using *Atg7* conditional knockout mice it is estimated that up to 20-30% of the mass of liver peroxisomes is degraded by Lon protease-mediated mechanisms and 15-LOX mediated autolysis of peroxisomes, whereas the remaining 70-80% are destroyed by autophagic mechanisms (98).

The peroxisomal isoform of the Lon protease is an ATP-dependent protease with chaperone-like activity that is involved in degradation of misfolded and unassembled peroxisomal proteins. Lon protease is upregulated in rats under peroxisome proliferation conditions (e.g.

administration of DEHP) and further increases its levels after withdrawal of the inducing drug while peroxisomal enzymes are quickly degraded (99). Subsequently, Lon protease activity catalyzes the breakdown of proteins resident in the peroxisomal matrix, indicating that it contributes to the reduction of peroxisome mass, if not quantity. Interestingly, the yeast ortholog of the Lon protease (encoded by the *PLN* gene in *H. polymorpha*) appears to be essentially involved in peroxisome quality control mechanisms, with only about a 25% contribution to reduction of peroxisome numbers, which increased only slightly from 2.6/cell to 3.3/cell in the absence of Pln, whereas the peroxisome number increased to 5.4/cell in the absence of the *ATG1* gene required for all forms of autophagy (100). Assuming that the Lon protease has similar roles in yeast and mammals, it is conceivable that relative to autophagic mechanisms, it plays a relatively modest role (in the range of 25%) in reducing peroxisome number.

The cytosolic enzyme, 15-LOX, can associate with peroxisomal membranes leading to localized membrane disruption (101). Structural breakdown subsequently exposes the peroxisomal content to cytosolic proteases resulting in its rapid degradation. This pathway appears to be initiated in parallel to pexophagy after drug-mediated accumulation of peroxisomes and accounts for removal of a limited fraction of excess peroxisomes.

While the abovementioned pathways contribute partially to peroxisome homeostasis under certain cellular conditions and other data argue for a role of the proteasome system by undefined mechanisms (102), the vast majority of selective peroxisome degradation is mediated by autophagosomal-lysosomal processes resembling yeast macropexophagy. As mentioned, early reports from the 1970's already noted the selective lysosomal degradation of mitochondria and peroxisomes during the diurnal cycle in rat inner organs (103), but it was only shown later that the autophagy machinery is specifically involved in degradation of surplus peroxisomes in mouse liver (104). This was demonstrated by comparing abundance and degradation efficiency of peroxisomes after treatment with phthalate ester for 2 weeks and chase after drug removal one week later in wild-type and autophagy-deficient *Atg7*$^{-/-}$ mice. The salient findings of this study emphasize mechanistic similarities to the above-mentioned yeast models used to study

pexophagy: environmental conditions that require peroxisomal enzymes (e.g. oleate/methanol for yeasts, chemical peroxisome proliferators for rodents) lead to peroxisome proliferation, followed by pexophagic degradation when the organelles are no longer required or can be used as a resource for alternative pathways. This biological theme of a metabolic switch involving adaptation to changing external factors and thereby triggering pexophagy is also reminiscent of organelle remodeling in pathogenic fungi and parasitic protozoa as will be outlined in the next section.

A detailed functional analysis of peroxisome degradation using an *in vitro* cell culture system showed for the first time that peroxisomes are preferentially degraded over cytosolic proteins under starvation/recultivation conditions (102). This study used Chinese Hamster Ovary (CHO) cells to describe autophagy-mediated peroxisome turnover when switching culture conditions from starvation in Hank's solution to reconstitution in nutrient-rich medium. The authors show convincingly that the peroxisomal membrane protein, Pex14, is bound by autophagosome-anchored LC3-II (i.e. the processed and lipidated form of LC3) under starvation conditions. Pex14 is an essential component of the peroxisomal translocon complex, which facilitates import of cytosolic proteins into the peroxisomal matrix. It is noteworthy that the dual role of Pex14 for both peroxisome assembly and selective degradation has also been shown for yeast systems (47). Moreover, this points to an involvement of the cytoskeleton in this process by demonstrating the requirement of intact microtubules for the LC3-II/Pex14 interaction (102). As an intriguing example of the competitive nature of the processes involved, binding of Pex14 to either LC3-II or the peroxisomal import receptor, Pex5, proved to be mutually exclusive. This might point to a general mechanism that ensures functional segregation of metabolically-active and degradation-prone organelles. Although this study uses an unusual experimental setup by applying starvation followed by re-cultivation in rich medium, it opens the avenue for future studies addressing the question of how exactly PMPs contribute to physical interactions with the autophagy-machinery. In line with these observations, a recent study describes the role of a Rab7-effector protein, FYCO1 (FYVE and coiled-coil domain-containing 1), as the physical link between LC3 family

members, PtdIns3P and microtubule plus end-directed transport (105,106), but the exact role of this mechanism for pexophagy in particular has not been addressed yet.

The dynamics of peroxisome turnover in mammalian cells under normal cultivation conditions have nicely been addressed in a recent publication (107). Using HaloTag-labelled peroxisomal marker proteins to follow the long-term fate of peroxisomes in cultured CHO cells and mouse fibroblasts, the authors show that mammalian peroxisomes have a half-life of approximately 2 days under normal cultivation conditions and that peroxisomes of different age display a different capacity to import newly synthesized proteins. In addition, this study shows that even under normal growth conditions, pexophagy contributes to the majority of turnover of this organelle as demonstrated by sensitivity to 3-methyl adenine (3-MA, an autophagy inhibitor) treatment. These findings emphasize the dual role of autophagy-related pathways: while autophagy principally serves to ensure nutrient recycling under starvation conditions, the same machinery fulfills the purpose of a quality control and homeostasis mechanism even in the presence of all nutrients.

Because the autophagy machinery in mammalian cells targets ubiquitinated protein aggregates, experiments were designed to address whether monoubiquitination of peroxisomal proteins could cause the autophagic clearance of peroxisomes (108). Using overexpression of PMPs, Pmp34 and Pex3, fused on the cytosolic side to a ubiquitin variant genetically tailored to block polyubiquitination, it was found that exposure of a single ubiquitin moiety on the cytosolic face of the peroxisomal membrane was sufficient to trigger turnover of this organelle. Specificity of this affect was demonstrated by analyzing sensitivity to protein topology and to the autophagy inhibitor, 3-MA, thus confirming the requirement of the autophagy machinery in degradation of the ubiquitin-labeled peroxisomes. Moreover, the study showed that the ubiquitin-binding autophagy adaptor, p62, is involved in selective degradation of peroxisomes under the chosen conditions. Although this study is primarily based on overexpression of ectopic proteins and the artificial placement of a ubiquitin tag on the peroxisomal membrane and does not identify the physiological target of this process, it has some interesting implications.

The general requirement of p62 for mammalian peroxisome homeostasis was demonstrated even in the absence of ectopic ubiquitin tagging, since knock-down of p62 significantly increased endogenous peroxisome numbers under the experimental conditions. Furthermore, of all mammalian autophagy adaptors identified so far (e.g. p62/SQSTM1, NDP52, NBR1), only p62 has as yet been shown to be involved in selective degradation of peroxisomes. Since these adaptors partly share mechanistic features such as bridging ubiquitinated cargo (e.g. cytoinvasive bacteria in the case of NDP52) to LC3 family members to link with the autophagy machinery, it is unclear to date how cargo selectivity is facilitated in mammals. An interesting finding on this theme comes from the field of xenophagy, the selective degradation of cytosolic pathogens (reviewed elsewhere in this Special Issue): As shown recently, the two ubiquitin-binding autophagy adaptors p62 and NDP52 are recruited independently to cytoinvasive *Salmonella sp*. and show distinct localization signals at the surface of the invaded pathogens (109). The authors argue that two individual adaptor complexes are required for effective xenophagy of *Salmonella sp*. and that these two complexes organize distinct microdomains associated with bacteria. With respect to pexophagy, it has not been analyzed whether or not different adaptor proteins are involved in selective degradation of peroxisomes and what their respective contribution is. Answers to this type of question will be informative not only for pexophagy, but for the whole field of selective autophagy pathways. A hypothetical mechanistic model of mammalian pexophagy is illustrated in Figure 1-7.

Pexophagy in plant and human pathogens

A very interesting and unexpected perspective originates from recent studies in the field of parasitology and infection biology showing that pexophagy is required for the phytopathogenicity of the cucumber anthracnose fungus, *Colletotrichum orbiculare* (110,111). This plant pathogen forms a specific structure termed the appressorium, which is required for penetration of the host epidermal cells in the course of infection. The authors used a random insertional mutagenesis screen to identify fungal genes that contribute to pathogenicity. They

identified the *C. orbiculare* ortholog of *P. pastoris ATG26* to be essential for host cell infection. *PpATG26* is a well characterized pexophagy gene encoding a sterol glucosyltransferase, which is essential for pexophagy in methylotrophic yeasts (46,68). In the case of *C. orbiculare*, the pathogen undergoes morphological changes reminiscent of pexophagy during development of its appressoria as indicated by vacuolar localization of peroxisomes and the requirement for the central autophagy protein, Atg8. While appressoria could still be formed in the *atg26* deletion mutant, the infection process was significantly delayed. Moreover, deletion of *atg8* completely abolished appressoria formation, suggesting an essential role of the autophagy machinery during infection. As the authors show, non-selective general autophagy is essential for early morphogenesis during pathogen development, while Atg26-dependent selective pexophagy is essential for later stages of direct host-pathogen infection steps. The authors conclude that Atg26-mediated pexophagy might be involved in maturation of the infection structures by providing molecular building blocks through organelle recycling.

Another report points to the role of pexophagy during developmental and environmental changes in the parasitic protozoan, *Trypanosoma brucei*. This human pathogen, which causes sleeping sickness and Chagas disease, harbors essential enzymes of glycolysis in its peroxisomal structures, which are therefore referred to as ‘glycosomes’. The parasitic life cycle of this pathogen, which comprises different developmental stages in the Tse-Tse fly vector and the human host, requires adaptation of its metabolism to the changing environment. The necessary dynamic remodeling of glycosomal structures is facilitated by fusion of glycosomes with acidic lysosomes through autophagy-related mechanisms resembling pexophagy (112). As shown recently, the acidic pH of the lysosomal compartment is responsible for inactivation of the key peroxisomal enzyme, Hexokinase (TbHK1), without affecting its protein level (113). In addition, the pH change renders the enzyme sensitive to metabolic feedback regulation by both its substrate and product (ATP and ADP, respectively) and to modulation by other glycosomal metabolites, most likely by subtle changes in the protein tertiary structure. Thus, pexophagy appears to allow for a novel mechanism of regulating enzymatic activity by facilitating pH-

dependent structural changes and concomitant feedback responses. These data point to an unexpected role of pexophagy as a regulator of essential enzyme activity in a parasitic protozoan during development and adaptation.

Moreover, the human fungal pathogen, *Candida glabrata,* requires adjustment of peroxisome number for survival after phagocytosis by immune cells (114). The authors used fluorescent fusion proteins of transcription factors and peroxisomal enzymes to assess the metabolic status of the engulfed parasite. Using this approach, they showed that the pathogen responds to phagocytosis by increasing peroxisome number initially, most likely to fight phagocyte-induced oxidative stress. However, prolonged phagocytosis resulted in carbon starvation and a pexophagy-mediated decrease of peroxisomes. The requirement of this mechanism was shown by the dramatic loss in parasite survival during phagocytosis when the selective autophagy gene, *CgATG11*, or the general autophagy gene, *CgATG17*, were knocked out. The authors conclude that autophagy-related mechanisms, including pexophagy, represent important survival mechanisms for *Candida* after engulfment by phagocytes, pointing to the pivotal role of these pathways for providing essential cellular resources.

A possible physiological role of pexophagy in yeast. This was achieved by exploring the relationship between the methylotrophic yeast *Candida boidinii* and the phyllosphere of growing *Arabidopsis thaliana* leaves (115). The authors developed a methanol sensing assay in live *C. boidinii* cells using a PTS1-tagged fluorescent protein expressed from a methanol-inducible promoter, whereby an increase in environmental methanol concentrations resulted in enhanced fluorescence levels. They then used this assay to measure local methanol concentrations at the phyllosphere of growing *A. thaliana* leaves and showed that methanol concentrations at the phyllosphere change throughout the day corresponding to the light-dark cycle, whereby methanol concentration increased in the dark period, compared to the light period. In addition, they showed that autophagy as well as pexophagy are both required for yeast growth and survival at the phyllosphere, as autophagy and pexophagy mutants exhibited impaired proliferation on growing *A. thaliana* leaves. These results reveal interesting mechanisms used by methylotrophic yeast to

survive at the phyllosphere, and how both autophagy and pexophagy are used to adapt to changes in environmental methanol dynamics, providing insight into plant-microbe interactions.

The common conclusion of the studies mentioned above is that pexophagy represents an important mechanism for survival and development under changing environmental conditions. Peroxisomes represent highly dynamic structures: Their biomass can easily be increased when peroxisomal functions are needed for specialized metabolic pathways or breakdown of damaging ROS, but they are quickly recycled when conditions change and they are not essential, so molecular building blocks and energy resources can be provided for alternative cellular functions. Taken together, these studies point to a pivotal role of pexophagy in the development and morphogenesis of important plant and human pathogens.

Future perspectives

Despite the great achievements of the last decade with respect to unraveling the molecular mechanisms contributing to pexophagy in various organisms, several aspects still remain to be resolved. The physiological role of pexophagy in model organisms such as yeast cells is still a matter of debate. With few exceptions, knock-out of genes specifically involved in yeast pexophagy does not necessarily result in reduced viability or increased cell death. In fact, the role of pexophagy may rather be associated with quick adaptation to changing environmental conditions and thus may only emerge under cellular stress conditions like nitrogen starvation after growth under peroxisome proliferation conditions. In line with this view, pexophagy in other organisms appears to play a role for removal and recycling of unwanted or non-essential peroxisomes under condition when the cell is in need of molecular building blocks for alternative pathways, e.g. for vital morphogenesis and development. In addition, the role of peroxisome turnover and linked changes in cellular redox state with cellular aging processes is increasingly recognized and warrants further investigation.

Although recent advances have pointed to a formerly unrecognized role of specific signal transduction pathways for the regulation of pexophagy (and mitophagy), the molecular framework

of this process still remains to be elucidated. Which upstream events activate MAPKs differentially? Which are the pivotal targets of the protein kinase activity in this context, and how do these contribute to pexophagy regulation? Is there a molecular link between mitophagy and pexophagy? Moreover, it is not known if this mechanism is restricted to yeasts or if other organisms share the same regulatory circuits and if they have functional homologs of all the selectivity factors. Future work will therefore focus on elucidating the underlying conserved (or distinct) mechanisms.

The identity and mode of action of autophagy adaptors for yeast pexophagy is one major aspect of current research efforts. While Atg30 has been identified as an Atg11-binding pexophagy adaptor, the identity of the (proposed) Atg8-binding partner remains unresolved. In addition, while the requirement of phosphorylation for adaptor protein binding to Atg11 is well established (34,73), it has not been addressed yet to what extent other posttranslational modifications, such as ubiquitination and/or alternative processing, of adaptor proteins contribute to the execution of pexophagy. Indeed, phosphorylation events in close proximity to Atg8-interaction motifs (AIMs) or LC3-interacting regions (LIRs) in the mammalian adaptor protein optineurin (OPTN) have been suggested as an important regulatory mechanism in xenophagy (116). Unraveling the corresponding mechanism in yeast and mammalian pexophagy therefore represents an intriguing perspective.

The origin of membrane material for the autophagosome/phagophore membrane is still an unanswered question. Several current models argue for a contribution of the ER to provide membrane lipids and structural components. Sar1, an ER protein required for the secretory pathway, has been shown to have a role in pexophagosome formation, but the data do not unambiguously show that the pexophagosome membrane derives from the ER (96). In addition, we have previously shown that Atg17 traffics from the peripheral ER and co-localizes with Atg35, which regulates MIPA formation (43) but there is not a decisive mechanism of membrane trafficking as of yet.

In addition, the sub-cellular sorting mechanisms, which would be required to facilitate this process of membrane recruitment are largely unknown yet recent advances towards membrane expansion and the requirement of SNAREs for autophagosome formation provide some insights (117). However, we still need to understand how various membrane fusion events are orchestrated during pexophagy

The role of cytoskeleton components for pexophagy is not yet fully understood. While pexophagy in yeast cells requires the actin skeleton (92), it appears that pexophagy in mammalian cells is dependent on tubulin-mediated interaction of LC3 family members with peroxisomal membrane proteins such as Pex14 (102). Another form of selective autophagy, xenophagy of intracellular *Listeria* and *Salmonella,* relies on components of the actin skeleton, a process mediated by the increasingly characterized class of septin proteins (118,119). Further work is needed to decipher the contribution of cytoskeleton elements and septins for different selective autophagy pathways.

While present studies have focused on experimental systems wherein pexophagy is induced by peroxisome proliferation followed by different starvation conditions, it will be a challenging task to analyze shared and distinct mechanisms for the degradation of damaged peroxisomes. Recent experiments have provided inroads to examine damage-induced pexophagy by destabilization of peroxisome membrane proteins (71). Whether or not this interesting finding relates to physiological processes, and if the same mechanism is conserved in other yeasts and higher eukaryotes, remains to be unraveled.

Given the emerging link between peroxisome biology and the infection cycle of important viral pathogens (e.g. HIV, influenza, rotavirus) on the one hand, and the contribution of peroxisomes to viral detection and innate immune responses on the other hand (120,121), it will be of utmost importance to define the role of pexophagy in the context of these important human pathogens.

Future work will shed light on these and other unanswered questions addressing the molecular basis of peroxisome turnover pathways. The resulting insights are estimated to further our understanding of selective autophagy in general.

Table 1-1: Genes involved in macro- and micropexophagy in methylotrophic yeasts. Involvement of the respective genes in the different modes of pexophagy is indicated by check marks. Genes denoted in bold font are (by current knowledge) exclusively involved in pexophagy, but not in other autophagy pathways. Genes denoted in regular font represent components of the core machinery involved in different autophagy pathways in the methylotrophic yeasts *Pichia pastoris* (Pp) and *Hansenula polymorpha* (Hp). Empty spaces and parentheses depict the current lack of conclusive evidence. Table adapted (138).

Gene	Description of molecular events	Macro-pexophagy		Micro-pexophagy	Reference
		Pp	***Hp***	***Pp***	
ATG1	serine/threonine kinase required for PAS formation	✓	✓	✓	(42,122,123)
ATG2	Peripheral membrane protein required for Atg9 recycling	✓		✓	(124)
ATG3	E2-like ubiquitin ligase that catalyzes lipidation of Atg8			✓	(125)
ATG4	protease that processes Atg8 as prerequisite for conjugation with phosphatidylethanolamine (PE)			✓	(65,126)
ATG6	subunit of PI3K complexes I and II	✓			(35)
ATG7	E1-(ubiquitin activating enzyme) – like protein involved in conjugation of Atg12-Atg5 and Atg8-PE conjugates	✓		✓	(42,127)
ATG8	ubiquitin-like protein that is anchored to the expanded phagophore membrane in its processed and lipidated form; involved in phagophore membrane expansion	✓	✓	✓	(33,65,126)
ATG9	transmembrane protein cycling between the PAS and a peripheral compartment	✓		✓	(95,123)
ATG11	coiled-coil adaptor protein that interacts with the core machinery and known receptors for selective autophagy	✓	✓	✓	(128)
ATG16	essential component of the Atg12-Atg5-Atg16 complex	(✓)		✓	(42)
ATG17	scaffold protein that is responsible for PAS organization	✓		✓	(34)
ATG18	PtdIns3P-binding protein whose localization is dependent Atg9 and PtdIns-3P; recruits Atg2 and needed for Atg9 recycling	✓		✓	(94,129)
ATG21	WD40 protein with phosphoinositide binding domain that is involved in pexophagosome formation		✓		(130)
ATG24	sorting nexin protein involved in fusion events with the vacuole	✓		✓	(33)

Table 1-1: Genes involved in macro- and micropexophagy in methylotrophic yeasts, continued

Gene	Description of molecular events	Macro-pexophagy		Micro-pexophagy	Reference
		Pp	*Hp*	*Pp*	
	role in phagophore membrane expansion	✓		✓	(131)
ATG28	coiled-coil protein required for peroxisome sequesteration during micropexophagy and vacuole fusion of pexophagosomes in macropexophagy	✓		✓	(34)
ATG30	pexophagy receptor that interacts with peroxins, Pex3 and Pex14, and adaptor proteins, Atg11 and Atg17				(43)
ATG35	localizes to the perinuclear structure; regulates MIPA formation and interacts with Atg28 and Atg17			✓	
				✓	(42)
GCN1-4	involved in general amino acid control		✓	✓	(96)
Sar1	Sec protein required for MIPA and proper pexophagosome formation			✓	(65)
PEP4	vacuolar protease	✓	✓	✓	(34,71,132)
PEX3	PMP peroxin required for peroxisome biogenesis and for recruitment of pexophagy receptor	✓	✓	✓	(34,133)
PEX14	PMP peroxin required for peroxisome biogenesis and for recruitment of pexophagy receptor			✓	(46)
PIK1	PtdIns-4-kinase required for MIPA formation			✓	(127)
PFK1	subunit of phosphofructokinase complex	✓			(134)
TUP1	transcriptional repressor			✓	(135,136)
VAC8	N-myristoylated armadillo-repeat protein of the vacuolar membrane; required for VSM formation		✓		(45)
VAM7	SNARE protein that is involved in vacuolar fusion events with the phagophore membrane	✓	✓	✓	(42,75)
VPS15	regulatory subunit of PI3K	✓	✓	✓	(36,88)
VPS34	phosphatidylinositol-3-kinase (PI3K)	✓	✓	✓	(71,137)
YPT7	Rab GTPase involved in phagophore membrane fusion				

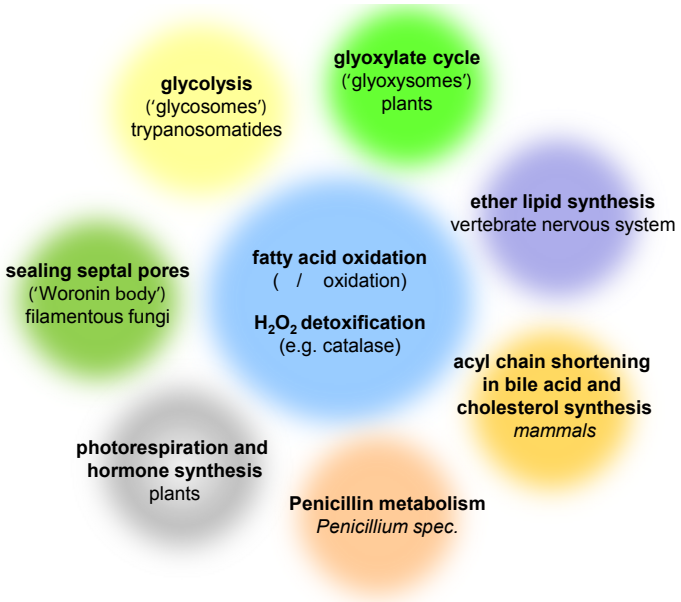

Figure 1-1: Overview of peroxisome functions in different organisms and tissues.
Peroxisomes display a great variety in metabolic pathways as defined by their respective enzymatic content. Most eukaryotes share peroxisomal enzymes for fatty-acyl-CoA metabolism (α- and β-oxidation) and detoxification of hydrogen peroxide by catalase. In addition, several specialized metabolic pathways housed in the peroxisomal matrix of various organisms or tissues are shown.

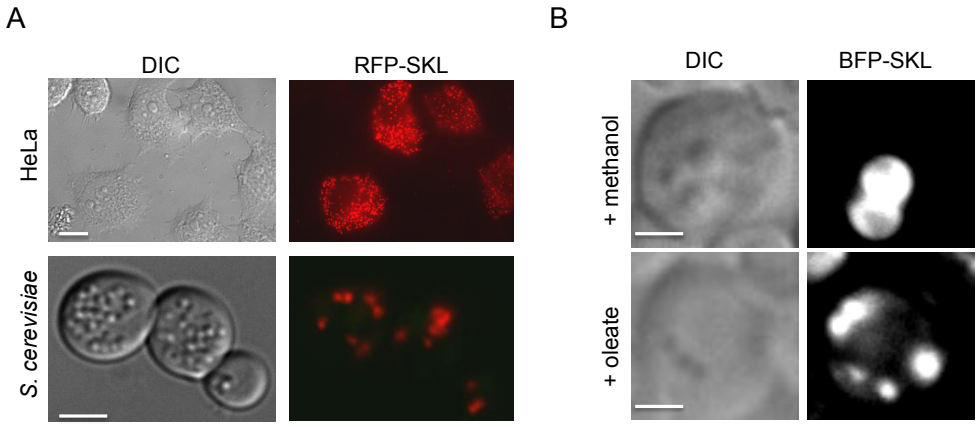

Figure 1-2: Comparison of peroxisome number and morphology in different eukaryotic cells and under different proliferation conditions. A) *Upper panel:* Human HeLa cells expressing the peroxisomal marker, RFP-SKL, under basal growth conditions. *Lower panel: S. cerevisiae* cells expressing RFP-SKL after peroxisome induction in oleate medium. The relative number of peroxisomes per cell differs greatly between different eukaryotic cell types. Size marker = 2 µm. B) Grayscale images of *P. pastoris* cells expressing BFP-SKL as peroxisomal marker. *Upper panel*: large, clustered methanol-induced peroxisomes; *lower panel:* small, unclustered oleate-induced peroxisomes. Note the difference in size and appearance of peroxisomes induced by different carbon sources. Size marker= 2µm.

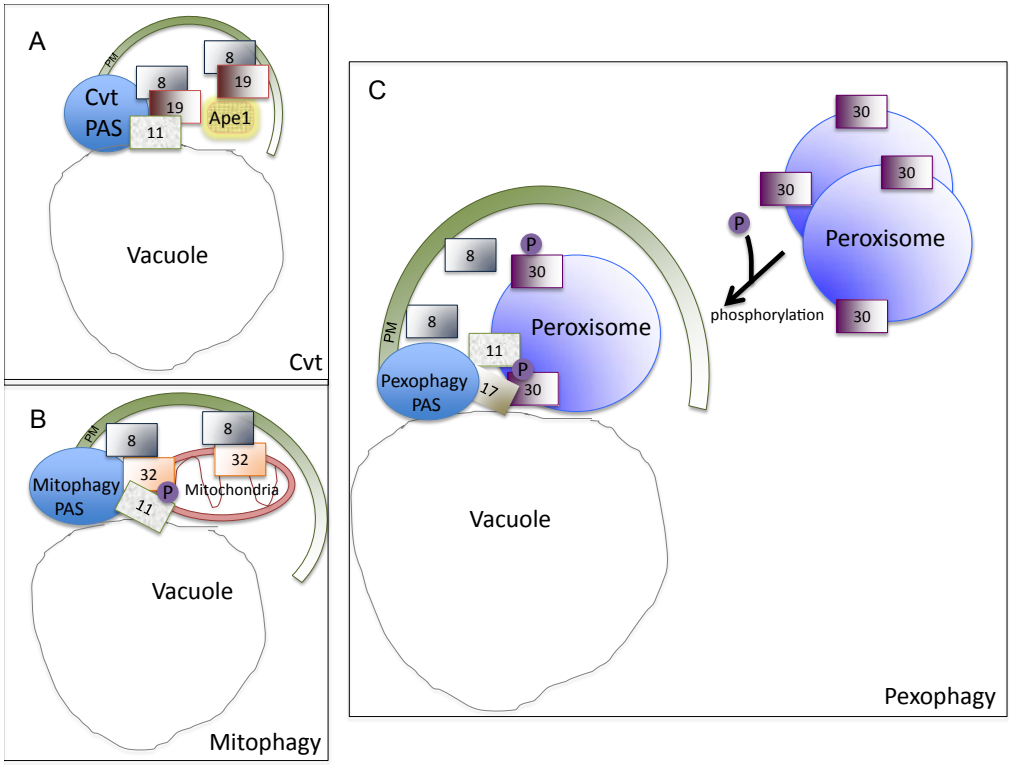

Figure 1-3: Similarities and differences between selective autophagy pathways. Various selective autophagy pathways share similar molecular mechanisms: They require a receptor that interacts with the cargo, recruits a scaffold protein (Atg11) that organizes the core autophagic machinery at the PAS, and mediates recruitment of Atg8, which initiates phagophore elongation from the PAS. In the Cvt pathway (A) Atg19 and Atg34 are the receptors for the cargo proteins aminopeptidase I (Ape1) and alpha-mannosidase, respectively. These receptors bind to Atg11 at the Cvt-specific PAS to initiate membrane expansion of the phagophore. B) The mitophagy-specific phagophore membrane expansion from the PAS is initiated by Atg32, a mitochondrial outer membrane protein. Atg32 also interacts with Atg11 and Atg8. C) The pexophagy receptor, Atg30, is localized at the peroxisome membrane, via interaction with the PMPs, Pex3 and Pex14. It is phosphorylated upon induction of pexophagy resulting in interaction of Atg30 with core autophagic machinery components, Atg11 and Atg17. In the case of pexophagy, the direct Atg8 interaction partner is still unknown.

Figure 1-4: Micropexophagy and Macropexophagy. A) Micropexophagy differs from macropexophagy in vacuole dynamics and formation of MIPA instead of the pexophagosome. A pexophagy-specific PAS, required for both forms of pexophagy, is characterized by its localization near the peroxisome and also touching the vacuolar membrane. Micropexophagy can target a peroxisome cluster for degradation by vacuole remodeling to form cup-like vacuolar sequestration membranes (VSM) and a lid-like cover called the MIPA (micropexophagy-specific membrane apparatus). Macropexophagy is characterized by individual sequestration of targeted peroxisomes into a pexophagosome, followed by its fusion with the vacuole for degradation and recycling. Pexophagy signaling is dependent on Mitogen-activated protein kinase (MAPK) pathways (Mid2 - Slt2 cascade), but may also be triggered by internal (unknown) factors, including signals related to the status of, or metabolic need for, (e. g. damaged or superfluous) peroxisomes. B) The upper panel depicts a single *P. pastoris* cell that has undergone peroxisome induction (in methanol) and has then been switched to micropexophagy conditions (glucose). The vacuole (red, FM 4-64) is shown surrounding the targeted peroxisome cluster (blue, BFP-SKL). The MIPA (green, GFP-Atg8) forms a lid over the cup-like VSMs. The lower panel illustrates pexophagosome formation around a single peroxisome under macropexophagy conditions (ethanol). C) *S. cerevisiae* cell labeled with GFP-tagged thiolase (a peroxisome matrix marker) and vacuole marker (FM 4-64, red) shows proliferated peroxisomes under nutrient-rich conditions (in oleate, top panel). When the cells are switched to glucose without nitrogen, peroxisomes are targeted to the vacuole by macropexophagy and GFP accumulates in the vacuole (lower panel).

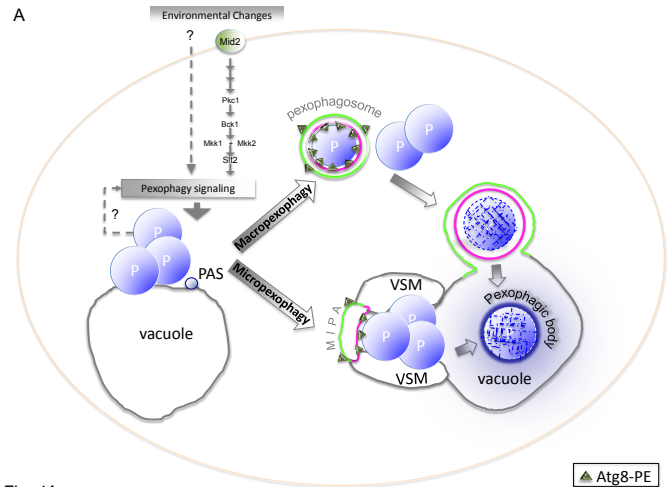
A
Environmental Changes
?
Mid2
Pkc1
Bck1
Mkk1
Mkk2
Slt2
Pexophagy signaling
?
P
PAS
vacuole
pexophagosome
Macropexophagy
Micropexophagy
VSM
M I P A
VSM
pexophagic body
vacuole
Atg8-PE

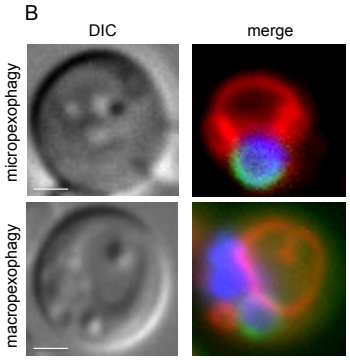
B
DIC
merge
micropexophagy
macropexophagy

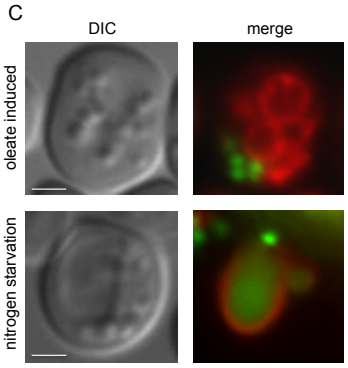
C
DIC
merge
oleate induced
nitrogen starvation

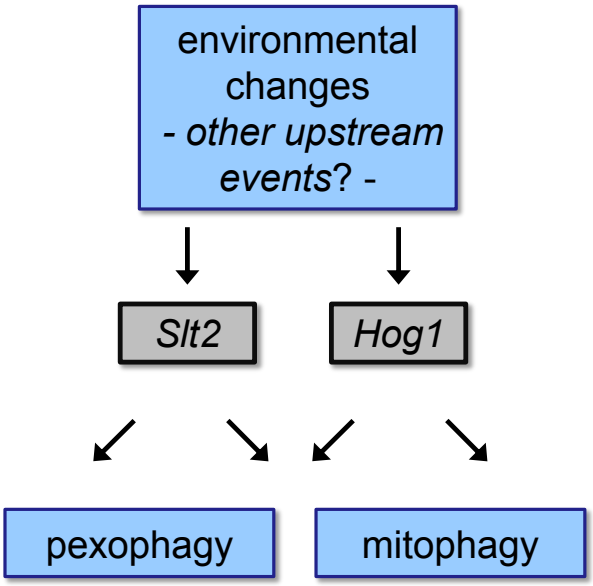

Figure 1-5: Signal transduction cascades regulating selective autophagy in yeast. Mitogen-activated protein kinase (MAPK) cascades contribute to differential regulation of selective autophagy pathways. As recently shown, the Slt2 and Hog1 signal transduction pathways regulate both mitophagy and pexophagy (37,73). Besides the obvious role of environmental factors such as nutritional conditions, details of other upstream events are poorly understood.

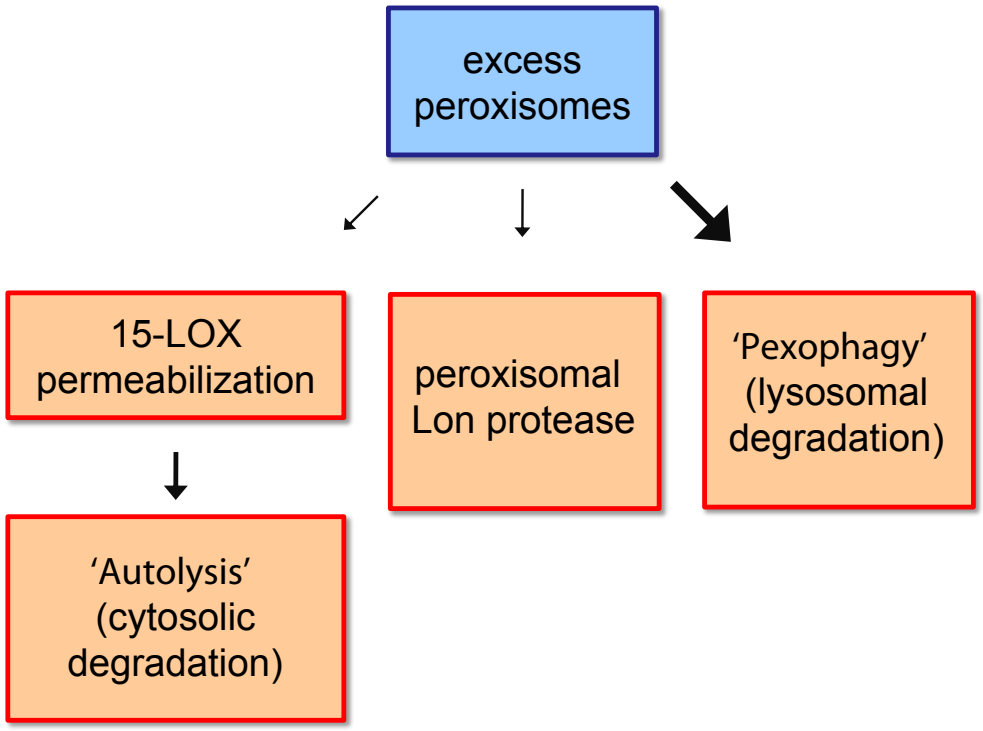

Figure 1-6: Peroxisome degradation pathways in mammalian cells. Surplus peroxisomes or their contents (e.g. peroxisomal matrix proteins) can be degraded by at least three distinct mechanisms: Lon protease-mediated proteolysis, 15-lipoxygenase (15-LOX)-mediated cytosolic degradation (autolysis), and pexophagy (autophagy-mediated lysosomal degradation). Current studies suggest that the majority of peroxisomes are degraded by pexophagy (indicated by bold arrow).

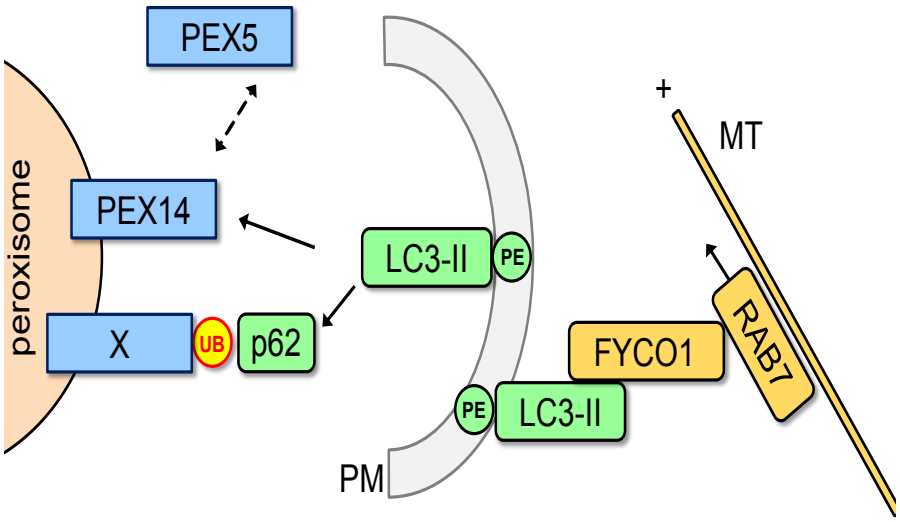

Figure 1-7: Hypothetical mechanistic model of pexophagy in mammalian cells. Processed and lipidated LC3 (LC3-II) is integrated into the expanding phagophore membrane (PM) and also may be involved in facilitating directed movement of the PM structure by interacting with microtubules (MT) via FYCO1/RAB7. Targeting of peroxisomes may either be accomplished by p62-mediated detection of ubiquitin (UB) motifs on still unknown peroxisomal membrane (or associated) proteins (X) or by direct binding of LC3 to PEX14, a process which is discussed to compete with the binding of PEX5 to PEX14 (dotted arrow). See text for details.

The text of Chapter 1 has been published in the *International Journal of Cell Biology.* The candidate wrote a large portion of the text and contributed to the figures as follows: sections on Peroxisome homeostasis, Methylotrophic yeasts as model systems for pexophagy, Modes of pexophagy: micropexophagy & micropexophagy, Nutrient conditions that induce pexophagy, The pexophagy-specific PAS, Requirement of specific proteins during the final stages of pexophagy and co-wrote General themes of selective autophagy pathways. In addition, the candidate made Table 1-1, Figure 1-2 B, Figure 1-3 A, B & C, and Figure 1-4 A & B.

References

1. Rhodin, J. (1954) Correlation of ultrastructural organization and function in normal and experimentally changed proximal tubule cells of the mouse kidney. *Doctorate Thesis. Karolinska Institute, Stockholm*

2. De Duve, C., and Baudhuin, P. (1966) Peroxisomes (microbodies and related particles). *Physiol Rev* **46**, 323-357

3. Hayashi, M., Toriyama, K., Kondo, M., Kato, A., Mano, S., De Bellis, L., Hayashi-Ishimaru, Y., Yamaguchi, K., Hayashi, H., and Nishimura, M. (2000) Functional transformation of plant peroxisomes. *Cell Biochem Biophys* **32**, 295-304

4. Michels, P. A., Moyersoen, J., Krazy, H., Galland, N., Herman, M., and Hannaert, V. (2005) Peroxisomes, glyoxysomes and glycosomes (review). *Mol Membr Biol* **22**, 133-145

5. Moyersoen, J., Choe, J., Fan, E., Hol, W. G., and Michels, P. A. (2004) Biogenesis of peroxisomes and glycosomes: trypanosomatid glycosome assembly is a promising new drug target. *FEMS Microbiol Rev* **28**, 603-643

6. Gould, S. G., Keller, G. A., and Subramani, S. (1987) Identification of a peroxisomal targeting signal at the carboxy terminus of firefly luciferase. *J Cell Biol* **105**, 2923-2931

7. Keller, G. A., Gould, S., Deluca, M., and Subramani, S. (1987) Firefly luciferase is targeted to peroxisomes in mammalian cells. *Proc Natl Acad Sci U S A* **84**, 3264-3268

8. Kiel, J. A., Hilbrands, R. E., Bovenberg, R. A., and Veenhuis, M. (2000) Isolation of Penicillium chrysogenum PEX1 and PEX6 encoding AAA proteins involved in peroxisome biogenesis. *Appl Microbiol Biotechnol* **54**, 238-242

9. van der Klei, I. J., and Veenhuis, M. (2006) Yeast and filamentous fungi as model organisms in microbody research. *Biochim Biophys Acta* **1763**, 1364-1373

10. Baes, M., and Aubourg, P. (2009) Peroxisomes, myelination, and axonal integrity in the CNS. *Neuroscientist* **15**, 367-379

11. Ma, C., Agrawal, G., and Subramani, S. (2011) Peroxisome assembly: matrix and membrane protein biogenesis. *J Cell Biol* **193**, 7-16

12. Subramani, S. (1998) Components involved in peroxisome import, biogenesis, proliferation, turnover, and movement. *Physiol Rev* **78**, 171-188

13. Gabaldon, T. (2010) Peroxisome diversity and evolution. *Philos Trans R Soc Lond B Biol Sci* **365**, 765-773

14. de Duve, C. (1996) The peroxisome in retrospect. *Ann N Y Acad Sci* **804**, 1-10

15. de Duve, C. (2007) The origin of eukaryotes: a reappraisal. *Nat Rev Genet* **8**, 395-403

16. Duhita, N., Le, H. A., Satoshi, S., Kazuo, H., Daisuke, M., and Takao, S. (2010) The origin of peroxisomes: The possibility of an actinobacterial symbiosis. *Gene* **450**, 18-24

17. Gabaldon, T., Snel, B., van Zimmeren, F., Hemrika, W., Tabak, H., and Huynen, M. A. (2006) Origin and evolution of the peroxisomal proteome. *Biol Direct* **1**, 8

18. Schluter, A., Fourcade, S., Ripp, R., Mandel, J. L., Poch, O., and Pujol, A. (2006) The evolutionary origin of peroxisomes: an ER-peroxisome connection. *Mol Biol Evol* **23**, 838-845

19. Geuze, H. J., Murk, J. L., Stroobants, A. K., Griffith, J. M., Kleijmeer, M. J., Koster, A. J., Verkleij, A. J., Distel, B., and Tabak, H. F. (2003) Involvement of the endoplasmic reticulum in peroxisome formation. *Mol Biol Cell* **14**, 2900-2907

20. Lam, S. K., Yoda, N., and Schekman, R. A vesicle carrier that mediates peroxisome protein traffic from the endoplasmic reticulum. *Proc Natl Acad Sci U S A* **107**, 21523-21528

21. Tabak, H. F., Murk, J. L., Braakman, I., and Geuze, H. J. (2003) Peroxisomes start their life in the endoplasmic reticulum. *Traffic* **4**, 512-518

22. Agrawal, G., Joshi, S., and Subramani, S. (2011) Cell-free sorting of peroxisomal membrane proteins from the endoplasmic reticulum. *Proc Natl Acad Sci U S A* **108**, 9113-9118

23. Wanders, R. J., and Waterham, H. R. (2006) Biochemistry of mammalian peroxisomes revisited. *Annu Rev Biochem* **75**, 295-332

24. Shimozawa, N., Tsukamoto, T., Suzuki, Y., Orii, T., Shirayoshi, Y., Mori, T., and Fujiki, Y. (1992) A human gene responsible for Zellweger syndrome that affects peroxisome assembly. *Science* **255**, 1132-1134

25. Fujiki, Y. (2000) Peroxisome biogenesis and peroxisome biogenesis disorders. *FEBS Lett* **476**, 42-46

26. Steinberg, S. J., Dodt, G., Raymond, G. V., Braverman, N. E., Moser, A. B., and Moser, H. W. (2006) Peroxisome biogenesis disorders. *Biochim Biophys Acta* **1763**, 1733-1748

27. Weller, S., Gould, S. J., and Valle, D. (2003) Peroxisome biogenesis disorders. *Annu Rev Genomics Hum Genet* **4**, 165-211

28. Kassmann, C. M., Quintes, S., Rietdorf, J., Mobius, W., Sereda, M. W., Nientiedt, T., Saher, G., Baes, M., and Nave, K. A. (2011) A role for myelin-associated peroxisomes in maintaining paranodal loops and axonal integrity. *FEBS Lett* **585**, 2205-2211

29. Baes, M., Gressens, P., Baumgart, E., Carmeliet, P., Casteels, M., Fransen, M., Evrard, P., Fahimi, D., Declercq, P. E., Collen, D., van Veldhoven, P. P., and Mannaerts, G. P. (1997) A mouse model for Zellweger syndrome. *Nat Genet* **17**, 49-57

30. Titorenko, V. I., and Terlecky, S. R. (2011) Peroxisome metabolism and cellular aging. *Traffic* **12**, 252-259

31. Ivashchenko, O., Van Veldhoven, P. P., Brees, C., Ho, Y. S., Terlecky, S. R., and Fransen, M. (2011) Intraperoxisomal redox balance in mammalian cells: oxidative stress and interorganellar cross-talk. *Mol Biol Cell* **22**, 1440-1451

32. Legakis, J. E., Koepke, J. I., Jedeszko, C., Barlaskar, F., Terlecky, L. J., Edwards, H. J., Walton, P. A., and Terlecky, S. R. (2002) Peroxisome senescence in human fibroblasts. *Mol Biol Cell* **13**, 4243-4255

33. Ano, Y., Hattori, T., Oku, M., Mukaiyama, H., Baba, M., Ohsumi, Y., Kato, N., and Sakai, Y. (2005) A sorting nexin PpAtg24 regulates vacuolar membrane dynamics during pexophagy via binding to phosphatidylinositol-3-phosphate. *Mol Biol Cell* **16**, 446-457

34. Farre, J. C., Manjithaya, R., Mathewson, R. D., and Subramani, S. (2008) PpAtg30 tags peroxisomes for turnover by selective autophagy. *Dev Cell* **14**, 365-376

35. Farre, J. C., Mathewson, R. D., Manjithaya, R., and Subramani, S. (2010) Roles of Pichia pastoris Uvrag in vacuolar protein sorting and the phosphatidylinositol 3-kinase complex in phagophore elongation in autophagy pathways. *Autophagy* **6**, 86-99

36. Kiel, J. A., Rechinger, K. B., van der Klei, I. J., Salomons, F. A., Titorenko, V. I., and Veenhuis, M. (1999) The Hansenula polymorpha PDD1 gene product, essential for the selective degradation of peroxisomes, is a homologue of *Saccharomyces cerevisiae* Vps34p. *Yeast* **15**, 741-754

37. Manjithaya, R., Jain, S., Farre, J. C., and Subramani, S. (2010) A yeast MAPK cascade regulates pexophagy but not other autophagy pathways. *J Cell Biol* **189**, 303-310

38. Manjithaya, R., Nazarko, T. Y., Farre, J. C., and Subramani, S. (2010) Molecular mechanism and physiological role of pexophagy. *FEBS Lett* **584**, 1367-1373

39. Monastyrska, I., Kiel, J. A., Krikken, A. M., Komduur, J. A., Veenhuis, M., and van der Klei, I. J. (2005) The *Hansenula polymorpha* ATG25 gene encodes a novel coiled-coil protein that is required for macropexophagy. *Autophagy* **1**, 92-100

40. Monastyrska, I., van der Heide, M., Krikken, A. M., Kiel, J. A., van der Klei, I. J., and Veenhuis, M. (2005) Atg8 is essential for macropexophagy in Hansenula polymorpha. *Traffic* **6**, 66-74

41. Monastyrska, I., and Klionsky, D. J. (2006) Autophagy in organelle homeostasis: peroxisome turnover. *Mol Aspects Med* **27**, 483-494

42. Mukaiyama, H., Oku, M., Baba, M., Samizo, T., Hammond, A. T., Glick, B. S., Kato, N., and Sakai, Y. (2002) Paz2 and 13 other PAZ gene products regulate vacuolar engulfment of peroxisomes during micropexophagy. *Genes Cells* **7**, 75-90

43. Nazarko, V. Y., Nazarko, T. Y., Farre, J. C., Stasyk, O. V., Warnecke, D., Ulaszewski, S., Cregg, J. M., Sibirny, A. A., and Subramani, S. (2011) Atg35, a micropexophagy-specific protein that regulates micropexophagic apparatus formation in *Pichia pastoris*. *Autophagy* **7**, 375-385

44. Oku, M., Warnecke, D., Noda, T., Muller, F., Heinz, E., Mukaiyama, H., Kato, N., and Sakai, Y. (2003) Peroxisome degradation requires catalytically active sterol glucosyltransferase with a GRAM domain. *EMBO J* **22**, 3231-3241

45. Stevens, P., Monastyrska, I., Leao-Helder, A. N., van der Klei, I. J., Veenhuis, M., and Kiel, J. A. (2005) *Hansenula polymorpha* Vam7p is required for macropexophagy. *FEMS Yeast Res* **5**, 985-997

46. Yamashita, S., Oku, M., Wasada, Y., Ano, Y., and Sakai, Y. (2006) PI4P-signaling pathway for the synthesis of a nascent membrane structure in selective autophagy. *J Cell Biol* **173**, 709-717

47. Zutphen, T., Veenhuis, M., and van der Klei, I. J. (2008) Pex14 is the sole component of the peroxisomal translocon that is required for pexophagy. *Autophagy* **4**, 63-66

48. Yokota, S. (1986) Quantitative immunocytochemical studies on differential induction of serine:pyruvate aminotransferase in mitochondria and peroxisomes of rat liver cells by administration of glucagon or di-(2-ethylhexyl)phthalate. *Histochemistry* **85**, 145-155

49. Latruffe, N., and Vamecq, J. (1997) Peroxisome proliferators and peroxisome proliferator activated receptors (PPARs) as regulators of lipid metabolism. *Biochimie* **79**, 81-94

50. Latruffe, N., Cherkaoui Malki, M., Nicolas-Frances, V., Clemencet, M. C., Jannin, B., and Berlot, J. P. (2000) Regulation of the peroxisomal beta-oxidation-dependent pathway by peroxisome proliferator-activated receptor alpha and kinases. *Biochem Pharmacol* **60**, 1027-1032

51. Kamendulis, L. M., Isenberg, J. S., Smith, J. H., Pugh, G., Jr., Lington, A. W., and Klaunig, J. E. (2002) Comparative effects of phthalate monoesters on gap junctional intercellular communication and peroxisome proliferation in rodent and primate hepatocytes. *J Toxicol Environ Health A* **65**, 569-588

52. Hasmall, S. C., James, N. H., Macdonald, N., Soames, A. R., and Roberts, R. A. (2000) Species differences in response to diethylhexylphthalate: suppression of apoptosis, induction of DNA synthesis and peroxisome proliferator activated receptor alpha-mediated gene expression. *Arch Toxicol* **74**, 85-91

53. Li, X., Baumgart, E., Dong, G. X., Morrell, J. C., Jimenez-Sanchez, G., Valle, D., Smith, K. D., and Gould, S. J. (2002) PEX11alpha is required for peroxisome proliferation in response to 4-phenylbutyrate but is dispensable for peroxisome proliferator-activated receptor alpha-mediated peroxisome proliferation. *Mol Cell Biol* **22**, 8226-8240

54. Sexton, J. Z., He, Q., Forsberg, L. J., and Brenman, J. E. (2010) High content screening for non-classical peroxisome proliferators. *Int J High Throughput Screen* **2010**, 127-140

55. Suzuki, K., and Ohsumi, Y. (2007) Molecular machinery of autophagosome formation in yeast, *Saccharomyces cerevisiae*. *FEBS Lett* **581**, 2156-2161

56. Santambrogio, L., and Cuervo, A. M. (2011) Chasing the elusive mammalian microautophagy. *Autophagy* **7**, 652-654

57. Sahu, R., Kaushik, S., Clement, C. C., Cannizzo, E. S., Scharf, B., Follenzi, A., Potolicchio, I., Nieves, E., Cuervo, A. M., and Santambrogio, L. (2011) Microautophagy of cytosolic proteins by late endosomes. *Dev Cell* **20**, 131-139

58. Noda, T., Kim, J., Huang, W. P., Baba, M., Tokunaga, C., Ohsumi, Y., and Klionsky, D. J. (2000) Apg9p/Cvt7p is an integral membrane protein required for transport vesicle formation in the Cvt and autophagy pathways. *J Cell Biol* **148**, 465-480

59. He, C., Song, H., Yorimitsu, T., Monastyrska, I., Yen, W. L., Legakis, J. E., and Klionsky, D. J. (2006) Recruitment of Atg9 to the preautophagosomal structure by Atg11 is essential for selective autophagy in budding yeast. *J Cell Biol* **175**, 925-935

60. Mari, M., Griffith, J., Rieter, E., Krishnappa, L., Klionsky, D. J., and Reggiori, F. (2010) An Atg9-containing compartment that functions in the early steps of autophagosome biogenesis. *J Cell Biol* **190**, 1005-1022

61. Yen, W. L., Legakis, J. E., Nair, U., and Klionsky, D. J. (2007) Atg27 is required for autophagy-dependent cycling of Atg9. *Mol Biol Cell* **18**, 581-593

62. Dunn, W. A., Jr., Cregg, J. M., Kiel, J. A., van der Klei, I. J., Oku, M., Sakai, Y., Sibirny, A. A., Stasyk, O. V., and Veenhuis, M. (2005) Pexophagy: the selective autophagy of peroxisomes. *Autophagy* **1**, 75-83

63. Farre, J. C., Krick, R., Subramani, S., and Thumm, M. (2009) Turnover of organelles by autophagy in yeast. *Curr Opin Cell Biol* **21**, 522-530

64. Oku, M., and Sakai, Y. (2010) Peroxisomes as dynamic organelles: autophagic degradation. *FEBS J* **277**, 3289-3294

65. Mukaiyama, H., Baba, M., Osumi, M., Aoyagi, S., Kato, N., Ohsumi, Y., and Sakai, Y. (2004) Modification of a ubiquitin-like protein Paz2 conducted micropexophagy through formation of a novel membrane structure. *Mol Biol Cell* **15**, 58-70

66. Ano, Y., Hattori, T., Kato, N., and Sakai, Y. (2005) Intracellular ATP correlates with mode of pexophagy in *Pichia pastoris*. *Biosci Biotechnol Biochem* **69**, 1527-1533

67. Hutchins, M. U., Veenhuis, M., and Klionsky, D. J. (1999) Peroxisome degradation in *Saccharomyces cerevisiae* is dependent on machinery of macroautophagy and the Cvt pathway. *J Cell Sci* **112 (Pt 22)**, 4079-4087

68. Nazarko, T. Y., Polupanov, A. S., Manjithaya, R. R., Subramani, S., and Sibirny, A. A. (2007) The requirement of sterol glucoside for pexophagy in yeast is dependent on the species and nature of peroxisome inducers. *Mol Biol Cell* **18**, 106-118

69. Tuttle, D. L., and Dunn, W. A., Jr. (1995) Divergent modes of autophagy in the methylotrophic yeast *Pichia pastoris*. *J Cell Sci* **108 (Pt 1)**, 25-35

70. Monastryska, I., Sjollema, K., van der Klei, I. J., Kiel, J. A., and Veenhuis, M. (2004) Microautophagy and macropexophagy may occur simultaneously in *Hansenula polymorpha*. *FEBS Lett* **568**, 135-138

71. van Zutphen, T., Veenhuis, M., and van der Klei, I. J. (2011) Damaged peroxisomes are subject to rapid autophagic degradation in the yeast *Hansenula polymorpha*. *Autophagy* **7**, 863-872

72. Mao, K., Wang, K., Zhao, M., Xu, T., and Klionsky, D. J. (2011) Two MAPK-signaling pathways are required for mitophagy in *Saccharomyces cerevisiae*. *J Cell Biol* **193**, 755-767

73. Aoki, Y., Kanki, T., Hirota, Y., Kurihara, Y., Saigusa, T., Uchiumi, T., and Kang, D. (2011) Phosphorylation of Serine 114 on Atg32 mediates mitophagy. *Mol Biol Cell* **22**, 3206-3217

74. Dagda, R. K., Zhu, J., Kulich, S. M., and Chu, C. T. (2008) Mitochondrially localized ERK2 regulates mitophagy and autophagic cell stress: implications for Parkinson's disease. *Autophagy* **4**, 770-782

75. Stasyk, O. V., van der Klei, I. J., Bellu, A. R., Shen, S., Kiel, J. A., Cregg, J. M., and Veenhuis, M. (1999) A *Pichia pastoris* VPS15 homologue is required in selective peroxisome autophagy. *Curr Genet* **36**, 262-269

76. Nazarko, V. Y., Thevelein, J. M., and Sibirny, A. A. (2008) G-protein-coupled receptor Gpr1 and G-protein Gpa2 of cAMP-dependent signaling pathway are involved in glucose-induced pexophagy in the yeast *Saccharomyces cerevisiae*. *Cell Biol Int* **32**, 502-504

77. Grunau, S., Lay, D., Mindthoff, S., Platta, H. W., Girzalsky, W., Just, W. W., and Erdmann, R. (2011) The phosphoinositide 3-kinase Vps34p is required for pexophagy in *Saccharomyces cerevisiae*. *Biochem J* **434**, 161-170

78. Chang, C. Y., and Huang, W. P. (2007) Atg19 mediates a dual interaction cargo sorting mechanism in selective autophagy. *Mol Biol Cell* **18**, 919-929

79. Suzuki, K., Kondo, C., Morimoto, M., and Ohsumi, Y. (2010) Selective transport of alpha-mannosidase by autophagic pathways: identification of a novel receptor, Atg34p. *J Biol Chem* **285**, 30019-30025

80. Watanabe, Y., Noda, N. N., Kumeta, H., Suzuki, K., Ohsumi, Y., and Inagaki, F. (2010) Selective transport of alpha-mannosidase by autophagic pathways: structural basis for cargo recognition by Atg19 and Atg34. *J Biol Chem* **285**, 30026-30033

81. Kanki, T., Wang, K., Cao, Y., Baba, M., and Klionsky, D. J. (2009) Atg32 is a mitochondrial protein that confers selectivity during mitophagy. *Dev Cell* **17**, 98-109

82. Okamoto, K., Kondo-Okamoto, N., and Ohsumi, Y. (2009) Mitochondria-anchored receptor Atg32 mediates degradation of mitochondria via selective autophagy. *Dev Cell* **17**, 87-97

83. Noda, N. N., Kumeta, H., Nakatogawa, H., Satoo, K., Adachi, W., Ishii, J., Fujioka, Y., Ohsumi, Y., and Inagaki, F. (2008) Structural basis of target recognition by Atg8/LC3 during selective autophagy. *Genes Cells* **13**, 1211-1218

84. Baxter, B. K., Abeliovich, H., Zhang, X., Stirling, A. G., Burlingame, A. L., and Goldfarb, D. S. (2005) Atg19p ubiquitination and the cytoplasm to vacuole trafficking pathway in yeast. *J Biol Chem* **280**, 39067-39076

85. Nazarko, T. Y., Farre, J. C., and Subramani, S. (2009) Peroxisome size provides insights into the function of autophagy-related proteins. *Mol Biol Cell* **20**, 3828-3839

86. Kawamata, T., Kamada, Y., Kabeya, Y., Sekito, T., and Ohsumi, Y. (2008) Organization of the pre-autophagosomal structure responsible for autophagosome formation. *Mol Biol Cell* **19**, 2039-2050

87. Suzuki, K., Kubota, Y., Sekito, T., and Ohsumi, Y. (2007) Hierarchy of Atg proteins in pre-autophagosomal structure organization. *Genes Cells* **12**, 209-218

88. Farre, J.-C., Mathewson, R., Manjithaya, R., and Subramani, S. (2009) UVRAG-like protein in *Pichia pastoris*. *Autophagy* **5**, 902

89. Stasyk, O. V., Nazarko, T. Y., Stasyk, O. G., Krasovska, O. S., Warnecke, D., Nicaud, J. M., Cregg, J. M., and Sibirny, A. A. (2003) Sterol glucosyltransferases have different functional roles in *Pichia pastoris* and Yarrowia lipolytica. *Cell Biol Int* **27**, 947-952

90. Reggiori, F., Tucker, K. A., Stromhaug, P. E., and Klionsky, D. J. (2004) The Atg1-Atg13 complex regulates Atg9 and Atg23 retrieval transport from the pre-autophagosomal structure. *Dev Cell* **6**, 79-90

91. Monastyrska, I., He, C., Geng, J., Hoppe, A. D., Li, Z., and Klionsky, D. J. (2008) Arp2 links autophagic machinery with the actin cytoskeleton. *Mol Biol Cell* **19**, 1962-1975

92. Reggiori, F., Monastyrska, I., Shintani, T., and Klionsky, D. J. (2005) The actin cytoskeleton is required for selective types of autophagy, but not nonspecific autophagy, in the yeast *Saccharomyces cerevisiae*. *Mol Biol Cell* **16**, 5843-5856

93. Sekito, T., Kawamata, T., Ichikawa, R., Suzuki, K., and Ohsumi, Y. (2009) Atg17 recruits Atg9 to organize the pre-autophagosomal structure. *Genes Cells* **14**, 525-538

94. Obara, K., and Ohsumi, Y. (2011) PtdIns 3-Kinase orchestrates autophagosome formation in yeast. *J Lipids* **2011**, 498768

95. Chang, T., Schroder, L. A., Thomson, J. M., Klocman, A. S., Tomasini, A. J., Stromhaug, P. E., and Dunn, W. A., Jr. (2005) PpATG9 encodes a novel membrane protein that traffics to vacuolar membranes, which sequester peroxisomes during pexophagy in *Pichia pastoris*. *Mol Biol Cell* **16**, 4941-4953

96. Schroder, L. A., Ortiz, M. V., and Dunn, W. A., Jr. (2008) The membrane dynamics of pexophagy are influenced by Sar1p in *Pichia pastoris*. *Molecular biology of the cell* **19**, 4888-4899

97. Chang, C. C., South, S., Warren, D., Jones, J., Moser, A. B., Moser, H. W., and Gould, S. J. (1999) Metabolic control of peroxisome abundance. *J Cell Sci* **112 (Pt 10)**, 1579-1590

98. Yokota, S., and Dariush Fahimi, H. (2009) Degradation of excess peroxisomes in mammalian liver cells by autophagy and other mechanisms. *Histochem Cell Biol* **131**, 455-458

99. Yokota, S., Haraguchi, C. M., and Oda, T. (2008) Induction of peroxisomal Lon protease in rat liver after di-(2-ethylhexyl)phthalate treatment. *Histochem Cell Biol* **129**, 73-83

100. Aksam, E. B., Koek, A., Kiel, J. A., Jourdan, S., Veenhuis, M., and van der Klei, I. J. (2007) A peroxisomal lon protease and peroxisome degradation by autophagy play key roles in vitality of *Hansenula polymorpha* cells. *Autophagy* **3**, 96-105

101. Yokota, S. (2003) Degradation of normal and proliferated peroxisomes in rat hepatocytes: regulation of peroxisomes quantity in cells. *Microsc Res Tech* **61**, 151-160

102. Hara-Kuge, S., and Fujiki, Y. (2008) The peroxin Pex14p is involved in LC3-dependent degradation of mammalian peroxisomes. *Exp Cell Res* **314**, 3531-3541

103. Pfeifer, U., Scheller, H., and Ormanns, W. (1976) [Diurnal rhythm of lysosomal organelle decomposition in liver, kidney and pancreas]. *Acta Histochem Suppl* **16**, 205-210

104. Iwata, J., Ezaki, J., Komatsu, M., Yokota, S., Ueno, T., Tanida, I., Chiba, T., Tanaka, K., and Kominami, E. (2006) Excess peroxisomes are degraded by autophagic machinery in mammals. *J Biol Chem* **281**, 4035-4041

105. Pankiv, S., Alemu, E. A., Brech, A., Bruun, J. A., Lamark, T., Overvatn, A., Bjorkoy, G., and Johansen, T. (2010) FYCO1 is a Rab7 effector that binds to LC3 and PI3P to mediate microtubule plus end-directed vesicle transport. *J Cell Biol* **188**, 253-269

106. Pankiv, S., and Johansen, T. (2011) FYCO1: Linking autophagosomes to microtubule plus end-directing molecular motors. *Autophagy* **6**

107. Huybrechts, S. J., Van Veldhoven, P. P., Brees, C., Mannaerts, G. P., Los, G. V., and Fransen, M. (2009) Peroxisome dynamics in cultured mammalian cells. *Traffic* **10**, 1722-1733

108. Kim, P. K., Hailey, D. W., Mullen, R. T., and Lippincott-Schwartz, J. (2008) Ubiquitin signals autophagic degradation of cytosolic proteins and peroxisomes. *Proc Natl Acad Sci U S A* **105**, 20567-20574

109. Cemma, M., Kim, P. K., and Brumell, J. H. (2011) The ubiquitin-binding adaptor proteins p62/SQSTM1 and NDP52 are recruited independently to bacteria-associated microdomains to target *Salmonella* to the autophagy pathway. *Autophagy* **7**, 341-345

110. Asakura, M., Ninomiya, S., Sugimoto, M., Oku, M., Yamashita, S., Okuno, T., Sakai, Y., and Takano, Y. (2009) Atg26-mediated pexophagy is required for host invasion by the plant pathogenic fungus *Colletotrichum orbiculare*. *Plant Cell* **21**, 1291-1304

111. Takano, Y., Asakura, M., and Sakai, Y. (2009) Atg26-mediated pexophagy and fungal phytopathogenicity. *Autophagy* **5**, 1041-1042

112. Herman, M., Perez-Morga, D., Schtickzelle, N., and Michels, P. A. (2008) Turnover of glycosomes during life-cycle differentiation of *Trypanosoma brucei. Autophagy* **4**, 294-308

113. Dodson, H. C., Morris, M. T., and Morris, J. C. (2011) Glycerol-3-phosphate alters *Trypanosoma brucei* hexokinase activity in response to environmental change. *J Biol Chem* **286**, 33150-33157

114. Roetzer, A., Gratz, N., Kovarik, P., and Schuller, C. (2010) Autophagy supports *Candida glabrata* survival during phagocytosis. *Cell Microbiol* **12**, 199-216

115. Kawaguchi, K., Yurimoto, H., Oku, M., and Sakai, Y. (2011) Yeast Methylotrophy and Autophagy in a Methanol-Oscillating Environment on Growing Arabidopsis thaliana Leaves. *PLoS One* **6**, e25257

116. Wild, P., Farhan, H., McEwan, D. G., Wagner, S., Rogov, V. V., Brady, N. R., Richter, B., Korac, J., Waidmann, O., Choudhary, C., Dotsch, V., Bumann, D., and Dikic, I. (2011) Phosphorylation of the autophagy receptor optineurin restricts *Salmonella* growth. *Science* **333**, 228-233

117. Nair, U., Jotwani, A., Geng, J., Gammoh, N., Richerson, D., Yen, W. L., Griffith, J., Nag, S., Wang, K., Moss, T., Baba, M., McNew, J. A., Jiang, X., Reggiori, F., Melia, T. J., and Klionsky, D. J. (2011) SNARE proteins are required for macroautophagy. *Cell* **146**, 290-302

118. Ogawa, M., Yoshikawa, Y., Mimuro, H., Hain, T., Chakraborty, T., and Sasakawa, C. (2011) Autophagy targeting of *Listeria* monocytogenes and the bacterial countermeasure. *Autophagy* **7**, 310-314

119. Mostowy, S., Sancho-Shimizu, V., Hamon, M. A., Simeone, R., Brosch, R., Johansen, T., and Cossart, P. (2011) p62 and NDP52 proteins target intracytosolic *Shigella* and *Listeria* to different autophagy pathways. *J Biol Chem* **286**, 26987-26995

120. Dixit, E., Boulant, S., Zhang, Y., Lee, A. S., Odendall, C., Shum, B., Hacohen, N., Chen, Z. J., Whelan, S. P., Fransen, M., Nibert, M. L., Superti-Furga, G., and Kagan, J. C. (2010) Peroxisomes are signaling platforms for antiviral innate immunity. *Cell* **141**, 668-681

121. Lazarow, P. B. (2011) Viruses exploiting peroxisomes. *Curr Opin Microbiol* **14**, 458-469

122. Komduur, J. A., Veenhuis, M., and Kiel, J. A. (2003) The Hansenula polymorpha PDD7 gene is essential for macropexophagy and microautophagy. *FEMS Yeast Res* **3**, 27-34

123. Schroder, L. A., and Dunn, W. A. (2006) PpAtg9 trafficking during micropexophagy in *Pichia pastoris*. *Autophagy* **2**, 52-54

124. Stromhaug, P. E., Bevan, A., and Dunn, W. A. (2001) GSA11 encodes a unique 208-kDa protein required for pexophagy and autophagy in *Pichia pastoris*. *J Biol Chem* **276**, 42422-42435

125. Ichimura, Y., Kirisako, T., Takao, T., Satomi, Y., Shimonishi, Y., Ishihara, N., Mizushima, N., Tanida, I., Kominami, E., Ohsumi, M., Noda, T., and Ohsumi, Y. (2000) A ubiquitin-like system mediates protein lipidation. *Nature* **408**, 488-492

126. Tamura, N., Oku, M., and Sakai, Y. (2010) Atg8 regulates vacuolar membrane dynamics in a lipidation-independent manner in *Pichia pastoris*. *J Cell Sci* **123**, 4107-4116

127. Yuan, W., Tuttle, D. L., Shi, Y. J., Ralph, G. S., and Dunn, W. A. (1997) Glucose-induced microautophagy in *Pichia pastoris* requires the alpha-subunit of phosphofructokinase. *J Cell Sci* **110 (Pt 16)**, 1935-1945

128. Kim, J., Kamada, Y., Stromhaug, P. E., Guan, J., Hefner-Gravink, A., Baba, M., Scott, S. V., Ohsumi, Y., Dunn, W. A., and Klionsky, D. J. (2001) Cvt9/Gsa9 functions in sequestering selective cytosolic cargo destined for the vacuole. *J Cell Biol* **153**, 381-396

129. Guan, J., Stromhaug, P. E., George, M. D., Habibzadegah-Tari, P., Bevan, A., Dunn, W. A., and Klionsky, D. J. (2001) Cvt18/Gsa12 is required for cytoplasm-to-vacuole transport, pexophagy, and autophagy in *Saccharomyces cerevisiae* and *Pichia pastoris*. *Mol Biol Cell* **12**, 3821-3838

130. Leao-Helder, A. N., Krikken, A. M., Gellissen, G., van der Klei, I. J., Veenhuis, M., and Kiel, J. A. (2004) Atg21p is essential for macropexophagy and microautophagy in the yeast *Hansenula polymorpha*. *FEBS Lett* **577**, 491-495

131. Stasyk, O. V., Stasyk, O. G., Mathewson, R. D., Farré, J. C., Nazarko, V. Y., Krasovska, O. S., Subramani, S., Cregg, J. M., and Sibirny, A. A. (2006) Atg28, a novel coiled-coil protein involved in autophagic degradation of peroxisomes in the methylotrophic yeast *Pichia pastoris*. *Autophagy* **2**, 30-38

132. Bellu, A. R., Salomons, F. A., Kiel, J. A., Veenhuis, M., and Van Der Klei, I. J. (2002) Removal of Pex3p is an important initial stage in selective peroxisome degradation in *Hansenula polymorpha*. *J Biol Chem* **277**, 42875-42880

133. Bellu, A. R., and Kiel, J. A. (2003) Selective degradation of peroxisomes in yeasts. *Microsc Res Tech* **61**, 161-170

134. Leao-Helder, A. N., Krikken, A. M., Lunenborg, M. G., Kiel, J. A., Veenhuis, M., and van der Klei, I. J. (2004) *Hansenula polymorpha* Tup1p is important for peroxisome degradation. *FEMS Yeast Res* **4**, 789-794

135. Oku, M., Nishimura, T., Hattori, T., Ano, Y., Yamashita, S., and Sakai, Y. (2006) Role of Vac8 in formation of the vacuolar sequestering membrane during micropexophagy. *Autophagy* **2**, 272-279

136. Fry, M. R., Thomson, J. M., Tomasini, A. J., and Dunn, W. A., Jr. (2006) Early and late molecular events of glucose-induced pexophagy in *Pichia pastoris* require Vac8. *Autophagy* **2**, 280-288

137. Polupanov, A. S., Nazarko, V. Y., and Sibirny, A. A. (2011) CCZ1, MON1 and YPT7 genes are involved in pexophagy, the Cvt pathway and non-specific macroautophagy in the methylotrophic yeast *Pichia pastoris*. *Cell Biol Int* **35**, 311-319

138. Sakai, Y., Oku, M., van der Klei, I. J., and Kiel, J. A. (2006) Pexophagy: autophagic degradation of peroxisomes. *Biochim Biophys Acta* **1763**, 1767-1775

Chapter 2: Defects in GABA metabolism affect selective autophagy pathways and are alleviated by mTOR inhibition

Abstract

In addition to key roles in embryonic neurogenesis and myelinogenesis, γ-aminobutyric acid (GABA) serves as the primary inhibitory mammalian neurotransmitter. In yeast, we have identified a new role for GABA that augments activity of the pivotal kinase, Tor1. GABA inhibits the selective autophagy pathways, mitophagy and pexophagy, through Sch9, the homolog of the mammalian kinase, S6K1, leading to oxidative stress, all of which can be mitigated by the Tor1 inhibitor, rapamycin. To confirm these processes in mammals, we examined the succinic semialdehyde dehydrogenase (SSADH)-deficient mouse model that accumulates supraphysiological GABA in the central nervous system and other tissues. Mutant mice displayed increased mitochondrial numbers in the brain and liver, expected with a defect in mitophagy, and morphologically abnormal mitochondria. Administration of rapamycin to these mice reduced mTOR activity, reduced the elevated mitochondrial numbers, and normalized aberrant antioxidant levels. These results confirm a novel role for GABA in cell signaling and highlight potential pathomechanisms and treatments in various human pathologies, including SSADH deficiency, as well as other diseases characterized by elevated levels of GABA.

Introduction

The non-protein amino acid γ-aminobutyric acid (GABA) is the chief inhibitory neurotransmitter, and is present in concentrations of between 1-10mM in the brain (1). It is also present in tissues outside the central nervous system (CNS) (2). GABA has been detected in the peripheral nervous and endocrine systems and is widely found in non-neuronal tissues, where it displays diverse physiological roles (3). Disorders due to defects in GABA metabolism cause severe neurological and neuromuscular symptoms. The autosomal-recessive metabolic disorder, succinic semialdehyde dehydrogenase (SSADH) deficiency, is the most common of the inherited

disorders of GABA metabolism (4). The clinical features of SSADH deficiency encompass developmental delay, psychomotor retardation, hypotonia, seizures, ataxia and other behavioral problems (5). Other diseases caused by defects in GABA metabolism include GABA transaminase deficiency, where patients have elevated levels of GABA in serum and cerebrospinal fluid causing abnormal development and seizures (4,6). A chronic excess of GABA may also cause sleep abnormalities (7,8,9). However, the exact role of GABA in the pathophysiology of these disorders remains unclear.

The GABA shunt is a closed loop metabolic pathway that bypasses two steps of the tricarboxylic acid (TCA) cycle, converting α-ketoglutarate to succinate, which feeds back into the TCA cycle (Supporting Information Fig. 2-S1). The bypass step occurs via the transamination of α-ketoglutarate to glutamate, which undergoes decarboxylation by glutamate decarboxylase to GABA. Next, the mitochondrial GABA transaminase converts GABA to the metabolic intermediate succinic semialdehyde (SSA), which is either oxidized to succinate to enter the TCA cycle, or reduced to γ-hydroxybutyric acid (GHB) (10). During normal physiological conditions, the GABA shunt allows constant replenishment of both the GABA and glutamate neurotransmitters.

It has been over thirty years since the first report of SSADH deficiency in a patient with neurological abnormalities (11). Later studies proved that the reduction or absence of SSADH activity was due to mutations in the *ALDH5A1* gene which encodes the SSADH enzyme, leading to increased levels of GABA and its metabolite, GHB, in patients (12). Due to the variety and severity in symptoms of the disease and difficulties in diagnosing patients, SSADH deficiency may be significantly under-diagnosed in clinical settings (13).

Currently, although the metabolic pathway of SSADH deficiency is known, how the accumulation of GABA contributes to the clinical manifestation of the disease is not known, and there is no established or universally effective treatment for the disease. Management of SSADH deficiency tends to treat the seizures, behavioral problems and other symptoms associated with the disorder (14). However, these symptoms may be secondary to the main cause of the

disease. The murine model of SSADH deficiency represents a relevant phenocopy of the human disease, with seizures and evidence of oxidative stress in tissues, along with increased levels of the peroxisomal enzyme catalase in the brain and elevated superoxide dismutase in the brain and liver (15).

In the current report, we evaluated the hypothesis that GABA impacts autophagy-related pathways. Towards this goal, we use yeast as a novel model system to elucidate the underlying mechanism by which GABA regulates autophagy-related pathways and translate the salient findings to a murine model of the disease.

Autophagy is a major catabolic pathway involved in the targeting and degradation of intracellular proteins and organelles to the lysosome/vacuole in a tightly regulated process (16) that is highly conserved from yeasts to humans (17). During this process, which allows cells to adapt to various environmental changes, a double-membrane vesicle known as an autophagosome sequesters organelles or cytosolic proteins and then fuses with the lysosome/vacuole, releasing its contents into the lumen, where they are degraded and recycled.

Autophagy can be either a non-selective process, gathering a bulk portion of the cytosol for degradation, or it operates specifically to degrade particular proteins or organelles, such as peroxisomes (pexophagy) (18), mitochondria (mitophagy) (19) or ribosomes (ribophagy) (20). Much of the same core machinery used for general autophagy also overlaps in the selective autophagy pathways. Defects in autophagy-related pathways have already been implicated in a wide variety of diseases, ranging from cancer and neurodegenerative disorders to aging (21), reflecting the theme that autophagy and autophagy-related pathways play essential roles in cellular homeostasis and quality control.

In this study, we find an unexpected role of GABA as a regulator of mitophagy and pexophagy. When GABA levels are increased, yeast cells are unable to specifically degrade mitochondria and peroxisomes via these selective autophagy pathways during starvation conditions, leading to oxidative stress due to the accumulation of these organelles. These effects mimic the oxidative stress observed in humans and the murine model of SSADH deficiency. The

GABA-induced defects can be overridden by the Tor1 inhibitor, rapamycin, via signaling pathways we have identified in this study. Furthermore, we show that rapamycin can reduce elevated mitochondrial numbers and normalize aberrant antioxidant levels found in the murine model of the disease. These results demonstrate a proof-of-concept for using autophagy-inducing or mTOR inhibiting drugs as treatment for disorders characterized by elevated levels of GABA.

Results

Increased levels of GABA inhibit pexophagy and mitophagy, but not other autophagy-related pathways

Patients with SSADH deficiency have up to a threefold increase in GABA levels (12). Previous research in yeast mutants of the GABA shunt pathway has demonstrated that deletion of the yeast SSADH, *uga2*, also increases intracellular GABA levels threefold (22), which is comparable with the human form of the disease. Mutants deleted for other genes in the GABA shunt, including *uga1* and *gad1*, have similar intracellular GABA levels as wild-type cells (22). We probed whether increased levels of GABA affect autophagy-related pathways in yeast. In *S. cerevisiae*, autophagy-related pathways can be monitored by transferring cells to starvation medium that lacks nitrogen and amino acids (SD-N) to induce autophagy, for which organelle-specific markers can be followed to monitor specific selective autophagy pathways. We found that the *UGA2*, but not the *UGA1* mutant of the GABA shunt pathway, partially inhibited pexophagy compared to the wild-type, as shown by the delay in degradation of the peroxisomal matrix protein, Pot1, at the 12 h time-point (Supporting Information Fig. 2-S2).

The addition of GABA to the starvation medium also inhibited autophagy-related pathways, because 10 mM GABA showed a severe defect in both pexophagy (Fig. 2-1A) and mitophagy (Fig. 2-1B and C). Both pexophagy and mitophagy assays assess degradation of superfluous organelles upon nutrient limitation. The defect in pexophagy was shown by the delay in degradation of the peroxisomal matrix protein, Pot1, fused to GFP (Pot1-GFP, Fig. 2-1A). In

this standard assay, wild-type cells are first grown in oleate medium for 15 h to increase peroxisome number and then transferred to starvation conditions, wherein pexophagy is activated and detected by the appearance of free GFP. The defect in mitophagy was shown by the delay in degradation of the mitochondrial outer membrane

protein, Om45, fused to GFP (Om45-GFP, Fig. 2-1B). In this assay, wild-type cells are grown in YPL medium, which contains lactic acid as a carbon source for 12-14 h to increase mitochondrial number and then transferred to starvation conditions, where mitophagy is detected by the appearance of free GFP. An alternative mitophagy assay using fluorescence microscopy showed a large number of mitochondria labeled by OM45-GFP outside of the vacuole after 12 h in YPL media. After transferring cells to starvation medium for 24 h, mitochondria were delivered to the vacuole as seen by GFP clearly located inside the vacuole lumen, However, when GABA was added to the starvation medium, OM45-GFP-labeled mitochondria remained outside of the vacuole (Fig. 2-1C).

Interestingly, the addition of 10 mM GABA did not block other selective-autophagy pathways such as the biosynthetic Cvt pathway, which was monitored by the maturation of the vacuolar aminopeptidase, Ape1, in growth conditions. This maturation of Ape1 was unaffected by elevated levels of GABA in the medium (Fig. 2-1D). Similarly, ribophagy, which was monitored by the degradation of the ribosomal fusion protein, Rpl25-GFP, in starvation conditions, remained unaffected by the addition of GABA. Free GFP accumulated at the same level as that seen in untreated cells (Fig. 2-1E). The non-selective general autophagy pathway also remained unaffected by the addition of 10 mM GABA, as judged by the normal degradation of the GFP-Atg8 fusion protein (Fig. 2-1F). Fluorescence microscopy confirmed that bulk autophagy was unaffected, because when wild-type cells were placed in starvation conditions for 6 h, GFP-Atg8 localized to the vacuole even when either 1 mM or 10 mM GABA was added to the nutrient-limited medium. As expected, the autophagy-deficient *atg1Δ* strain was blocked in GFP-Atg8 localization to the vacuole (Supporting Information Fig. 2-S3).

As GABA functions as a nitrogen source in *S. cerevisiae*, we asked if GABA blocked pexophagy and mitophagy in strains that cannot use GABA as a nitrogen source. Previous studies in *S. cerevisiae* have shown that strains deficient in either *UGA1* (utilize GABA) or *UGA2* cannot grow in medium with GABA as the source of nitrogen (23). Both pexophagy and mitophagy were blocked when 10 mM GABA was added to test *uga1Δ* mutants (Supporting Information Fig. 2-S4A and B). We also tested SSA, a GABA metabolite formed downstream of GABA by the GABA transaminase (Uga1).

Neither pexophagy nor mitophagy were inhibited by elevated levels of SSA (Supporting Information Fig. 2-S5A and B). These results show that the inhibition of pexophagy and mitophagy occurs even when cells cannot utilize GABA as a source of nitrogen, implicating a signaling process involving GABA itself, but not its metabolite(s).

The GABA-induced block in pexophagy and mitophagy is overridden by rapamycin

Rapamycin is a pleiotropic bacteria-derived drug molecule that is commonly used to trigger autophagy pathways via its ability to inhibit the pivotal kinase Tor1 (target of rapamycin) (24). We tested if rapamycin could override the GABA-induced block in pexophagy and mitophagy by performing the above-mentioned assays in the presence of rapamycin and GABA.

Rapamycin did override the block in pexophagy caused by the addition of GABA (Fig. 2-2A). An alternative pexophagy assay using fluorescence microscopy showed a large number of peroxisomes labeled by Pot1-GFP outside of the vacuole, and low levels of free GFP in the vacuole at 6 h after GABA addition to the starvation medium. However, when both rapamycin and GABA were added to the starvation medium, the number of Pot1-GFP labeled peroxisomes decreased dramatically and GFP was clearly located in the vacuole (Fig. 2-2B). Rapamycin also overrode the block in mitophagy caused by the addition of GABA, as measured by OM45-GFP degradation to yield free GFP (Fig. 2-2C).

Increasing GABA level endogenously also inhibits pexophagy and mitophagy and these defects are overridden by rapamycin

Cellular GABA levels were increased genetically using a high copy-number plasmid to over-express the glutamate decarboxylase gene, *GAD1*, which catalyses the conversion of glutamate to GABA, (23). Experiments were performed in the *uga2Δ* background strain to keep GABA levels elevated in the cells by slowing down GABA catabolism. Mitophagy was significantly inhibited when *GAD1* was over-expressed compared to the wild-type strain (Fig. 2-3A). Pexophagy was also significantly delayed compared to the wild-type strain (Fig. 2-3B). However, autophagy was unaffected (Fig. 2-3C).

Much like the exogenous addition of GABA, the defects in mitophagy and pexophagy found in the *GAD1* over-expression strains could be rescued with the addition of rapamycin (Fig. 2-3A and B).

Increased GABA levels activate Tor1 while inhibiting pexophagy and mitophagy through Sch9

We wanted to see if the increase in GABA levels affected Tor1 activity during nutrient limitation, because Tor1 is the mechanistic target of rapamycin (24). In starvation medium, autophagy and autophagy-related pathways are induced by the inactivation of Tor1 (25). Tor1 activity can be measured by the phosphorylation of the S6 ribosomal protein, as inhibition of autophagy and phosphorylation of the S6 ribosomal protein are controlled by the same signal transduction pathway (26).

Despite starvation conditions that normally inhibit Tor1, the increase in GABA partially activated Tor1 during pexophagy and mitophagy. As expected, when cells were transferred to starvation medium for 6 h to induce pexophagy, the levels of S6 phosphorylation were markedly decreased. However, in the same conditions with the addition of GABA, there was a small increase in S6 phosphorylation, suggesting that GABA activated Tor1 (Fig. 2-4A). This was also observed during mitophagy conditions, where S6 phosphorylation was absent in starvation conditions but increased upon addition of GABA after 6 h (Fig. 2-4B).

The addition of rapamycin to inhibit Tor1 function leads to the induction of autophagy even in nutrient-rich conditions (27). We found that rapamycin overrides the increase in Tor1 activity caused by the addition of GABA to the starvation medium, as seen by the complete reduction in S6 phosphorylation during both pexophagy and mitophagy conditions (Fig. 2-4A and B).

To confirm that GABA acts through Tor1, we tested the *tor* mutant strain *tor1Δ tor2*^{ts} and found that the addition of GABA lost its inhibitory effect on selective autophagy in this strain, whereas GABA inhibited the WT strain (Supporting Information Fig. 2-S6).

The Ser/Thr kinase, Tor1, has a number of potential downstream targets. The AGC family protein kinase, Sch9, which is analogous to the mammalian TORC1 substrate S6K1, is directly phosphorylated by TORC1 at multiple sites to activate the protein kinase (28).

Therefore, we wanted to see if the inhibition of pexophagy and mitophagy caused by elevated GABA functioned through Sch9. We tested the *sch9Δ* strain and found that the addition of GABA lost its inhibitory effect on both pexophagy (Fig. 2-4C) and mitophagy (Fig. 2-4D) even though both pathways were blocked when GABA was added to WT strains. The inhibition of selective autophagy by GABA in the *atg13Δ* strain (Supporting Information Fig. 2-S7) suggests that GABA does not operate through the Atg1/Atg13 complex. Therefore, mechanistically our model suggests that elevated GABA activates Tor1 in starvation conditions and inhibits pexophagy and mitophagy through Sch9 (Fig. 2-4E).

Varying levels of Tor activity may inhibit specific autophagy-related pathways

Previous research has shown the role amino acids play in mTOR activation in mammalian cells (29), as well as the involvement of amino acids in the regulation of the mTOR pathway, whereby addition of amino acids inhibited autophagy and increased S6 phosphorylation in rat hepatocytes (26). The over-activation of the mTOR signaling pathway has been implicated in many types of cancer (30), tissue hypertrophy (31) and other diseases (32). However, the molecular mechanism of amino acid signaling in mTOR activation is only just emerging (33).

To test the hypothesis that there may be a threshold of Tor1 activity required to inhibit non-selective autophagy compared to mitophagy and pexophagy, we predicted that autophagy would be inhibited by increasing the concentration of GABA, which would increase Tor1 activity. We found that 10 mM GABA partially activated Tor1 in autophagy conditions (Fig. 2-5A), to similar levels as those observed in pexophagy (Fig. 2-4A) and mitophagy (Fig. 2-4B) conditions. 50 mM GABA showed a much larger increase in Tor1 activity compared to 10 mM GABA (Fig. 2-5A). However, 10 mM GABA did not inhibit autophagy, as shown by the normal degradation of the GFP-Atg8 fusion protein, comparable to the wild-type (Fig. 2-5B), whereas 50 mM GABA did inhibit autophagy, as shown by the delay in GFP-Atg8 degradation, compared to the wild-type. Thus a partial activation of Tor1 activity by GABA is enough to inhibit mitophagy and pexophagy, but higher levels of Tor1 activity may be required to inhibit autophagy.

The GABA-induced block of pexophagy and mitophagy increases reactive oxygen species levels that can be reduced by rapamycin

Mitochondria are the main source of cellular reactive oxygen species (ROS) (34) and aberrant and dysfunctional mitochondria increase ROS levels in the cell (35) leading to oxidative stress (36). Defective peroxisomes are also known to increase ROS levels (37), and impaired pexophagy promotes oxidative stress in mammalian cells (38). We hypothesized that the GABA-induced block in pexophagy and mitophagy may cause an increase in intracellular ROS levels.

Relative intracellular ROS levels of wild-type cells in four different treatment conditions were tested under both pexophagy and mitophagy conditions; wild-type cells, wild-type with GABA, wild-type with GABA plus the antioxidant glutathione and wild-type with GABA plus rapamycin. We chose glutathione as an antioxidant as it has previously been shown to be taken up by yeast when supplemented to the medium (39,40). After 24 h in starvation medium, cells were assayed for intracellular ROS levels using the redox sensitive fluorescent probe Dihydrorhodamine-123 (DHR-123). Propidium iodide was used to distinguish living cells from dead cells (36).

In the presence of GABA, we observed significant increases (**p<0.01) of intracellular ROS, compared to the untreated wild-type strain in both pexophagy and mitophagy conditions (Fig. 2-6A and B). The addition of the antioxidant glutathione along with GABA could significantly reduce ROS levels (*p<0.05). However, the addition of rapamycin along with GABA reduced ROS levels much further (**p<0.01) compared to glutathione (Fig. 2-6A and B). The increase in intracellular ROS caused by elevated levels of GABA was also confirmed employing an alternative assay using the redox sensitive fluorescent probe 2′,5′-dichlorofluorescein diacetate (DCFH-DA) (**p<0.01). The enhanced ROS levels could be significantly decreased by rapamycin (**p<0.01) (Supporting Information Fig. 2-S8A). In addition, the *atg32Δ* strain, which is defective in mitophagy (41), was also tested under mitophagy conditions and was also found to have increased ROS levels compared to the WT strain (**p<0.01), Again, rapamycin was able to significantly reduce elevated ROS levels in the *atg32Δ* strain (**p<0.01) (Supporting Information Fig. 2-S8B). These results show that the block in pexophagy and mitophagy caused by elevated levels of GABA increase cellular oxidative stress, probably due to the presence of longer-lived or damaged peroxisomes and mitochondria.

It is also noteworthy that we observed significantly increased cell death induced by elevated GABA after 24 h, when comparing the number of live cells to dead cells by propidium iodide uptake in both pexophagy and mitophagy conditions compared to the WT strain (**p<0.01) (Fig. 2-6C and D) using a gate for high signals in the propidium iodide specific channel (Supporting Information Fig. 2-S9A). This effect was significantly reversed by parallel treatment with rapamycin (**p<0.01) (Fig. 2-6C and D). The percentage of dead cells positively correlate with increased ROS levels in live cells, suggesting a mechanistic link between GABA-induced redox stress and cell death (Supporting Information Fig. 2-S9B and C).

To evaluate whether it was the block in selective autophagy pathways that caused the accumulation of ROS, or whether selective autophagy pathways are blocked as a consequence of increased ROS levels, we aimed to assess whether the inhibition of selective autophagy pathways caused by GABA could be suppressed by reducing ROS levels using glutathione.

However, glutathione did not override the block in pexophagy or mitophagy caused by GABA, the way rapamycin did (Fig. 2-6E and F), suggesting that it is the block in selective autophagy pathways that contributes to the increased levels of ROS.

Elevated GABA inhibits mitophagy in mammalian cells

To determine if elevated GABA could also inhibit basal mitophagy in mammalian cells, we performed an image based *in vitro* mitophagy assay using a tandem fluorochrome protein (mito-RFP-GFP) in human HeLa cells over-expressing human Parkin (42, 43), whereby fluorescently tagged mitochondria undergo a color change upon delivery to the lysosome after 3 days in DMEM medium (Fig. 2-7A and B). HeLa cells were either untreated, or treated with 1mM GABA, with or without rapamycin. We found that 1mM GABA significantly inhibited mitophagy (**p<0.01) as quantified by the percentage of cells displaying mitophagy compared to untreated cells, and that rapamycin was able to significantly mitigate the inhibition of mitophagy caused by elevated levels of GABA (**p<0.01) (Fig. 2-7C).

SSADH-deficient mice have increased numbers of mitochondria and aberrant antioxidant levels that can be normalized by rapamycin

In order to elucidate the evolutionary conservation of the mechanism found in yeast and its potential role in a clinical setting, we assessed the role of rapamycin treatment in a murine model of SSADH deficiency that represents a viable model for the human disease, characterized by elevated levels of GABA in physiological fluids and tissues up to threefold higher than wild-type mice (44).

Using transmission electron microscopy (TEM) images of SSADH-deficient mice homozygous for a targeted mutation of the aldehyde dehydrogenase family 5, subfamily A1 gene (*Aldh5a1*$^{-/-}$) and wild-type liver cells, we noticed morphological differences between mitochondria in *Aldh5a1*$^{-/-}$ mice compared to wild-type, whereby mitochondria appeared significantly larger, as judged by mitochondria area (**p<0.01) (Fig. 2-8A and B). In humans, mitochondrial proliferation

often expresses as mitochondrial DNA depletion. We found that mitochondrial DNA was not depleted in *Aldh5a1*$^{-/-}$ mice compared to wild-type mice (Supporting Information Fig. 2-S10). Our results from the yeast model indicated that SSADH-deficient mice should possess increased numbers of mitochondria. Indeed, we found significantly increased numbers of mitochondria in *Aldh5a1*$^{-/-}$ mice compared to wild-type mice in both the liver (Fig. 2-8C) and brain (Fig. 2-8D) (**$p<0.01$). Moreover, rapamycin treatment lowered mitochondria numbers to levels not significantly different from wild-type mice (Fig. 2-8C and D).

Previous studies using the SSADH-deficient mouse model have shown increased levels of the antioxidant superoxide dismutase (SOD) in the liver compared to wild-type mice (15). Our data also found the same trend, whereby SOD enzyme activity was elevated in the liver of *Aldh5a1*$^{-/-}$ mice by 25% compared to wild-type mice. We found that rapamycin treatment could significantly reduce elevated SOD levels in the *Aldh5a1*$^{-/-}$ mice (*$p<0.05$) compared to diseased mice treated with the vehicle alone (Fig. 2-8E). Next, to see if the elevated SOD levels were specifically associated with mitochondrial SOD (SOD2), the level of this protein was quantified from microsections of liver biopsies using immunofluorescence microscopy and automated image analysis. SOD2 levels in the *Aldh5a1*$^{-/-}$ mice also increased by 25% compared to wild-type mice and rapamycin treatment significantly reduced SOD2 levels in the *Aldh5a1*$^{-/-}$ mice (**$p<0.01$) compared to diseased mice treated with the vehicle alone (Fig. 2-8F). Raw data from at least 10 individual images per treatment were normalized to nuclear staining (DAPI, blue) to measure SOD2 staining (red) for differences between wild-type, *Aldh5a1*$^{-/-}$ mice and *Aldh5a1*$^{-/-}$ mice with rapamycin treatment (Fig. 2-8G).

We predicted that the mechanism of Tor1 activation by elevated GABA levels in yeast should also be found in SSADH-deficient mice, as measured by S6 phosphorylation. We found the same trend in mice liver and brain samples as we did in yeast. On average when normalized, SSADH-deficient mice showed a 58% increase in S6 phosphorylation levels in the liver (Fig. 2-9A and B), and a 20% increase in S6 phosphorylation levels in the brain compared to wild-type mice (Fig. 2-9C and D), indicating increased levels of mTOR activity. Rapamycin treatment

significantly reduced the elevated S6 phosphorylation levels in SSADH-deficient mice (Fig. 2-9A-D). This demonstrates that SSADH deficiency in mammals may follow the same mechanistic pathway to inhibit selective autophagy pathways as shown in yeast (Fig. 2-4E), and further supports the model that the increased levels of mTOR activity, as well as the accumulation of mitochondria associated with elevated GABA levels, can be reversed by mTOR inhibition.

Discussion

Many disorders with varying symptoms present with increased levels of GABA in the brain as well as outside the CNS. These include sleep abnormalities (7) to more severe diseases such as SSADH deficiency (12) and GABA transaminase deficiency (6). Our results show for the first time how elevated levels of GABA inhibit the selective degradation of both peroxisomes and mitochondria, but not general autophagy cargo (Fig. 2-1).

These findings are in line with previous work conducted on the murine model of the SSADH deficiency disease which found significantly higher levels of the peroxisomal enzyme catalase in the thalamus, as well as increased levels of SOD (a mitochondrial enzyme) in the liver and cerebellum (15), suggesting that there could be similar defects in peroxisomal and mitochondrial turnover in human cells, but this hypothesis remains to be tested directly.

Interestingly, we also found that the block in both of these selective autophagy pathways caused by increased levels of GABA can be overridden with the autophagy-inducing drug and Tor1 inhibitor, rapamycin (Fig. 2-2).

Previous studies in a plant model of SSADH deficiency showed the accumulation of ROS (45), but the physiological reason was unclear. Our results demonstrate that the increase in GABA levels increases Tor1 activity, leading to the inhibition of both pexophagy and mitophagy, probably causing the retention of longer-lived and damaged peroxisomes and mitochondria, which could be the underlying cause for a concomitant increase in ROS levels (Fig. 2-6A and B). Mitochondria are well known to be the primary source of cellular ROS, which could potentially cause severe oxidative stress to the cell (34).

Consistent with our hypothesis that the block in selective autophagy is the cellular cause of ROS increase, the GABA-induced ROS elevation is also reversed with rapamycin or partially with an antioxidant (Fig. 2-6A and B). We also found that the increase in oxidative stress caused by elevated GABA significantly increased cell death in both pexophagy and mitophagy conditions, and that rapamycin, by overriding the inhibition of selective autophagy caused by GABA, significantly reduced cell death (Fig. 2-6C and D). While the antioxidant glutathione reduced ROS levels significantly, it could not override the block in pexophagy or mitophagy caused by GABA, whereas rapamycin could (Fig. 2-6E and F). As rapamycin reduced ROS levels more than glutathione, and is known to induce pexophagy and mitophagy, we suggest that rapamycin overcomes the underlying cause of the disorder by reducing elevated mTOR activity to induce autophagy, thus clearing away old and damaged peroxisomes and mitochondria causing the high levels of ROS.

We find that the mechanism causing the inhibition of pexophagy and mitophagy is that increased GABA levels cause the partial activation of Tor1 during starvation conditions, which in turn inhibits the selective autophagy pathways through Sch9, the yeast homolog of the mammalian S6K1 kinase (28). Our data show that both pexophagy and mitophagy are not blocked by increasing GABA levels in the *sch9*Δ strain (Fig. 2-4).

During starvation conditions when Tor1 is inactive, non-selective autophagy is initiated. We believe that there may be a certain threshold value that needs to be surpassed when describing the relationship between Tor1 activation and the inhibition of autophagy and autophagy-related pathways. A partial increase in Tor1 activity caused by the increase in GABA levels may be enough to block specific selective autophagy pathways such as pexophagy and mitophagy, but a higher level of Tor1 activity may need to be reached before autophagy and other selective autophagy pathways are inhibited (Fig. 2-5).

Translating our results from yeast to mammalian cells, we found that elevated levels of GABA could also inhibit mitophagy in HeLa cells, and that this inhibition could be mitigated by rapamycin (Fig. 2-7). In the murine model of SSADH deficiency, we found as predicted,

increased numbers of mitochondria in SSADH-deficient mice liver (Fig. 2-8C) and brain (Fig. 2-8D) compared to wild-type mice, probably due to a defect in mitophagy, and that the elevated numbers of mitochondria could be normalized to levels not significantly different from wild-type upon rapamycin treatment (Fig. 2-8C and D). We also found that mitochondria were on average larger in the *Aldh5a1*$^{-/-}$ mice liver compared to wild-type (Fig. 2-8A and B). We show that the elevated levels of SOD previously reported in *Aldh5a1*$^{-/-}$ mice (15), and mitochondrial SOD2, can be significantly reduced with rapamycin treatment (Fig. 2-8E and F), which may have important treatment relevance for the human disorder.

SSADH-deficient mice also have increased levels of S6 phosphorylation in the liver (Fig. 2-9A and B) and brain (Fig. 2-9C and D) compared to wild-type mice, indicating increased levels of mTOR activity. Rapamycin treatment reduced elevated S6 phosphorylation levels in SSADH-deficient mice significantly (Fig. 2-9A-D). This trend follows the same mechanistic pathway as we found in yeast (Fig. 2-4A and B).

We demonstrate for the first time the applicability of yeast to study the molecular mechanisms linked to human SSADH deficiency, as well as other disorders caused by defects in GABA metabolism. Our data indicate a pivotal role of the induction of selective autophagy pathways for restoring cellular organelle homeostasis in this disease setting. Interestingly, autophagy has emerged as a promising target mechanism for the treatment of a variety of neurological disorders, including Huntington's disease (46), Alzheimer's and Parkinson's disease (21,47). The data presented here further emphasize the vital role of tightly regulated autophagy for cellular homeostasis and provide a proof of principle for using autophagy-inducing drugs or mTOR inhibitors for the treatment of SSADH deficiency and other disorders characterized by elevated levels of GABA.

Further work would be required to identify if mammalian cells follow the same mechanistic pathway as we have described in yeast. However, as the autophagy pathway is conserved from yeast to mammals, the unexpected role of GABA as a regulator of selective autophagy pathways may be an evolutionarily conserved one.

Materials and methods

Yeast strains and growth conditions

Yeast strains and plasmids used in this study are listed in Table 2-1 and 2-2, respectively. *S. cerevisiae* strains were grown in rich medium (YPD; 1% yeast extract, 2% peptone and 2% glucose) or defined synthetic medium (SD; 0.17% yeast nitrogen base, 0.5% ammonium sulfate, 2% glucose and auxotrophic amino acids as required) at 30°C on a shaker set at 250 rpm. For induction of peroxisomes, cells were transferred to oleate medium (1% oleate, 5% Tween-40, 0.25% yeast extract, 0.5% peptone, and 5 mM phosphate buffer). For induction of mitochondria, cells were grown in lactate medium (YPL; 1% yeast extract, 2% peptone and 2% lactate, pH 5.5). Pexophagy, mitophagy, ribophagy and autophagy were induced by transferring cells to SD-N medium, which contained no nitrogen or amino acids (0.17% yeast nitrogen base without ammonium sulfate or amino acids and 2% glucose).

Reagents

1M stock solution of GABA (Acros Organics) was dissolved in water and diluted down to either 1 mM or 10 mM in SD-N medium. 200 nM rapamycin (Sigma-Aldrich) was added to SD-N to induce autophagy. 5 µg/ml of FM 4-64 (Life Technologies) diluted from a 1 mg/ml stock solution in DMSO was added to label the vacuolar membrane. Succinic semialdehyde (SSA) was added to SD-N from a 1.5 M stock solution (Aldrich). 50 mM of the redox sensitive dye Dihydrorhodamine-123 (DHR-123, Molecular Probes). 5 µM of propidium iodide (PI, Sigma-Aldrich) was used to label dead cells.

Measurement of intracellular reactive oxygen species

Intracellular ROS levels were measured using a modification of a protocol previously described (36). Relative ROS levels were analyzed using either the redox sensitive fluorescent probe, Dihydrorhodamine-123 (DHR-123) or 2′,5′-dichlorofluorescein diacetate (DCFH-DA) (Molecular Probes). Propidium iodide (PI, Sigma-Aldrich) was used to distinguish living from

dead cells. After treatment, cells were incubated in medium containing 50 mM DHR-123 or DCFH-DA and 5 μM PI for 1 h. Fluorescence was detected using a FACScalibur flow cytometer (Beckton-Dickinson). PI signal was detected in channel FL3 (deep red fluorescence, Ex 488nm, Em 670LP), DHR-123/DCFH-DA was detected in channel FL1 (green fluorescence, Ex 488nm, Em 535/30nm). Only living cells were used to quantify DHR-123/DCFH-DA fluorescence by gating for PI-negative cells. At least 20,000 living cells per sample were analyzed. Specific fluorescence in channel FL1 was normalized to cells lacking DHR-123/DCFH-DA (background control). Each treatment was done in triplicate and repeated at least twice. Data are represented as mean plus standard deviation. Student's t-test was used to calculate p values between treatments (*$p<0.05$, **$p<0.01$).

Fluorescence microscopy

For the autophagy assay, cells were cultured to log-phase (A_{600} ~ 0.8/ml) in SD medium containing 5 μg/ml FM 4-64 to stain the vacuole membrane and transferred to SD-N, with or without GABA. For the pexophagy assay, cells were cultured to log-phase (A_{600} ~ 0.8/ml) in oleate medium containing 5 μg/ml FM 4-64 and transferred to SD-N, with or without GABA and rapamycin. Images were captured at room temperature using a Plan Apochromat 100× 1.40 NA oil immersion objective on a motorized fluorescence microscope (Axioskop 2 MOT plus; Carl Zeiss, Inc.) coupled to a monochrome digital camera (AxioCam MRm; Carl Zeiss, Inc.) and processed using AxioVision software (version 4.5; Carl Zeiss, Inc.).

Immunoblotting

Samples were prepared by precipitation with trichloroacetic acid and A_{600} 0.1 equivalent was resolved using 12% SDS-PAGE followed by Western blotting with anti-Pot1 (1:5,000 Subramani Laboratory), anti-Ape1 (1:5,000 Klionsky Laboratory), anti-GFP (1:2,000; Roche), anti-phospho-S6 (1:2000 Ser235/236) all from Cell Signaling Technology. Secondary antibodies were

either anti-rabbit or anti-mouse polyclonal (both 1:10,000; Roche) followed by enhanced chemiluminescence (GE Healthcare).

***In vitro* mammalian mitophagy assay**

The assay to quantify basal mitophagy in mammalian cells is based on differential stability of a tandem protein (mito-RFP-GFP) as previously described [Kim, 2013, Hepatitis B virus disrupts mitochondrial dynamics: induces fission and mitophagy to attenuate apoptosis]. In short, HeLa cells over-expressing human Parkin (42) were quantified for basal mitophagy. Transfection was performed on cells growing on cover slips using XtremeGene 9 (Invitrogen) according to the manufacturer's recommendations (1µg plasmid + 3µl XtremeGene in 200µl serum free medium for transfection of one well of a 6 well plate). 1 day after transfection, cells were either left untreated, or treated with 1mM GABA with or without 0.05µM rapamycin (1:20,000 dilution of a 1mg/ml stock) in DMEM medium for 3 days. Next, cells were fixed in 4%PFA/PBS and analyzed by fluorescence microscopy. Cells were defined to display signs of mitophagy when areas of red fluorescence caused by lysosomal delivery of mitochondria was detected within the cytosol. The percentage of cells showing red structures among all transfected cells (as evident from red + green mitochondrial signals) was used to quantify basal mitophagy. At least 80 cells were analyzed per treatment.

Animals

Monogamous breeding colonies were established with heterozygous breeders of the B6.129-Aldh5a1$^{tm1KMG/J}$ mouse model, which is an established model representing SSADH deficiency. Tail snips were collected at day of life 15 for DNA extraction, and genotyping was performed with 3 primer 2 reaction polymerase chain reaction and 1.5% agarose gel electrophoresis, as described previously (44).

Animal work in the present study was approved by the animal use and care committee at Washington State University (04276).

Rapamycin treatment for mice to measure superoxide dismutase and S6 phosphorylation

Rapamycin (LC Laboratories) stock was prepared at 25 mg/mL in DMSO (Sigma) and delivered to mice comprising both sexes daily via intraperitoneal injections of 10 mg/kg body weight with a final injection volume of 100 µL. 100 µL aliquots of stock solution were stored at -20°C. Mice were injected every 24 hours beginning at the 10th day of life and continuing for 10 successive days. After 10 days of injection the animals were euthanized by CO_2 anesthesia and cervical dislocation. The livers and brains from all experimental animals were collected and snap frozen in dry ice.

Rapamycin treatment for mice for transmission electron microscopy

Rapamycin was delivered to mice via intraperitoneal injection. Litters comprising both sexes were injected with either DMSO (vehicle) or 5 mg rapamycin per kg body weight diluted with 1XPBS to a final injection volume of 100 µL. Mice were injected intraperitoneally from day 7 to day 10 of life (3 day duration). On the eleventh day, animals were anesthetized with ketamine/xylazene and underwent perfusion fixation through the left ventricle. Post flush with physiological saline (0.9 M NaCl), 4% paraformaldehyde (in PBS) was circulated for 4 min at 15 mL/min with a peristaltic pump. Liver and brain tissues were collected into 2% glutaraldehyde/2% paraformaldehyde (in 0.1 M phosphate buffer) overnight. The next day the samples were rinsed in phosphate buffer, and the median lobe of the liver, as well as the cerebral cortex were sectioned and cut into 1mm cubic pieces.

Tissue processing for transmission electron microscopy

Samples were rinsed in 0.1 M phosphate buffer three times for 10 min, and then fixed with 1% osmium tetroxide for 5 hours.

Tissues were again rinsed once each with 0.1 M phosphate then 0.1 M cacodylate buffers for 10 min each. Next, tissue was dehydrated with a 7 step ethanol series for 10 min each, 100% acetone, and left in 1:1 acetone:SPURRs overnight. The next day, tissue was

placed in 100% SPURRs resin for three days and then polymerized in an oven at 65°C for 24 h. Thin sections were obtained on a Reichert-Jung ultramicrotome (Leica) set to 60 nm and collected onto formvar coated copper grids. In a grid stick pipette, samples were immersed in 2 mL of filtered 4% uranyl acetate and 10 µL $KMnO_4$

for 10 min in the dark and subsequently rinsed thirty times in three separate beakers with filtered DI H_2O. The samples were then rinsed once with 0.1N NaOH before staining with Reynold's lead (pH = 12) for 10 min and rinsed with DI water as above. Grids were dried under a heat lamp for 30 min before viewing with the TEM.

Mitochondrial quantification

Images were taken with a FEI Tecnai G^2 from at least three separate sections positioned to capture the cytoplasm of random cells (excluding the nucleus). 9.6K images were collected for wild-type, *Aldh5a1*$^{-/-}$ and *Aldh5a1*$^{-/-}$ mice treated with rapamycin. Mitochondria were counted based on evidence of the double membrane and cristae. The number of mitochondria were counted and averaged across multiple micrographs of equal areas from comparable regions of mouse liver or brain regions.

Calculation of mitochondrial areas

AxioVision software was used to outline TEM 9.6K images of individual mitochondria and calculate area (μM^2) of whole mitochondria from wild-type (n=44 micrographs) and *Aldh5a1*$^{-/-}$ (n=80 micrographs) mice and taking an average of each group. Student's t-test was used to calculate the p value between the two groups of mice (**$p<0.01$).

Methods for Quantifying Mitochondria to Nuclear DNA Ratio

Genomic DNA extracted from the tails of wild-type and *Aldh5a1*$^{-/-}$ mice and re-suspended in water. Concentrations of DNA were calculated using a Nanodrop 2000 spectrophotometer (Thermo Scientific).

Novaquant Mouse Mitochondrial to Nuclear DNA Ratio Kit (Novagen) was used as per manufacturer's directions, using 1ng of isolated genomic DNA. qPCR was performed using Fast Sybr Green Mastermix (Applied Biosystems) with Step One Plus Real Time PCR System (Applied Biosystems) with the following program: 95°C x 10 min; 95°C x 3 sec; 60°C x 30 sec; 95°C x 15 sec; 60°C x 1 min for 45 cycles. Experiments were performed in duplicate.

Quantification of mtDNA relative copy number to nuclear DNA was done by averaging the copy numbers calculated from trLEV/BECN1 gene pair and the 12s/NEB pair. The counts (Cts) from the trLEV gene were subtracted from BECN1 Ct to obtain ΔCt_1; and 12s Ct was subtracted from NEB to obtain ΔCt_2. To calculate the copy number, the average of the two sets of gene pairs (trLEV/BECN1) and (12s/NEB) were used. Calculation of the individual ratios used the formula $N=2^{\wedge}\Delta Ct$ where $\Delta Ct_1 = Ct^{Nuc1} - Ct^{Mito1}$ and $\Delta Ct_2 = Ct^{Nuc2} - Ct^{Mito2}$. Lastly, the average of the two copy number results was taken.

Enzymatic assay for SOD activity

Livers were halved and homogenized 1:5 (w/v) with ice cold 1 mM EDTA dissolved in 1XPBS (pH = 7.8) with an Omni TH tissue homogenizer. Homogenates were centrifuged at 14,000 rpm for 10 min at 8°C and supernatant harvested. SOD colorimetric-based activity assays were performed according to the methods described by the vendor (Cell Biolabs, Inc. STA-340). Absorbance was measured on a Synergy HT microplate reader (Biotek) for duplicate samples and standards. A 7 point standard curve was used to determine the optimal absorbance range. The relative SOD activity was determined by inhibition of chromagen reduction by free xanthine/xanthane oxidase produced superoxide anions. An unpaired two-tailed t-test was used to compare genotype and treatment groups (Graphpad Prism 5) (*$p<0.05$). Enzyme assays for liver were processed for enzyme activity within two weeks of homogenization.

Immunofluorescence of mice biopsies

Liver tissue sections (5 micron) were obtained from snap frozen biopsies using a Leica CM1800 Cryostat. Staining of mitochondrial marker SOD2 was performed using rabbit anti-

SOD2 (NB100-1969, Novus Biologicals) at 1:200, followed by incubation with a biotinylated goat anti-rabbit secondary antibody (Jackson ImmunoResearch Laboratories Inc.) and Cy3-Streptavidin (Jackson ImmunoResearch Lab. Inc.). Tissues were counterstained for DNA using DAPI (Roche Diagnostics Corp.). Images were captured and processed as described for immunofluorescence microscopy. Automated image analysis for quantification of subcellular SOD2 protein content was performed using the CellProfiler software (http://www.cellprofiler.org) (48) and a self-made analysis pipeline. Briefly, channel intensity was calculated for at least 10 individual images per treatment for the DAPI (blue) channel and for the Cy3 (red) channel. Specific signal intensity for SOD2 staining was calculated by normalizing the Cy3 channel intensity to DAPI intensity. Data were normalized to the wild-type signal (set as 1) and are depicted as an average + SD. Student's t-test was used to calculate p values between treatments (**$p<0.01$).

Table 2-S1: List of strains used in this study

Strain	Genotype	Source or reference!
BY4741	*MATa, his3Δ1, leu2Δ0, met15Δ0, ura3Δ0*	Invitrogen
BY4742!	*MATα, his3Δ1, leu2Δ0, lys2Δ0, ura3Δ0*	Invitrogen
POT1-GFP	*MATα, his3Δ1, leu2Δ0, lys2Δ0, ura3Δ0, pot1::POT1-GFP (HIS5)*	19
OM45-GFP	*MATα, his3Δ1, leu2Δ0, lys2Δ0, ura3Δ0, pot1::OM45-GFP (HIS5)*	19
atg1Δ!	*MATa, his3Δ1, leu2Δ0, met15Δ0, ura3Δ0, atg1::KanMX4*	Invitrogen
atg32Δ	*MATa, his3Δ1 leu2Δ0 met15Δ0 ura3Δ0, atg32::KanMX4*	Invitrogen
uga1Δ	*MATa, his3Δ1 leu2Δ0 met15Δ0 ura3Δ0, uga1::KanMX4*	Invitrogen
uga2Δ	*MATa, his3Δ1 leu2Δ0 met15Δ0 ura3Δ0, uga2::KanMX4*	Invitrogen
sch9Δ	*MATa, trp1, his3, ura3, leu2, rme1, sch9::kanMX4*	28
tor1Δ tor2^{ts}	*MATa, leu2, ura3, rme1, trp1, his3Δ GAL+ HMLa tor1::HIS3MX6 tor2::KanMX4/YCplac33::tor2-21ts*	Dr Michael Hall
TB50a	*MATa, leu2, ura3, rme1, trp1, his3Δ GAL+ HMLa*	Dr Michael Hall

Table 2-S2: List of plasmids used in this study.

Name	Relevant characteristics	Source or reference
pCK5	*pRS316 RPL25-GFP*	20
2µm GAD1	*YEp352-GAD1*	23
GFP-ATG8	*pRS315 GFP-ATG8*	41
AT016	*p-mito-mRFP-EGFP*	18
Human Parkin	*pPARKIN*	42

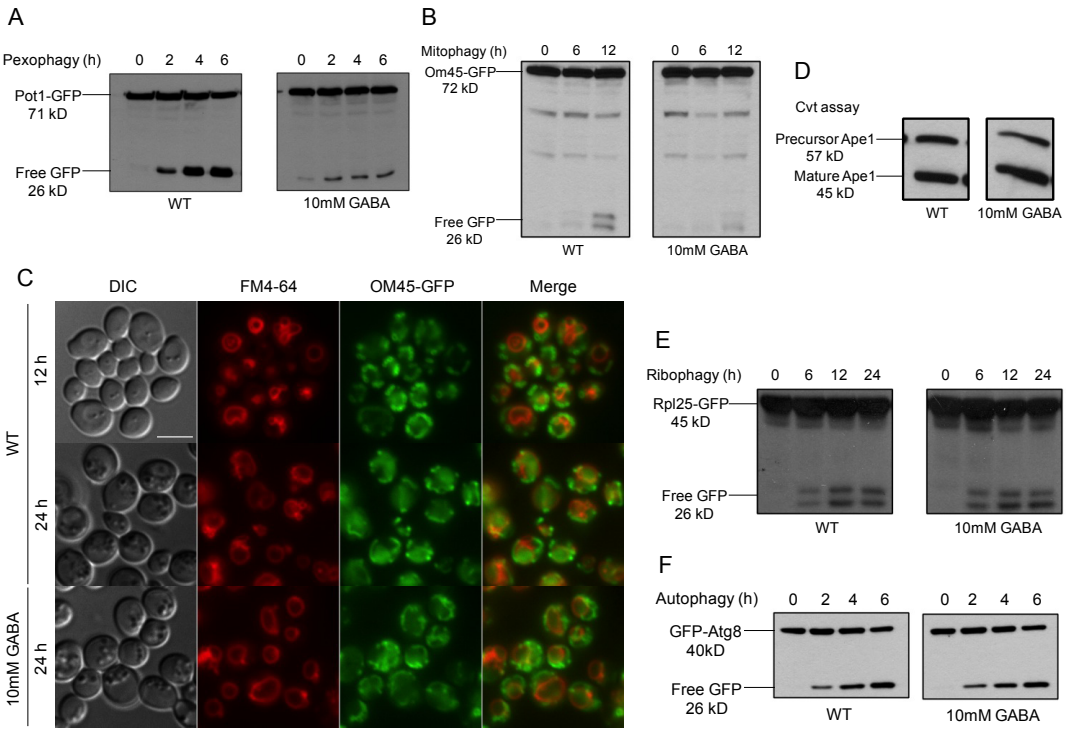

Fgure 2-1: Increased levels of GABA inhibit pexophagy and mitophagy, but not other autophagy-related pathways. (A) Peroxisomes were induced by growing the wild-type (WT) strain expressing Pot1-GFP in oleate medium to mid-log phase then transferred to SD-N starvation medium with or without GABA to trigger pexophagy for 6 h. GFP cleavage was analyzed at the indicated time points by immunoblotting. (B) Mitochondria were induced by growing the WT strain expressing OM45-GFP in YPL medium to mid-log phase and subsequently transferring cells to either SD-N with or without GABA to trigger mitophagy for 12 h. GFP cleavage was analyzed at the indicated time points by immunoblotting. (C) Mitophagy was monitored by fluorescence microscopy using a WT strain expressing OM45-GFP grown in YPL medium for 12 h to mid-log phase in the presence of FM4-64, and transferred to either SD-N medium with or without GABA for 24 h. Bar, 5 μm. (D) The Cvt pathway was monitored using the WT strain with or without GABA and grown in SD medium to mid-log phase, after which samples were analyzed for Ape1 maturation. (E) Ribophagy was monitored by growing the WT strain expressing Rpl25-GFP in SD medium to mid-log phase and transferring cells to SD-N either with or without GABA for 24 h. (F) Autophagy was monitored by growing the WT strain expressing GFP-Atg8 in SD medium to mid-log phase and transferring cells to SD-N either with or without GABA for 6 h.

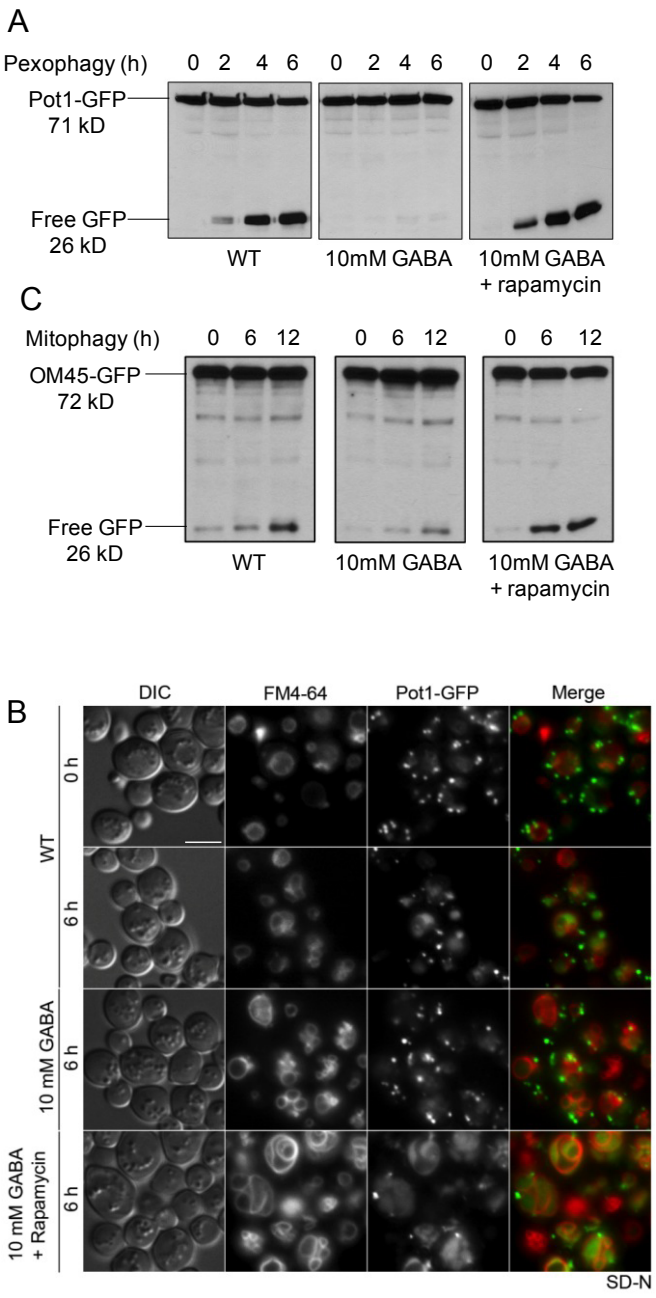

Figure 2-2: The GABA-induced block in pexophagy and mitophagy is overridden by rapamycin. (A) Peroxisomes were induced in oleate and pexophagy was monitored as described for Figure 1. (B) Pexophagy was monitored by fluorescence microscopy using a WT strain expressing Pot1-GFP grown in oleate medium to mid-log phase in the presence of FM4-64, and transferred to either SD-N medium with or without GABA or to SD-N with GABA and rapamycin for 6 h. Bar, 5 μm. (C) Mitochondria were induced and mitophagy was assessed as described for Figure 2-1.

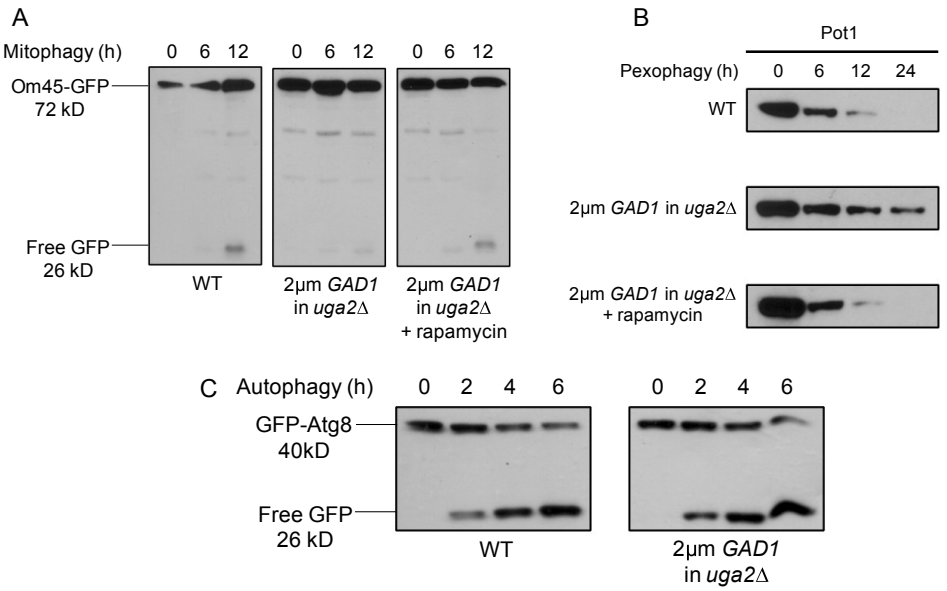

Figure 2-3: Increasing GABA levels endogenously also inhibits pexophagy and mitophagy and these defects are suppressed by rapamycin. (A) WT cells expressing OM45-GFP, along with the *uga2*Δ strain over-expressing the *GAD1* gene and expressing OM45-GFP were grown in YPL medium to mid-log phase. To monitor mitophagy, strains were transferred to SD-N starvation medium (with or without rapamycin). (B) WT, along with the *uga2*Δ strain over-expressing the *GAD1* gene were grown in oleate and pexophagy was monitored as described in Figure 2-1, with or without rapamycin. Samples were taken at the indicated time points and Pot1 degradation was analyzed by immunoblotting (45kD). (C) To monitor autophagy, WT cells expressing GFP-Atg8, along with the *uga2*Δ strain over-expressing the *GAD1* gene and expressing GFP-Atg8 were grown in SD medium and transferred to SD-N.

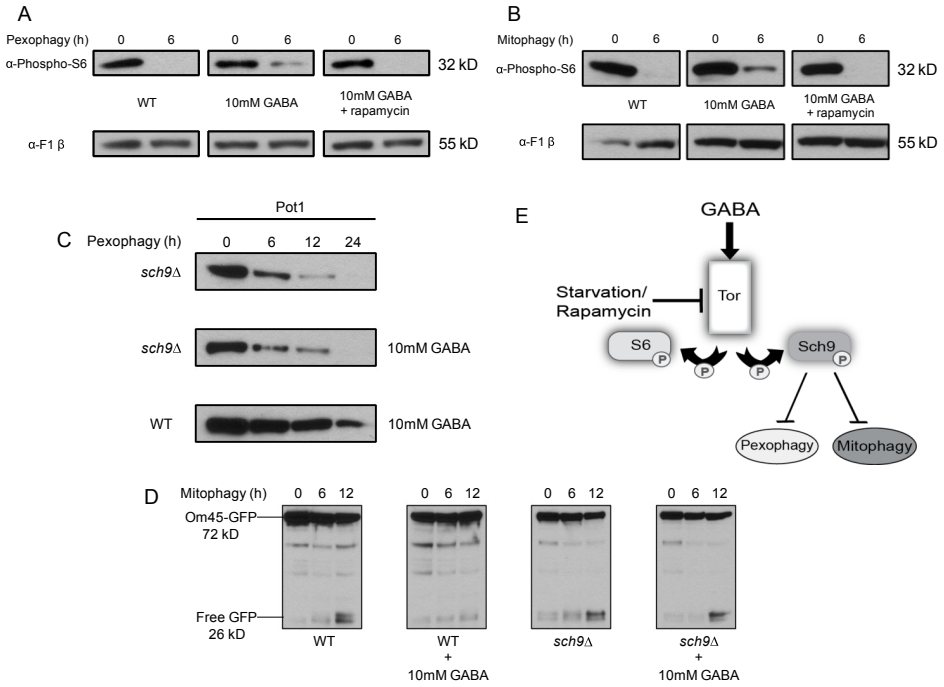

Figure 2-4: Increased GABA levels activate Tor in starvation conditions and inhibit pexophagy and mitophagy by acting through Sch9. WT cells were cultured under pexophagy (A) or mitophagy (B) conditions with or without GABA and rapamycin. S6 phosphorylation at the indicated time points was analyzed by immunoblotting with a loading control. WT and *sch9*Δ strains were grown, as described earlier, for pexophagy or mitophagy assays with or without GABA. (C) Samples were analyzed for Pot1 degradation by immunoblotting (45kD). (D) GFP production during mitophagy was analyzed by immunoblotting. (E) Proposed model for the regulation of pexophagy and mitophagy by GABA. Elevated GABA activates Tor1 in starvation conditions and inhibits pexophagy and mitophagy by activating Sch9.

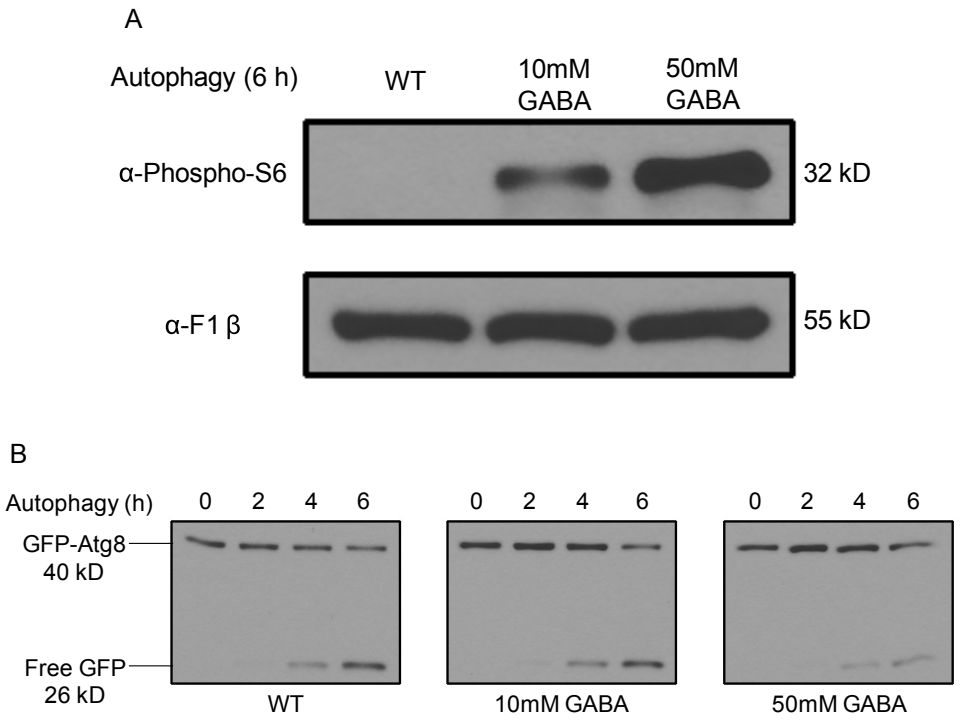

Figure 2-5: Increasing GABA concentration further increases Tor activity and inhibits autophagy. WT cells were cultured under autophagy conditions with or without GABA for 6 h. (A) S6 phosphorylation after 6 h in SD-N was analyzed by immunoblotting with a loading control. (B) GFP production monitoring autophagy at the indicated time points was analyzed by immunoblotting.

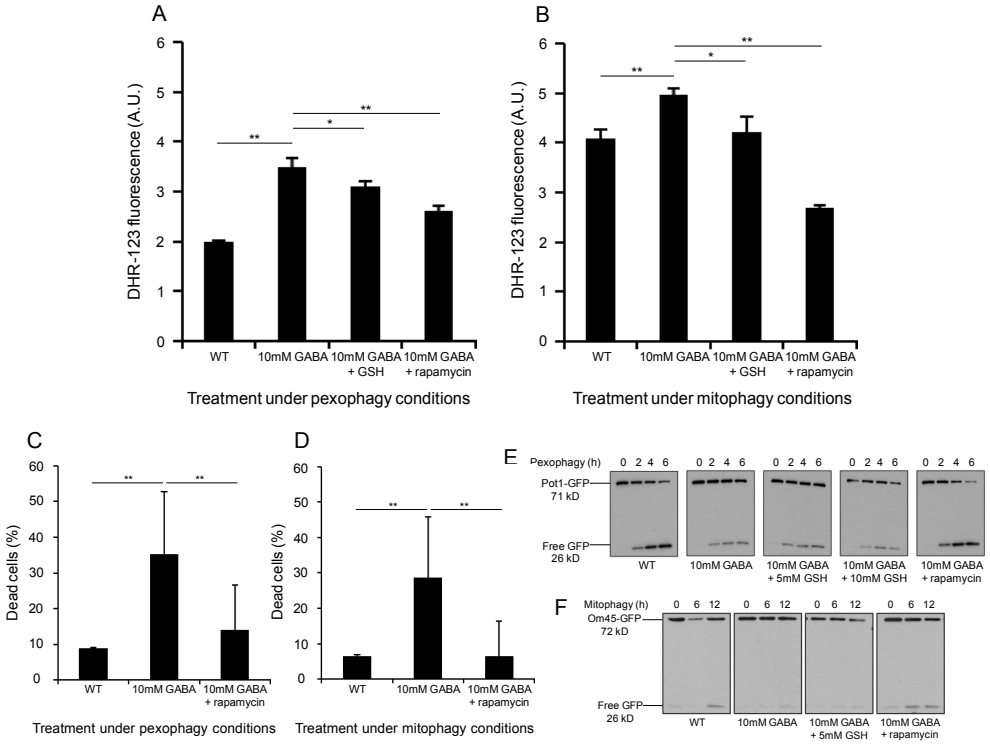

Figure 2-6: The GABA-induced block of pexophagy and mitophagy increases reactive oxygen species levels that can be reduced by rapamycin. WT, WT with GABA, WT with GABA and 10mM GSH and WT with GABA and 200nM rapamycin were tested for intracellular ROS levels under (A) pexophagy and (B) mitophagy conditions. After 24 h incubation, cells were stained with DHR-123 and propidium iodide for 1 h. Living cells were analyzed for DHR-123 fluorescence by flow cytometry. Data represent mean (n=3) plus standard deviation. Significant differences between treatments and strains were determined using a two-tailed t-test. (*p<0.05, **p<0.01). Yeast cells stained with 5 μM propidium iodide were used to differentiate between living and dead cells under (C) pexophagy or (D) mitophagy conditions. (E) Pexophagy assay was monitored by the degradation of Pot1-GFP and analyzed for GFP cleavage by immunoblotting. (F) Mitophagy assay was monitored by the degradation of Om45-GFP and analyzed for GFP cleavage by immunoblotting.

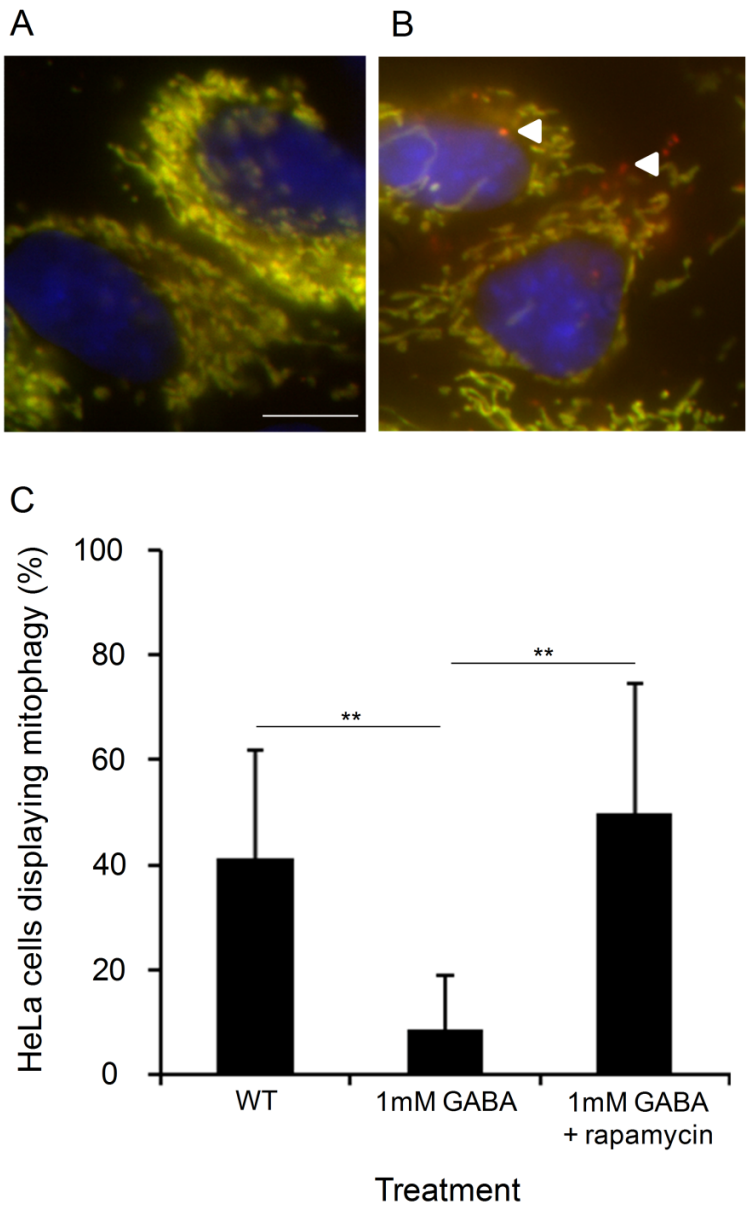

Figure 2-7: Elevated GABA inhibits mitophagy in mammalian cells. (A, B) Example images of Parkin expressing HeLa cells analyzed using a tandem fluorochrome protein (mito-RFP-GFP) mitophagy assay under (A) control conditions or (B) displaying mitophagy depicted by the red mitochondrial structures localized to lysosomes. Bar, 10 μm. (C) Percentage of cells displaying mitophagy + SD (**p<0.01, n>80).

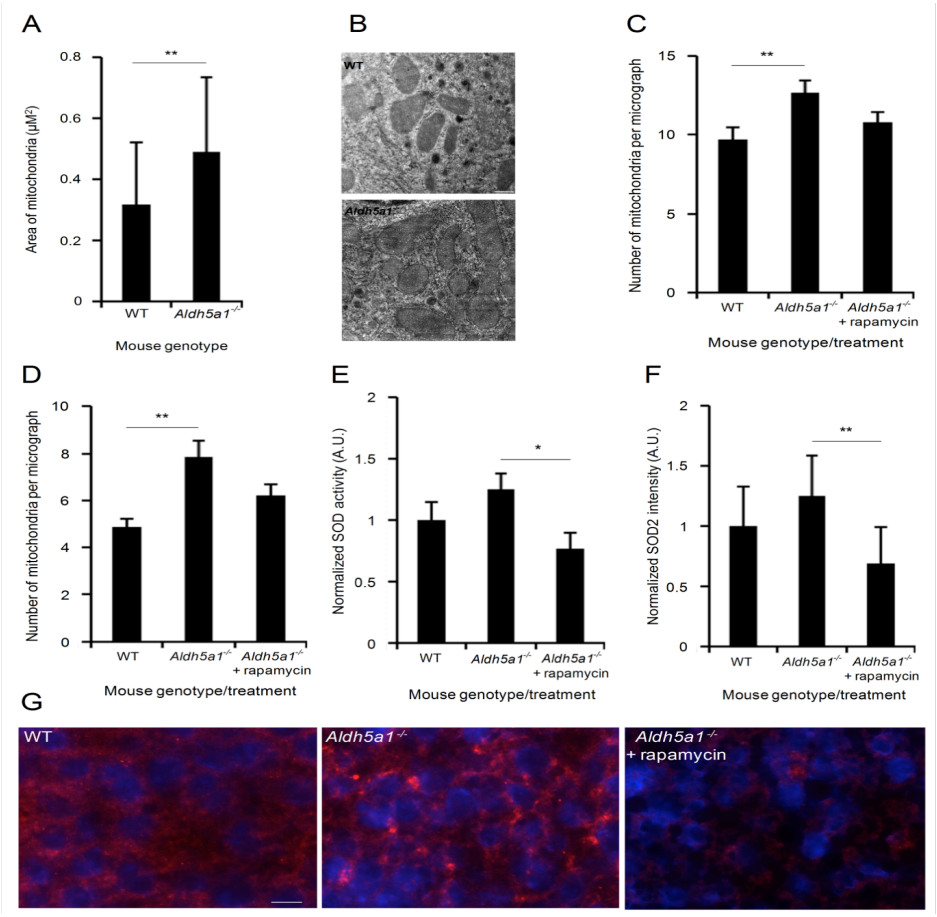

Figure 2-8. SSADH-deficient mice have increased numbers of mitochondria and aberrant antioxidant levels that can be normalized by rapamycin. (A) Electron microscopy images of mitochondria from WT (n=44) and SSADH-deficient mice (*Aldh5a1*$^{-/-}$) (n=80) were calculated for area size. (B) Electron microscopy images showing typical sizes of WT and *Aldh5a1*$^{-/-}$ mice liver mitochondria. Bar, 0.5 μm. (C) Quantification of mitochondrial numbers from electron microscopy images of liver from WT (n=31) and *Aldh5a1*$^{-/-}$ mice treated with vehicle (n=39) or rapamycin (n=34) (5 mg/kg body weight per day) via intraperitoneal injections for 3 successive days starting at day 7 of life. (D) Quantification of mitochondrial numbers from electron microscopy images of brain from WT (n=23) and *Aldh5a1*$^{-/-}$ mice treated with vehicle (n=30) or rapamycin (n=41) (5 mg/kg body weight per day) via intraperitoneal injections for 3 successive days starting at day 7 of life. (E) *Aldh5a1*$^{-/-}$ mice were treated with vehicle or rapamycin (10 mg/kg body weight per day) via intraperitoneal injections for 10 successive days starting at day 10 of life. WT mice served as non-disease controls (set to 1). After sacrifice, liver homogenates were used to measure SOD enzyme activity using a colorimetric SOD activity assay. (F) Mitochondrial SOD2 protein levels were quantified from liver microsections using immunofluorescence microscopy and automated image analysis (WT set to 1). (G) Immunofluorescence images showing typical nuclear staining (DAPI, blue) and SOD2 staining (red) from WT, *Aldh5a1*$^{-/-}$ mice treated with vehicle and *Aldh5a1*$^{-/-}$ mice treated with rapamycin. Bar, 10 μm. (**p<0.01, *p<0.05 using a two-tailed t-test). Data represent average + SD.

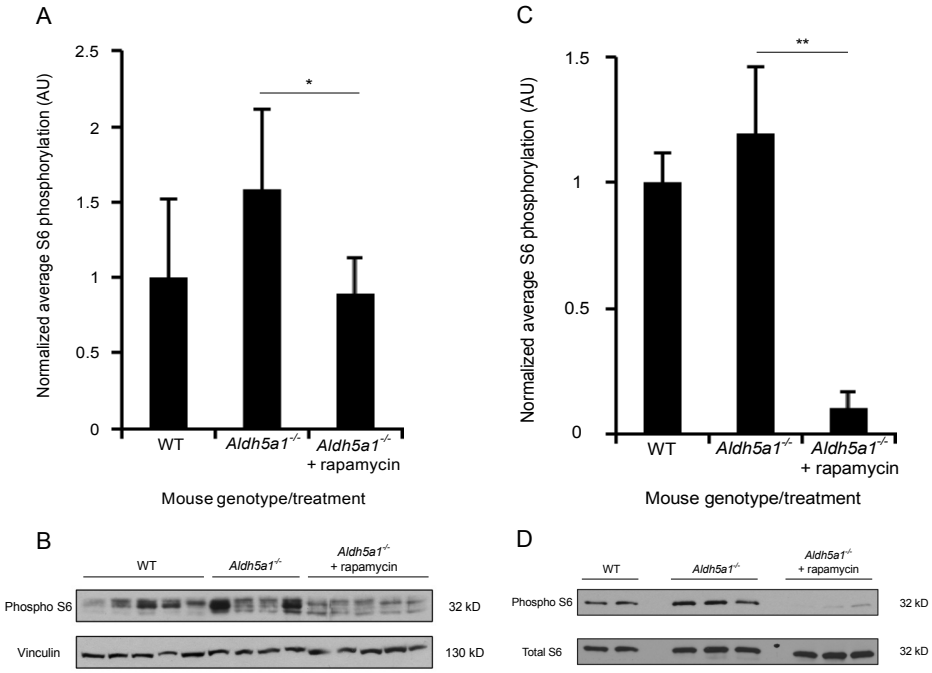

Figure 2-9: SSADH-deficient mice have increased levels of S6 phosphorylation compared to wild-type mice that can be reduced by rapamycin treatment. *Aldh5a1*$^{-/-}$ mice were treated with vehicle or rapamycin (10 mg/kg body weight per day) via intraperitoneal injections for 10 successive days starting at day 10 of life. WT mice served as non-disease controls. After sacrifice, homogenates were used to measure S6 phosphorylation. (A) Quantification of S6 phosphorylation of liver lysates from WT (n=5) and *Aldh5a1*$^{-/-}$ mice treated with vehicle (n=4) or rapamycin (n=5) after normalization (WT set to 1). (B) S6 phosphorylation of liver lysates analyzed by immunoblotting. (C) Quantification of S6 phosphorylation of brain lysates from WT (n=2) and *Aldh5a1*$^{-/-}$ mice treated with vehicle (n=3) or rapamycin (n=3) after normalization (WT set to 1). (D) S6 phosphorylation of brain lysates analyzed by immunoblotting. (**p<0.01, *p<0.05, using a two-tailed t-test). Data represent average + SD.

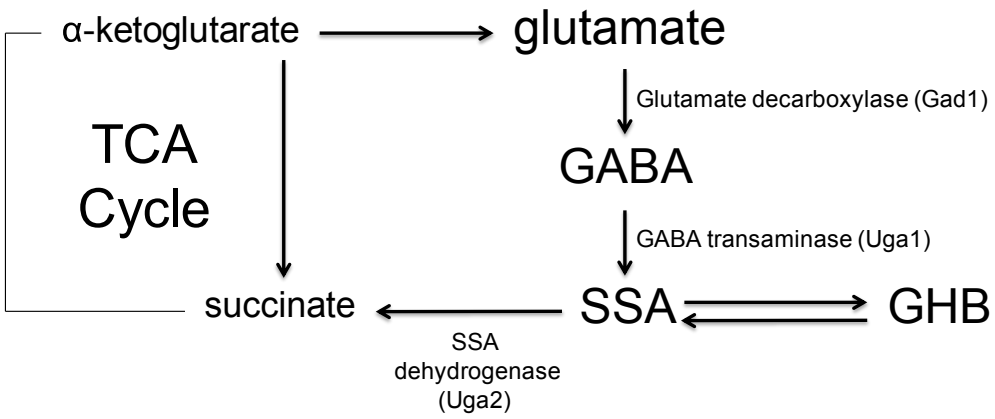

Figure 2-S1: Metabolic pathway of GABA. The GABA shunt showing the formation and degradation of GABA in the yeast *S. cerevisiae* including the major enzymes involved in GABA metabolism.

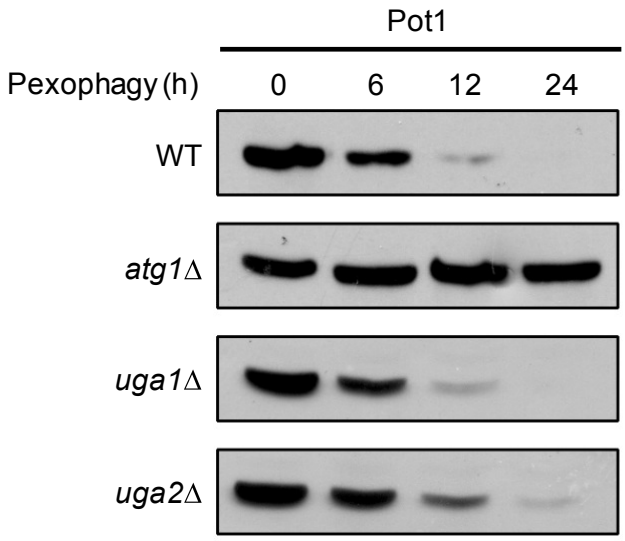

Figure 2-S2: Deletion of the yeast *UGA2* gene encoding SSADH partially inhibits pexophagy but deletion of *UGA1* does not affect pexophagy. Pexophagy assay was monitored by the degradation of Pot1 after transferring cells from oleate to SD-N for 24 h and analyzed by immunoblotting (45kD).

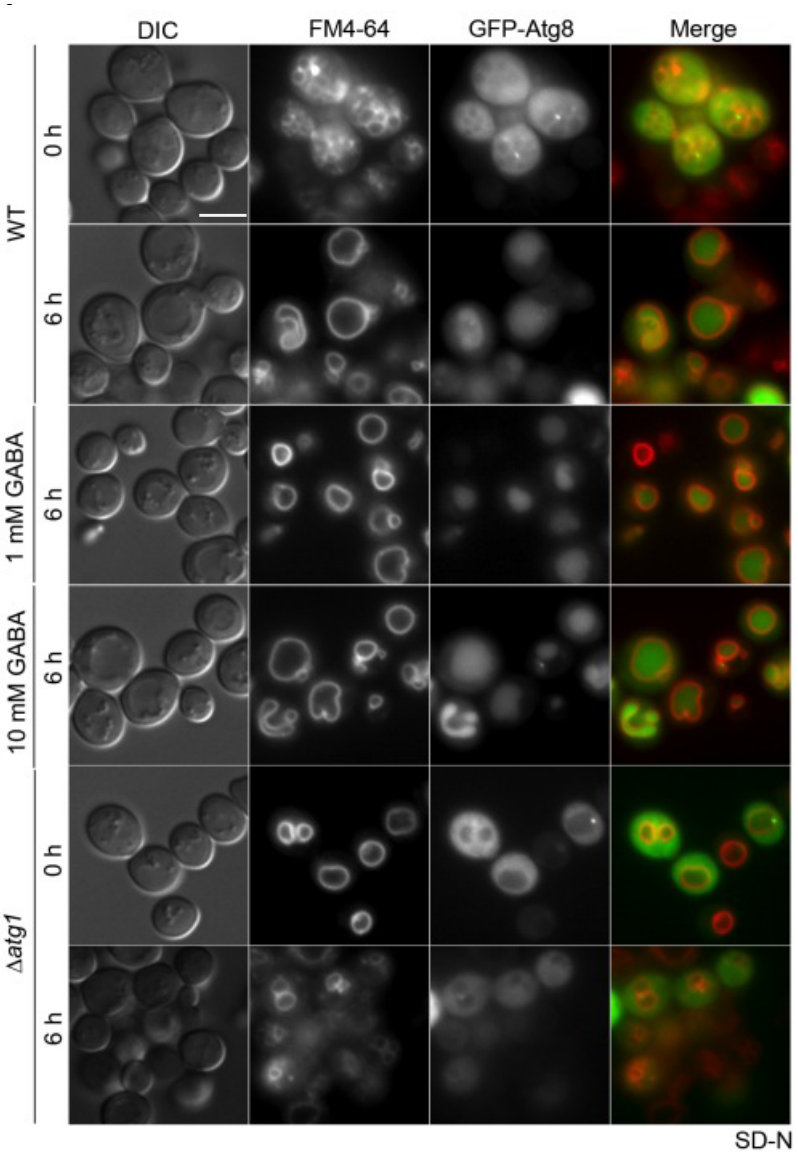

Figure 2-S3: Elevated levels of GABA do not inhibit autophagy. Autophagy analyzed by fluorescence microscopy in the presence of the vacuolar membrane dye, FM4-64. The differential interference contrast (DIC), FM4-64 and GFP-Atg8 images are shown. Bar, 5 μm.

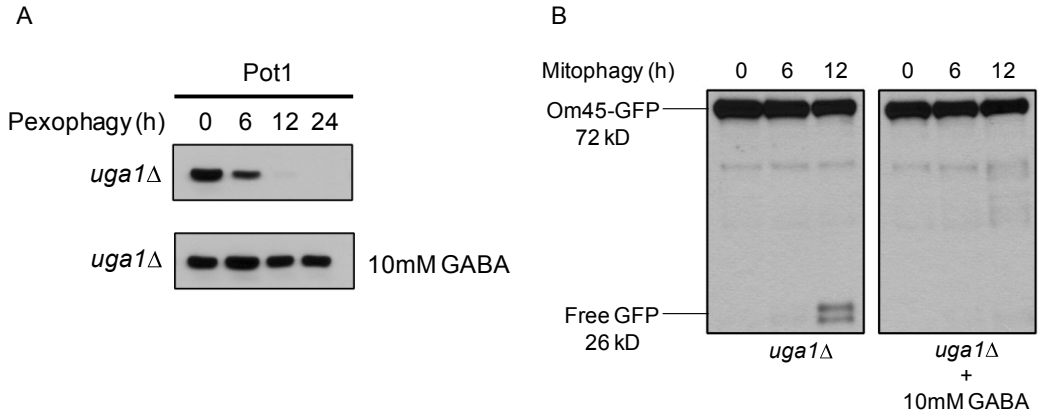

Figure 2-S4: Increased GABA levels inhibit pexophagy and mitophagy even in mutants that cannot utilize GABA as a source of nitrogen. (A) Utilization of GABA mutant *uga1*Δ was subjected to pexophagy conditions as described in Figure 1. Samples were monitored for Pot1 degradation. (B) The *uga1*Δ strain expressing OM45-GFP was subjected to mitophagy conditions and analyzed for GFP cleavage.

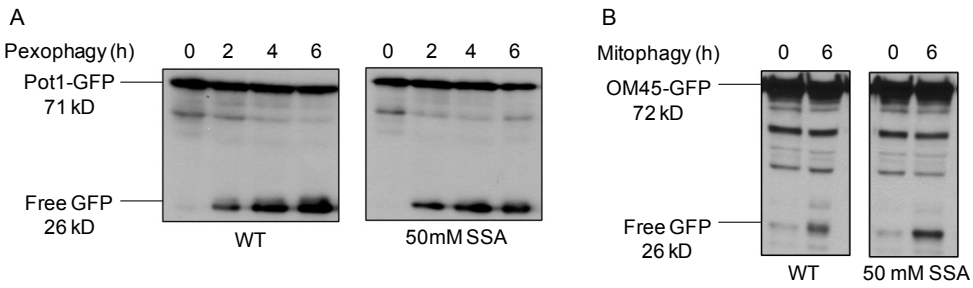

Figure 2-S5: Increased levels of succinic semialdehyde (SSA) do not inhibit pexophagy or mitophagy. (A) Pexophagy in the Pot1-GFP wild-type strain (+/- SSA) was analyzed for GFP cleavage by immunoblotting. (B) Mitophagy assays with and without SSA analyzed for GFP cleavage by immunoblotting.

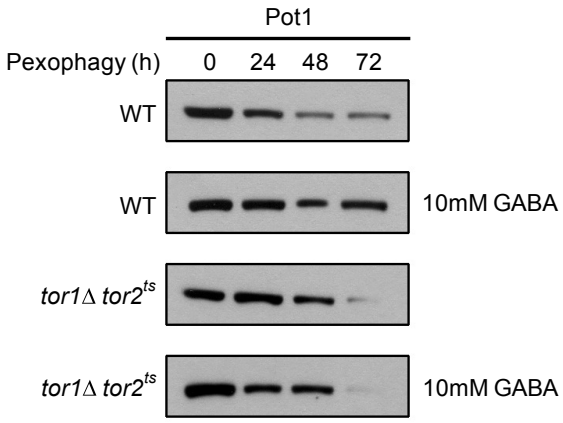

Figure 2-S6: Increased GABA levels inhibit selective autophagy by acting through Tor. WT and *tor1*Δ *tor2*^{ts} strains were cultured under pexophagy conditions at 37°C for 72 h with or without GABA and samples were analyzed for Pot1 degradation by immunoblotting (45kD).

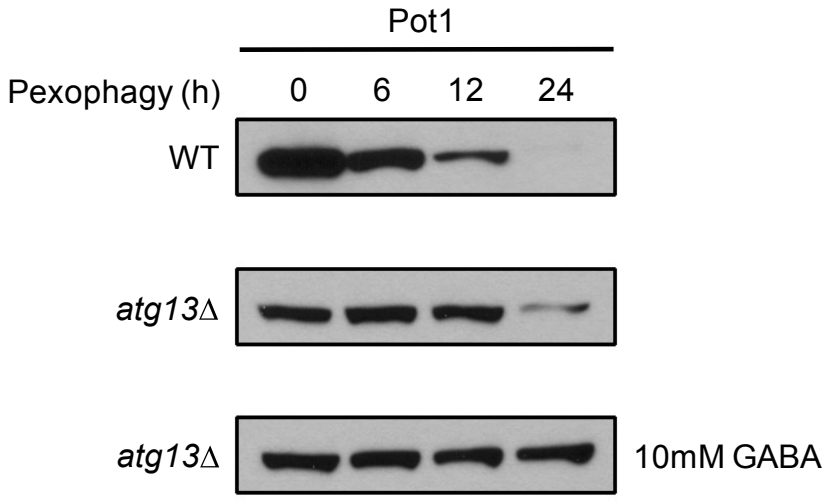

Figure 2-S7: GABA does not act through Atg13. WT and *atg13*Δ strains were cultured under pexophagy conditions with or without GABA and samples were analyzed for Pot1 degradation by immunoblotting (45kD).

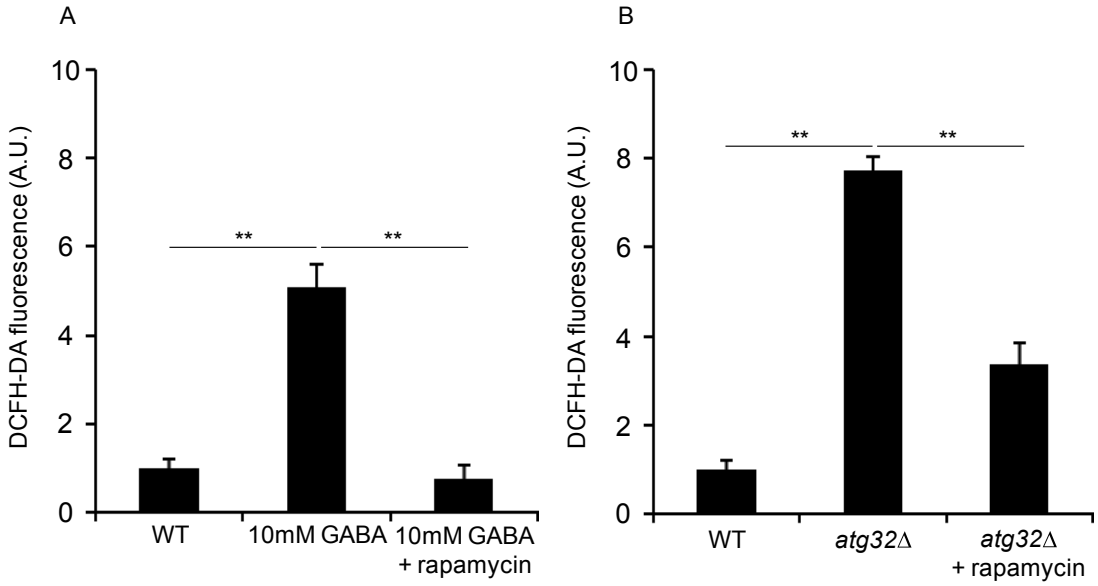

Figure 2-S8: The GABA induced block in mitophagy increases reactive oxygen species levels that can be mitigated by rapamycin treatment. (A) WT, WT with GABA and WT with GABA and rapamycin were tested for intracellular ROS levels under mitophagy conditions for 24 h, along with (B) WT and the mitophagy mutant strain *atg32*Δ with and without rapamycin. After incubation, cells were stained with DCFH-DA and PI for 1 h. Living cells were analyzed for DCFH-DA fluorescence by flow cytometry. Data represent mean (n=4) plus standard deviation and are normalized to the WT condition (set to 1). (**p<0.01 using a two-tailed t-test). Data represent average + SD.

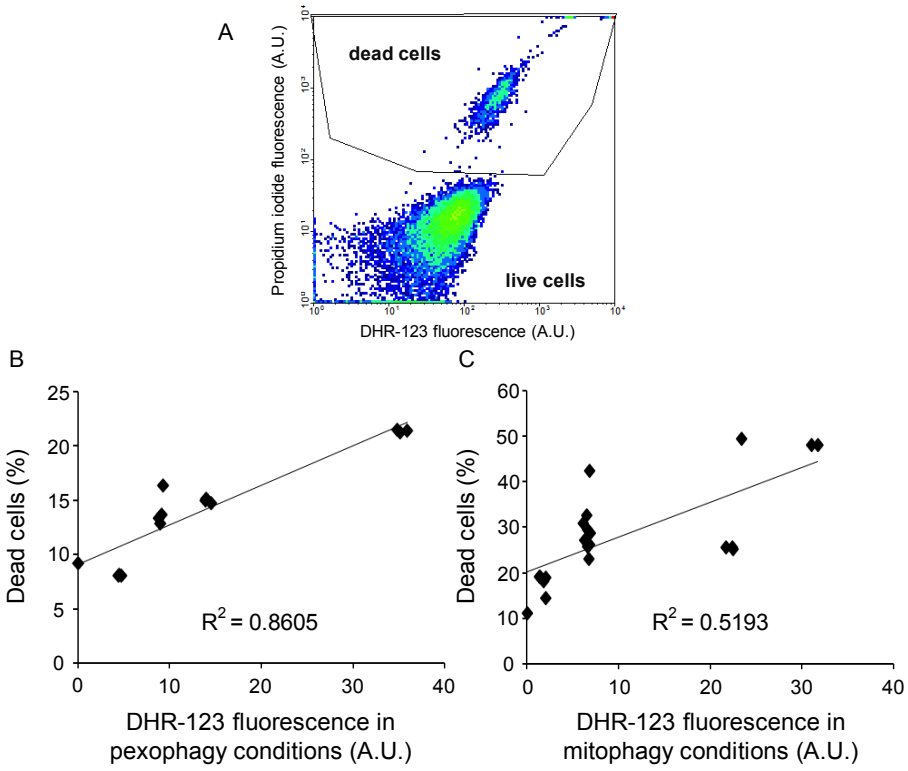

Figure 2-S9: Strategy for parallel assessment of cell death and ROS levels in live cells with correlation analysis. Yeast cells were stained with 5 μM of propidium iodide (PI) to differentiate between living and dead cells along with 50mM of the ROS sensitive dye DHR-123. (A) A high signal in fluorescence channel FL3 (high pass >670nm) was used to create a gate for quantifying dead cells. Only live cells (outside of the dead cell gate) were used to measure intracellular ROS levels in fluorescence channel FL1 (band pass filter 530/40). The percentage of dead cells (PI positive cells) positively correlates with increased intracellular ROS levels (as measured by DHR-123) of live cells in both (B) pexophagy and (C) mitophagy conditions. R^2; correlation coefficient.

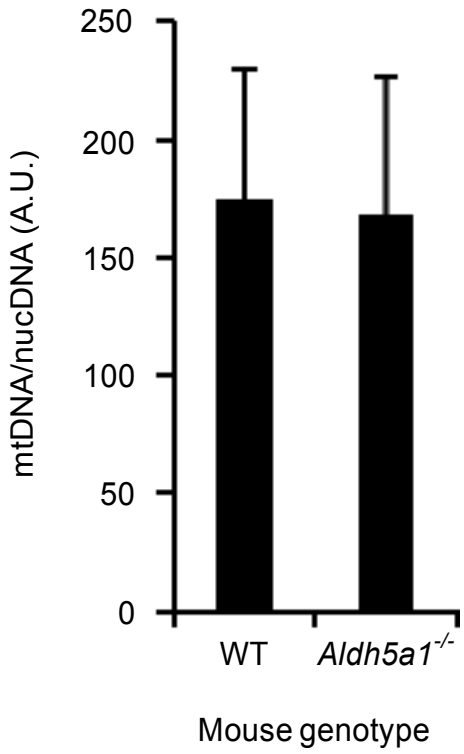

Figure 2-S10: The increased size of liver mitochondria in *Aldh5a1*$^{-/-}$ mice is not due to the depletion of mitochondria DNA. WT (n=5) and *Aldh5a1*$^{-/-}$ (n=5) mice DNA was quantified to determine the ratio of mitochondrial to nuclear DNA relative copy numbers. Data represent average + SD.

Refernces

1. Young, A. B., and Chu, D. (1990) Distribution of GABAA and GABAB receptors in mammalian brain: Potential targets for drug development. *Drug Development Research* **21**, 161-167

2. Watanabe, M., Maemura, K., Kanbara, K., Tamayama, T., and Hayasaki, H. (2002) GABA and GABA receptors in the central nervous system and other organs. *Int Rev Cytol* **213**, 1-47

3. Tillakaratne, N. J., Medina-Kauwe, L., and Gibson, K. M. (1995) gamma-Aminobutyric acid (GABA) metabolism in mammalian neural and nonneural tissues. *Comp Biochem Physiol A Physiol* **112**, 247-263

4. Pearl, P. L., Hartka, T. R., Cabalza, J. L., Taylor, J., and Gibson, M. K. (2006) Inherited disorders of GABA metabolism *Future Neurology* **1**, 631-636

5. Gibson, K. M., Christensen, E., Jakobs, C., Fowler, B., Clarke, M. A., Hammersen, G., Raab, K., Kobori, J., Moosa, A., Vollmer, B., Rossier, E., Iafolla, A. K., Matern, D., Brouwer, O. F., Finkelstein, J., Aksu, F., Weber, H. P., Bakkeren, J. A., Gabreels, F. J., Bluestone, D., Barron, T. F., Beauvais, P., Rabier, D., Santos, C., Lehnert, W. (1997) The clinical phenotype of succinic semialdehyde dehydrogenase deficiency (4-hydroxybutyric aciduria): case reports of 23 new patients. *Pediatrics* **99**, 567-574

6. Tsuji, M., Aida, N., Obata, T., Tomiyasu, M., Furuya, N., Kurosawa, K., Errami, A., Gibson, K. M., Salomons, G. S., Jakobs, C., and Osaka, H. (2010) A new case of GABA transaminase deficiency facilitated by proton MR spectroscopy. *J Inherit Metab Dis* **33**, 85-90

7. Arnulf, I., Konofal, E., Gibson, K. M., Rabier, D., Beauvais, P., Derenne, J. P., and Philippe, A. (2005) Effect of genetically caused excess of brain gamma-hydroxybutyric acid and GABA on sleep. *Sleep* **28**, 418-424

8. Kim, S. J., Lyoo, I. K., Lee, Y. S., Sung, Y. H., Kim, H. J., Kim, J. H., Kim, K. H., and Jeong, D. U. (2008) Increased GABA levels in medial prefrontal cortex of young adults with narcolepsy. *Sleep* **31**, 342-347

9. Pearl, P. L., Shamim, S., Theodore, W. H., Gibson, K. M., Forester, K., Combs, S. E., Lewin, D., Dustin, I., Reeves-Tyer, P., Jakobs, C., and Sato, S. (2009) Polysomnographic abnormalities in succinic semialdehyde dehydrogenase (SSADH) deficiency. *Sleep* **32**, 1645-1648

10. Bach, B., Meudec, E., Lepoutre, J. P., Rossignol, T., Blondin, B., Dequin, S., and Camarasa, C. (2009) New insights into {gamma}-aminobutyric acid catabolism: Evidence for {gamma}-hydroxybutyric acid and polyhydroxybutyrate synthesis in *Saccharomyces cerevisiae*. *Appl Environ Microbiol* **75**, 4231-4239

11. Jakobs, C., Bojasch, M., Mönch, E., Rating, D., Siemes, H., and Hanefeld, F. (1981) Urinary excretion of gamma-hydroxybutyric acid in a patient with neurological abnormalities. The probability of a new inborn error of metabolism. *Clin Chim Acta* **111**, 169-178

12. Gibson, K. M., Gupta, M., Pearl, P. L., Tuchman, M., Vezina, L. G., Snead, O. C., Smit, L. M., and Jakobs, C. (2003) Significant behavioral disturbances in succinic semialdehyde dehydrogenase (SSADH) deficiency (gamma-hydroxybutyric aciduria). *Biol Psychiatry* **54**, 763-768

13. Pearl, P. L., Gibson, K. M., Acosta, M. T., Vezina, L. G., Theodore, W. H., Rogawski, M. A., Novotny, E. J., Gropman, A., Conry, J. A., Berry, G. T., and Tuchman, M. (2003) Clinical spectrum of succinic semialdehyde dehydrogenase deficiency. *Neurology* **60**, 1413-1417

14. Kim, K. J., Pearl, P. L., Jensen, K., Snead, O. C., Malaspina, P., Jakobs, C., and Gibson, K. M. (2011) Succinic semialdehyde dehydrogenase: biochemical-molecular-clinical disease mechanisms, redox regulation, and functional significance. *Antioxid Redox Signal* **15**, 691-718

15. Latini, A., Scussiato, K., Leipnitz, G., Gibson, K. M., and Wajner, M. (2007) Evidence for oxidative stress in tissues derived from succinate semialdehyde dehydrogenase-deficient mice. *J Inherit Metab Dis* **30**, 800-810

16. Yang, Z., and Klionsky, D. J. (2009) An overview of the molecular mechanism of autophagy. *Curr Top Microbiol Immunol* **335**, 1-32

17. Meijer, W. H., van der Klei, I. J., Veenhuis, M., and Kiel, J. A. (2007) ATG genes involved in non-selective autophagy are conserved from yeast to man, but the selective Cvt and pexophagy pathways also require organism-specific genes. *Autophagy* **3**, 106-116

18. Till, A., Lakhani, R., Burnett, S. F., and Subramani, S. (2012) Pexophagy: the selective degradation of peroxisomes. *Int J Cell Biol* **2012**, 512721

19. Kanki, T., and Klionsky, D. J. (2008) Mitophagy in yeast occurs through a selective mechanism. *J Biol Chem* **283**, 32386-32393

20. Kraft, C., Deplazes, A., Sohrmann, M., and Peter, M. (2008) Mature ribosomes are selectively degraded upon starvation by an autophagy pathway requiring the Ubp3p/Bre5p ubiquitin protease. *Nat Cell Biol* **10**, 602-610

21. Mizushima, N., Levine, B., Cuervo, A. M., and Klionsky, D. J. (2008) Autophagy fights disease through cellular self-digestion. *Nature* **451**, 1069-1075

22. Kamei, Y., Tamura, T., Yoshida, R., Ohta, S., Fukusaki, E., and Mukai, Y. (2011) GABA metabolism pathway genes, UGA1 and GAD1, regulate replicative lifespan in *Saccharomyces cerevisiae*. *Biochem Biophys Res Commun* **407**, 185-190

23. Coleman, S. T., Fang, T. K., Rovinsky, S. A., Turano, F. J., and Moye-Rowley, W. S. (2001) Expression of a glutamate decarboxylase homologue is required for normal oxidative stress tolerance in *Saccharomyces cerevisiae*. *J Biol Chem* **276**, 244-250

24. Raught, B., Gingras, A. C., and Sonenberg, N. (2001) The target of rapamycin (TOR) proteins. *Proc Natl Acad Sci U S A* **98**, 7037-7044

25. Kamada, Y., Sekito, T., and Ohsumi, Y. (2004) Autophagy in yeast: a TOR-mediated response to nutrient starvation. *Curr Top Microbiol Immunol* **279**, 73-84

26. Blommaart, E. F., Luiken, J. J., Blommaart, P. J., van Woerkom, G. M., and Meijer, A. J. (1995) Phosphorylation of ribosomal protein S6 is inhibitory for autophagy in isolated rat hepatocytes. *J Biol Chem* **270**, 2320-2326

27. Noda, T., and Ohsumi, Y. (1998) Tor, a phosphatidylinositol kinase homologue, controls autophagy in yeast. *J Biol Chem* **273**, 3963-3966

28. Urban, J., Soulard, A., Huber, A., Lippman, S., Mukhopadhyay, D., Deloche, O., Wanke, V., Anrather, D., Ammerer, G., Riezman, H., Broach, J. R., De Virgilio, C., Hall, M. N., and Loewith, R. (2007) Sch9 is a major target of TORC1 in *Saccharomyces cerevisiae*. *Mol Cell* **26**, 663-674

29. Hara, K., Yonezawa, K., Weng, Q. P., Kozlowski, M. T., Belham, C., and Avruch, J. (1998) Amino acid sufficiency and mTOR regulate p70 S6 kinase and eIF-4E BP1 through a common effector mechanism. *J Biol Chem* **273**, 14484-14494

30. Guertin, D. A., and Sabatini, D. M. (2007) Defining the role of mTOR in cancer. *Cancer Cell* **12**, 9-22

31. Lee, C. H., Inoki, K., and Guan, K. L. (2007) mTOR pathway as a target in tissue hypertrophy. *Annu Rev Pharmacol Toxicol* **47**, 443-467

32. Inoki, K., Corradetti, M. N., and Guan, K. L. (2005) Dysregulation of the TSC-mTOR pathway in human disease. *Nat Genet* **37**, 19-24

33. Kim, J., and Guan, K. L. (2011) Amino acid signaling in TOR activation. *Annu Rev Biochem* **80**, 1001-1032

34. Wallace, D. C. (2005) A mitochondrial paradigm of metabolic and degenerative diseases, aging, and cancer: a dawn for evolutionary medicine. *Annu Rev Genet* **39**, 359-407

35. Giaime, E., Yamaguchi, H., Gautier, C. A., Kitada, T., and Shen, J. (2012) Loss of DJ-1 Does Not Affect Mitochondrial Respiration but Increases ROS Production and Mitochondrial Permeability Transition Pore Opening. *PLoS One* **7**, e40501

36. Zuin, A., Gabrielli, N., Calvo, I. A., García-Santamarina, S., Hoe, K. L., Kim, D. U., Park, H. O., Hayles, J., Ayté, J., and Hidalgo, E. (2008) Mitochondrial dysfunction increases oxidative stress and decreases chronological life span in fission yeast. *PLoS One* **3**, e2842

37. Bonekamp, N. A., Völkl, A., Fahimi, H. D., and Schrader, M. (2009) Reactive oxygen species and peroxisomes: struggling for balance. *Biofactors* **35**, 346-355

38. Vasko, R., Ratliff, B. B., Bohr, S., Nadel, E., Chen, J., Xavier, S., Chander, P., and Goligorsky, M. S. (2013) Endothelial peroxisomal dysfunction and impaired pexophagy promotes oxidative damage in lipopolysaccharide-induced acute kidney injury. *Antioxid Redox Signal* **19**, 211-230

39. Yano, T., Takigami, E., Yurimoto, H., and Sakai, Y. (2009) Yap1-regulated glutathione redox system curtails accumulation of formaldehyde and reactive oxygen species in methanol metabolism of Pichia pastoris. *Eukaryot Cell* **8**, 540-549

40. Ayer, A., Tan, S. X., Grant, C. M., Meyer, A. J., Dawes, I. W., and Perrone, G. G. (2010) The critical role of glutathione in maintenance of the mitochondrial genome. *Free Radic Biol Med* **49**, 1956-1968

41. Kanki, T., Wang, K., Cao, Y., Baba, M., and Klionsky, D. J. (2009) Atg32 is a mitochondrial protein that confers selectivity during mitophagy. *Dev Cell* **17**, 98-109

42. Lazarou, M., Narendra, D. P., Jin, S. M., Tekle, E., Banerjee, S., and Youle, R. J. (2013) PINK1 drives Parkin self-association and HECT-like E3 activity upstream of mitochondrial binding. *J Cell Biol* **200**, 163-172

43. Allen, G. F., Toth, R., James, J., and Ganley, I. G. (2013) Loss of iron triggers PINK1/Parkin-independent mitophagy. *EMBO Rep* **14**, 1127-1135

44. Hogema, B. M., Gupta, M., Senephansiri, H., Burlingame, T. G., Taylor, M., Jakobs, C., Schutgens, R. B., Froestl, W., Snead, O. C., Diaz-Arrastia, R., Bottiglieri, T., Grompe, M., and Gibson, K. M. (2001) Pharmacologic rescue of lethal seizures in mice deficient in succinate semialdehyde dehydrogenase. *Nat Genet* **29**, 212-216

45. Bouché, N., Fait, A., Bouchez, D., Møller, S. G., and Fromm, H. (2003) Mitochondrial succinic-semialdehyde dehydrogenase of the gamma-aminobutyrate shunt is required to restrict levels of reactive oxygen intermediates in plants. *Proc Natl Acad Sci U S A* **100**, 6843-6848

46. Ravikumar, B., Vacher, C., Berger, Z., Davies, J. E., Luo, S., Oroz, L. G., Scaravilli, F., Easton, D. F., Duden, R., O'Kane, C. J., and Rubinsztein, D. C. (2004) Inhibition of mTOR induces autophagy and reduces toxicity of polyglutamine expansions in fly and mouse models of Huntington disease. *Nat Genet* **36**, 585-595

47. Chong, Z. Z., Shang, Y. C., Zhang, L., Wang, S., and Maiese, K. (2010) Mammalian target of rapamycin: hitting the bull's-eye for neurological disorders. *Oxid Med Cell Longev* **3**, 374-391

48. Carpenter, A. E., Jones, T. R., Lamprecht, M. R., Clarke, C., Kang, I. H., Friman, O., Guertin, D. A., Chang, J. H., Lindquist, R. A., Moffat, J., Golland, P., and Sabatini, D. M. (2006) CellProfiler: image analysis software for identifying and quantifying cell phenotypes. *Genome Biol* **7**, R100

Chapter 3: Phosphoregulation of selective autophagy receptors

Abstract

The selective autophagy receptors Atg19 and Atg32 interact with two proteins of the core autophagic machinery: the scaffold protein Atg11 and the ubiquitin-like protein Atg8. We found that the *Pichia pastoris* pexophagy receptor, Atg30, also interacts with Atg8. Both Atg30 and Atg32 interactions were regulated by phosphorylation close to Atg8-interaction motifs. Extending this finding to *Saccharomyces cerevisiae*, we confirmed phospho-regulation for the mitophagy and pexophagy receptors Atg32 and Atg36. Each Atg30 molecule must interact with both Atg8 and Atg11 for full functionality, and these interactions occur independently and not simultaneously, but rather in random order. We present a common model for the phospho-regulation of selective autophagy receptors.

Introduction

Macroautophagy (hereafter called autophagy) is an intracellular bulk degradation system, and is distinct from selective autophagy, which facilitates degradation of specific cargos (1). Autophagy in yeast is primarily a survival response to nutrient starvation, whereas selective autophagy plays a variety of roles, such as cell remodeling to adapt to different environmental conditions and elimination of damaged organelles. Cargo selectivity is mediated via autophagy receptors that simultaneously bind cargos and components of the autophagic machinery (2). In yeast, four receptors have been described: three in *S. cereivisae*, Atg19 (cytoplasm-to-vacuole targeting [Cvt] pathway), Atg32 (mitophagy) and Atg36 (pexophagy), and one in *P. pastoris*, Atg30 (pexophagy) (3-7). Atg19 interacts directly with the cargo (aminopeptidase I, Ape1) to form the Cvt complex, and subsequently with two autophagy proteins, Atg11 and Atg8 (8). Atg11 is a required protein for most selective autophagy pathways in yeast and functions as a basic scaffold in assembling the specific phagophore assembly site (PAS) by interacting directly with the receptor, with itself and several other proteins such as Atg1, Atg9 and Atg17 (9) to form the PAS.

Selective autophagy receptors interact with Atg8 through WxxL-like sequences, called Atg8-family interacting motifs (AIMs in yeast) or LC3-interacting regions (LIRs in animals) (10). Atg19 has such an AIM motif near its carboxy-terminus (8). The hierarchical assembly of Atg8 at the PAS depends on many other autophagy-related (Atg) proteins, suggesting that the binding between Atg19 and Atg8 likely succeeds the Atg11 interaction in growing conditions (11,12).

Much like Atg19, other autophagy receptors including *P. pastoris* Atg30 and *S. cerevisiae* Atg32 and Atg36 (hereafter called Atg30, ScAtg32 and Atg36, respectively) localize with their respective cargos and interact with autophagy proteins. Atg30, and ScAtg32 localize at the cargo surface during organelle biogenesis (4-6). During pexophagy and mitophagy, these receptors are phosphorylated by an unknown kinase(s), facilitating their interaction with Atg11 and subsequent PAS formation (4,13). In addition, Atg30 interacts directly with another scaffold protein, Atg17. Moreover, as a classic autophagy receptor, ScAtg32 interacts with Atg8 through an AIM, but such an interaction is yet to be described for Atg30 and Atg36 (7).

Despite studies involving individual selective autophagy receptors and their interacting partners, little is known about whether and how these interactions are regulated: whether they proceed sequentially or simultaneously; in the same molecule or in two separate molecules; or whether common mechanisms exist for different forms of selective autophagy. We show the existence of a phospho-regulatable AIM on Atg30, Atg32 and Atg36 required for their interactions with Atg8. In addition, we describe putative consensus motifs for Atg8 and Atg11 binding on the receptors. Mutations of these consensus motifs allowed us to study the mechanism of interactions between the receptors and the autophagic proteins. These studies reveal a conserved mode of regulation of selective autophagy pathways, illuminating shared mechanistic principles.

Results and Discussion

Atg30 interacts with Atg8

The selective autophagy receptors (Atg19 and ScAtg32) in yeast bind both Atg8 and Atg11 [5, 6, 8]. So far, only Atg11, but not Atg8, is known to interact with Atg30 (4). By co-immunoprecipitation experiments, we found that Atg30 also interacts with Atg8 (Fig. 3-1A), suggesting that Atg30 forms complexes with Atg8 and Atg11 during pexophagy, like the other selective autophagy receptors.

Atg30 has a cryptic AIM motif

Mutation of a putative AIM (YxxL, amino acids (aa) 330-333 in Atg30), that is not conserved between Atg30 homologs (Fig. 3-S1A), showed it was unnecessary for pexophagy (Fig. 3-S1B). The *S. cerevisiae* mitophagy receptor, ScAtg32, has a phosphorylation-dependent Atg11-binding site with a proximal AIM (13), which led us to another putative AIM-like sequence in Atg30. Atg30 is phosphorylated on Ser112 (S112) and this modification is essential for Atg11 binding and pexophagy (4). Interestingly, the sequences surrounding the phosphorylation sites, S112 in Atg30 and S114 in ScAtg32, required for Atg11 binding, were similar (Fig. 3-1B). Multiple sequence alignments of Atg30 and Atg32 homologs highlighted a conserved motif (D/S)IL<u>S</u>SS surrounding the phosphosite required for Atg11 binding (underlined). The AIM in the Atg32 proteins is in close proximity and upstream of the Atg11-binding site, a situation mimicked in Atg30 proteins. The putative AIM in Atg30 (aa 73-76) does not conform to the strict consensus W/F/YxxL/I/V, but has the sequence, W/YxxF (14). We mutated this cryptic AIM sequence ($Atg30^{W73A\ F76A}$) and checked its effect on pexophagy (Fig. 3-1C, D and 3-S2A, B, C). The Δ*atg30* cells expressing $Atg30^{W73A\ F76A}$ degraded peroxisomes slower than did wild-type cells, suggesting that this AIM could bind Atg8. The pexophagy defect in this mutant was only partial (Fig. 3-1D), but comparable to the mitophagy defect found in the AIM mutant of ScAtg32 (6).

Phosphorylation upstream of the AIMs of Atg30 and Atg32 modulates Atg8 binding

In a previous study (4), we had not detected the Atg8-Atg30 interaction by two-hybrid in *S. cerevisiae* (Y2H), but the recent discovery of the phosphorylation requirement upstream of the AIM/LIR of the OPTN receptor in mammals (15), together with our knowledge that the heterologous *P. pastoris* Atg30 used in the Y2H was not phosphorylated in *S. cerevisiae*, suggested that the absence of phosphorylation of Atg30 may have caused the failure of interaction in *S. cerevisiae*. Interestingly, the hydrophobic core sequences of the AIMs of Atg30 and Atg32 are preceded by multiple Ser and Thr residues (Fig. 3-1B). We mutated these residues upstream of the putative AIMs, replacing them with a phosphomimic amino acid (Asp or Glu) or a non-phosphorylatable amino acid (Ala), and assessed interactions by Y2H (Fig. 3-1E). Atg30 and *P. pastoris* Atg32 (hereafter called Atg32) with phosphomimic mutations upstream of the AIMs ($Atg30^{S71E}$ and $Atg32^{T119E}$) did interact with Atg8, but the wild-type proteins and the non-phosphorylatable mutants (Atg30, Atg32, $Atg30^{S71A}$ and $Atg32^{T119A}$) did not, suggesting that the absence of interaction of wild-type Atg30 with Atg8 was indeed due to the lack of Atg30 phosphorylation in *S. cerevisiae.* In addition, we mutated the AIMs of Atg30 to $Atg30^{W73A\ F76A}$, $Atg30^{S71E}$ to $Atg30^{S71E\ W73A\ F76A}$, Atg32 to $Atg32^{W121A\ V124A}$ and $Atg32^{T119E}$ to $Atg32^{T119E\ W121A\ V124A}$. Mutation of the AIMs in $Atg30^{S71E}$ and $Atg32^{T119E}$ abolished the interactions with Atg8, confirming that both Atg30 and Atg32 contain phospho-regulatable AIMs.

We validated independently the phosphorylation requirement for Atg30-Atg8 binding in *P. pastoris* by Atg30-HA co-immunoprecipitation from different mutants cells (as indicated in the Fig. 3-1F) in the presence (+) or absence (-) of phage λ protein phosphatase (λPP). The interactions of both Atg8 and Atg11, but not the control Pex3, with Atg30 were severely affected by the phosphatase treatment. The AIM and S71A mutations in Atg30 also abolished the interaction with Atg8, but not with Atg11 or Pex3. In contrast, and as expected the phosphomimic mutation ($Atg30^{S71E}$) did not impair the Atg30-Atg8 interaction.

Definitive evidence of phosphorylation at S71 of Atg30 was obtained by mobility shift detection of phosphorylated proteins and mass spectrometry (MS) of Atg30 purified from *P. pastoris* cells. First, we confirmed the presence of a phosphorylation site upstream of the AIM of

Atg30 (S71) using Phos-Tag acrylamide to improve the separation of phosphoproteins (Fig. 3-S3A). When S71 was mutated to a non-phosphorylatable S71A ($Atg30^{S71A}$), some phospho-Atg30 forms shifted to a lower molecular weight, but this protein mobility was rescued by $Atg30^{S71E}$. Additionally, affinity-purified Atg30-HA subjected to MS revealed that Atg30 was phosphorylated at S71 (Fig. 3-S3B, C).

The physiological relevance of the Atg30 phosphorylation was tested by pexophagy assays (Fig. 3-1G and 3-S2A, B) wherein $Atg30^{S71A}$ exhibited delayed pexophagy, similar to the AIM mutant ($Atg30^{W73A\ F76A}$). These results indicate that both pexophagy and mitophagy receptors in *P. pastoris* interact with Atg8 in a phosphorylation-dependent manner and are regulated by an unknown kinase(s). This finding reveals a conserved mode of regulation of Atg8/LC3 binding to autophagy receptors that is likely to be a general and recurring theme across the evolutionary spectrum (15).

Mode of interaction of Atg11 and Atg8 with Atg30

The sequences of Atg32 homologs in yeasts such as *Vanderwaltozyma polyspora* and *Tetrapisispora phaffii* contain an Atg11-binding site overlapping the AIM motif, suggesting that Atg8 and Atg11 may interact sequentially on the same receptor molecule (specific or random order) or bind independently to separate receptors (Fig. 3-1B). The overlapping binding domains and steric interference preclude the simultaneous interaction of Atg8 and Atg11 with the receptor(s). We tested this hypothesis by deleting the amino acids between the AIM and the Atg11-binding motif of Atg30 (Fig. 3-$2A_1$) and testing the mutants in pexophagy assays (Fig. 3-$2A_2$). Two Atg30 truncations (preserving the AIM consensus, underlined in Fig. 3-$2A_1$) analogous to the *Vp*Atg32 and *Tp*Atg32 sequences were tested: 1) $Atg30^{WDILSSS}$ mutant, in which the AIM and Atg11-binding sites overlap and, 2) $Atg30^{WSILSSS}$ mutant, the Asp of the $Atg30^{WDILSSS}$ mutant (underlined) was replaced by Ser to mimic a highly conserved amino acid near the Atg11-binding site in Atg32 (Fig. 3-1B). The two Atg30 truncations produced distinctive results (Fig. 3-$2A_2$). The $Atg30^{WDILSSS}$ mutant partially complemented the Δ*atg30* cells, exhibiting a phenotype similar to

the Atg8-binding site mutants (Atg30^{S71A} or Atg30$^{W73A\ F76A}$), suggesting that this mutant might bind Atg11, but not Atg8. Finally, the Atg30^{WSILSSS} mutant fully complemented Δ*atg30* cells, showing not only that the overlapping AIM and Atg11-binding sites could function in Atg30, but also that Atg8 and Atg11 need not bind simultaneously to a single Atg30 molecule. As expected, the mutant Atg30^{WSILSSS} did indeed interact with Atg8 by Y2H (Fig. 3-2A$_3$).

The hypothetical interaction of Atg8 and Atg11 with two different receptor molecules was excluded by an experiment involving the co-expression of two copies of Atg30 in D*atg30* cells, one with the AIM mutation (S71A or W73A F76A) and a second with the Atg11-binding mutation (S112A), followed by pexophagy assays using either endogenous thiolase or thiolase-GFP (Fig. 2B and S2C). Atg30^{S112A} did not complement the pexophagy delay of either Atg30^{S71A} or Atg30$^{W73A\ F76A}$ (Fig. 3-2B$_2$ and 3-S2C), thereby indicating that Atg8 and Atg11 must interact with the same Atg30 molecule.

Based on our findings that the Atg8- and Atg11-binding sites in Atg30 can overlap while maintaining receptor function and the result that both molecules must interact with the same Atg30 for a fully functional receptor, we asked whether there is any obligatory order of binding, using mutants (Atg30$^{S71A\ S112A}$ and Atg30$^{W73A\ F76A\ S112A}$) that are unable to interact with Atg8 and Atg11 (3-Fig2C and S2A). We reasoned that an obligatorily sequential binding of the proteins to Atg30, as part of a single pathway, should not have a cumulative effect, but should mimic instead the loss of one or other binding site (Fig. 3-2C$_1$). However, Atg30$^{S71A\ S112A}$ and Atg30$^{W73A\ F76A\ S112A}$ were fully blocked in pexophagy (Fig. 3-2C$_2$ and 3-S2A), showing that both Atg8 and Atg11 interaction with Atg30 are independently required for optimal pexophagy.

These combined results indicate that Atg8 and Atg11 need to bind to the same Atg30 molecule, neither interaction (Atg8-Atg30 or Atg11-Atg30) is a prerequisite for the other and finally, the two interactions cannot occur simultaneously when their binding sites overlap. We call this mode of interactions independent (on the same molecule) and randomly sequential.

Independence of Atg8 and Atg11 binding to Atg30 during pexophagy

Disruption of the Atg30-Atg8 interaction only partially affects selective autophagy (6), Fig. 3-1D, G, Fig. 3-2 and Fig. 3-S2). To compare this result in the absence of Atg8, we tested Δ*atg8* cells for pexophagy and phagophore membrane elongation during pexophagy of both small, oleate-induced and large, methanol-induced peroxisomes (Fig. 3-S4A, B). In contrast to the delayed pexophagy in the absence of Atg8-Atg30 interaction, Atg8 was indispensable for pexophagy and phagophore membrane elongation (Δ*atg8*, Fig. 3-S4). This suggests that Atg8 may interact with other unknown "peroxisomal" proteins or that the interaction between Atg30 and Atg8 is non-essential but a different Atg8 function is crucial for pexophagy.

To understand why pexophagy was delayed in the absence of Atg30-Atg8 interaction, we studied Atg8 localization to the phagophore membrane (Fig. 3-3A). No characteristic phagophore membrane was found when the Atg30-Atg8 interaction was abolished (Fig. 3-3A, see S71A and W73A F76A), but instead small Atg8-containing punctae overlapped with peroxisomes. Since pexophagy occurs slowly in these mutants, it suggests that Atg8-Atg30 interaction may be required to extend the phagophore membrane, and the Atg8-containing punctae may be phagophore membranes enclosing only small peroxisomes.

The interaction of Atg11 with the receptor seems to play a more significant role during pexophagy because the disruption of the Atg30-Atg11 interaction ($Atg30^{S112A}$) strongly delayed peroxisomes degradation (16) (Fig. 3-2C_2 and Fig. 3-S2A, B), and this delay was comparable to the absence of Atg11 (D*atg11*, Fig. S4A). Surprisingly, Atg8-labeled phagophore membranes were found in cells expressing $Atg30^{S112A}$ (7.9% of cells) to the same extent as in wild-type (8.1% of cells), despite the severe delay in pexophagy (Fig. 3-2C_2, 3-3A and Fig. 3-S2A, B).

By analogy to the weak phenotype of the $Atg30^{S71A}$ mutant compared to Δ*atg8* (strong phenotype), Atg11 has another function in pexophagy beyond its interaction with Atg30, because Δ*atg11* did not accumulate any phagophore membranes (Fig. 3-S4B), when compared to the $Atg30^{S112A}$ mutant, which had normal phagophore membranes. This conclusion is not unexpected because Atg11 interacts with and recruits many other proteins.

Finally, we visualized Atg11 in cells impaired in the Atg8-Atg30 and Atg11-Atg30 interactions (Fig. 3-3B). During pexophagy, Atg11 accumulated in the vacuolar membrane region, where the peroxisomes contact the vacuole (17). Atg11 localization was dependent on Atg11-Atg30 interaction (S112A), but independent of Atg8-Atg30 interaction (S71A or W73A F76A), in agreement with independent binding of Atg11 to Atg30.

In conclusion, the complete loss of Atg8 and Atg11 had a stronger phenotype than just loss of the interaction between Atg8 and Atg11 with the receptors. The likely explanation is that Atg8 and Atg11 interact with several other Atg proteins and therefore are likely to perform other functions in autophagy and selective-autophagy, beyond just the interactions with Atg30. Additionally, it is known that Atg17 can substitute for Atg11 to facilitate Ape1 transport to the vacuole during nitrogen starvation (18, 19), and partially for Atg11 during pexophagy (16), which could explain why loss of Atg8 has a more severe effect on pexophagy than the loss of Atg11. The *atg11*Δ cells are partially complemented by Atg17 and this would also explain why the isolation membrane elongates in the absence of Atg30-Atg11 interaction (Fig. 3-3A). The dependence of the localization of Atg8 and Atg11 exclusively on just their own binding sites in the receptor (Fig. 3-1F and 3-3), corroborate their independent binding to Atg30. These results are in agreement with the interaction study of ScAtg32 with Atg8 and Atg11 in several autophagy mutants such as Δ*atg8* and Δ*atg11*, which show that the mitophagy receptor interacts with Atg8 in the absence of Atg11 binding and vice versa (20), and with the finding that Atg19 also mediates an independent dual interaction prApe1-sorting mechanism (21). An alternative explanation is the possibility of a weak but undetectable interaction under our experimental conditions, between Atg30 mutants and Atg8 or Atg11, which could be enough to support pexophagy and/or phagophore membrane elongation. However, this is very unlikely at least for the Atg11-binding mutant (S112A), because phagophore membrane formation was completely normal (size and number, Fig. 3-3A) but the pexophagy rate was strongly delayed (Fig. 3-2C2).

Common mechanisms for mitophagy and pexophagy receptors in *P. pastoris* and *S. cerevisiae*

To extend the model of interaction proposed for Atg30 and the autophagic core machinery proteins, we subjected *P. pastoris* Atg32 mutants to mitophagy assays. Mitophagy was followed by Tom20 localization (Tom20-mCherry) and Tom20 degradation (free GFP appearance from Tom20-GFP). Atg32 and Tom20 colocalized to mitochondria during growth condition in YPL medium (mid-log growth phase) and were degraded only after cells had reached stationary phase or shifted to SD-N (Fig. 3-4A, B and Fig.3-S5). Tom20 degradation was depended on Ypt7, Atg5 and Atg32 (Fig. 3-4A, B), as expected for mitophagy.

First, the amino acids between the AIM and the Atg11 binding motif of Atg32 (Met123 to Ser156) were deleted, generating a truncated Atg32 (Atg32^{WQVLSSS}) with overlapping binding motifs (Fig. 3-S6A). Atg32^{WQVLSSS} fully complemented the mitophagy defect of D*atg32* cells (Fig. 3-4A, B) and interacted with Atg8 (Fig. 3-S6B), suggesting that interactions of the Atg32 with Atg8 and Atg11 may not occur simultaneously. Next, we mutated the AIM on Atg32 (Atg32$^{W121A\ V124A}$) and the threonine upstream of the AIM (Atg32^{T119A}) and found slight defects in mitophagy (Fig. 3-4A, B), comparable to the pexophagy defect seen for the equivalent mutation in Atg30 (Fig. 3-1D, G and Fig. 3-S2). In contrast, the mutation, S159A, required for Atg11 binding (Atg32^{S159A}) severely impaired mitophagy, comparable to the Δ*atg32* cells. These results confirmed that Atg32 and Atg30 share the same motif organization for Atg8 and Atg11 binding sites and probably the same molecular mechanisms.

We extended our studies to *S. cerevisiae*, where Atg36 is the pexophagy receptor (7). Atg36 does not share sequence homology with Atg30, yet is functionally homologous, by interacting with the same set of proteins such as Pex3, Atg8 and Atg11. We used our consensus sequence logo (Fig. 3-1B) to screen for a putative AIM followed by an Atg11-binding site in Atg36, and found an N-terminal region with similar sequence organization (Fig. 3-4C). The putative AIM, the Ser (S31) upstream of the AIM and the Ser (S97) in the Atg11-binding site of Atg36 were mutated to Ala and tested by Y2H (Fig. 3-4D). The interaction studies of Atg36 confirmed the

presence of a classical AIM (F33 -L36), with S31 upstream of the AIM also being required for ScAtg8 binding. Similarly, the Atg11-binding site in Atg36 was confirmed by Y2H with wild-type Atg36 and the mutation, S97A. The physiological roles of these interactions were assayed by free GFP appearance caused by degradation of Thiolase-GFP during pexophagy (Fig. 3-4E). Similarly to Atg30 and Atg32 point mutations, Atg36 mutants affecting the AIM and upstream Ser (S31) delayed pexophagy to the same extent.

A yeast three-hybrid (Y3H) analysis confirmed the hypothesis that Atg8 and Atg11 cannot interact simultaneously with the receptors, as suggested by the overlapping Atg8 and Atg11 binding motifs found in some receptors in nature (Fig. 3-1B) or recreated by truncation (Fig. 3-2A, Fig. 3-4A, B and Fig. 3-S6). We studied this with *S. cerevisiae* Atg36 because phosphorylation during the Y2H happens normally, making it unnecessary to use phosphimimic mutations of Atg36 to study its interactions with ScAtg8 and ScAtg11. The Y3H analysis revealed that ScAtg11 fused to a nuclear localization signal (NLS-ScAtg11) competes with ScAtg8 (BD-ScAtg8) for interaction with ScAtg36 (AD-ScAtg36) and this competition was inhibited by mutation of the Atg11 binding site on ScAtg36 ($ScAtg36^{S97A}$; Fig. 3-4F). These data confirm that ScAtg11 can displace ScAtg8 for interaction with Atg36. Interestingly, ScAtg8 (NLS-ScAtg8) did not compete with ScAtg11 (BD-ScAtg11) for ScAtg36 (AD-ScAtg36) interaction, in agreement with the pexophagy experiments wherein Atg30 S71E behaved like WT (Fig. 3-S2A, B). This suggests that Atg11 has a higher affinity for the receptor than Atg8. So, if Atg8 binds first, Atg11 can displace Atg8. However, if Atg11 binds first, modulation of the respective binding affinities perhaps by phosphorylation of the Atg8 site and/or dephosphorylation at the Atg11 site would allow Atg8 to displace Atg11.

Finally, we showed the mitophagy receptor ScAtg32 requires Ser81, 83, 85 upstream of the published AIM to bind ScAtg8 [6] (Fig. 3-S7). Our studies illustrate the evolutionary conservation of selective autophagy receptors in yeast that are characterized by a tripartite interaction with cargo, Atg8 and Atg11, and these interactions are regulated by phosphorylation events.

We summarize the receptor interactions in Fig. 3-S8. During organelle biogenesis, the selective autophagy receptors are transported to the target organelle in an inactive form that does not interfere with organelle biogenesis. When selective autophagy is induced, an unknown kinase(s) activates the receptor by phosphorylation of the serine(s)/threonine(s) at the Atg11-binding site (model 1) or upstream of the phospho-regulated AIM (model 2), to allow interactions with Atg11 and Atg8, respectively. Atg11 or Atg8 then dissociates from the receptor, likely via competition based on their intrinsic affinities for the receptor or via the action of an unknown phosphatase(s). A second phosphorylation event happens on the same receptor molecule to facilitate the interaction with the other molecule, Atg8 (model 1) or Atg11 (model 2), as applicable.

Mitophagy and pexophagy display added complexities relative to the Cvt pathway in that their turnover is regulated and their engulfment may be more complex. Mitochondria and peroxisomes must be targeted to the vacuole in a manner that depends on environmental changes, but they must also be degraded in the absence of external cues when they are dysfunctional. The mechanisms proposed here for Atg30, Atg32 and Atg36 outline a general mechanistic framework for most of the selective autophagic receptors in yeast. Whether different types of selective autophagy use the same or different kinases/phosphatases for the regulation of selective autophagy remains to be determined.

Methods

Strains and plasmids are described in tables 3-S1 to 3-S4. Media and growth conditions are in the Supplementary information.

***In silico* analysis.** Putative Atg30 and Atg32 homologs were identified using Atg30 (GenBank accession number: AAQ63446) and ScAtg32 (GenBank accession number: DAA08407) protein sequences as described in the Supplementary information.

Biochemical studies of pexophagy and mitophagy. In *P. pastoris*, peroxisomes were induced by incubation of cells in oleate medium (starting OD_{600} of 0.2) for 15 h and transferred to SD-N medium at an OD_{600} of 2, to induce pexophagy. One ml of cells were collected at different times as described in the Figures, TCA precipitated and analyzed by Western blot. In *S. cerevisiae*,

pexophagy was performed as described earlier (18). Mitophagy in *P. pastoris* was induced by growth in YPL medium up to stationary phase, as described earlier (19). Cells were grown in YPL medium starting at 0.1 OD_{600} and at 12, 18 and 36 h, one ml of cells was TCA precipitated and analyzed by Western blot.

Yeast two- and three-hybrid analysis. The *GAL4*-based Matchmaker yeast two-hybrid system (CLONTECH Laboratories, Inc.) was used. Full-length open reading frames were inserted in pGAD-GH (Activation Domain, AD) and pGBT9 (Binding Domain, BD) plasmids, except for *P. pastoris* and *S. cerevisiae* Atg8, where the BD was fused to a truncated Atg8 (Met1 to Phe115). The pBridge plasmid from CLONTECH Laboratories (for co-expression of a BD fusion protein and a NLS fusion protein) was used exclusively for the three-hybrid assay. The *S. cerevisiae* strains AH109 and HF7c were used for the two- and three-hybrid assays, respectively. Two transformants from each strain were tested in duplicate in both assays. All strains were plated on SD medium (Leu^-, Trp^-) as well as SD medium (His^-, Leu^-, Trp^-) containing 3-amino-1,2,4-triazole (3AT) at the concentration indicated in the figure.

Fluorescence microscopy. Pexophagy assays were performed as described for biochemical studies and pictures were acquired after 3 h in SD-N medium. Large phagophore membrane detection and Atg11 localization: cells were grown in methanol medium (starting OD_{600} of 0.2) for 15 h and transferred to SD-N medium at an OD_{600} of 2 for 1 h. The phagophore membrane was labeled with GFP-Atg8 or GFP-Atg26. Mitophagy assays: cells were grown in YPL medium (starting OD_{600} of 0.2) for 12 h and transferred to SD-N medium at an OD_{600} of 1, as described in *S. cerevisiae* (19). To quantify selective-autophagy defects during experiments, the fluorescence microscopy parameters such as exposition time, gain and binning were kept constant.

Co-immunoprecipitation, protein purification and mass spectrometry. We used Δ*ypt7* D*atg30* cells, expressing Atg30-Flag or Flag-Atg11 and Atg30-HA, and either GFP-Atg8 or myc-Atg8 expressed from their endogenous promoters. The experiments were performed as described (20), using 1% CHAPS as detergent for Fig. 3-1A or as described in Supplementary methods for Fig. 3-1F. Protein purification of a mutated Atg30(A81R) to facilitate mass

spectrometry studies was performed as described in Supplementary methods.

Figure 3-1: Atg30 interacts with Atg8 through a cryptic AIM and phosphorylation upstream of the AIM regulates their interaction. (A) Immunoprecipitation (IP) of GFP–Atg8 (α-GFP), Atg30-Flag (α-Flag) and Pex3 (α-Pex3) under pexophagy conditions. The abundant peroxisome matrix protein, alcohol oxidase (AOX), was used as a negative control. Input: total lysate; ϕ: IP without antibody. (B) Two multiple sequence alignments, including 11 Atg30 homologs and 11 Atg32 homologs (identical residues are indicated with black boxes, and similar residues with grey boxes), and a sequence logo of the combined multiple sequence alignments from Atg30 and Atg32 homologs currently listed in GenBank. (C and D). Pexophagy experiments of Δ*atg30* (ϕ), wild-type (Atg30) and Atg30 AIM mutant ($Atg30^{W73A\ F76A}$) cells were done by fluorescence microscopy, following the degradation of peroxisomes labeled with BFP fused at its C-terminus to the Ser-Lys-Leu peroxisomal targeting signal 1 (BFP-SKL) and biochemically by monitoring peroxisomal thiolase degradation. Vacuoles were labeled with FM4-64. Scale bar: 5 μm. (E) AH109 cells were transformed with two yeast two-hybrid assay plasmids, AD (activation domain) and BD (binding domain), which encode the indicated domains fused with Atg30, Atg32 and Atg8 or an empty vector, as negative controls and grown on +His and −His + 40 mM 3-AT plates. (F). Δ*atg30* (ϕ) and Δ*atg30* cells complemented with Atg30-HA (Atg30) and several Atg30-HA mutants were immunoprecipitated (α-HA IP) under pexophagy conditions. In addition, α-HA IP of Δ*atg30* cells (ϕ) and Δ*atg30* cells complemented with Atg30-HA (Atg30) were incubated with (+) and without (-) λPP. Input: total lysate. (G) Pexophagy in Atg30 mutants was monitored by following thiolase levels of oleate-induced peroxisomes after shifting cells to SD-N.

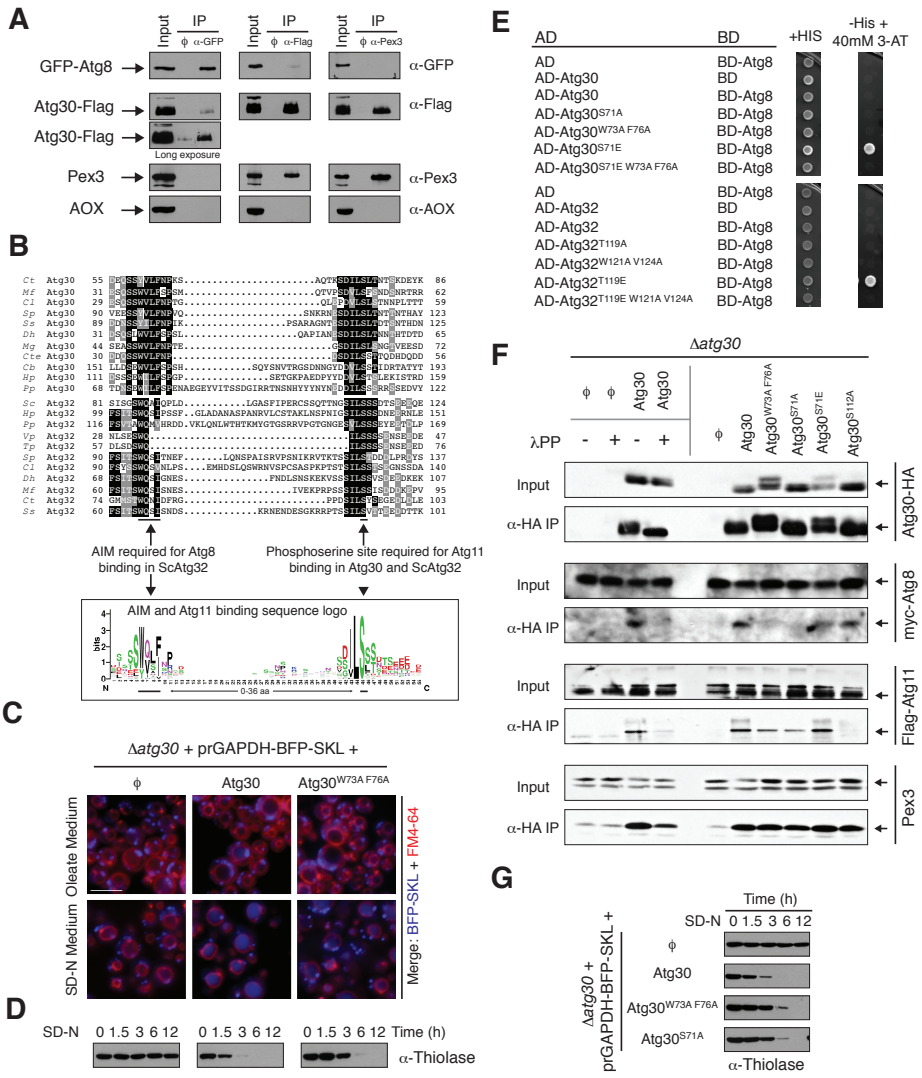
A
Input
IP
ϕ α-GFP
ϕ α-Flag
ϕ α-Pex3
GFP-Atg8
Atg30-Flag
Atg30-Flag
Long exposure
Pex3
AOX
α-GFP
α-Flag
α-Pex3
α-AOX
B
AIM required for Atg8 binding in ScAtg32
Phosphoserine site required for Atg11 binding in Atg30 and ScAtg32
AIM and Atg11 binding sequence logo
0-36 aa
C
Δatg30 + prGAPDH-BFP-SKL +
ϕ
Atg30
Atg30W73A F76A
SD-N Medium Oleate Medium
SD-N Medium
Merge: BFP-SKL + FM4-64
D
SD-N 0 1.5 3 6 12 0 1.5 3 6 12 0 1.5 3 6 12 Time (h)
α-Thiolase
E
AD
BD
+HIS
-His + 40mM 3-AT
AD BD-Atg8
AD-Atg30 BD
AD-Atg30 BD-Atg8
AD-Atg30S71A BD-Atg8
AD-Atg30W73A F76A BD-Atg8
AD-Atg30S71E BD-Atg8
AD-Atg30S71E W73A F76A BD-Atg8
AD BD-Atg8
AD-Atg32 BD
AD-Atg32 BD-Atg8
AD-Atg32T119A BD-Atg8
AD-Atg32W121A V124A BD-Atg8
AD-Atg32T119E BD-Atg8
AD-Atg32T119E W121A V124A BD-Atg8
F
Δatg30
ϕ
ϕ
Atg30
Atg30
λPP - + - +
ϕ
Atg30
Atg30W73A F76A
Atg30S71A
Atg30S71E
Atg30S112A
Input
α-HA IP
Atg30-HA
myc-Atg8
Flag-Atg11
Pex3
G
Time (h)
SD-N 0 1.5 3 6 12
Δatg30 + prGAPDH-BFP-SKL +
ϕ
Atg30
Atg30W73A F76A
Atg30S71A
α-Thiolase

Figure 3-2: Interactions between Atg30, Atg8 and Atg11. (A_1) Atg30 sequences from aa 68-122 of wild-type (Atg30), the S71A mutant ($Atg30^{S71A}$) and two different deletions of the sequence between the AIM and phosphosite required for Atg11 binding in Atg30 ($Atg30^{WDILSSS}$ and $Atg30^{WSILSSS}$). (A_2) Pexophagy experiments of D*atg30* cells complemented with appropriate wild-type or mutant Atg30 proteins described in A_1. (A_3) Two-hybrid assays between Atg30 wild-type or mutants (described in A_1) and Atg8. Phosphomimic S71E was included to detect the interaction with Atg8. (B_1) Schematic of the two Atg30 molecules, one with an Atg8-binding site mutated and a second with an Atg11-binding site (A11-BS) mutated, used to complement D*atg30* cells by co-expression. P: indicates phosphorylation in vivo. (B_2) Pexophagy experiments of D*atg30* cells complemented with the two Atg30 molecules described in B_1. (C_1) Schematic of the Atg30 mutations, S71A and S112A that impair Atg8 and Atg11 binding, respectively. (C_2) Pexophagy assays of D*atg30* cells complemented with Atg30 wild-type and mutants.

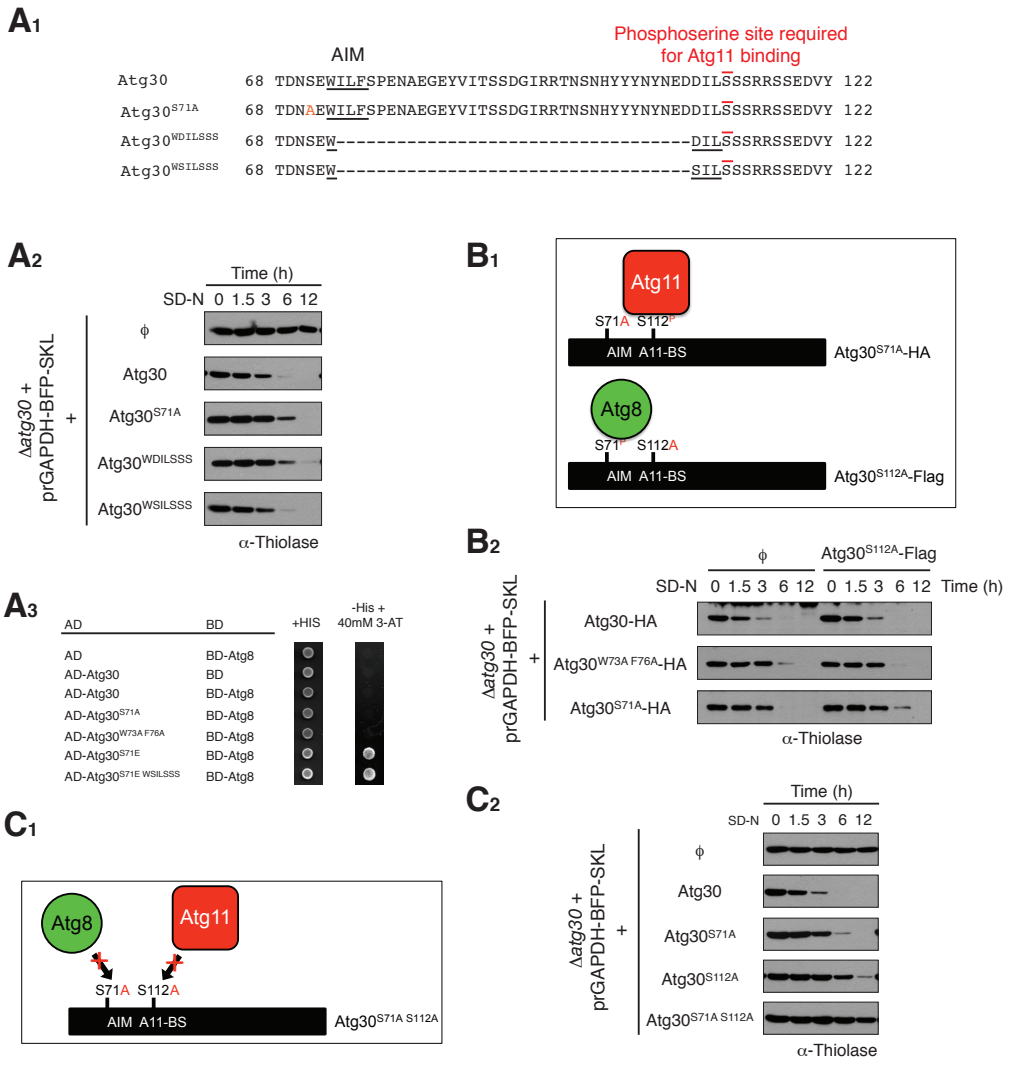
A1
AIM
Phosphoserine site required for Atg11 binding
Atg30 68 TDNSEWILFSPENAEGEYVITSSDGIRRTNSNHYYYNYNEDDILSSSRRSSEDVY 122
Atg30S71A 68 TDNAEWILFSPENAEGEYVITSSDGIRRTNSNHYYYNYNEDDILSSSRRSSEDVY 122
Atg30WDILSSS 68 TDNSEW----------DILSSSRRSSEDVY 122
Atg30WSILSSS 68 TDNSEW----------SILSSSRRSSEDVY 122
A2
Time (h)
SD-N 0 1.5 3 6 12
Δatg30 + prGAPDH-BFP-SKL
+
ϕ
Atg30
Atg30S71A
Atg30WDILSSS
Atg30WSILSSS
α-Thiolase
A3
AD
BD
+HIS
-His + 40mM 3-AT
AD BD-Atg8
AD-Atg30 BD
AD-Atg30 BD-Atg8
AD-Atg30S71A BD-Atg8
AD-Atg30W73A F76A BD-Atg8
AD-Atg30S71E BD-Atg8
AD-Atg30S71E WSILSSS BD-Atg8
B1
Atg11
S71A S112A
AIM A11-BS
Atg30S71A-HA
Atg8
S71A S112A
AIM A11-BS
Atg30S112A-Flag
B2
ϕ
Atg30S112A-Flag
SD-N 0 1.5 3 6 12 0 1.5 3 6 12 Time (h)
Δatg30 + prGAPDH-BFP-SKL
+
Atg30-HA
Atg30W73A F76A-HA
Atg30S71A-HA
α-Thiolase
C1
Atg8
Atg11
S71A S112A
AIM A11-BS
Atg30S71A S112A
C2
Time (h)
SD-N 0 1.5 3 6 12
Δatg30 + prGAPDH-BFP-SKL
+
ϕ
Atg30
Atg30S71A
Atg30S112A
Atg30S71A S112A
α-Thiolase

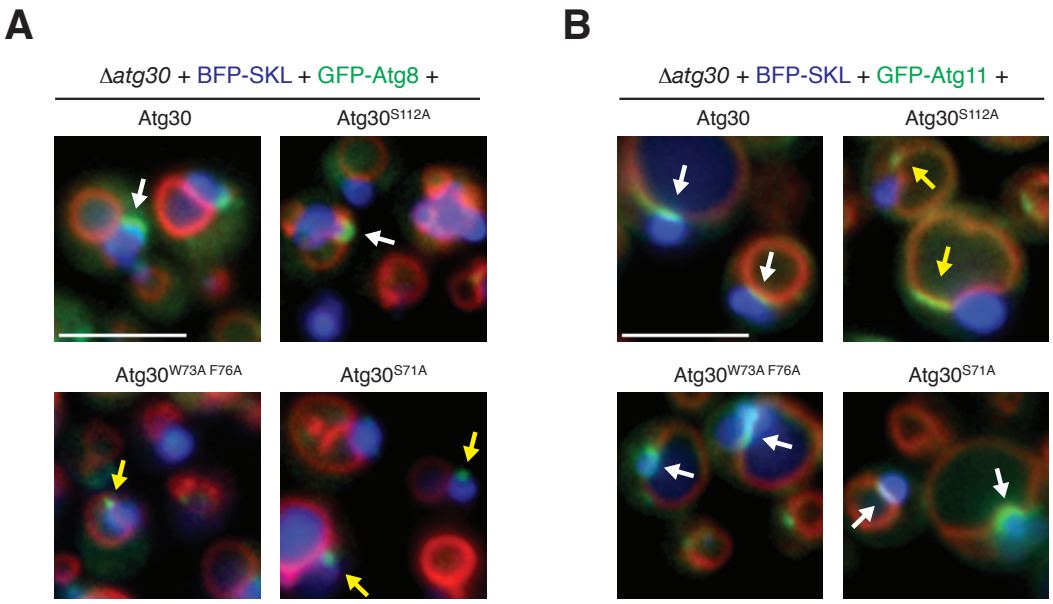

Figure 3-3: Atg8 and Atg11 localization during pexophagy. (A) Large phagophore membrane formation in WT and the Atg30 mutant cells monitored by GFP-Atg8 during pexophagy conditions. (B) Localization of GFP-Atg11 during pexophagy of methanol-induced peroxisomes in cells expressing WT or mutant Atg30 proteins. White arrows indicate correct localization and, yellow arrows indicate mislocalization or in case of Atg8 localization, indicate absence of phagophore membrane elongation. Peroxisomes were labeled with BFP-SKL and vacuoles with FM4-64. Scale bar: 5 μm.

Figure 3-4: Atg32, ScAtg32 and Atg36 use similar interaction mechanisms as Atg30. (A) Mitophagy experiments of WT (PPY12), Δ*atg5*, Δ*atg32* (ϕ), and Δ*atg32* complemented with wild-type Atg32 (Atg32), Atg32 with a deletion of the sequence between the AIM and phosphosite required for Atg11 binding (Atg32^{WQVLSSS}), Atg32 AIM mutant (Atg32$^{W121A\ V124A}$), mutants of the Thr upstream of the Atg32 AIM (Atg32^{T119A}) and mutants altered in the Ser required for Atg11 binding (Atg32^{S159A}). The cells were grown in YPL medium and shifted to SD-N. Mitophagy was followed by the transport of Tom20-mCherry to the vacuole by fluorescence microscopy. Mitophagy was classified as – no mitophagy, + few cells show mitophagy, +++ most cells show mitophagy and ++++ almost all the cells show mitophagy (the intensity and numbers of cells containing Tom20-mCherry in the vacuole was considered). Scale bar: 5 μm. (B) *P. pastoris* Ä*atg32* cells (ΔPp*atg32*) expressing Tom20-GFP and expressing the indicated Atg32 mutants were cultured in YPL medium for 12, 18 and 36 h. Mitophagy was monitored by GFP appearance by immunoblotting with α-GFP antibodies. (C) N-terminal sequence of Atg36 manually-aligned against the multiple sequence alignments of Atg30, Atg32 and ScAtg32. Identical residues are indicated with black boxes, and similar residues with grey boxes. (D) Two-hybrid protein-protein interaction analysis of ScAtg36, ScAtg8 and ScAtg11. The receptors were mutated at the AIM (Atg36$^{F33A\ L36A}$), at Serine(s) upstream of the AIM (Atg36^{S31A}) and at the Atg11-binding site (Atg36^{S97A}). (E) *S. cerevisiae* Δ*atg36* cells (ΔSc*atg36*) expressing Thiolase-GFP and expressing the indicated Atg36 mutants were cultured in oleate medium until mid-log growth and then shifted to SD-N. Pexophagy was monitored by GFP appearance by immunoblotting with α-GFP antibodies. (F) Yeast Three-Hybrid analysis of ScAtg36 with ScAtg8 and ScAtg11. The Y3H technology is based on the yeast two-hybrid system but with the co-expression of third protein as a competitor and indicated in the figure (NLS-ScAtg11 or NLS-ScAtg8). The positive control was the ScAtg36 mutant affected in Atg11 binding (ScAtg36^{S97A}) or in Atg8 binding (ScAtg36^{S31A}), which should be unaffected by the competition of NLS-ScAtg11 or NLS-ScAtg8, respectively. Appropriate auto-activation and interaction controls were also included.

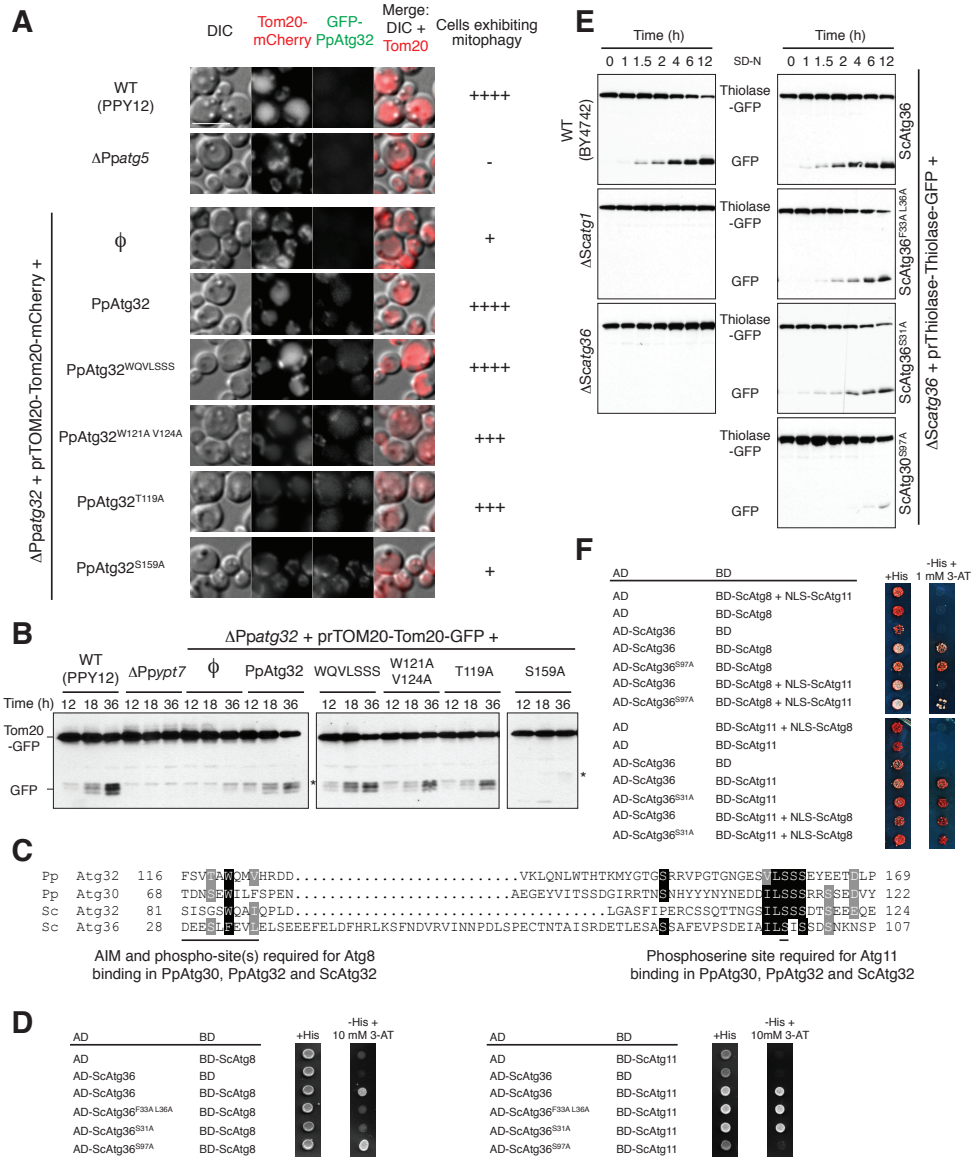
A
DIC
Tom20-mCherry
GFP-PpAtg32
Merge: DIC + Tom20
Cells exhibiting mitophagy
WT (PPY12)
ΔPpatg5
ϕ
PpAtg32
PpAtg32WQVLSSS
PpAtg32W121A V124A
PpAtg32T119A
PpAtg32S159A
ΔPpatg32 + prTOM20-Tom20-mCherry +
++++
-
+
++++
++++
+++
+++
+
B
ΔPpatg32 + prTOM20-Tom20-GFP +
WT (PPY12)
ΔPpypt7
ϕ
PpAtg32
WQVLSSS
W121A V124A
T119A
S159A
Time (h)
12 18 36
Tom20-GFP
GFP
C
Pp Atg32 116 FSVLAWQMHRDD.....VKLQNLWTHTKMYGTGSRRVPGTGNGESVLSSSEYEETTLP 169
Pp Atg30 68 TDNSPWILFSPEN.....AEGEYVITSSDGIRRTNSNHYYYNYNEDDILSSSRRSSEEVY 122
Sc Atg32 81 SISGSWQALQPLD.....LGASFIPERCSSQTTNGSILSSSDTSEELQE 124
Sc Atg36 28 DEESLFEVLELSEEEFELDFHRLKSFNDVRVINNPDLSPECTNTAISRDETLESASSAFEVPSDEIAILSISSDSNKNSP 107
AIM and phospho-site(s) required for Atg8 binding in PpAtg30, PpAtg32 and ScAtg32
Phosphoserine site required for Atg11 binding in PpAtg30, PpAtg32 and ScAtg32
D
AD
BD
+His
-His + 10 mM 3-AT
AD
BD-ScAtg8
AD-ScAtg36
BD
AD-ScAtg36
BD-ScAtg8
AD-ScAtg36F33A L36A
BD-ScAtg8
AD-ScAtg36S31A
BD-ScAtg8
AD-ScAtg36S97A
BD-ScAtg8
AD
BD-ScAtg11
AD-ScAtg36
BD
AD-ScAtg36
BD-ScAtg11
AD-ScAtg36F33A L36A
BD-ScAtg11
AD-ScAtg36S31A
BD-ScAtg11
AD-ScAtg36S97A
BD-ScAtg11
+His
-His + 10mM 3-AT
E
Time (h)
0 1 1.5 2 4 6 12
SD-N
WT (BY4742)
ΔScatg1
ΔScatg36
Thiolase-GFP
GFP
ScAtg36
ScAtg36F33A L36A
ScAtg36S31A
ScAtg30S97A
ΔScatg36 + prThiolase-Thiolase-GFP +
F
AD
BD
+His
-His + 1 mM 3-AT
AD
BD-ScAtg8 + NLS-ScAtg11
AD
BD-ScAtg8
AD-ScAtg36
BD
AD-ScAtg36
BD-ScAtg8
AD-ScAtg36S97A
BD-ScAtg8
AD-ScAtg36
BD-ScAtg8 + NLS-ScAtg11
AD-ScAtg36S97A
BD-ScAtg8 + NLS-ScAtg11
AD
BD-ScAtg11 + NLS-ScAtg8
AD
BD-ScAtg11
AD-ScAtg36
BD
AD-ScAtg36
BD-ScAtg11
AD-ScAtg36S31A
BD-ScAtg11
AD-ScAtg36
BD-ScAtg11 + NLS-ScAtg8
AD-ScAtg36S31A
BD-ScAtg11 + NLS-ScAtg8

The text of Chapter 2 has been published in the journal *EMBO Molecular Medicine,* volume 6, pages 551-566. The candidate made Figure 2-4E and Figure 2-S1, carried out the experiment for Figure 2-S10. In addition, major contributions were made to the writing of the manuscript.

References

1. Farre, J. C., Krick, R., Subramani, S., and Thumm, M. (2009) Turnover of organelles by autophagy in yeast. *Curr Opin Cell Biol* **21**, 522-530

2. Johansen, T., and Lamark, T. (2011) Selective autophagy mediated by autophagic adapter proteins. *Autophagy* **7**, 279-296

3. Scott, S. V., Guan, J., Hutchins, M. U., Kim, J., and Klionsky, D. J. (2001) Cvt19 is a receptor for the cytoplasm-to-vacuole targeting pathway. *Mol Cell* **7**, 1131-1141

4. Farre, J. C., Manjithaya, R., Mathewson, R. D., and Subramani, S. (2008) PpAtg30 tags peroxisomes for turnover by selective autophagy. *Dev Cell* **14**, 365-376

5. Kanki, T., Wang, K., Cao, Y., Baba, M., and Klionsky, D. J. (2009) Atg32 is a mitochondrial protein that confers selectivity during mitophagy. *Dev Cell* **17**, 98-109

6. Okamoto, K., Kondo-Okamoto, N., and Ohsumi, Y. (2009) Mitochondria-anchored receptor Atg32 mediates degradation of mitochondria via selective autophagy. *Dev Cell* **17**, 87-97

7. Motley, A. M., Nuttall, J. M., and Hettema, E. H. (2012) Pex3-anchored Atg36 tags peroxisomes for degradation in *Saccharomyces cerevisiae*. *EMBO J* **31**, 2852-2868

8. Shintani, T., Huang, W. P., Stromhaug, P. E., and Klionsky, D. J. (2002) Mechanism of cargo selection in the cytoplasm to vacuole targeting pathway. *Dev Cell* **3**, 825-837

9. Yorimitsu, T., and Klionsky, D. J. (2005) Atg11 links cargo to the vesicle-forming machinery in the cytoplasm to vacuole targeting pathway. *Mol Biol Cell* **16**, 1593-1605

10. Noda, N. N., Ohsumi, Y., and Inagaki, F. (2010) Atg8-family interacting motif crucial for selective autophagy. *FEBS Lett* **584**, 1379-1385

11. Suzuki, K., Kubota, Y., Sekito, T., and Ohsumi, Y. (2007) Hierarchy of Atg proteins in pre-autophagosomal structure organization. *Genes Cells* **12**, 209-218

12. Itakura, E., and Mizushima, N. (2010) Characterization of autophagosome formation site by a hierarchical analysis of mammalian Atg proteins. *Autophagy* **6**, 764-776

13. Aoki, Y., Kanki, T., Hirota, Y., Kurihara, Y., Saigusa, T., Uchiumi, T., and Kang, D. (2011) Phosphorylation of Serine 114 on Atg32 mediates mitophagy. *Mol Biol Cell* **22**, 3206-3217

14. Noda, N. N., Kumeta, H., Nakatogawa, H., Satoo, K., Adachi, W., Ishii, J., Fujioka, Y., Ohsumi, Y., and Inagaki, F. (2008) Structural basis of target recognition by Atg8/LC3 during selective autophagy. *Genes Cells* **13**, 1211-1218

15. Wild, P., Farhan, H., McEwan, D. G., Wagner, S., Rogov, V. V., Brady, N. R., Richter, B., Korac, J., Waidmann, O., Choudhary, C., Dotsch, V., Bumann, D., and Dikic, I. (2011) Phosphorylation of the autophagy receptor optineurin restricts *Salmonella* growth. *Science* **333**, 228-233

16. Nazarko, T. Y., Farre, J. C., and Subramani, S. (2009) Peroxisome size provides insights into the function of autophagy-related proteins. *Mol Biol Cell* **20**, 3828-3839

17. Kim, J., Kamada, Y., Stromhaug, P. E., Guan, J., Hefner-Gravink, A., Baba, M., Scott, S. V., Ohsumi, Y., Dunn, W. A., Jr., and Klionsky, D. J. (2001) Cvt9/Gsa9 functions in sequestering selective cytosolic cargo destined for the vacuole. *J Cell Biol* **153**, 381-396

18. Manjithaya, R., Jain, S., Farre, J. C., and Subramani, S. (2010) A yeast MAPK cascade regulates pexophagy but not other autophagy pathways. *J Cell Biol* **189**, 303-310

19. Kanki, T., Kang, D., and Klionsky, D. J. (2009) Monitoring mitophagy in yeast: the Om45-GFP processing assay. *Autophagy* **5**, 1186-1189

20. Farre, J. C., Mathewson, R. D., Manjithaya, R., and Subramani, S. (2010) Roles of *Pichia pastoris* Uvrag in vacuolar protein sorting and the phosphatidylinositol 3-kinase complex in phagophore elongation in autophagy pathways. *Autophagy* **6**, 86-99

Chapter 3: Supplementary Information

Methods

Media used to grow strains include: YPD (2% glucose, 2% bacto-peptone, 1% yeast extract); YNB (0.17% yeast nitrogen base without amino acids and ammonium sulfate, 0.5% ammonium sulfate); nitrogen starvation medium or SD-N (0.17% yeast nitrogen base without amino acids and ammonium sulfate; 2% glucose); oleate medium for *P. pastoris* (YNB; 0.079% complete supplement mixture [CSM], 0.05% yeast extract, 0.02% Tween-40, 0.2% oleate), oleate medium for *S. cerevisiae* (1% oleate, 5% Tween-40, 0.25% yeast extract, 0.5% peptone, and 5 mM phosphate buffer) and methanol medium (YNB; 0.079% CSM, 0.05% yeast extract, 0.5% methanol); YPL (2% lactic acid, 2% bacto-peptone, 1% yeast extract, pH 5.5). All cultures were grown at 30°C.

In silico analysis

Atg30 and ScAtg32 protein sequences were used as queries in Standard Protein BLAST analyses on dataset of the non-redundant (nr) protein sequences, using default parameters and the algorithm PSI-BLAST (Position-Specific Iterated BLAST) at the National Center for Biotechnology Information (NCBI). The organism names, abbreviations and GenBank accession numbers of Atg30 homologs are the following: *Candida boidinii* (*Cb*, BAL15150), *Clavispora lusitaniae* (*Cl*, EEQ38313), *Spathaspora passalidarum* (*Sp*, EGW35335), *Candida tropicalis* (*Ct*, EER31772), *Millerozyma farinosa* (*Mf*, CCE81513), *Meyerozyma guilliermondii* (EDK37477), *Candida parapsilosis* (*Cp*, CCE40725), *Candida dubliniensis* (*Cd*, CAX44784), *Lodderomyces elongisporus* (*Le*, EDK43552), *Scheffersomyces stipitis* (*Ss*, EAZ63411), *Candida albicans* (*Ca*, EEQ42629), *Debaryomyces hansenii* (*Dh*, CAG86787), *Candida tenuis* (*Cte*, EGV64948) and *Hansenula polymorpha* (*Hp*, EFW95627). The Atg32 homologs: *Hansenula polymorpha* (EFW94927), *Pichia pastoris* (*Pp*, CAY71556), *Kluyveromyces lactis* (*Kl*, CAH02615), *Zygosaccharomyces rouxii* (*Zr*, CAR29352), *Ashbya gossypii* (*Ag*, AAS53654), *Candida glabrata* (*Cg*, CAG60013), *Vanderwaltozyma polyspora* (*Vp*, EDO18565), *Tetrapisispora phaffii* (*Tp*,

CCE63093), *Lachancea thermotolerans* (*Lt*, CAR23100), *Torulaspora delbrueckii* (*Td*, CCE90351), *Kazachstania africana* (*Ka*, CCF57872), *Eremothecium cymbalariae* (*Ec*, AET39104), *Naumovozyma castellii* (*Nc*, CCC70913), *Scheffersomyces stipitis* (ABN68377), *Spathaspora passalidarum* (EGW34613), *Candida tropicalis* (EER35239), *Debaryomyces hansenii* (CAG88355), *Millerozyma farinosa* (CCE81282) and *Clavispora lusitaniae* (EEQ41615). Multiple sequence alignments were done using ClustalW2 and manually adjusted if required. The sequence logo was obtained using the combined multiple sequence alignments of all Atg30 and Atg32 homologs in the GenBank database (up to Nov 2011, described the supplementary information) and the default setup of the WebLogo server (http://weblogo.berkeley.edu/logo.cgi).

Mobility shift detection of phosphorylated proteins

One ml of D*ypt7* D*atg30* cells expressing Atg30, Atg30^{S71A} and Atg30^{S71E} was collected after peroxisome proliferation in oleate medium for 15 h and shifted to nitrogen starvation for 30 min. and TCA precipitated. Samples were resolved in a 10% SDS-PAGE gel with 25 mM Phos-Tag acrylamide (Wako Cat. #300-93523) and 25 mM $MnCl_2$ to improve the separation of phosphoproteins. Phos-Tag acrylamide gels were treated according manufacturer's recommendation and analyzed by Western blot.

Co-immunoprecipitation with and without phosphatase treatement

A) Peroxisomes purification: 300 hundred OD of cells were grown 15-16 h in oleate medium, washed twice with dH_2O and transferred to glucose medium, SD-N at 2 OD/ml for 0.5 h. The pellet weight was used to determine the volume of Zymolase buffer (0.5 M KCl, 5 mM MOPS/KOH buffer [pH 7.2] 10 mM Na_2SO_4; 4 ml/g of cells) and concentration of Zymolase-100T (Nacalai Tesque) to add to cells (0.5 mg/1g cells). Cells were then incubated at 30°C (80 rpm for 45 min) and spheroplasts were centrifuged (2200 x g, 8 min, 4°C) before being resuspended in 1 homogenization buffer (5 mM MES/KOH [pH 5.5], 1 M Sorbitol with 10 mM NaF, 1 mM PMSF, 1 mM protease inhibitors: PIC yeast, Leupeptin and Aprotinin; 2 mL/g of cells) and subjected to 20

strokes in a Dounce homogenizer. The cell homogenate was centrifuged twice at low speed to remove cell debris (500 x g, 10 min, 4°C) and the supernatant spun at high speed (200, 000 x g, 30 min, 4°C). The pellet was retrieved and resuspended in 0.8 mL of IP lysis buffer (50 mM Tris-HCl [pH 7.5], 100 mM NaCl, 0.1 mM EDTA, 0.2% Triton X-100, and 10 mM NaF, 1 mM PMSF, 1 mM protease inhibitors: PIC yeast, Leupeptin and Aprotinin). The addition of 250 µl acid-washed glass beads and vortexing (1 min x 5 times) lysed the peroxisome fraction, which was further solubilized with rotation (30 min, 4°C). The supernatant was recovered after centrifugation (20, 000 x g, 10 min, 4°C) and total protein concentration was measured using the Bradford assay. The supernatant was diluted to 200 µg of protein in 1mL with IP lysis buffer; 10 µl of sample was used for the input lane (Input). (B) Co-immunoprecipitation: 100 µl of EZ-View HA-beads (Sigma) were added to the supernatant containing 200 µg of protein in 1 ml and rotated for 16 hr, 4°C. The samples were either washed four times with IP lysis buffer (5 mL for 10 min) or were further phosphatase treated. HA-Beads after the wash were resuspended in 100 µL of 1% SDS and 1x loading buffer and boiled at 100°C for 10 min to elute, followed by SDS-PAGE and immunoblotting.(C) Lambda Protein Phosphatase (λPP) treatment: the protein complex purified using EZ-View HA-beads from D*atg30* cells, with or without Atg30-HA expression, was collected in duplicate and washed once with 5 ml of IP lysis buffer and twice with 500 ml of NEBuffer for PMP (50 mM HEPES, 100 mM NaCl, 2 mM DTT, 0.01% Brij 35, pH 7.5). The HA-bead complex was resuspended in 50 ml of NEBuffer for PMP with 1.5 ml of λPP (+; NEB, 400,000 U/ml) and without λPP (-), and incubated at 30°C for 1 h. To stop the reaction and clean the HA-bead complex, two 5 ml short washes with IP lysis buffer, as well as two 5 ml washes for 10 min with IP lysis buffer were used. Finally, samples were eluted with 100 ml of 1% SDS and 1x loading buffer, boiled and subjected to SDS-PAGE and immunoblotting.

Proteins purification and sequencing

A) Proteins purification: HA-tagged Atg30, mutated at position 81 (A81R) to reduce the size of the tryptic peptide encompassing S71 (from 33 to 20 aa), was expressed in D*atg30* cells. Cells

were grown overnight on oleate medium and transferred for 30 min into SD-N before extraction. Atg30-HA purification was performed from 3000 OD equivalents of yeast cells. The cells pellet was washed in phosphate-buffered saline (pH 7.4) and lysed with 5 mL of glass beads (vortexed 5 times for 2 min at 4°C) in 20 ml IP lysis buffer (50 mM Tris-HCl, pH 7.5, 100mM NaCl, 0.1mM EDTA, 0.2% Triton X-100, 10 mM NaF, 1mM PMSF, 1mM protease inhibitors cocktail: PIC yeast, Leupeptin and Aprotinin). The cells debris was removed by centrifugation at low speed (500 × g, 10 min). The membrane protein solubilization was performed by incubation of the supernatant at 4°C for 1 h with rotation followed by centrifugation (21,000 × g, 10 min). One mL of EZ-View HA-beads (Sigma) was added to the supernatant and incubated overnight. Beads were washed five times with 10 mL of the IP lysis buffer for 5 min and three times with 5 mL of 50 mM HEPES pH 7.2. B) Mass spectrometry: proteins bound to EZ-View HA-beads were digested with 0.5 µg trypsin at 37°C overnight. Phosphopeptides were enriched by metal oxide affinity capture (CeO2) and analyzed by 2D LC MS/MS using an LTQ tandem mass spectrometer.

An Agilent 1200 HPLC system (Agilent Technologies) delivered a flow rate of 600 nL min^{-1} to a 3-phase capillary chromatography column through a splitter. Using a custom pressure cell, 5 µm Zorbax SB-C18 (Agilent) was packed into fused silica capillary tubing (250 µm ID, 360 µm OD, 30 cm long) to form the first dimension reverse phase column (RP1). A 5 cm long strong cation exchange (SCX) column packed with 5 µm PolySulfoethyl (PolyLC) was connected to RP1 using a zero dead volume 1 µm filter (Upchurch, M548) attached to the exit of the RP1 column. A fused silica capillary (200 µm ID, 360 µm OD, 20 cm long) packed with 5 µm Zorbax SB-C18 (Agilent) was connected to SCX as the analytical column (RP2). The electrospray tip of the fused silica tubing was pulled to a sharp tip using a laser puller (Sutter P-2000). The peptide mixtures were loaded onto the RP1 column using the custom pressure cell. Peptides were first eluted from the RP1 column to the SCX column using a 0 to 80% acetonitrile gradient for 150 min. The peptides were then fractionated by the SCX column using a series of salt gradients (from 5 mM to 1 M ammonium acetate for 20 min), followed by high resolution reverse phase separation using an acetonitrile gradient of 0 to 80% for 120 min.

Spectra were acquired on LTQ-XL linear ion trap tandem mass spectrometers (Thermo Electron Corporation, San Jose, CA) employing automated, data dependent acquisition. The mass spectrometer was operated in positive ion mode with a source temperature of 250 °C. As a final fractionation step, gas phase separation in the ion trap was employed to separate the peptides into 3 mass classes prior to scanning; the full MS scan range was divided into 3 smaller scan ranges (400–800, 800–1,200, and 1,200–2,000 Da) to improve dynamic range. Each MS scan was followed by 5 MS/MS scans of the most intense ions from the parent MS scan. A dynamic exclusion of 1 min was used to improve the duty cycle.

The raw data were extracted and searched using Spectrum Mill v4.01 (Agilent Technologies). MS/MS spectra with a sequence tag length of 1 or less were considered to be poor spectra and were discarded. The remaining MS/MS spectra were searched against NCBI non-redundant protein database limited to *P. pastoris* taxonomy. The enzyme parameter was limited to full tryptic peptides with a maximum mis-cleavage of 1. All other search parameters were set to SpectrumMill's default settings (carbamidomethylation of cysteines, +/- 2.5 Da for precursor ions, +/- 0.7 Da for fragment ions, and a minimum matched peak intensity of 50%). Ox-Met, n-term pyro-Gln, and phosphorylation on Serine, Threonine, or Tyrosine were defined as variable modifications. A maximum of 2 modifications per peptide was used. Spectra with score of 10 or higher were manually inspected. Phosphorylation sites were localized to a particular amino acid within a peptide using the variable modification localization (VML) score in Agilent's Spectrum Mill software (1).

Figure 3-S1: Non-conserved and non-functional AIM in Atg30. (A) Multiple sequence alignments of Atg30 homologs (identical residues are indicated with black boxes and similar residues with grey boxes). Sequences, accession numbers, abbreviation of organism names and methodology used for the alignments are in Materials and Methods. Red box indicates a putative AIM in Atg30. (B) Pexophagy assay by fluorescence microscopy analysis of methanol-induced peroxisomes labeled with BFP-SKL and Atg30-GFP. ϕ: Δ*atg30*; Atg30: WT; Atg30$^{Y330A\ L333A}$: putative AIM mutant. Vacuoles are labeled with FM4-64. Scale bar: 5 μm.

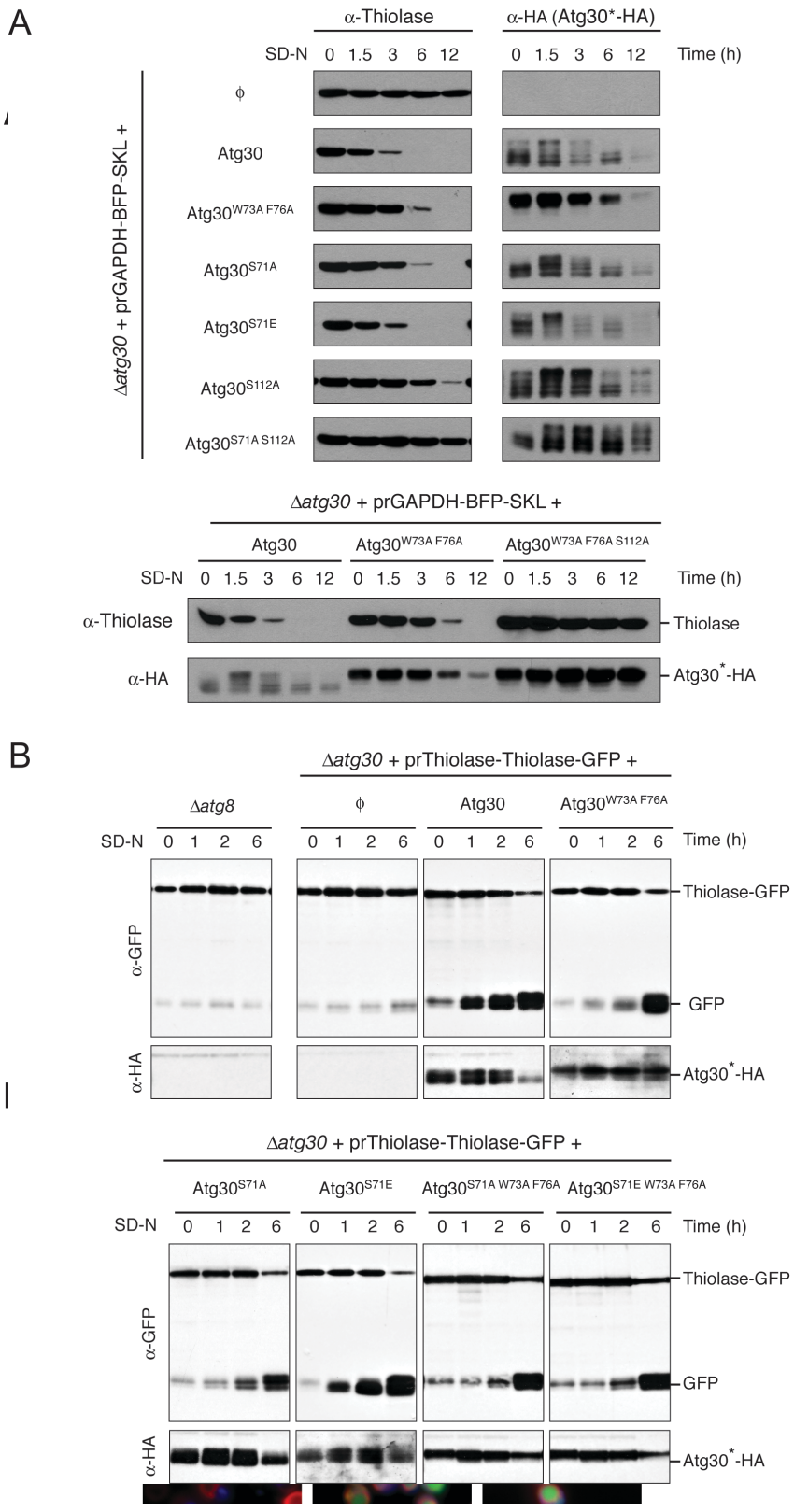
A
α-Thiolase
α-HA (Atg30*-HA)
SD-N 0 1.5 3 6 12
0 1.5 3 6 12 Time (h)
Δatg30 + prGAPDH-BFP-SKL +
ϕ
Atg30
Atg30W73A F76A
Atg30S71A
Atg30S71E
Atg30S112A
Atg30S71A S112A
Δatg30 + prGAPDH-BFP-SKL +
Atg30
Atg30W73A F76A
Atg30W73A F76A S112A
SD-N 0 1.5 3 6 12 0 1.5 3 6 12 0 1.5 3 6 12 Time (h)
α-Thiolase
Thiolase
α-HA
Atg30*-HA
B
Δatg30 + prThiolase-Thiolase-GFP +
Δatg8
ϕ
Atg30
Atg30W73A F76A
SD-N 0 1 2 6 0 1 2 6 0 1 2 6 0 1 2 6 Time (h)
α-GFP
Thiolase-GFP
GFP
α-HA
Atg30*-HA
Δatg30 + prThiolase-Thiolase-GFP +
Atg30S71A
Atg30S71E
Atg30S71A W73A F76A
Atg30S71E W73A F76A
SD-N 0 1 2 6 0 1 2 6 0 1 2 6 0 1 2 6 Time (h)
α-GFP
Thiolase-GFP
GFP
α-HA
Atg30*-HA

C

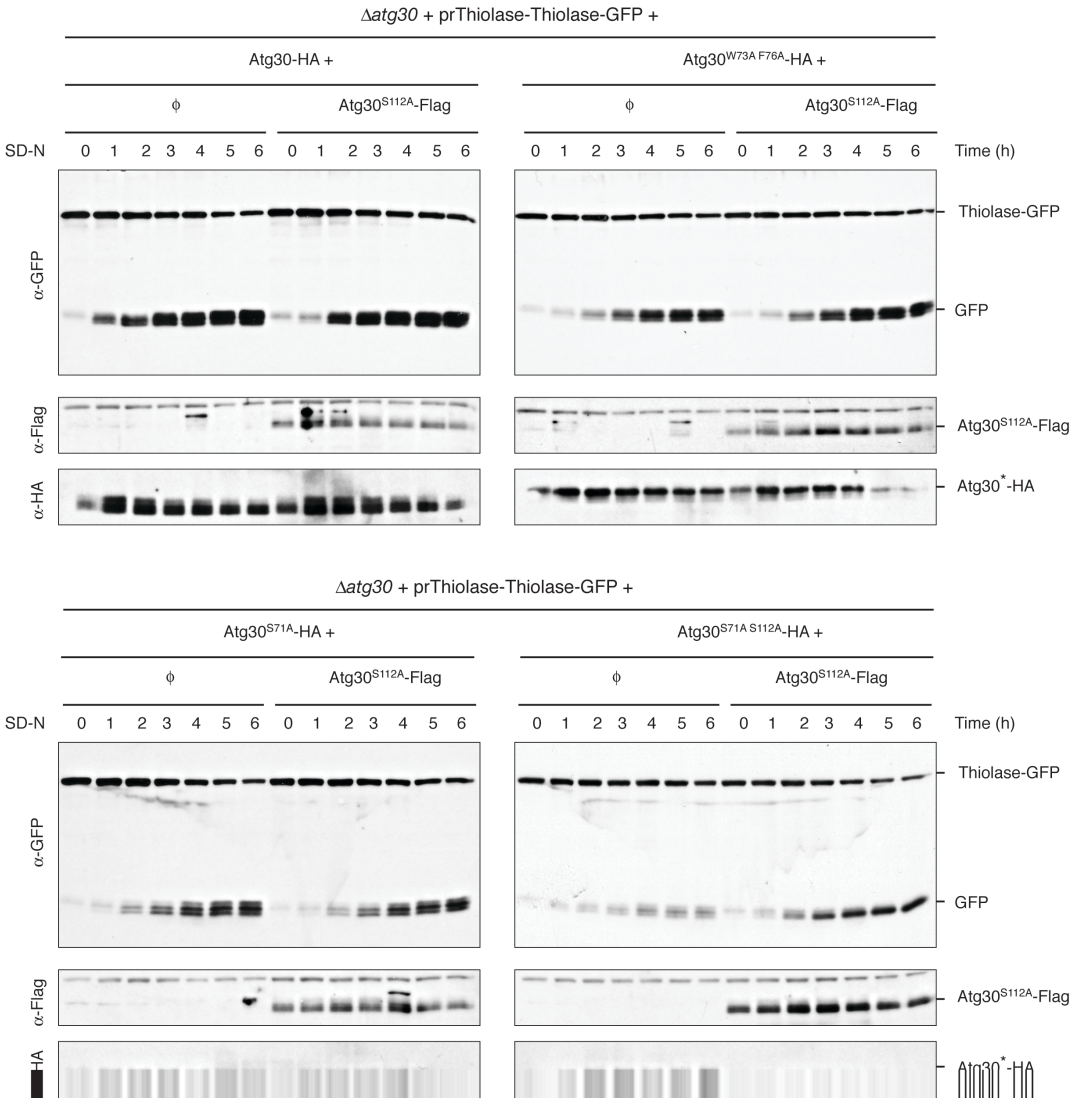

Figure 3-S2: Pexophagy experiments monitored by degradation of thiolase. (A) or by appearance of free GFP (B and C). Degradation of oleate-induced peroxisomes was stimulated by shifting cells to SD-N. The presence of the specified proteins was examined by immunoblotting using a-*Sc*thiolase, a-GFP, a-HA and/or a-Flag antibody. (A) Pexophagy in D*atg30* (f), WT (Atg30) and Atg30 mutants was monitored by thiolase levels. (B and C) Pexophagy was monitored by appearance of free GFP. *: Atg30 wild-type or mutant forms.

Figure 3-S3: Phosphorylation of S71 in the Atg30 protein. (A) Mobility shift detection of Atg30 and Atg30 phosphomutants ($Atg30^{S71A}$ and $Atg30^{S71E}$) proteins. Phosphorylated molecules were separated using Phos-tag acrylamide as described in the Methods section of Supplementary information. Cells were grown in oleate medium for 15 h and shifted to SD-N for 30 min. Ponceau S staining and Atp2 were used as a loading control. Red arrow indicates a band absent in $Atg30^{S71A}$. (B) Table containing result of Spectrum Mill search result of S71 phospho-peptide. SPI (%): Score Peak Intensity. VML: Variable Modification Localization score [1]. The site is considered localized when VML > 1.1. *: / = y ions; | = both b and y ions. (C) MS2 spectra revealing the S71 phospho-peptide.

A

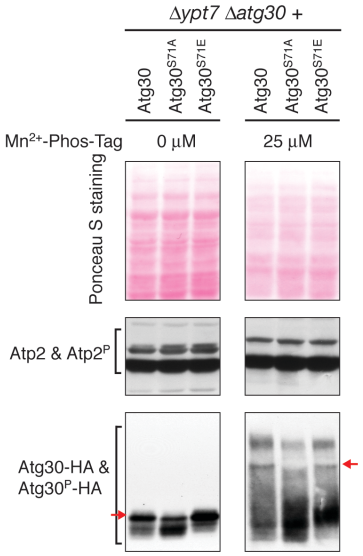

B

Rank	Score	SPI (%)	VML	Variable sites	Sequence
1	10.41	60.7	1.3	S71s	(R) T S S I L T/D N s E W/I|L|F/S|P E N R (E) *

C

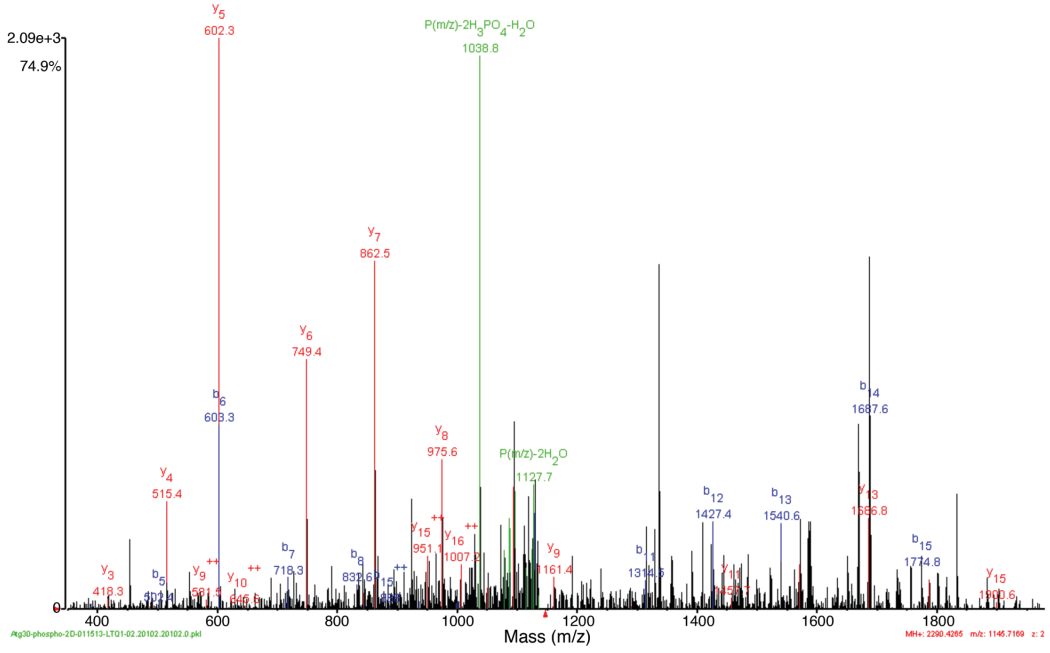

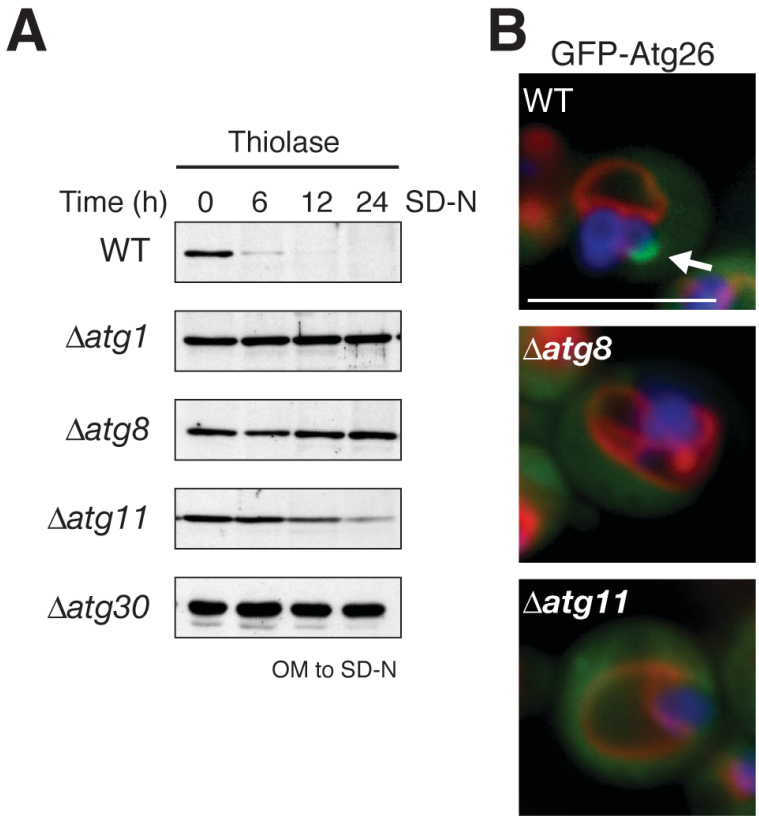

Figure 3-S4: Atg8 and Atg11 are indispensable for pexophagy. (A) Pexophagy experiments of oleate-induced peroxisomes shifted to SD-N followed by degradation of thiolase. (B) Large phagophore membrane formation in WT, Δ*atg8* and Δ*atg11* cells monitored with GFP-Atg26 during pexophagy upon switch from methanol to SD-N (9).

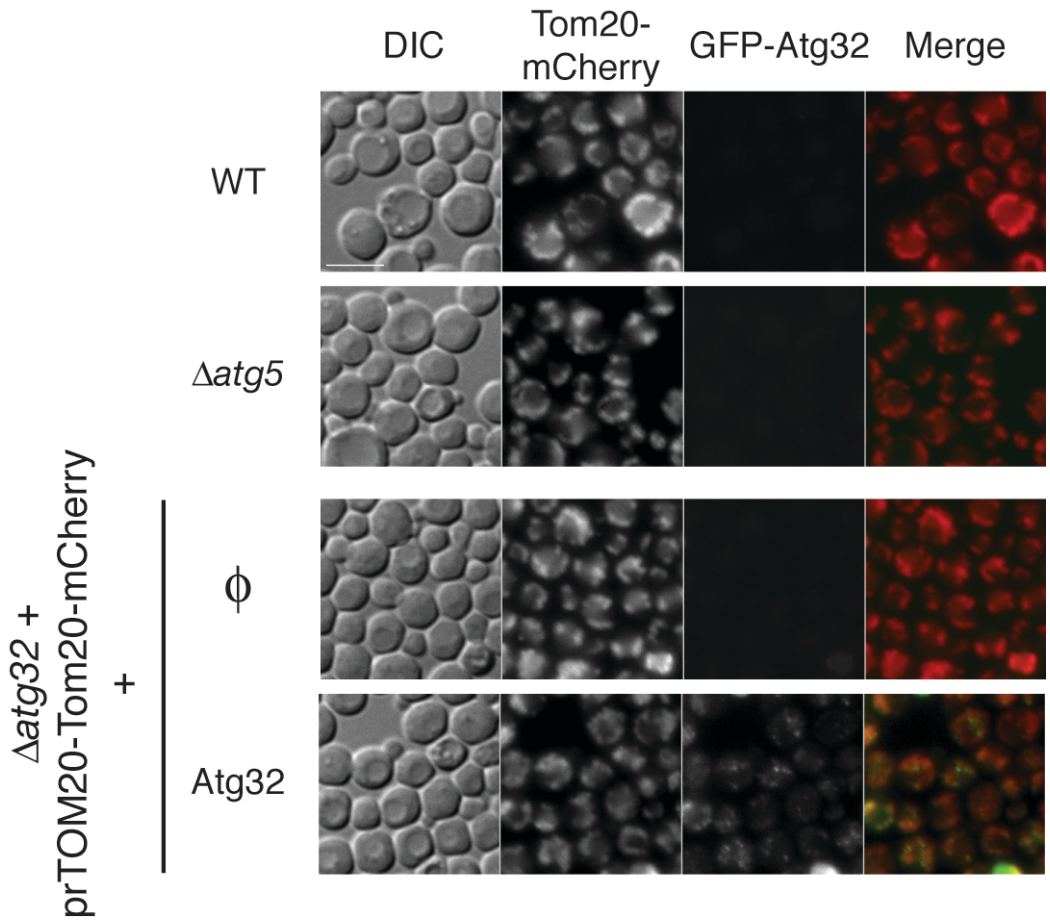

Figure 3-S5: The *P. pastoris* Atg32 localizes on mitochondria. Cells grown in YPL medium for 12 h. The fusion protein, GFP-Atg32, colocalized with Tom20-mCherry at the mitochondria. prTOM represents the promoter of the *TOM20* gene. Scale bar: 5 μm.

A

B

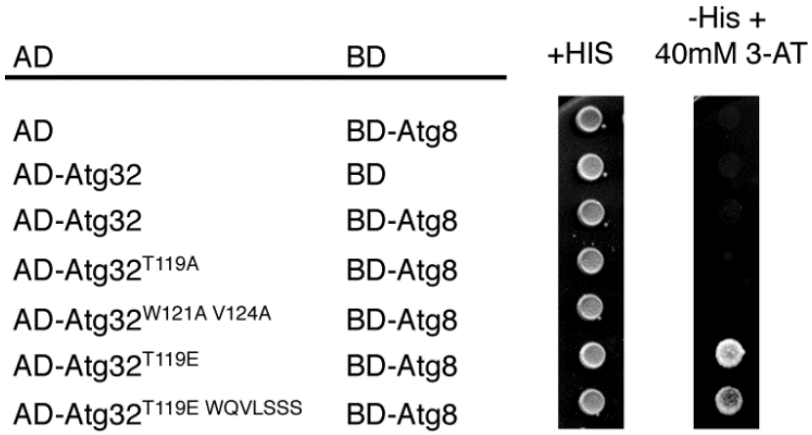

Figure 3-S6: Interactions between *P. pastoris* Atg32 and Atg8. (A) Atg32 sequences from aa 116-169 of wild-type (Atg32), the T119A mutant, the AIM mutant (Atg32$^{W121A\ V124A}$), the S159A mutant (Atg32^{S159A}) affecting the Atg11 binding site and a deletion of the sequence between the AIM and phosphosite required for Atg11 binding in Atg32 (Atg32^{WQVLSSS}). (B) Two-hybrid assays between Atg32 wild-type or mutants and Atg8. Phosphomimic T119E was included in Atg32^{WQVLSSS} to detect the interaction with Atg8 because this site on the heterologous protein is not phosphorylated in *S. cerevisiae*.

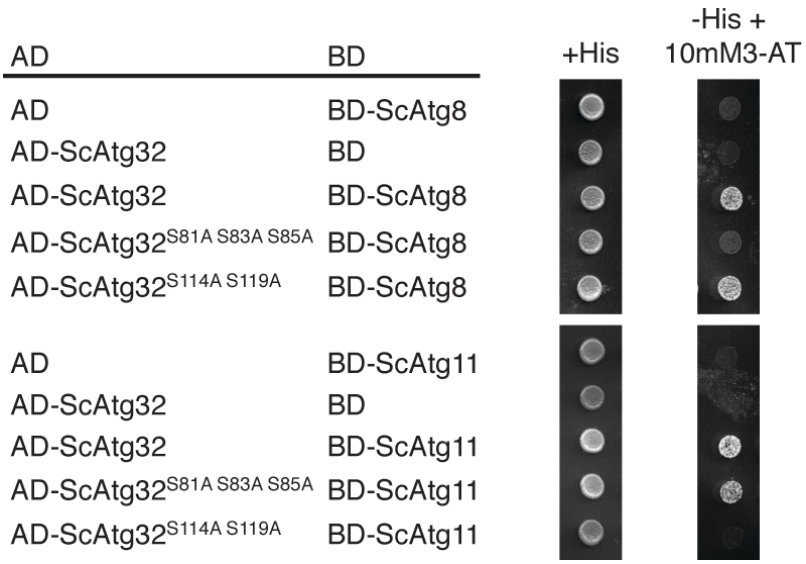

Figure 3-S7: Two-hybrid protein-protein interaction analysis of ScAtg32, ScAtg8 and ScAtg11. The receptor was mutated at Serine(s) upstream of the AIM (ScAtg32$^{S81A\ S83A\ S85A}$) and at the Atg11-binding site (ScAtg32$^{S114A\ S119A}$).

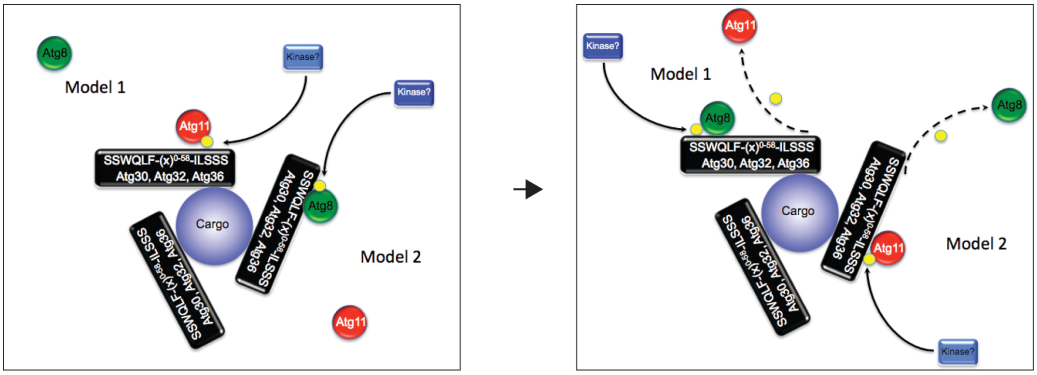

Figure 3-S8: Model for interactions between autophagy receptors and the core autophagic machinery. See text for details.

Table 3-S1: *Pichia pastoris* strains

Description	Strain	Genotype	Reference
	GS115	*his4*	[3]
WT	PPY12	*his4, arg4*	[4]
D*atg1*	R12	GS115 D*atg1::Zeocin*	[5]
D*atg5*	Sjcf935	PPY12 D*atg5::Zeocin*	This study
D*atg8*	Sjcf925	PPY12 D*atg8::KanMX*	[6]
D*atg11*	R8	GS115 D*atg11::Zeocin*	[7]
D*atg30*	Sjcf959	PPY12 D*atg30*::*KanMX*	This study
D*atg30*	Sjcf936	PPY12 D*atg30::Zeocin*	[6]
D*atg32*	Sjcf1715	PPY12 D*atg32::KanMX*	This study
D*ypt7*	Srrm197	PPY12 D*ypt7*::*KanMX*	[8]
D*ypt7* D*atg30*	Sjcf1736	PPY12 D*ypt7*::*KanMX* D*atg30::Zeocin*	This study

Table 3-S2: *Saccharomyces cerevisiae* strains

Strain	Description	Genotype	Reference
WT	BY4742 + Thiolase-GFP	MATa, his3D1, leu2D0, lys2D0, ura3D0, pot1::Thiolase-GFP (HIS5)	[9]
ΔSc*atg1*	Δ*atg1* + Thiolase-GFP	MATa, his3D1, leu2D0, lys2D0, ura3D0, atg1::KanMX4, pot1:: Thiolase -GFP (HIS5)	[9]
ΔSc*atg36*	Δ*atg36* + Thiolase-GFP	MATa, his3D1, leu2D0, lys2D0, ura3D0, atg36::KanMX4, pot1:: Thiolase-GFP (HIS5)	This study

Table 3-S3: *Pichia pastoris* plasmid

Plasmid	Promoter	Fusion protein	Integration locus	Selectable marker
pJCF143	*ATG30*	Atg30-Flag	*ATG30*	Zeocin
pJCF208	*ATG8*	GFP-Atg8	*HIS4*	*HIS4*
pJCF213	*ATG30*	Atg30-GFP	*HIS4*	*HIS4*
pJCF291	*ATG11*	GFP-Atg11	*ARG4*	*ARG4*
pJCF388	*ATG11*	Flag-Atg11	*ARG4*	*ARG4* or Zeocin
pJCF392	*GAPDH*	GFP-Atg26	*HIS4*	*HIS4*
pJCF401	*GAPDH*	BFP-SKL	*HIS4*	*HIS4* or Geneticin
pJCF402	*GAPDH*	BFP-SKL	*ARG4*	*ARG4*
pJCF419	*ATG8*	GFP-Atg8	*HIS4*	*HIS4* or Hygromycin
pJCF523	*TOM20*	Tom20-mCherry	*ARG4*	*ARG4* or Hygromycin
pJCF592	*ATG32*	Atg32-GFP	*HIS4*	*HIS4*
pJCF648	*ATG30*	Atg30-HA	*HIS4*	*HIS4*
pJCF681	*ATG32*	Atg32-HA	*HIS4*	*HIS4*
pJCF688	*TOM20*	Tom20-GFP	*ARG4*	*ARG4* or Hygromycin
pJCF694	*ATG8*	myc-Atg8	*HIS4*	*HIS4* or Hygromycin
pJCF701	*THIOLASE*	Thiolase-GFP	*ARG4*	*ARG4*

Table 3-S4: *Saccharomyces cerevisiae* plasmids

Plasmid	Fusion protein 1	Fusion Protein 2	Background vector	Selectable marker
pJCF589-F115	BD-PpAtg8	none	pGBT9	*TRP1*
pJCF226	AD-PpAtg30	none	pGAD-GH	*LEU2*
pJCF590	AD-PpAtg32	none	pGAD-GH	*LEU2*
pJCF659	BD-ScAtg8	none	pGBT9	*TRP1*
pJCF660	BD-ScAtg11	none	pGBT9	*TRP1*
pJCF652	AD-ScAtg32	none	pGAD-GH	*LEU2*
pJCF653	AD-ScAtg36	none	pGAD-GH	*LEU2*
pJCF800	AD-ScAtg8	none	pGBT9	*TRP1*
pJCF801	BD-ScAtg8	NLS-ScAtg11	pBridge	*TRP1*
pJCF804	BD-ScAtg11	NLS-ScAtg8	pBridge	*TRP1*
pJCF805	HA-ScAtg36	none	pRS415	*LEU2*

The text of Chapter 3 has been published in the journal *EMBO Reports,* volume 14, pages 441-449. The candidate contributed to the immunoprecipitations in Figure 3-1, the *S. cerevisiae* pexophagy assays in the paper, Fig 3-S3A. In addition, major contributions were made to the writing of the manuscript.

References

1. Chalkley RJ, Clauser KR (2012) Modification site localization scoring: strategies and performance. *Mol Cell Proteomics* **11:** 3-14

2. Oku M, Warnecke D, Noda T, Muller F, Heinz E, Mukaiyama H, Kato N, Sakai Y (2003) Peroxisome degradation requires catalytically active sterol glucosyltransferase with a GRAM domain. *EMBO J* **22:** 3231-3241

3. Cregg JM, Barringer KJ, Hessler AY, Madden KR (1985) *Pichia pastoris* as a host system for transformations. *Mol Cell Biol* **5:** 3376-3385

4. Gould SJ, McCollum D, Spong AP, Heyman JA, Subramani S (1992) Development of the yeast *Pichia pastoris* as a model organism for a genetic and molecular analysis of peroxisome assembly. *Yeast* **8:** 613-628

5. Stromhaug PE, Bevan A, Dunn WA, Jr. (2001) GSA11 encodes a unique 208-kDa protein required for pexophagy and autophagy in *Pichia pastoris*. *J Biol Chem* **276:** 42422-42435

6. Nazarko TY, Farre JC, Subramani S (2009) Peroxisome size provides insights into the function of autophagy-related proteins. *Mol Biol Cell* **20:** 3828-3839

7. Kim J (2001) Cvt9/Gsa9 functions in sequestering selective cytosolic cargo destined for the vacuole. *J Cell Biol* **153:** 381-396

8. Manjithaya R, Anjard C, Loomis WF, Subramani S (2010) Unconventional secretion of *Pichia pastoris* Acb1 is dependent on GRASP protein, peroxisomal functions, and autophagosome formation. *J Cell Biol* **188:** 537-546

9. Saleem RA, Knoblach B, Mast FD, Smith JJ, Boyle J, Dobson CM, Long-O'Donnell R, Rachubinski RA, Aitchison JD (2008) Genome-wide analysis of signaling networks regulating fatty acid-induced gene expression and organelle biogenesis. *J Cell Biol* **181:** 281-292

Chapter 4: Activation of pexophagy receptor Atg30 by Pex3

Abstract

Pexophagy is a process that selectively degrades peroxisomes by autophagy. The *Pichia pastoris* pexophagy receptor, Atg30, is recruited to peroxisomes during peroxisome proliferation conditions. During pexophagy, Atg30 undergoes phosphorylation, a pre-requisite for its interactions with the autophagy scaffold protein, Atg11, and the ubiquitin-like protein, Atg8. Atg30 is subsequently shuttled to the vacuole along with the targeted peroxisome for degradation. Here, we defined the binding site for Atg30 on the peroxisomal membrane protein (PMP), Pex3, and uncovered a role for Pex3 in the activation of Atg30 via phosphorylation, and in the recruitment of Atg11 to the receptor protein complex (RPC). Pex3 is classically a docking protein for other proteins that affect peroxisome biogenesis, division and segregation. We conclude that Pex3 has a role beyond simple docking of Atg30 and that its interaction with Atg30 regulates pexophagy in the yeast *P. pastoris*.

Introduction

Autophagy exists in yeasts, plants and mammalian cells as a homeostatic regulator for the destruction of superfluous or damaged cytosolic components or organelles and its dysregulation has implications in many diseases (1,2). Autophagy is referred as a non-selective bulk degradation process (3,4). However, many selective types of autophagy have been described that lead to the elimination of specific organelles or protein aggregates. All the autophagy-related pathways share common components, which can be broken down into the following steps: phagophore assembly site (PAS) organization, elongation of the phagophore membrane around the cargo, vesicle formation to generate an autophagosome, fusion of the autophagosome with the vacuole (lysosome in mammals) and degradation of the cargo by vacuolar (lysosomal) hydrolases (5). Autophagy-related (Atg) proteins involved in the formation of the autophagosome are considered as the core autophagic machinery. Selective autophagy

requires additional factors. Cargo selection is achieved by specific autophagy receptor proteins interacting both with the cargo and the autophagic machinery (6). Receptors have been described in yeast for the cytoplasm-to-vacuole targeting (Cvt) pathway (Atg19, Atg34), the selective autophagy of mitochondria (called mitophagy) (Atg32) and peroxisomes (pexophagy) (*P. pastoris* (*Pp)* Atg30 and *Saccharomyces cerevisiae (Sc)* Atg36) (7-11). The organelle selective autophagy receptors localize to their respective cargo surfaces and upon phosphorylation by kinases (casein kinase 2 for Atg32 (12), Hrr25 for Atg19 (13) and Atg36 (14) and an unknown kinase for Atg30) are then able to interact with the scaffold protein, Atg11, and an ubiquitin-like component of the PAS and phagophore, Atg8, in a random-sequential manner (15). In addition, Atg30 interacts with others autophagy proteins at the RPC, such as the scaffold protein, Atg17, and the acyl-CoA binding protein, Atg37, as well as two PMPs, Pex3 and Pex14 (16,17).

Peroxisomes are single-membrane bound organelles that perform essential cellular functions such as ß-oxidation of fatty acids and detoxification of reactive oxygen species. Peroxisome biogenesis factors or peroxins (encoded by *PEX* genes) are responsible for the biogenesis of the peroxisomal membrane and for the delivery of proteins carrying peroxisomal targeting signals (PTS1 and PTS2) to the organelle matrix (18). Biogenesis of the peroxisome membrane requires Pex3 and Pex19 in all species and additionally requires Pex16 in mammals (19).

Pex3 has a dynamic role at the peroxisome membrane, binding to many proteins and serving as a master regulator of peroxisome dynamics. Pex3 regulates peroxisome biogenesis by acting as a docking factor for Pex19, the protein that recognizes the membrane peroxisomal targeting signal (mPTS) on PMPs and facilitates their post-translational insertion into the peroxisomal membrane (20-23); as a tether for the peroxisome inheritance factor, Inp1 (24,25); as the receptor for Myo2 for peroxisome segregation in *Yarrowia lipolytica* (26); and as an anchor at the peroxisomal membrane for *Pp*Atg30 and *Sc*Atg36 (10,16). Additionally, Pex3 has been implicated in pexophagy in other species, such as the methylotrophic yeast, *Hansenula polymorpha*, wherein removal of ubiquitinated Pex3 from the peroxisome membrane induced

pexophagy, and in mammals, where Pex3 overexpression induced pexophagy through an ubiquitin-dependent mechanism (27,28).

The crystal structure of human PEX3 has been determined with a peptide of PEX19 (23,29-31) elucidating the PEX3-PEX19 interaction region that is likely similar in yeast based on a high degree of conservation of Pex3. Other highly conserved domains of PEX3 have also been described: the hydrophobic domain, which may play a role in PMP-binding and peroxisome maturation; and a patch of acidic residues that does not have an assigned function (32). The Inp1 binding site on *Sc*Pex3 was also determined by mutations affecting only inheritance, while leaving biogenesis function intact (25). These data suggest that Pex3 has distinct regulatory domains that have been evolutionarily separated on the protein to maintain regulation of different processes.

Recently, pexophagy in higher eukaryotes has gained a lot of attention, and several breakthrough findings have emerged. A physiological association has been made between disease states and altered peroxisome turnover in primary endothelial cells, wherein impaired peroxisome homeostasis and function resulted from induced renal toxicity or sepsis (33). Artificial induction of pexophagy has been reported in mammalian cells by fusing ubiquitin moieties to PEX3 and PMP34 (34). NBR1 has been identified as a pexophagy receptor in mammalian cells and SQSTM1/p62 was suggested to act as the pexophagy co-receptor (35). Interestingly, the peroxisome itself may be a signaling node for general autophagy regulation as the peroxisome-localized (and peroxin-binding) tuberous sclerosis protein complex, TSC, acts in the signaling cascade to suppress mTORC1 and induce autophagy in responses to reactive oxygen species (ROS) (36). The peroxisome membrane could be the site of multiple signaling pathways.

The selective autophagy receptors in yeasts (Atg19, Atg30, Atg32 and Atg36) depend on phosphoregulation for their interactions with components of the autophagy machinery, such as Atg8 and Atg11 (15). However, the upstream regulation of signaling for these receptors at the organelle membrane level is poorly understood. Both *Pp*Atg30 and *Sc*Atg36 bind Pex3 suggesting that Pex3 is a docking site at the peroxisome membrane for both Atg30 and Atg36. In peroxisome proliferation conditions the synthesis of both Atg30 and Atg36 is up-regulated

(15,16). These proteins localize to the peroxisome membrane and are then post-translationally modified during pexophagy conditions, which require at least glucose in *P. pastoris* and also nitrogen limitation in *S. cerevisiae* (10,16). It is unclear whether the signal to degrade the peroxisome comes from the peroxisome itself. In view of the central role of Pex3 in coordinating many aspects of peroxisome dynamics, we wondered whether Pex3 might be a transducer protein that could inform the cell of nutrients or other signals regulating pexophagy. Understanding the role of Pex3 in pexophagy could provide further insight into the relationship between the targeted organelle or cargo and the selective autophagy machinery.

In this study, we report the identification of the Atg30-binding domain on *P. pastoris* Pex3. This domain is separate from other known protein-interacting domains implicated in peroxisome biogenesis. The Atg30-binding domain of Pex3 is not required to localize the pexophagy receptor to the peroxisome, but instead it affects the Atg30 phosphorylation status and the interaction of Atg30 with Atg11. Consequently, Atg11 is not targeted to the RPC and the phagophore membrane (MIPA) is not formed. We conclude that Pex3 could serve a regulatory role in pexophagy rather than just serving as a docking factor as previously described.

Experimental Procedures

Strains used and media – Yeast strains and plasmids used in this study are listed in Table 4-1. Media used to grow strains are as previously described (15,16). Yeast starvation medium, SD-N (0.17% [w/v] yeast nitrogen base without amino acids and ammonium sulfate, 2% [w/v] glucose) and methanol medium (0.67% [w/v] yeast nitrogen base without amino acids, 0.5% [v/v] methanol, supplemented with the complete supplement mixture (CSM)).

Yeast two-hybrid (Y2H) analysis – The *GAL4*-based yeast two-hybrid Matchmaker system was used (Clontech Laboratories, Inc.). Full-length *PpPEX3* was inserted into pGBKT7 (Gal4 DNA Binding Domain, BD) and subsequently the QuikChange XL Site-Directed Mutagenesis Kit (Stratagene) was used to produce the *pex3* mutant plasmids in the figure. All BD plasmids were co-transformed into Y2H Gold strain (Clontech) in a pairwise manner with full-

length *PpATG30* (inserted into pGAD-GH, Gal4 Activation Domain, AD) as seen in Fig. 4-3A. All strains were first selected on SD medium without Leu and Trp, and then streaked in duplicate on SD media without His, Leu and Trp and containing 2.5 mM 3-Amino-1,2,4-triazole (3-AT).

Peroxisome biogenesis & pexophagy assays – Peroxisome biogenesis was induced by incubation of cells in methanol media at a starting OD_{600} of 0.2. For pexophagy assay, cells were grown from 8 to 16 h in methanol media and then transferred to SD-N at an OD_{600} of 2 in order to induce pexophagy. One mL samples were prepared using TCA precipitation and analyzed by Western blot.

Fluorescence microscopy – Pexophagy assays were performed as described above with the addition of FM 4-64 to the media. Cells were visualized at 0 h and 3 h in SD-N. For Atg30 localization, Atg8 and Atg11 studies: cells were grown as described above to induce peroxisomes and then transferred to SD-N for 0.5 to 1 h at an OD_{600} of 2. GFP-Atg8 labeled the PAS/MIPA. Quantification was performed by taking ten Z-stack images 0.2 microns apart and deconvoluting images using Zeiss software. Microscopy parameters such as exposure time and gain were constant for all samples pictured per figure.

Co-immunoprecipitation – The Δ*ypt7* strains expressing Atg30-TAP (Tandem Protein A and calmodulin binding protein domains) and FLAG-Atg11 (with endogenous *PEX3* replaced by the *PEX3(HYGROMYCIN [HYGRO^R])* or *pex3m(HYGRO^R)*) were used in all experiments as previously described (15,16). Peroxisome proliferation was induced by methanol media (8 h) and pexophagy by transfer to SD-N. The relative levels of Pex3, Atg30-TAP and FLAG-Atg11 were calculated by densitometry using ImageJ (Version 1.48t, National Institutes of Health).

Protein modeling – Protein modeling was done using 3D-JIGSAW software (Cancer Research UK) and human PEX3 (PMID: 3MK4 (30)). A PDB format of *Pp*Pex3 was generated and then visualized using PyMOL software.

Protein purification – GST-Pex3ΔN was mutated to obtain GST-Pex3mΔN. The GST-Pex3ΔN and GST-Pex3mΔN proteins were purified as described (17). *ATG30* from plasmid pJCF226 (16) was digested with the restriction enzymes *EcoRV* and *SalI* and the full-length

ATG30 gene was ligated into pET-32b (Novagen) after digestion with *SmaI* and *SalI* enzymes. The resulting fusion protein (His-Atg30) contained a His-tag, followed by the S-tag, at the N-terminus of Atg30. This plasmid, pSFB342, was transformed into *Escherichia coli* BL21 (DE3) cells. His-Atg30 expression was induced by adding 0.3mM IPTG for 3 h at 30º C and the fusion protein was purified using Ni-NTA agarose (Qiagen). Cells were resuspended in lysis buffer (50 mM Tris-Cl, pH 7.5, 150 mM NaCl, 20mM imidazole, 0.05% NP-40) with lysozyme and protease inhibitors and disrupted by sonication. The 14,000 g supernatant was incubated with the Ni-NTA agarose for 1 h at 4º C. The beads were washed twice with wash buffer (50 mM Tris-Cl, pH 7.5, 500 mM NaCl, 20mM imidazole, 0.05% NP-40) and the bound protein was collected using elution buffer (lysis buffer containing 100mM imidazole). Pooled fractions were subjected to buffer exchange and de-salted using Amicon filters with a 30kDA molecular weight cut-off (Millipore).

In vitro binding – Purified recombinant proteins GST-Pex3ΔN, GST-Pex3mΔN and His-Atg30 were quantified by Coomassie-staining following SDS-PAGE and by comparing the intensities of the protein bands against a BSA standard. For the binding assay, we mixed GST-Pex3ΔN, GST-Pex3mΔN or GST (23 μM) with His-Atg30 (81 μM) in 200 μL binding buffer (20 mM Tris-HCl, pH 7.5, 150 mM NaCl, and 0.05% vol/vol NP-40) for 1 h at 4ºC. The His-Atg30/GST-Pex3ΔN, His-Atg30/GST-Pex3mΔN, and His-Atg30/GST reaction mixtures were used along with Atg30 alone as an additional control. For each binding assay, 50 μL of the reaction volume was taken as input and 150 μL was incubated 1 h at 4º C with 50 μL of prewashed glutathione-Sepharose 4B media (GE Healthcare) to bind the GST and GST-tagged Pex3 species. The beads were washed three times with binding buffer at room temperature. Elution of bound proteins was done with 150 μL of 2x SDS loading buffer and the samples were boiled for 5 min. Equivalent samples were subjected to SDS-PAGE and analyzed by immunoblotting with α-S-tag or α-GST antibodies (Novagen).

Results

A Pex3 mutant has a pexophagy defect – P. pastoris Pex3 has a known interaction with Atg30 and has been suggested as a docking factor for the pexophagy receptor on the peroxisomal membrane (16). In order to determine the nature of the Pex3-Atg30 interaction, we used *pex3* mutant strains generated from a previous screen in the lab. We rescreened the *pex3* mutants for the following attributes: they expressed the full-length *PEX3* protein, grew on peroxisome proliferation media, imported PTS1 proteins and did not degrade GFP-PTS1 by pexophagy. Two mutants were selected: *pex3*^{L320P} and *pex3*$^{I152V, Q218H, N325D}$ (Fig. 4-1A, B). In an effort to confine the important residues of *pex3*$^{I152V, Q218H, N325D}$, single mutants *pex3*^{152V}, *pex3*^{Q218H} and *pex3*^{N325D} were also tested. Only *pex3*^{N325D} had a pexophagy phenotype (Fig. 4-1A, B). Leucine-320 and Asparagine-325 are in close proximity and when these two residues were combined (*pex3*$^{L320P, N325D)}$, the pexophagy phenotype was exaggerated (Fig. 4-1A, B).

In another test of pexophagy, we examined the ability of the *pex3* mutant, *pex3*$^{L320P, N325D}$, to affect peroxisome degradation as measured by the loss of peroxisomal matrix protein, AOX, after the shift of cells to pexophagy-inducing conditions. Partial degradation of AOX was seen after 24 h, as compared to 0 h levels, in *pex3*^{L320P} and *pex3*^{N325D}, while Δ*atg30* and *pex3*$^{L320P, N325D}$ showed a complete block of pexophagy, with similar AOX levels at 0 h and 24 h (Fig. 4-1C).

The *pex3*$^{L320P, N325D}$ mutant, hereafter referred to as *pex3m*, had a severe block in pexophagy (Fig. 4-1), but not in peroxisome biogenesis, as evidenced by the presence of peroxisomes, by normal peroxisomal import of PTS1-containing proteins (Fig. 4-1B) and by its growth in the methanol-containing media, which requires peroxisome metabolism (Fig. 4-2A). Pex3 is an essential protein for peroxisome biogenesis, so Δ*pex3* cells did not contain peroxisomes, could not import GFP-PTS1 (Fig. 4-1B) or grow in methanol media (Fig. 4-2A), as expected, while the *pex3m* allele partially complemented Δ*pex3* cells.

We used the crystal structure of the cytosolic domain of human PEX3 (29,30) to create a hypothetical model of *Pp*Pex3 (Fig. 4-2B). Leucine-320 and Asparagine-325 are found in a

structural loop that is distinct from any defined protein interaction domains of yeast Pex3 thus far (25,32).

Pex3 mutants defective in binding Atg30 – To elucidate if Leucine-320 and Asparagine-325 are the crux of the Pex3-Atg30 interaction domain, we then analyzed Pex3m by yeast two-hybrid analysis for interaction with the full-length Atg30. WT maintained interaction with Atg30, while Pex3m no longer interacted with Atg30 suggesting the importance of these residues of Pex3 in Pex3-Atg30 interaction (Fig. 4-3A). Therefore, mutation of the key residues in this structural loop might affect pexophagy through disruption of Atg30 interaction.

In vivo interaction and localization of Atg30 with Pex3m were performed in order to test whether or not Pex3 acts as the docking factor for Atg30, as well as to test the importance of the Leucine-320- and Asparagine-325-containing structural loop in Pex3 as the potential domain mediating Pex3-Atg30 interaction. Verification of the Y2H data that Pex3m interaction with Atg30 is impaired (Fig. 4-3A) was obtained by immunoprecipitation of the Pex3 and Pex3m proteins in *P. pastoris* cells defective in autophagosome-vacuole fusion (Δ*ypt7*) in order to accumulate Atg30 and Pex3 on cytosolic pexophagosomes (Fig. 4-3B). Using densitometry, Atg30 levels were always ~2 times lower in *pex3m* than in WT. This ratio was considered during interpretation of our immunoprecipitation experiments. Furthermore, the Atg30 interacting proteins (Pex3 and Atg11) were not a limiting factor, since their levels were comparable in the input and unbound fractions (Fig. 4-3B).

Atg30 was immunoprecipitated with WT Pex3, as expected, but pulled down much less Pex3m, even when the difference of Atg30 levels between WT and *pex3m* was accounted for (Fig. 4-3B).

To address whether Atg30 and Pex3 associate directly, an *in vitro* interaction assay of His-Atg30 with GST-Pex3ΔN, GST-Pex3mΔN and GST was performed using purified recombinant proteins. His-Atg30 interacted with GST-Pex3ΔN, but not with GST-Pex3mΔN or GST alone (Fig. 4-3C). This clearly indicates that this interaction is direct and that the *pex3m* mutation disrupts the binding with Atg30.

Peroxisomal localization of Atg30 is unaffected in pex3m cells – In WT cells, Atg30 targets to the peroxisomal membrane where it interacts with Pex3 (16). As interaction is impaired between Atg30 and Pex3m, Atg30 localization on the peroxisomal membrane was studied by fluorescence microscopy with genomically tagged Atg30-YFP. Atg30 localization was unaffected by *pex3m*, as seen by colocalization of Atg30-YFP with the peroxisomal BFP-PTS1 in 48±6% of WT and 56±7% of *pex3m* cells (p is non-significant) (Fig. 4-3D, white arrows). Taken together, the Pex3-Atg30 interaction is not essential for the peroxisomal localization of Atg30, as the localization of Atg30 was similar between WT and *pex3m* cells.

Atg30 is differentially phosphorylated in pex3m cells – The ability of Atg30-YFP to localize to the peroxisomal membrane in *pex3m* cells as efficiently as in WT cells was an unexpected result. Pex3 has been postulated to be the peroxisomal docking factor for Atg30 not only because of their interaction but also because of the altered localization of Atg30 in Δ*pex3* cells (16). Atg30 is massively phosphorylated by an unknown kinase as a trigger for peroxisome degradation. It is differentially phosphorylated at Serine-71 to regulate Atg8 binding and at Serine-112 to modulate its interaction with Atg11 (15). It is also known that Atg30 is hypophosphorylated in Δ*pex3* cells (16), however the rational explanation for this phenotype was the mislocalization of Atg30. Interestingly, in *pex3m* cells, where Atg30 is properly localized, it was also hypophosphorylated (Fig. 4-4A). These results suggest that efficient Pex3-Atg30 interaction is required to induce the correct phosphorylation of Atg30, which is necessary for pexophagy.

Impaired recruitment of Atg11 to the RPC in pex3m cells – In the absence of Atg11, the recruitment of the core autophagy machinery is impeded, as Atg11 is required for the organization of the PAS for selective autophagy pathways (16,37,38). Phosphorylation of Atg30 at Serine-112 is required for its interaction with Atg11 (15,16) and as Atg30 is hypophosphorylated in *pex3m* cells, we postulated that Atg30-Atg11 interaction might be impaired in the *pex3m* background. When either WT or *pex3m* lysates co-expressing Atg30-TAP and FLAG-Atg11 were used for co-immunoprecipitation studies, we observed no interaction

between Atg30-TAP and FLAG-Atg11 in *pex3m* cells, while WT cells maintained a strong interaction, even when the difference of Atg30 levels between WT and *pex3m* was accounted for (Fig. 4-3B).

Atg11 is normally found at the PAS and vacuole membrane in close proximity to the targeted peroxisome after re-localization from a diffuse location around the vacuole prior to the activation of pexophagy (42). In *pex3m* cells, GFP-Atg11 maintained solely vacuole membrane fluorescence, similar to that observed at the onset of pexophagy in Δ*atg30* cells, and did not re-localize to the vacuole sequestering membranes (VSMs) or accumulate at the base of the targeted peroxisome, as often as seen in WT cells (61±14% in WT, 11±7% in *pex3m*, 7±6% in Δ*atg30)* (Fig. 4-4B, C). Therefore, Pex3 could play an indirect role in the recruitment of Atg11 to the pexophagic RPC.

Phagophore formation is affected in pex3m cells – We also wondered how the mislocalization of Atg11 in *pex3m* cells affects the downstream process of phagophore formation. In WT cells, GFP-Atg8 accumulates at the PAS, which is a punctate structure at the vacuole rim in proximity to the peroxisome. During pexophagy, the transient PAS extends into the phagophore (also known as micropexophagic apparatus or MIPA). Fluorescence microscopy images revealed that *pex3m* cells expressing BFP-PTS1 and GFP-Atg8 had GFP-Atg8 localized properly at the pexophagy-specific PAS (Fig. 4-4D). However, the MIPA did not surround targeted peroxisomes in *pex3m* cells, as opposed to WT cells. The MIPA and PAS were each present in roughly 5% of WT cells, while *pex3m* cells accumulated only the PAS (8.5% of cells) as determined by Z-stack analysis (Fig. 4-4E) with a p value of <0.001. Therefore, likely the lack of Atg11 at the RPC in *pex3m* cells leads to defective phagophore formation.

Discussion

Here we report the identification of a distinct Atg30-binding domain in Pex3 that modulates the phosphorylation of Atg30 and the recruitment of Atg11 by Atg30 to the RPC in *P.*

pastoris cells. We highlight that Pex3 has signaling roles beyond just docking of the pexophagy receptor at the peroxisomal membrane.

Previous studies concluded that in the absence of Pex3, Atg30 would be mislocalized (16). However, those studies shed no light on the nature or physiological role of the interaction of Atg30 with Pex3. Our findings reveal a specific interaction domain of Pex3 that binds directly to Atg30. Additionally, we show that post-translational modifications of Atg30 that trigger the onset of pexophagy in yeast can be disrupted by mutations in this interaction domain of Pex3. This is evident when Atg30, which is hypophosphorylated in *pex3m* cells, fails in the subsequent pexophagy-related interaction with Atg11.

Atg30-YFP properly localized to the peroxisomal membrane in *pex3m* cells, despite the lack of interaction between Atg30 and Pex3m as judged by both co-immunoprecipitation, *in vitro* binding with recombinant proteins, and Y2H studies. This shows that Pex3 is not the sole protein on the peroxisomal membrane that docks Atg30. Our previous study showied that Atg30 also interacts with a peroxisomal integral membrane protein, Atg37 (7). Since Pex3 is needed for peroxisome biogenesis, previous studies using Δ*pex3* cells might have missed additional PMPs, like Atg37 that recruit Atg30 to the peroxisomes.

Pex3 is positioned to be a signaling platform for the peroxisome as it is a PMP that interacts with many proteins involved in peroxisome biogenesis and dynamics. Atg30 is highly phosphorylated during pexophagy, but likely kept in an inactive state during peroxisome proliferation. During pexophagy, an activation of unknown factor or signal that depends on Atg30-Pex3 interaction leads to the phosphorylation of the residues on Atg30 responsible for Atg11 interaction.

How might Pex3 regulate the phosphorylation status of Atg30? During pexophagy, (i) a conformational change of Atg30, mediated by Pex3, could expose phosphorylation sites to the kinase(s) to activate Atg30; (ii) Pex3 might act directly or indirectly as a docking site for kinase(s) that may phosphorylate Atg30 (Fig. 4-5). The kinase(s) and phosphatase(s), responsible for coordinated phosphorylation events on Atg30 have not been discovered yet and we are in an

active pursuit of this. We conclude that peroxisomal Pex3 is more than just a docking factor and it would be interesting to determine if other selective autophagy receptors are post-translationally regulated by the organelle-specific protein ligands to control the organelle fate.

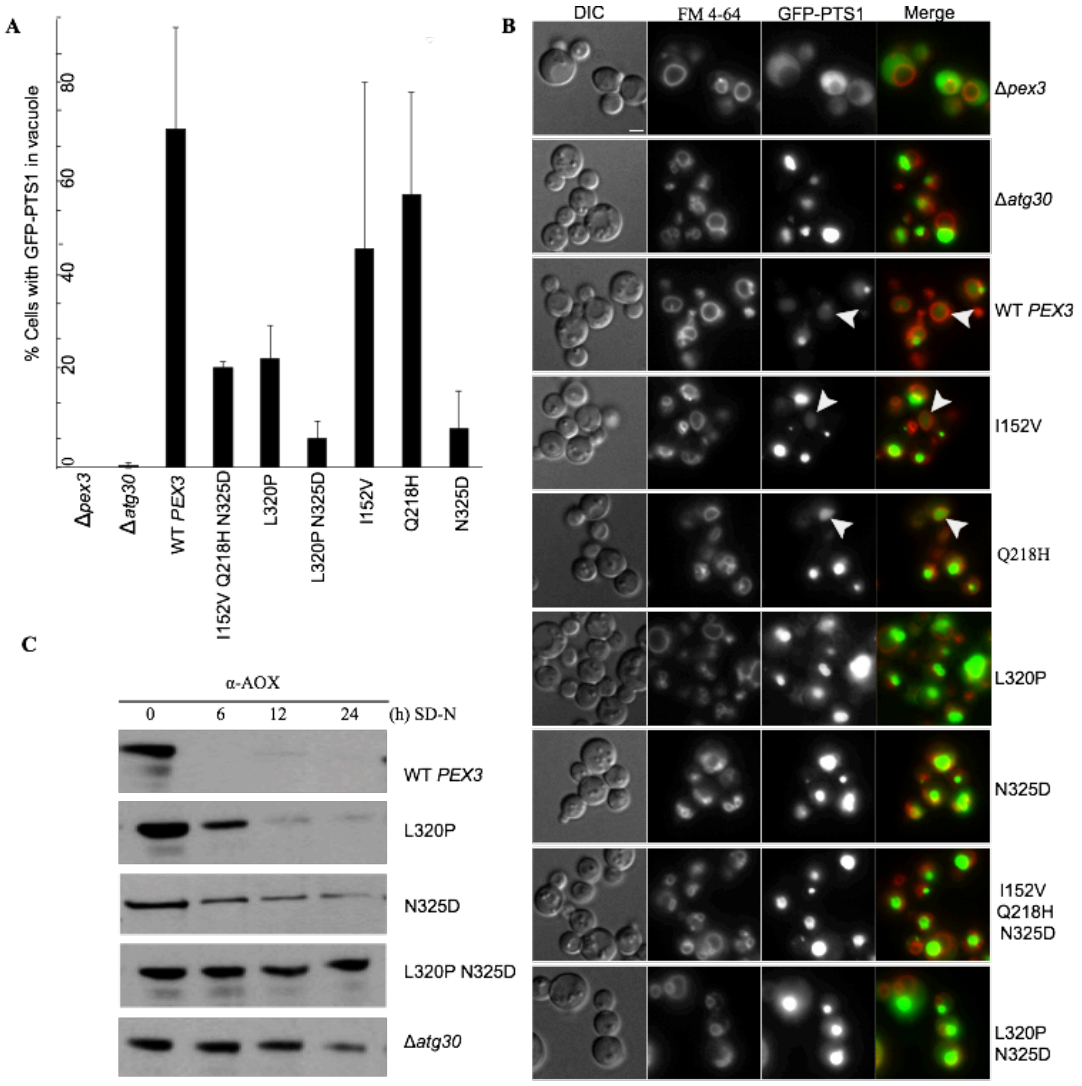

Figure 4-1: Pex3 mutants with pexophagy defect. A) The strain Δ*pex3* expressing a peroxisome reporter (GFP-PTS1) was transformed with plasmids either expressing wild-type *PEX3* or mutant *pex3* ORFs. The strains Δ*pex3* and Δ*atg30* were used as controls. The percentage of cells that contained GFP fluorescence in the vacuole after 3 h in SD-N was estimated (mean % of 3 experiments ± S.E.M). Quantification was done on at least 300 cells of each strain. B) Representative images of (A) showing cells under pexophagy conditions. FM 4-64 was used to stain the vacuolar membrane. Arrows indicate GFP fluorescence in the vacuole. Bar, 2μM. C) Biochemical pexophagy assay. Cell lysates were prepared as described in Experimental Procedures and resolved by SDS-PAGE. Western blot was performed with antibodies against *Pp*AOX.

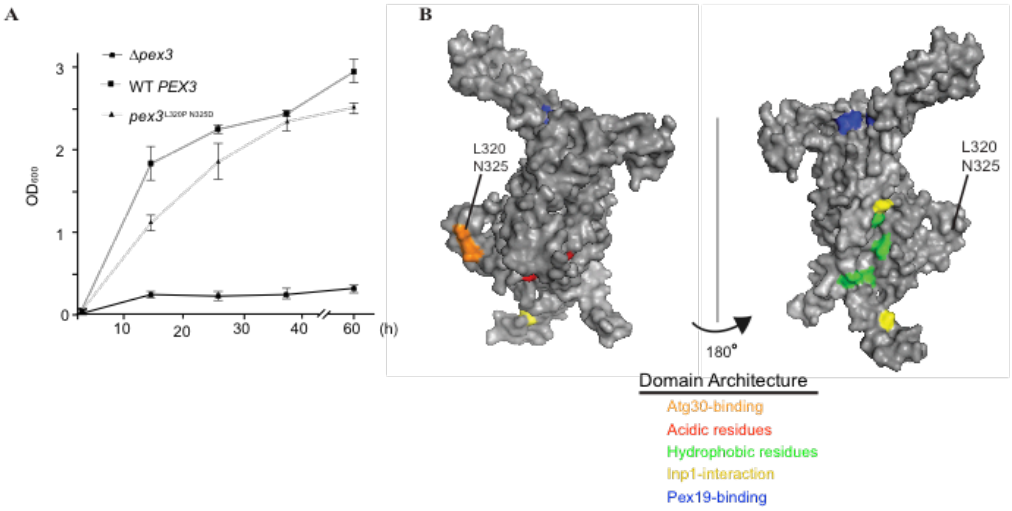

Figure 4-2: Novel pexophagy-specific domain identified. A) The strains Δ*pex3* and Δ*pex3* complemented with the plasmid containing WT *PEX3* or *pex3*$^{L320P\ N325D}$ were evaluated for proper peroxisome proliferation via the growth in methanol media. Presented are average ODs ± S.E.M from three individual experiments. B) Hypothetical predicted structure of *Pp*Pex3 modeled in PyMol based on human PEX3. The surface of the protein is visualized in grey and protein-binding domains in colors, as indicated.

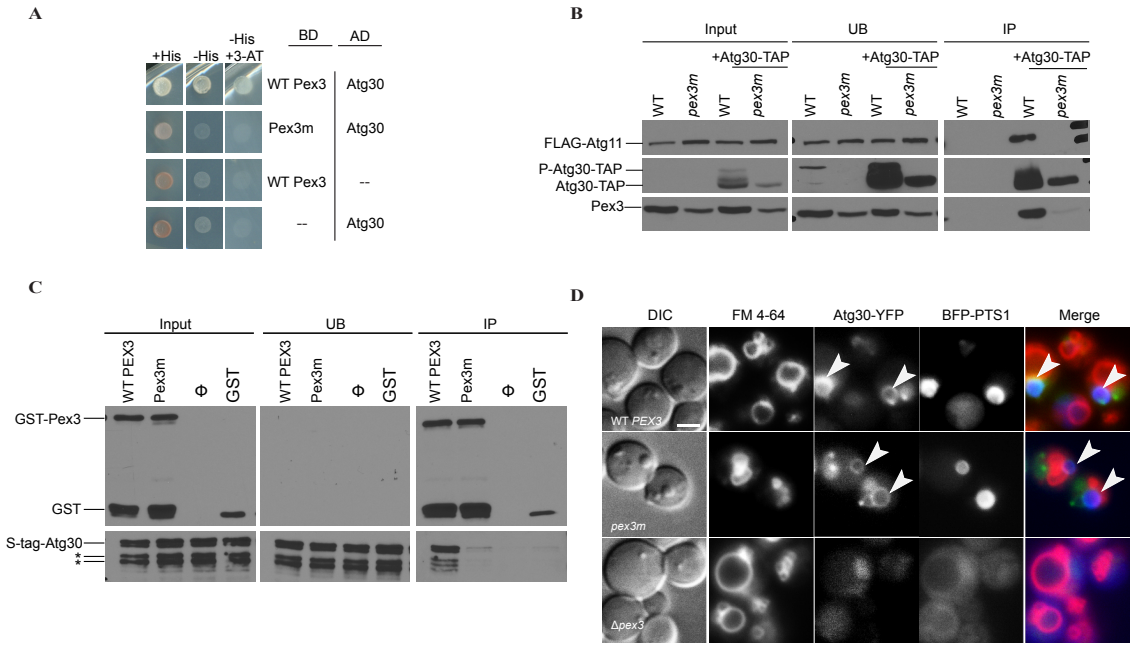

Figure 4-3: Pex3-Atg30 interaction is not required to localize Atg30 to the peroxisome. A) Yeast two-hybrid analysis for interaction between Atg30 and WT Pex3 or Pex3m. The Atg30 was fused to the Gal4-activation domain (AD-Atg30) and Pex3 to the Gal4-DNA binding domain (BD-Pex3). Cell growth in the absence of histidine was used as a measure of protein-protein interaction. Dashes denote empty plasmids used as controls, pGBKT7 (BD) and pGADGH (AD). B) Δ*ypt7* cells with endogenous *PEX3* replaced by the WT *PEX3-HYGRO*^{R} or *pex3m-HYGRO*^{R} were transformed with FLAG-Atg11 and Atg30-TAP (denoted as +Atg30-TAP). Immunoprecipitation (IP) was performed using IgG-Agarose beads in pexophagy conditions (SD-N). Lysates of cells taken at absorbances of 0.8, 29.2 and 0.8 ODs were loaded as Input, IP and UB (long exposure), respectively. Proteins immunoprecipitated were visualized with α-FLAG, α-CBP and α-*Pp*Pex3. P-Atg30 denotes phosphorylated species. UB, unbound fractions. C) His-Atg30 binds GST-Pex3ΔN, but not to GST-Pex3mΔN or GST *in vitro*. Equivalent loading in the Input; UB, unbound; IP, pull-down lanes. Ø, contains His-Atg30, but no GST-species. Immunoblot was performed with α-S-tag, to detect Atg30, and α-GST antibodies D) Δ*pex3* cells were transformed with Atg30-YFP, BFP-PTS1 and either a plasmid containing WT *PEX3* or *pex3m* and subjected to peroxisome proliferation and subsequent pexophagy conditions (SD-N, 1 h) followed by the localization of Atg30 to peroxisome membranes (white arrows). FM 4-64 labels the vacuolar membrane. Δ*pex3* cells do not form peroxisomes and Atg30 is cytosolic (lower panel). Bar, 2μM.

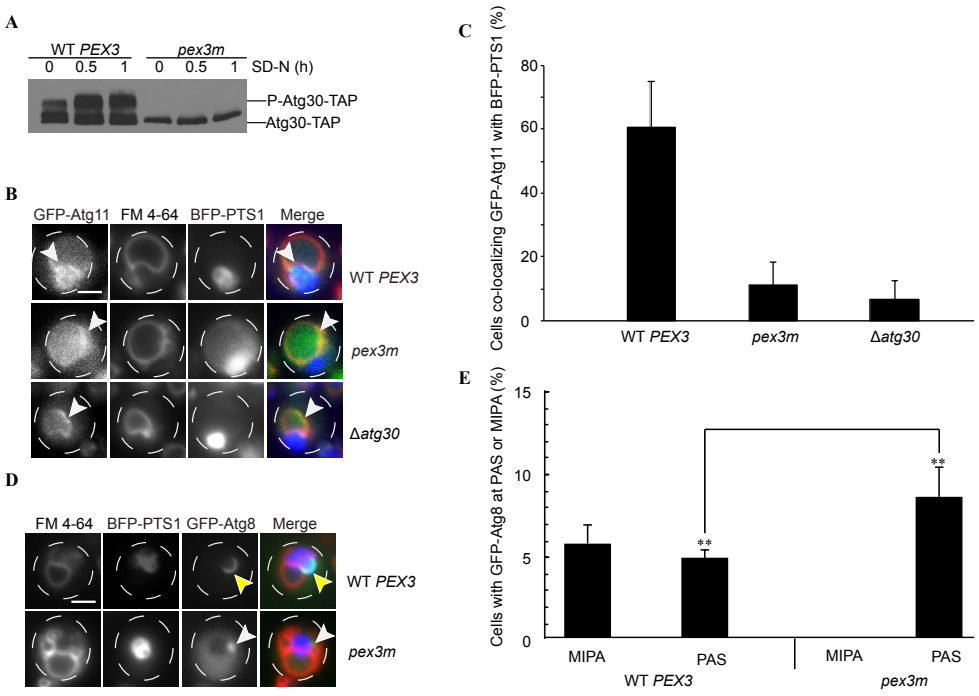

Figure 4-4: *pex3m* affects Atg30 phosphorylation, Atg11 localization and phagophore formation. A) Δ*ypt7* (WT *PEX3-HYGRO*^{R} or *pex3m-HYGRO*^{R}) cells containing Atg30-TAP were followed after peroxisome induction to monitor the phosphorylation status of Atg30 upon switching media to SD-N. P-Atg30-TAP denotes phosphorylated Atg30 species. B) WT *PEX3-HYGRO*^{R}, *pex3m-HYGRO*^{R} and Δ*atg30* cells containing GFP-Atg11, BFP-PTS1 and FM 4-64 were visualized after switching to SD-N (1 h). White arrow indicates GFP-Atg11 localization. Bar, 2μM. C) Cells from (B) were quantified for GFP-Atg11 accumulation in the interface of vacuole (FM 4-64) and peroxisomes (BFP-PTS1) (mean % of 3 experiments ± S.E.M). D. Δ*pex3* cells were transformed with WT *PEX3* or *pex3m* plasmids along with GFP-Atg8 and BFP-PTS1 to monitor phagophore (MIPA) formation (yellow arrow) or PAS organization (white arrow) upon induction of pexophagy. Bar, 2μM. E. MIPA and PAS structures from (D) were quantified (mean % of 3 experiments ± S.E.M, ** $p < 0.001$).

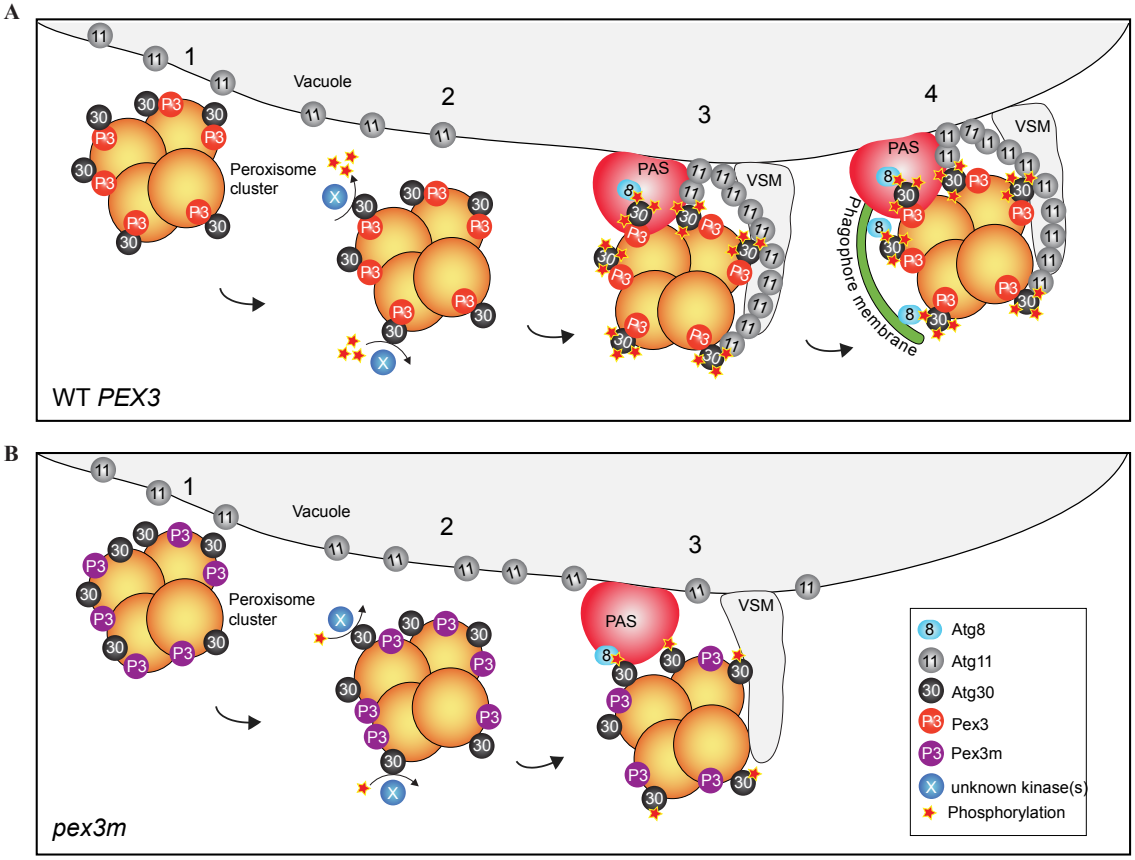

Figure 4-5: Model for Atg30 activation by Pex3. A) In WT cells, Atg30 and Pex3 localize at the peroxisome membrane (1); after pexophagy induction, Atg30 is phosphorylated by an unknown kinase(s) in a Pex3-Atg30 interaction-dependent manner (2); Atg8 and Atg11 interact with phosphorylated Atg30, leading to the PAS formation and Atg11 accumulation at the interface between peroxisomes and vacuolar membranes (3); the phagophore (decorated by Atg8) extends from the PAS and engulfs the peroxisome cluster (4) to allow for fusion with the vacuolar membranes and peroxisome degradation inside the vacuole. B) In *pex3m* cells, Atg30 is targeted to the peroxisome in a Pex3-independent manner (1); Atg30 is not properly phosphorylated (2); despite being hypophosphorylated, Atg8 is still recruited to the PAS yet Atg11 does not accumulate in the proximity of the peroxisome cluster (3).

Table 4-1: Strains used in study

Name	Genotype and plasmid used for construction	Source
PPY12h	*arg4 his4*	(39)
Sew1	PPY12h Δ*pex3::ARG4*	(40)
Sjcf936	PPY12h Δ*atg30*::ZEO^R	(41)
Sjcf959	PPY12h Δ*atg30*::KAN^R	(15)
Stn98	Sjcf936 *his4*::pTW51 *(P_{AOX1}-GFP-SKL, HIS4)*	This study
Stn636	PPY12h P_{AOX1} :: pPICz-BFP-PTS1 (P_{AOX1}-*BFP-PTS1*, ZEO^R), *arg4*::pJCF291 *(P_{ATG11}-GFP-ATG11, ARG4)*	(17)
Stn640	Sjcf959 P_{AOX1} :: pPICz-BFP-PTS1 (P_{AOX1}-*BFP-PTS1*, ZEO^R), *arg4*::pJCF291 *(P_{ATG11}-GFP-ATG11, ARG4)*	(17)
Srrm197	PPY12h Δ*ypt7*::KAN^R	(43)
Ssl12	Sew1 P_{AOX1}::pSJ7 (P_{AOX1}-*GFP-PTS1*, ZEO^R)	This study
Ssl13	Ssl12 *his4*::pSJ40 (P_{PEX3}-*PEX3, HIS4*)	This study
Ssl20	Ssl12 *his4*::pSJ56 (P_{PEX3}-$PEX3^{L320P}$, *HIS4*)	This study
Ssfb20	Ssl12 *his4*::pSFB127 (P_{PEX3}-$PEX3^{I152V, N325D, L320P}$, *HIS4*)	This study
Ssfb24	Ssl12 *his4*::pSFB139 (P_{PEX3}-$PEX3^{N325D}$, *HIS4*)	This study
Ssfb28	Ssl12 *his4*::pSFB145 (P_{PEX3}-$PEX3^{Q218H}$, *HIS4*)	This study
Ssfb40	Ssl12 *his4*::pIB1 (*HIS4*)	This study
Ssfb52	Sew1 *his4*::pSJ40 (P_{PEX3}-*PEX3, HIS4*), *his4*::pJCF419 (P_{ATG8}-*GFP-ATG8, HIS4,* $HYGRO^R$), *his4*::pJCF401 (P_{GAP}-*BFP-PTS1, HIS4,* KAN^R)	This study
Ssfb58	Ssl12 *his4*::pSFB165 (P_{PEX3}-$PEX3^{L320P, N325D}$, *HIS4*)	This study
Ssfb64	Ssl12 *his4*::pSFB164 (P_{PEX3}-$PEX3^{I152V}$, *HIS4*)	This study
Ssfb82	Sew1 *his4*::pSFB165 (P_{PEX3}-$PEX3^{L320P, N325D}$, *HIS4*), *his4*::pJCF419 (P_{ATG8}-*GFP-ATG8, HIS4,* $HYGRO^R$), *his4*::pJCF401 (P_{GAP}-*BFP-PTS1, HIS4,* KAN^R)	This study
Ssfb83	Sew1 *his4*::pSJ40 (P_{PEX3}-*PEX3*, *HIS4*), *ATG30*::pJCF105 (P_{ATG30}-*ATG30-YFP,* ZEO^R), *his4*::pJCF401 (P_{GAP}-*BFP-PTS1*, *HIS4*, KAN^R)	This study
Ssfb86	Sew1 *ATG30*::pJCF105 (P_{ATG30}-*ATG30-YFP,* ZEO^R), *his4*::pJCF401 (P_{GAP}-*BFP-PTS1*, *HIS4*, KAN^R)	This study
Ssfb87	Sew1 *his4*::pSFB165 (P_{PEX3}-$PEX3^{L320P\ N325D}$, *HIS4*), *ATG30*::pJCF105 (P_{ATG30}-*ATG30-YFP,* ZEO^R), *his4*::pJCF401 (P_{GAP}-*BFP-PTS1, HIS4,* KAN^R)	This study
Ssfb431	Srrm197 *PEX3*::pSFB202 (P_{PEX3}-$PEX3^{L320P, N325D}$, $HYGRO^R$), *arg4*::pJCF340 (P_{ATG11}-*FLAG-ATG11, ARG4*)	This study
Ssfb432	Srrm197 *PEX3*::pSFB203 (P_{PEX3}-*PEX3,* $HYGRO^R$), *arg4*::pJCF340 (P_{ATG11}-*FLAG-ATG11, ARG4*)	This study
Ssfb435	Srrm197 *PEX3*::pSFB202 (P_{PEX3}-$PEX3^{L320P, N325D}$, $HYGRO^R$), *arg4*::pJCF340 (P_{ATG11}-*FLAG-ATG11, ARG4*), *ATG30::*pJCF75 (P_{ATG30}-*ATG30-TAP,* ZEO^R)	This study

Table 4-1: Strains used in study, continued

Name	Genotype and plasmid used for construction	Source
Ssfb436	Srrm197 *PEX3*::pSFB203 (P_{PEX3}-*PEX3, HYGRO*^{R}), *arg4*::pJCF340 (P_{ATG11}-*FLAG-ATG11, ARG4*), *ATG30*::pJCF75 (P_{ATG30}-*ATG30-TAP*, *ZEO*^{R})	This study
Y2H Gold	*S. cerevisiae MAT*a, *trp1-901*, *leu2-3*, *112*, *ura3-52*, *his3-200*, *gal4*Δ, *gal80*Δ, *LYS2*::*GAL1UAS–Gal1TATA–His3*, *GAL2UAS–Gal2TATA–Ade2*, *URA3*::*MEL1UAS–Mel1TATA*, *AUR1-C MEL1*	Clontech
Ssfb461	Y2H Gold *trp1*::pKSN65 (*GAL4BD-PEX3, TRP1*), *leu2*::pJCF226 (*GAL4AD-ATG30, LEU2*)	This study
Ssfb462	Y2H Gold *trp1*::pSFB171 (*GAL4BD-PEX3*$^{L320P, N325D}$, *TRP1*), *leu2*::pJCF226 (*GAL4AD-ATG30, LEU2*)	This study
Ssfb463	Y2H Gold *trp1*::pKSN65 (*GAL4BD-PEX3, TRP1*), *leu2*::pGAD-GH (*GAL4AD, LEU2*)	This study
Ssfb464	Y2H Gold *trp1*::pGBKT7 (*GAL4BD, TRP1*), *leu2*::pJCF226 (*GAL4AD-ATG30, LEU2*)	This study

Addendum:
Table 4-2: Plasmids used in the study

Name	Description	Parent Plasmid	Bacterial Selection	Yeast Selection	Linearize With	Locus Insertion	Notes
pSFB127	P_{PEX3}-*PEX3*$^{I152V, N325D, L320P}$, *HIS4*	pSJ40	Amp	*HIS4*	SalI	*HIS4*	KpnI/SpeI
pSFB139	P_{PEX3}-*PEX3*^{N325D}, *HIS4*	pSJ40	Amp	*HIS4*	SalI	*HIS4*	KpnI/SpeI
pSFB145	P_{PEX3}-*PEX3*^{Q218H}, *HIS4*	pSJ40	Amp	*HIS4*	SalI	*HIS4*	KpnI/SpeI
pSFB164	P_{PEX3}-*PEX3*^{I152V}, *HIS4*	pSJ40	Amp	*HIS4*	SalI	*HIS4*	KpnI/SpeI
pSFB165	P_{PEX3}-*PEX3*$^{L320P, N325D}$, *HIS4*	pSJ40	Amp	*HIS4*	SalI	*HIS4*	KpnI/SpeI
pSFB202	P_{PEX3}-*PEX3*$^{L320P, N325D}$, *HYGRO*^{R}	pAG32/pSJ40	Hygro	*HygroR*	EcoRV	*PEX3*	SacII/HpaI
pSFB203	P_{PEX3}-*PEX3, HYGRO*^{R}	pAG32/pSJ40	Hygro	*HygroR*	EcoRV	*PEX3*	SacII/HpaI
pSFB171	*GAL4BD-PEX3*$^{L320P, N325D}$, *TRP1*	pKSN65	Kan	*TRP1*	N/A	N/A	NdeI/Pst1
pSFB342	S-tag/His-Atg30	pET32b/pJCF226	Amp	*N/A*	N/A	N/A	SmaI/SalI (Bacterial)
pSFB247	GST-Δ41*PEX3m*	pGEX2TK	Amp	*N/A*	N/A	N/A	XmaI (Bacterial)
pTW51	P_{AOX1}-*GFP-PTS1, HIS4*	pIB4	Amp	*HIS4*	SalI	*AOX*	EcoRI
pPICz-BFP-PTS1	P_{AOX1}-*BFP-PTS1*, *ZEO*^{R}	pPICz	Zeo	Zeo	PmeI	*AOX*	EcoRI
pJCF291	P_{ATG11}-*GFP-ATG11, ARG4*	pJCF281/pJCF264	Amp	*ARG4*	NruI	ARG4	NotI/HindIII
pSJ7	P_{AOX1}-*GFP-PTS1, ZEO*^{R}	pTW51/pPICZA	Zeo	*HIS4*	DraI	AOX	EcoRI
pSJ40	P_{PEX3}-*PEX3, HIS4*	pIB1	Amp	*HIS4*	SalI	*HIS4*	KpnI/SpeI
pSJ56	P_{PEX3}-*PEX3*^{L320P}, *HIS4*	pGBKT7/pSJ40	Kan	*HIS4*	SalI	*HIS4*	KpnI/SpeI
pJCF419	P_{ATG8}-*GFP-ATG8, HIS4, HYGRO*^{R}	pJCF208	Amp	*HygroR*	SalI	*HIS4*	BsrBI/EcoRI
pJCF401	P_{GAP}-*BFP-PTS1, HIS4, KAN*^{R}	pSFB386	Amp	*G418*	StuI	*HIS4*	EcoRI/SacII
pJCF105	P_{ATG30}-*ATG30-YFP, ZEO*^{R}	pMY75	Zeo	*Zeo*	PflmI	*ATG30*	ClaI/AflII
pJCF340	P_{ATG11}-*FLAG-ATG11, ARG4*	pJCF281	Amp	*ARG4*	NruI	*ATG30*	NotI
pJCF75	P_{ATG30}-*ATG30-TAP, ZEO*^{R}	pMY62	Zeo	*Zeo*	PflmI	*ATG30*	ClaI/AflII
pKSN65	*GAL4BD-PEX3, TRP1*	pGBKT7	Kan	*TRP1*	N/A	N/A	NdeI/PstI (Y2H)
pJCF226	*GAL4AD-ATG30, LEU2*	pGADGH	Amp	*LEU2*	N/A	N/A	SmaI/SalI (Y2H)
pGAD-GH	*GAL4AD, LEU2*	commerical	Amp	*LEU2*	N/A	N/A	N/A (Y2H)
pGBKT7	*GAL4BD, TRP1*	commerical	Kan	*TRP1*	N/A	N/A	N/A (Y2H)

The text of Chapter 4 has been published in the *Journal of Biological Chemistry*, *2015*. The candidate performed all experiments.

References

1. Tan, C. C., Yu, J. T., Tan, M. S., Jiang, T., Zhu, X. C., and Tan, L. (2013) Autophagy in aging and neurodegenerative diseases: implications for pathogenesis and therapy. *Neurobiol Aging* **35**, 00587-00583

2. Feng, Y., He, D., Yao, Z., and Klionsky, D. J. (2013) The machinery of macroautophagy. *Cell Res* **24**, 24-41

3. Nakatogawa, H., Suzuki, K., Kamada, Y., and Ohsumi, Y. (2009) Dynamics and diversity in autophagy mechanisms: lessons from yeast. *Nature reviews. Molecular cell biology* **10**, 458-467

4. Yang, Z., and Klionsky, D. J. (2009) An overview of the molecular mechanism of autophagy. *Curr Top Microbiol Immunol* **335**, 1-32

5. Till, A., Lakhani, R., Burnett, S. F., and Subramani, S. (2012) Pexophagy: the selective degradation of peroxisomes. *Int J Cell Biol* **2012**, 512721

6. Johansen, T., and Lamark, T. (2011) Selective autophagy mediated by autophagic adapter proteins. *Autophagy* **7**, 279-296

7. Shintani, T., Huang, W. P., Stromhaug, P. E., and Klionsky, D. J. (2002) Mechanism of cargo selection in the cytoplasm to vacuole targeting pathway. *Dev Cell* **3**, 825-837

8. Kanki, T., Wang, K., Cao, Y., Baba, M., and Klionsky, D. J. (2009) Atg32 is a mitochondrial protein that confers selectivity during mitophagy. *Developmental cell* **17**, 98-109

9. Okamoto, K., Kondo-Okamoto, N., and Ohsumi, Y. (2009) Mitochondria-anchored receptor Atg32 mediates degradation of mitochondria via selective autophagy. *Developmental cell* **17**, 87-97

10. Motley, A. M., Nuttall, J. M., and Hettema, E. H. (2012) Pex3-anchored Atg36 tags peroxisomes for degradation in *Saccharomyces cerevisiae*. *EMBO J* **13**, 2852-2868

11. Suzuki, K., Kondo, C., Morimoto, M., and Ohsumi, Y. (2010) Selective transport of alpha-mannosidase by autophagic pathways: identification of a novel receptor, Atg34p. *J Biol Chem* **285**, 30019-30025

12. Kanki, T., Kurihara, Y., Jin, X., Goda, T., Ono, Y., Aihara, M., Hirota, Y., Saigusa, T., Aoki, Y., Uchiumi, T., and Kang, D. (2013) Casein kinase 2 is essential for mitophagy. *EMBO reports* **14**, 788-794

13. Pfaffenwimmer, T., Reiter, W., Brach, T., Nogellova, V., Papinski, D., Schuschnig, M., Abert, C., Ammerer, G., Martens, S., and Kraft, C. (2014) Hrr25 kinase promotes selective autophagy by phosphorylating the cargo receptor Atg19. *EMBO Rep* **15**, 862-870

14. Tanaka, C., Tan, L. J., Mochida, K., Kirisako, H., Koizumi, M., Asai, E., Sakoh-Nakatogawa, M., Ohsumi, Y., and Nakatogawa, H. (2014) Hrr25 triggers selective autophagy-related pathways by phosphorylating receptor proteins. *J Cell Biol* **207**, 91-105

15. Farré, J. C., Burkenroad, A., Burnett, S. F., and Subramani, S. (2013) Phosphorylation of mitophagy and pexophagy receptors coordinates their interaction with Atg8 and Atg11. *EMBO Rep* **14**, 441-449

16. Farré, J. C., Manjithaya, R., Mathewson, R. D., and Subramani, S. (2008) *Pp*Atg30 tags peroxisomes for turnover by selective autophagy. *Dev Cell* **14**, 365-376

17. Nazarko, T. Y., Ozeki, K., Till, A., Ramakrishnan, G., Lotfi, P., Yan, M., and Subramani, S. (2014) Peroxisomal Atg37 binds Atg30 or palmitoyl-CoA to regulate phagophore formation during pexophagy. *J Cell Biol* **204**, 541-557

18. Ma, C., Agrawal, G., and Subramani, S. (2011) Peroxisome assembly: matrix and membrane protein biogenesis. *J Cell Biol* **193**, 7-16

19. Pinto, M. P., Grou, C. P., Alencastre, I. S., Oliveira, M. E., Sá-Miranda, C., Fransen, M., and Azevedo, J. E. (2006) The import competence of a peroxisomal membrane protein is determined by Pex19p before the docking step. *J Biol Chem* **281**, 34492-34502

20. Snyder, W. B., Faber, K. N., Wenzel, T. J., Koller, A., Lüers, G. H., Rangell, L., Keller, G. A., and Subramani, S. (1999) Pex19p interacts with Pex3p and Pex10p and is essential for peroxisome biogenesis in *Pichia pastoris*. *Mol Biol Cell* **10**, 1745-1761

21. Hettema, E. H., Girzalsky, W., van Den Berg, M., Erdmann, R., and Distel, B. (2000) *Saccharomyces cerevisiae* Pex3p and Pex19p are required for proper localization and stability of peroxisomal membrane proteins. *EMBO J* **19**, 223-233

22. Fang, Y., Morrell, J. C., Jones, J. M., and Gould, S. J. (2004) PEX3 functions as a PEX19 docking factor in the import of class I peroxisomal membrane proteins. *J Cell Biol* **164**, 863-875

23. Hattula, K., Hirschberg, D., Kalkkinen, N., Butcher, S. J., and Ora, A. (2014) Association between the intrinsically disordered protein PEX19 and PEX3. *PLoS One* **9**, e103101

24. Munck, J. M., Motley, A. M., Nuttall, J. M., and Hettema, E. H. (2009) A dual function for Pex3p in peroxisome formation and inheritance. *J Cell Biol* **187**, 463-471

25. Knoblach, B., Sun, X., Coquelle, N., Fagarasanu, A., Poirier, R. L., and Rachubinski, R. A. (2013) An ER-peroxisome tether exerts peroxisome population control in yeast. *EMBO J* **32**, 2439-2453

26. Chang, J., Mast, F. D., Fagarasanu, A., Rachubinski, D. A., Eitzen, G. A., Dacks, J. B., and Rachubinski, R. A. (2009) Pex3 peroxisome biogenesis proteins function in peroxisome inheritance as class V myosin receptors. *J Cell Biol* **187**, 233-246

27. Williams, C., and van der Klei, I. J. (2013) Pexophagy-linked degradation of the peroxisomal membrane protein Pex3p involves the ubiquitin-proteasome system. *Biochem Biophys Res Commun* **438**, 395-401

28. Yamashita, S. I., Abe, K., Tatemichi, Y., and Fujiki, Y. (2014) The membrane peroxin PEX3 induces peroxisome-ubiquitination-linked pexophagy. *Autophagy* **10,** 1549-64

29. Sato, Y., Shibata, H., Nakatsu, T., Nakano, H., Kashiwayama, Y., Imanaka, T., and Kato, H. (2010) Structural basis for docking of peroxisomal membrane protein carrier Pex19p onto its receptor Pex3p. *EMBO J* **29**, 4083-4093

30. Schmidt, F., Treiber, N., Zocher, G., Bjelic, S., Steinmetz, M. O., Kalbacher, H., Stehle, T., and Dodt, G. (2010) Insights into peroxisome function from the structure of PEX3 in complex with a soluble fragment of PEX19. *J Biol Chem* **285**, 25410-25417

31. Schueller, N., Holton, S. J., Fodor, K., Milewski, M., Konarev, P., Stanley, W. A., Wolf, J., Erdmann, R., Schliebs, W., Song, Y. H., and Wilmanns, M. (2010) The peroxisomal receptor Pex19p forms a helical mPTS recognition domain. *EMBO J* **29**, 2491-2500

32. Schmidt, F., Dietrich, D., Eylenstein, R., Groemping, Y., Stehle, T., and Dodt, G. (2012) The role of conserved PEX3 regions in PEX19-binding and peroxisome biogenesis. *Traffic* **13**, 1244-1260

33. Vasko, R., Ratliff, B. B., Bohr, S., Nadel, E., Chen, J., Xavier, S., Chander, P., and Goligorsky, M. S. (2013) Endothelial peroxisomal dysfunction and impaired pexophagy promotes oxidative damage in lipopolysaccharide-induced acute kidney injury. *Antioxid Redox Signal* **19**, 211-230

34. Kim, P. K., Hailey, D. W., Mullen, R. T., and Lippincott-Schwartz, J. (2008) Ubiquitin signals autophagic degradation of cytosolic proteins and peroxisomes. *Proceedings of the National Academy of Sciences of the United States of America* **105**, 20567-20574

35. Deosaran, E., Larsen, K. B., Hua, R., Sargent, G., Wang, Y., Kim, S., Lamark, T., Jauregui, M., Law, K., Lippincott-Schwartz, J., Brech, A., Johansen, T., and Kim, P. K. (2013) NBR1 acts as an autophagy receptor for peroxisomes. *J Cell Sci* **126**, 939-952

36. Zhang, J., Kim, J., Alexander, A., Cai, S., Tripathi, D. N., Dere, R., Tee, A. R., Tait-Mulder, J., Di Nardo, A., Han, J. M., Kwiatkowski, E., Dunlop, E. A., Dodd, K. M., Folkerth, R. D., Faust, P. L., Kastan, M. B., Sahin, M., and Walker, C. L. (2013) A tuberous sclerosis complex signalling node at the peroxisome regulates mTORC1 and autophagy in response to ROS. *Nat Cell Biol* **15**, 1186-1196

37. Aoki, Y., Kanki, T., Hirota, Y., Kurihara, Y., Saigusa, T., Uchiumi, T., and Kang, D. (2011) Phosphorylation of Ser114 on Atg32 mediates mitophagy. *Mol Biol Cell* **22**, 3206-3217

38. Cheong, H., Yorimitsu, T., Reggiori, F., Legakis, J. E., Wang, C. W., and Klionsky, D. J. (2005) Atg17 regulates the magnitude of the autophagic response. *Mol Biol Cell* **16**, 3438-3453

39. Gould, S. J., McCollum, D., Spong, A. P., Heyman, J. A., and Subramani, S. (1992) Development of the yeast *Pichia pastoris* as a model organism for a genetic and molecular analysis of peroxisome assembly. *Yeast* **8**, 613-628

40. Wiemer, E. A., Luers, G. H., Faber, K. N., Wenzel, T., Veenhuis, M., and Subramani, S. (1996) Isolation and characterization of Pas2p, a peroxisomal membrane protein essential for peroxisome biogenesis in the methylotrophic yeast *Pichia pastoris*. *J Biol Chem* **271**, 18973-18980

41. Nazarko, T. Y., Farré, J. C., and Subramani, S. (2009) Peroxisome size provides insights into the function of autophagy-related proteins. *Mol Biol Cell* **20**, 3828-3839

42. Kim, J., Kamada, Y., Stromhaug, P. E., Guan, J., Hefner-Gravink, A., Baba, M., Scott, S. V., Ohsumi, Y., Dunn, W. A., Jr., and Klionsky, D. J. (2001) Cvt9/Gsa9 functions in sequestering selective cytosolic cargo destined for the vacuole. *J Cell Biol* **153**, 381-396

43. Manjithaya, R., Jain, S., Farre, J. C., and Subramani, S. (2010) A yeast MAPK cascade regulates pexophagy but not other autophagy pathways. *The Journal of cell biology* **189**, 303-310

Chapter 5: The role of Rvs167 in pexophagy mechanisms in yeast

Introduction:

In the previous chapter, I showed that the peroxisomal membrane protein *P. pastoris* Pex3 plays a dynamic regulatory role in determining the level of phosphorylation of the pexophagy receptor, Atg30. The phosphorylation of Atg30, in turn, affects the recruitment of the core autophagy machinery to peroxisomes, thereby impacting pexophagy. We wished to explore which proteins interact with Atg30 in the presence of wild-type Pex3, but less strongly with the mutant Pex3m, in the hope of finding interaction partners (such as kinases) that might account for the lower level of phosphorylation of Atg30 in cells expressing Pex3m relative to wild-type Pex3. In this chapter, I introduce hypothetical interacting proteins that were uncovered in a screen looking for protein-protein interactions via IP/MS using *P. pastoris* Atg30 as bait.

A tagged version of the protein, HA-Atg30, was purified from yeast lysates undergoing pexophagy in both wild-type and in *pex3m* cells, and the interaction partners for HA-Atg30 in the two cell backgrounds were then compared for similarities and differences (Table 5-1). Here we focus on the potential interaction between Atg30 and Rvs167, which was seen in wild-type, but not in *pex3m* cells. Although not a kinase, Rvs167 had a variety of potentially interesting links with autophagy and pexophagy that warranted further exploration of its role, including a structure similarity to a mammalian homolog, the endophilin Bif-1 (19).

As we have discussed previously, autophagy can be induced by changing the nutrient requirements in the cell. In selective autophagy, an organelle (or other selective cargo) can be targeted for destruction (1). In yeast cells, peroxisomes can proliferate when the cells are grown in the presence of oleate as a carbon source. When cells are shifted to a different carbon source, like glucose, and lack nitrogen, the extraneous peroxisomes are degraded by pexophagy (2).

Yeast Rvs167 and Rvs161 are highly conserved proteins, most similar to mammalian amphiphysins I and II, respectively. The proteins Rvs167 and Rvs161 are termed “reduced viability upon starvation” in yeast as they are negative cell cycle regulators that link cell cycle

progression to nutrient availability (3). The proteins associate with actin patches and play active roles in endocytosis and exocytosis (4-6). Rvs167 has sequence homology with three characteristic domains: an N-terminal region for protein-protein interactions (7,8), termed the BAR domain (9) (10); a C-terminal Src-homology domain (SH3); and a variable intermediate domain (Fig. 5-1A).

Mammalian amphiphysin I has been described as having a role in synaptic vesicle formation in the brain, as well as in non-neuronal endocytosis (11,12). The yeast homologs, Rvs161 and Rvs167, were originally found in a screen for reduced viability and abnormal morphology during starvation and the *rvs* mutants were found to have a depolarized actin cytoskeleton network (3). The actin cytoskeleton may be of particular interest in terms of pexophagosome motility, maturation and fusion; in fact, the actin cytoskeleton plays a role in pexophagy, but not in nonselective autophagy (13). Indeed, Rvs167 physically interacts with actin (14) and forms a heterodimer with Rvs161 (8).

The phenotypes shown by the *rvs* mutants, especially the reduced viability upon starvation, are hallmarks of autophagy-related proteins. Mutants of Rvs161 and Rvs167 have several features that make them interesting candidates for further testing their role in pexophagy. For example, they have an endocytic defect which is similar to other autophagy-defective mutants (15,16). This means the mutants are unable to internalize plasma membrane, ligands, particles and fluids from the extracellular compartment by invagination of the plasma membrane and formation of endocytic vesicles (17). The endocytic machinery may be involved in membrane generation to form the phagophore or in fusion events during autophagy (16). However, *S. cerevisiae rvs167*Δ was previously tested for general autophagy defect and was found to have normal autophagy (18), making the study of selective autophagy in the mutant intriguing.

The source of the membrane for the autophagosome has eluded many researchers. BAR proteins like Rvs161 and Rvs167, which sense and induce membrane curvature (14), may play a part in generating the membrane tubules that connect donor membranes to the burgeoning autophagosome. In the mutants of these proteins, the autophagosome formation would then be

blocked. In fact, the mammalian BAR domain protein, Bif-1, when mutated in this domain, is affected in the ability of Atg9 to traffic from the membrane source, (a key component of the core autophagy machinery) (19). The ability of Rvs167 to affect Atg9 trafficking, like Bif-1 does, is a very interesting concept that we will explore in the future.

Rvs167 has many known protein interactions, which may be important for a putative role in pexophagy. It was shown to interact with dynamin-related protein, Vps1, at the Golgi endocytic sites and associating at the sites before recruitment of Vps1 while possibly having coordinated association/dissociation during tubulation and assembly/disassembly (20). The mutant, Vps1 (P564A) behaves like a Δ*rvs167* in *Saccharomyces cerevisiae*, via the loss of interaction between Vps1 and Rvs167 (20) (Figure 5-1B). Interestingly, the mutant Vps1 has no affect on peroxisome morphology, although the role of Vps1 in peroxisome fission is well described (21). This mutant Vps1 (P564A) has not been tested for a pexophagy phenotype yet theoretically would behave like *rvs176*Δ cells.

Vps1 has previously been implicated in pexophagy (22). It interacts with the peroxisome degradation machinery Atg11 and Atg36 (22), which is the *S. cerevisiae* pexophagy receptor (23), along with another protein involved in the peroxisome fission machinery, Dnm1 (22). Based on the Rvs167-Vps1 interaction and localization at the peroxisome, the role that Rvs167 plays in pexophagy remains unknown.

While screening for proteins interacting with the pexophagy adapter Atg30 in *P. pastoris* via mass spectrometry, we found Rvs167 as a potential interacting protein, yet it is not associated with Atg30 in *pex3m* cells. As *S. cerevisiae* is a more genetically tractable organism, we confirmed that *rvs167Δ* cells had a pexophagy phenotype and then knocked out the gene in *P. pastoris*, which also had a pexophagy phenotype (Fig. 5-2B). Peroxisome homeostasis is visualized well in *P. pastoris*, and a tagged version of overexpressed RFP-Rvs167 co-localized with the phagophore assembly site (PAS) labeled with GFP-Atg8. This signifies that likely Rvs167 plays some membrane-associated role in pexophagy in yeasts, as the PAS is the site of

membrane curvature of the micropexophagic apparatus or MIPA. Future studies using Rvs167 in both yeasts are planned.

Results

In *P. pastoris*, peroxisomes proliferate in number and size when the cells are grown in methanol as a carbon source; in S. *cerevisiae,* oleic acid is the carbon source that promotes peroxisome biogenesis. In both organisms, when exposed to nitrogen limitation conditions and in the presence of glucose, the peroxisomes become superfluous and pexophagy is induced (1). The pexophagy receptor, Atg30, in *P. pastoris* interacts with several peroxins (proteins involved in peroxisome biogenesis), such as Pex3 and Pex14, as well as with autophagy-related proteins, Atg11, Atg17 and Atg37 (24,25).

In order to study other interesting protein-protein interactions of the Atg30 complex during the onset of pexophagy, *P. pastoris* lysates containing Atg30 tagged with HA were subjected to immunoprecipitation. The Δ*pex3* cells were used as a negative control for the immunoprecipitation, as Atg30 is mislocalized in the absence of Pex3 (24); we also used *pex3m* cells in order to differentiate proteins involved in pexophagy, as *pex3m* is blocked in pexophagy. Upon immunoprecipitation of the Atg30 complex, samples were submitted for mass spectrometry analysis of protein-protein interactions. The list of proteins was whittled down to 22 interesting proteins and separated into a few classes, defined by previous literature. The generated protein hits were screened against a decoy library of false peptides in order to establish confidence in the peptides identified in the immunoprecipitate (26) (Figure 5-1C).

Of particular interest initially was the class of proteins that have already been associated with pexophagy or autophagy in previous annotations. For these reasons, we first focused on ergosterol proteins associated with ergosterol metabolism and BAR-domain proteins. Atg26 is an ergosterol glucoside synthesizing protein. The sterol conversion by Atg26 is necessary for MIPA formation and expansion; Atg26 is recruited to the MIPA by phosphatidylinositol-4-phosphate, PI-4P, generated by Pik1 (27). We screened the viable mutants of the *S. cerevisiae* deletion library

for pexophagy. Specifically we tested pexophagy in *sla1*, *erg6*, *mcr1* and *rvs167* mutants. In addition, we tested the *vps70* mutant for pexophagy as other Vps proteins have autophagic roles, including Vps34 and Vps21 (15,28) (Figure 5-2A).

Experimentally, we can test for pexophagy defects in *S. cerevisiae* by first inducing peroxisome proliferation using oleic acid in the medium and subsequently shifting the medium to nitrogen limitation conditions (SD-N) and monitoring the degradation of peroxisomal protein, thiolase. Here, we found a slight pexophagy defect in *rvs167*Δ cells, but no detectable defect in the other mutants tested. Therefore, only *rvs167*Δ was pursued further.

Because Rv167 was identified as an interaction partner with Atg30, a *P. pastoris*-specific protein, we extended our analysis to the molecular role Rvs167 could have during pexophagy. *P. pastoris* is a great model organism for studying the molecular details of pexophagy, especially membrane contributions to pexophagy (29). The coding region of *RVS167* was replaced by a kanamycin cassette (*KanMx*) flanked by two 500bp regions of homology to the 5'UTR and 3'UTR of RVS167. The confirmed *rvs167*Δ cells were then subjected to pexophagy assays. Our results show that Δ*rvs167* in *P. pastoris* is defective in pexophagy (Figure 5-2B).

In order to determine if Rvs167 and Atg30 interact in live cells with a dependence on either Pex3 or Atg30, we performed an immunoprecipitation of HA-Atg30 in cells containing RFP-Rvs167 in the following strains: Δ*pex3*, Δ*atg30*, WT and *pex3m* cells (Figure 5-3C). RFP-Rvs167 interacted with HA-Atg30 in Δ*pex3,* WT and *pex3m* cells but failed to be immuniprecipitated in Δ*atg30* cells. This is particularly interesting because in these experiments interaction with Atg30-Rvs167 is similar in the presence or absence of Pex3 or Pex3m. Here, we use *pex3m* (from Chapter 4) as a tool for studying interactions that are dependent on functional pexophagy and determined that Rvs167 may play a role in pexophagy by interaction with Atg30 (Figure 5-1C). By testing this interaction in an immunoprecipitation, we found that Atg30 and Rvs167 may indeed interact in pexophagy conditions (Figurue 5-3C).

The study of the hierarchical recruitment of autophagy proteins is the logical next step to analyze in order to identify at which point Rvs167 could play a role in pexophagy. We first

analyzed the localization of Atg8, a core autophagy protein. Atg8 is recruited to the PAS during pexophagy along with Atg11, and dependent on phosphorylation of Atg30 at Serine-71 upstream of the Atg8-interacting motif (AIM) (30). Atg8 localization at the vacuole periphery and adjacent the targeted peroxisome is an indication that pexophagy has been signaled. The vacuole rearranges and the core machinery recruited to the PAS will extend to the MIPA and act like a cap to the vacuole-engulfed peroxisome. In Pex3 WT cells, GFP-Atg8 and overexpressed RFP-Rvs167 did not localize at the peroxisome-vacuole intersection. However, Atg8 and RFP-Rvs167 did co-localize at the PAS in pexophagy conditions in *pex3m* cells (Figure 5-3). The results are interesting because Rvs167 was not present in the *pex3m* IP/MS protein list however *in vivo* it seems to co-localize better with GFP-Atg8 in *pex3m* cells than in WT cells suggesting that when pexophagy is blocked, RFP-Rvs167 remains tethered to the membrane with GFP-Atg8.

Discussion

In this chapter we describe the finding that in *S. cerevisiae*, *rvs167*Δ was partially blocked in pexophagy. The results indicate that Rvs167 may play a role specifically in pexophagy (Figure 5-2B). Another possibility is that Rvs167 acts as a heterodimer with another BAR protein, Rvs161 (6) during pexophagy in this species of yeast. As this case has not been tested, the double mutant *rvs161*Δ *rvs167*Δ needs to be tested for an exacerbated pexophagy phenotype.

Physical interaction between Atg30 and Rvs167 is likely, as determined by preliminary immunoprecipitation data suggesting that RFP-Rvs167 cannot be pulled down in the absence of Atg30 (Δ*atg30*) (Figure 5-2D). The physiological significance of this interaction remains to be explored, but is worth pursuing with respect to the previously described role of Rvs167 in membrane curvature suggesting a role in phagophore formation or fusion events during selective autophagy (4).

When we overexpressed *P. pastoris* RFP-Rvs167, it did not co-localize with GFP-Atg8 in WT cells; however when pexophagy is blocked in *pex3m* cells, RFP-Rvs167 does co-localize with GFP-Atg8 at the pexophagy-specific PAS (Figure 5-3). These results could likely be explained by

a dominant-negative effect of the Rvs167 overexpression. Consequently, endogenous levels of Rvs167 expression will need to be used for the localization of Rvs167 with the autophagy machinery in order to dissect the point at which the pexophagy mechanism intersects at this novel Atg30-interacting protein. However, it is also interesting to postulate that possibly the role of Rvs167 is transiently required to facilitate membrane bending or fusion events during pexophagy. The function of Rvs167 may need to be that releasing from the membrane interaction with Atg30 is required in order for pexophagy to progress. In the case of blocked pexophagy phenotype of *pex3m* cells, the presence of Rvs167 at the PAS may be preventing further advancement of the MIPA. The formation of the pexophagosome or MIPA requires donation of membrane from another source or recruited by membrane tubules connected to other compartments of the cell. Because Rvs167 has a role in interacting with, as well as forming, curved membranes, this role in pexophagy is conceivable. In addition, if *P. pastoris* Δ*rvs167* is fully blocked in pexophagy, and the accumulation of membrane is at the PAS but the extension of the membrane does not occur, then the hypothetical role of Rvs167 in pexophagy fits this model.

Figure 5-1: Rvs167 is a potential Atg30-interacting protein. A) Rvs167 tertiary structure consists of the conserved highly organized domains made up of a BAR domain, middle domain and SH3 domain. B) Vps1 contains a GTPase domain, a middle domain, and a GTPase effector domain. Proline-564 in the middle domain of Vps1 is responsible for binding to Rvs167 in *S. cerevisiae*. C) Atg30 interacting proteins found in *P. pastoris* that have sequence homology to annotated *S. cerevisiae* proteins, as determined by whole-genome BLAST search. All proteins are found in Pex3 WT while those in the green box were absent in *pex3m* cells. Ergosterol synthesis-related proteins are in red, BAR-protein related in blue. Vps70 is a protein that was in a class of proteins associated with autophagy (15).

A.

B.

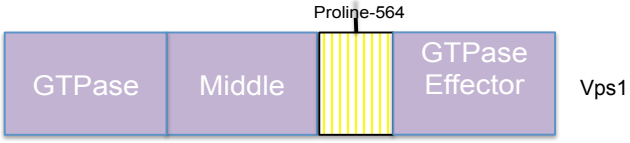

C.

Atg30-interacting

Absent in *pex3m*

ERG13	**ATG30**
ERG6	TKL2
MCR1	YIA6
CMD1	YDR541C
NUP42/RIP1	AHP1
VMA6	ATP14
ERG11	PSA1
ERG25	RNA binding domain
SEC22	PEX11
NADH UBIQUINONE	HTA2
COX1	RHO1
PHB1	GAP1
AGC1	GTO3
SEG1	ARF1
SLA2	PMT1
RNA BINDING MOTIF	TEF4
VTI1	RPL23
HEM13	L23
GVP36	HTA1
VPS70	YIM1
UBIQUINONE	Rpl11B
RVS167	DAK1
IRC22	CHS1
	DAL4
	RPL34
	HHF2
	YPL142C
	SEC4
	FBP1
	RP51
	RPL12A
	TRANSCRIPTION FACTOR E3-LIKE
	COX13
	NADH UBIQUINONE RELATED
	AYR1
	VMA6
	Gas1

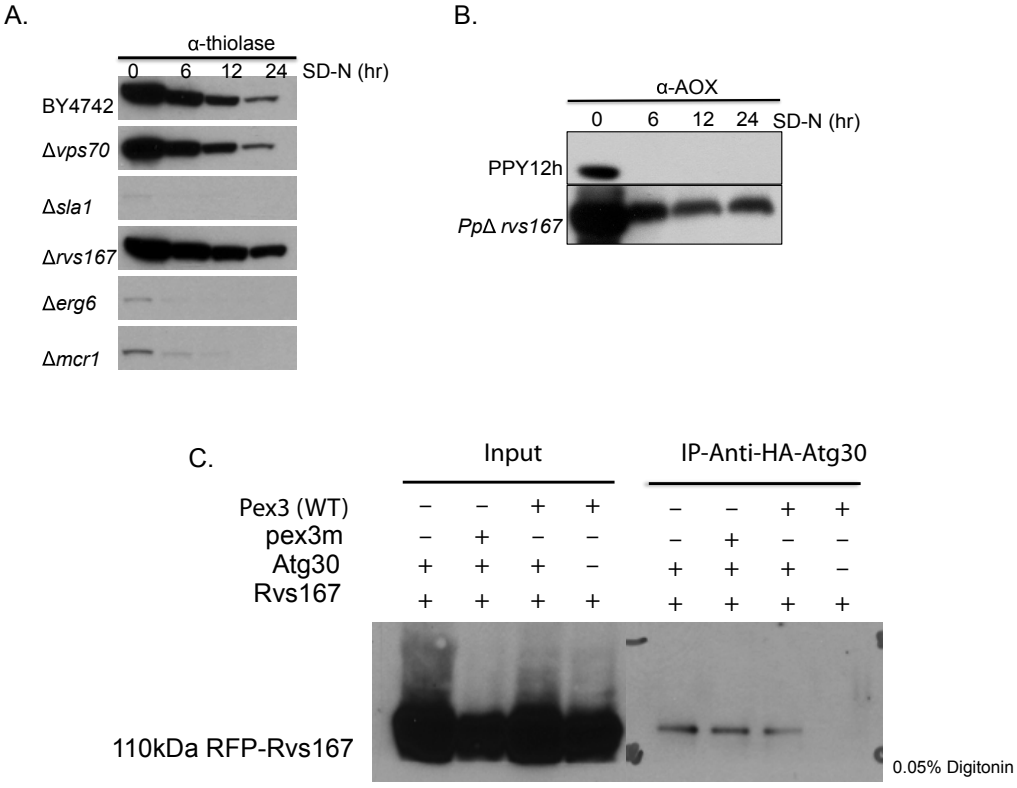

Figure 5-2. Yeast Rvs167 has a role in pexophagy and is an Atg30-interacting protein. A) Pexophagy phenotype measured via degradation of the peroxisomal enzyme thiolase over 24 hours in the following gene knock out strains: WT (31), Δ*vsp70*, Δ*sla1*, Δ*rvs167*, Δ*erg6* and Δ*mcr1*. B) Conservation of the pexophagy phenotype in *P. pastoris* was measured via alcohol oxidase degradation over 24 hours in a WT (PPY12h) and in Δ*rvs167* cells. C) In *P. pastoris* cells, overexpression of RFP-Rvs167 was used for an *in vivo* interaction studies with HA-Atg30. In four strains, Δ*pex3*, Δ*atg30*, WT Pex3 and *pex3m* the interaction was tested in pexophagy conditions. IP: HA-Atg30, WB: RFP.

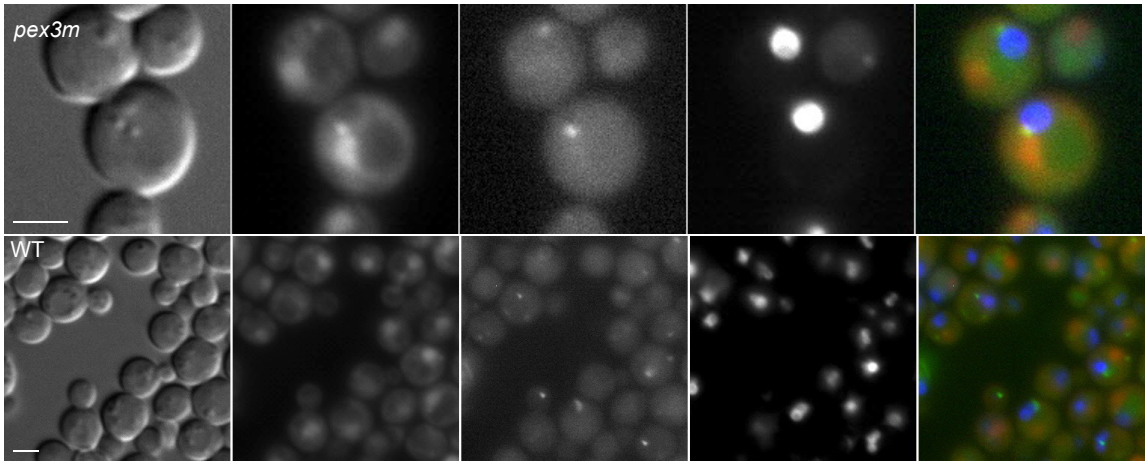

Figure 5-3. Co-localization of RFP-Rvs167 with GFP-Atg8 in *P. pastoris* cells. GFP-Atg8 localization was analyzed in both Pex3 WT (bottom) and *pex3m* cells (top) in pexophagy conditions. P_{GAP}-RFP-Rvs167 (red) was used as well as BFP-SKL for a peroxisomal marker. The merged channel with the yellow triangle shows the co-localization of RFP-Rvs167, GFP-Atg8 and BFP-SKL. Scale 4μm (top), 2μm (bottom

References

1. Till, A., Lakhani, R., Burnett, S. F., and Subramani, S. (2012) Pexophagy: the selective degradation of peroxisomes. *Int J Cell Biol* **2012**, 512721

2. Polupanov, A. S., Nazarko, V. Y., and Sibirny, A. A. (2011) CCZ1, MON1 and YPT7 genes are involved in pexophagy, the Cvt pathway and non-specific macroautophagy in the methylotrophic yeast *Pichia pastoris*. *Cell Biol Int* **35**, 311-319

3. Bauer, F., Urdaci, M., Aigle, M., and Crouzet, M. (1993) Alteration of a yeast SH3 protein leads to conditional viability with defects in cytoskeletal and budding patterns. *Mol Cell Biol* **13**, 5070-5084

4. Balguerie, A., Sivadon, P., Bonneu, M., and Aigle, M. (1999) Rvs167p, the budding yeast homolog of amphiphysin, colocalizes with actin patches. *J Cell Sci* **112** , 2529-2537

5. David, C., Solimena, M., and De Camilli, P. (1994) Autoimmunity in stiff-Man syndrome with breast cancer is targeted to the C-terminal region of human amphiphysin, a protein similar to the yeast proteins, Rvs167 and Rvs161. *FEBS Lett* **351**, 73-79

6. Lombardi, R., and Riezman, H. (2001) Rvs161p and Rvs167p, the two yeast amphiphysin homologs, function together in vivo. *J Biol Chem* **276**, 6016-6022

7. Sivadon, P., Crouzet, M., and Aigle, M. (1997) Functional assessment of the yeast Rvs161 and Rvs167 protein domains. *FEBS Lett* **417**, 21-27

8. Navarro, P., Durrens, P., and Aigle, M. (1997) Protein-protein interaction between the RVS161 and RVS167 gene products of *Saccharomyces cerevisiae*. *Biochim Biophys Acta* **1343**, 187-192

9. Peter, B. J., Kent, H. M., Mills, I. G., Vallis, Y., Butler, P. J., Evans, P. R., and McMahon, H. T. (2004) BAR domains as sensors of membrane curvature: the amphiphysin BAR structure. *Science* **303**, 495-499

10. Sakamuro, D., Elliott, K. J., Wechsler-Reya, R., and Prendergast, G. C. (1996) BIN1 is a novel MYC-interacting protein with features of a tumour suppressor. *Nat Genet* **14**, 69-77

11. Folli, F., Solimena, M., Cofiell, R., Austoni, M., Tallini, G., Fassetta, G., Bates, D., Cartlidge, N., Bottazzo, G. F., Piccolo, G., and De Camilli, P. (1993) Autoantibodies to a 128-kd synaptic protein in three women with the stiff-man syndrome and breast cancer. *N Engl J Med* **328**, 546-551

12. Wigge, P., and McMahon, H. T. (1998) The amphiphysin family of proteins and their role in endocytosis at the synapse. *Trends Neurosci* **21**, 339-344

13. Reggiori, F., Monastyrska, I., Shintani, T., and Klionsky, D. J. (2005) The actin cytoskeleton is required for selective types of autophagy, but not nonspecific autophagy, in the yeast *Saccharomyces cerevisiae*. *Mol Biol Cell* **16**, 5843-5856

14. Breton, A. M., and Aigle, M. (1998) Genetic and functional relationship between Rvs, myosin and actin in *Saccharomyces cerevisiae*. *Curr Genet* **34**, 280-286

15. Chen, Y., Zhou, F., Zou, S., Yu, S., Li, S., Li, D., Song, J., Li, H., He, Z., Hu, B., Björn, L. O., Lipatova, Z., Liang, Y., Xie, Z., and Segev, N. (2014) A Vps21 endocytic module regulates autophagy. *Mol Biol Cell* **25**, 3166-3177

16. Polupanov, A. S., Nazarko, V. Y., and Sibirny, A. A. (2011) CCZ1, MON1 and YPT7 genes are involved in pexophagy, the Cvt pathway and non-specific macroautophagy in the methylotrophic yeast *Pichia pastoris*. *Cell biology international* **35**, 311-319

17. Munn, A. L., Stevenson, B. J., Geli, M. I., and Riezman, H. (1995) end5, end6, and end7: mutations that cause actin delocalization and block the internalization step of endocytosis in *Saccharomyces cerevisiae*. *Mol Biol Cell* **6**, 1721-1742

18. Nair, U., Jotwani, A., Geng, J., Gammoh, N., Richerson, D., Yen, W. L., Griffith, J., Nag, S., Wang, K., Moss, T., Baba, M., McNew, J. A., Jiang, X., Reggiori, F., Melia, T. J., and Klionsky, D. J. (2011) SNARE Proteins Are Required for Macroautophagy. *Cell* **146**, 290-302

19. Takahashi, Y., Coppola, D., Matsushita, N., Cualing, H. D., Sun, M., Sato, Y., Liang, C., Jung, J. U., Cheng, J. Q., Mulé, J. J., Pledger, W. J., and Wang, H. G. (2007) Bif-1 interacts with Beclin 1 through UVRAG and regulates autophagy and tumorigenesis. *Nat Cell Biol* **9**, 1142-1151

20. Smaczynska-de Rooij, I. I., Allwood, E. G., Mishra, R., Booth, W. I., Aghamohammadzadeh, S., Goldberg, M. W., and Ayscough, K. R. (2012) Yeast dynamin Vps1 and amphiphysin Rvs167 function together during endocytosis. *Traffic* **13**, 317-328

21. Hoepfner, D., van den Berg, M., Philippsen, P., Tabak, H. F., and Hettema, E. H. (2001) A role for Vps1p, actin, and the Myo2p motor in peroxisome abundance and inheritance in *Saccharomyces cerevisiae*. *J Cell Biol* **155**, 979-990
22. Mao, K., Liu, X., Feng, Y., and Klionsky, D. J. (2014) The progression of peroxisomal degradation through autophagy requires peroxisomal division. *Autophagy* **10**, 652-661

23. Motley, A. M., Nuttall, J. M., and Hettema, E. H. (2012) Pex3-anchored Atg36 tags peroxisomes for degradation in *Saccharomyces cerevisiae*. *EMBO J* **13**, 2852-2868

24. Farré, J. C., Manjithaya, R., Mathewson, R. D., and Subramani, S. (2008) *Pp*Atg30 tags peroxisomes for turnover by selective autophagy. *Dev Cell* **14**, 365-376

25. Nazarko, T. Y., Ozeki, K., Till, A., Ramakrishnan, G., Lotfi, P., Yan, M., and Subramani, S. (2014) Peroxisomal Atg37 binds Atg30 or palmitoyl-CoA to regulate phagophore formation during pexophagy. *J Cell Biol* **204**, 541-557

26. Elias, J. E., and Gygi, S. P. (2010) Target-decoy search strategy for mass spectrometry-based proteomics. *Methods Mol Biol* **604**, 55-71

27. Yamashita, S., Oku, M., Wasada, Y., Ano, Y., and Sakai, Y. (2006) PI4P-signaling pathway for the synthesis of a nascent membrane structure in selective autophagy. *J Cell Biol* **173**, 709-717

28. Cao, Y., and Klionsky, D. J. (2007) Physiological functions of Atg6/Beclin 1: a unique autophagy-related protein. *Cell Res* **17**, 839-849

29. Oku, M., and Sakai, Y. (2008) Pexophagy in *Pichia pastoris*. *Methods Enzymol* **451**, 217-228

30. Farré, J. C., Burkenroad, A., Burnett, S. F., and Subramani, S. (2013) Phosphorylation of mitophagy and pexophagy receptors coordinates their interaction with Atg8 and Atg11. *EMBO Rep* **5**, 441-449

31. Wurtz, C., Schliebs, W., Erdmann, R., and Rottensteiner, H. (2008) Dynamin-like protein-dependent formation of Woronin bodies in *Saccharomyces cerevisiae* upon heterologous expression of a single protein. *FEBS J* **275**, 2932-2941

Chapter 6: Future Directions

Introduction

Because studying pexophagy is technically complex in mammals, the molecular details of pexophagy have been elucidated using a variety of yeast species as model organisms. In this thesis, a multitude of approaches have been taken to deconstruct this complex process. Using yeast as a model system, we found that an elevated level of GABA can activate Tor1 kinase to inhibit mitophagy and pexophagy specifically. The oxidative stress from a block in mitophagy and pexophagy can be relieved by the addition of rapamycin. We explored the mechanism of phosphoregulation of selective autophagy receptors in yeast whereby their phosphorylation status at certain sites on the proteins determines their ability to bind to core autophagy machinery proteins, Atg11 and Atg8.

In addition, we found an unexpected role of Pex3 as a phosphoregulator of the pexophagy receptor in *P. pastoris.* Finally, we identified a new Atg30-interacting protein, Rvs167 that may play a role in pexophagy in yeast. These studies have set up a solid foundation for the signaling mechanisms of pexophagy and have furthered contributed to the field of selective autophagy, with the hope that others will build upon this research in both yeast and mammalian models.

Future Studies

Atg30-related

Our studies define a domain of *Pp*Pex3 that is distinct from other known domains on the highly conserved Pex3 protein (1-6). This study, along with the preceding study on Atg30 phosphorylation status affecting Atg11 and Atg8 recruitment (7) are the first to give insight into the biochemistry of the pexophagy receptor, Atg30. However, nothing is known of its structure and the predicted structure algorithms also are inconclusive. Using the *in vitro* interaction study of Atg30 and Pex3 in this dissertation as a proof-of-principle experiment, the Atg30-Pex3 crystallization and study by X-ray diffraction would be very useful for structure-function assays. It

would be valuable to identify structurally where Atg8 and Atg11 binding sites are on the tertiary structure and to identify other binding pockets. As there is no predicted structure, Atg30 may be a disordered protein without a interacting with a protein at the peroxisome membrane. We hypothesize that the protein interactions above, as well as the other known interacting proteins like Atg37 (8), Atg17 and Pex14 (9) could give valuable insight onto the regulatory domains of Atg30 and could likely be applied to other selective autophagy receptors.

The pexophagy receptor in *S. cerevisiae*, Atg36, is phosphorylated by the casein kinase 1 Hrr25 to regulate binding to Atg11 (10). Hrr25 phosphorylates not only the pexophagy receptor, but other selective autophagy receptors (11,12). Interestingly, in *S. cerevisiae*, casein kinase 2 phosphorylates the mitophagy receptor (13). It is very likely that *Pp*Hrr25 is the kinase for Atg30 activation during pexophagy. An experiment to perform would be to do a simple purification of native, tagged Hrr25 from *P. pastoris* cells under pexophagy conditions and study the phosphorylation of recombinant Atg30 with or without Pex3, Pex3m and/or Atg37. These experiments would settle whether Hrr25 is the kinase for Atg30 (Fig. 6-1).

Another Atg30 interacting protein that could uncover more about the biochemistry of pexophagy is Atg37. Atg37 interacts directly with both Atg30 and Pex3 and affect the Atg30-Atg11 interaction. Furthermore, the Atg30-Atg37 interaction can be out-competed by the binding of Atg37 to palmitoyl-CoA (8); how Atg30 interacts with Atg37 and Pex3 is unknown . Is there one binding site for both proteins or do Atg37 and Pex3 compete for binding to Atg30? In addition, it would be interesting to know if Pex3m perturbs the Atg30-Atg37 interaction or if there are modifications on Atg37 that could be affected by Pex3m.

Pex3m can be used as a tool to dissect pexophagy mechanisms in *P. pastoris* (6). As we already know the sites of phosphorylation of Atg30 for interaction with Atg8 (Serine-71) and Atg11 (Serine-112) (7,9), it would be interesting to know which sites are phosphorylated or de-phosphorylated, in contrast to wild-type cells, in a *pex3m* background via phospho-peptide mapping by mass spectrometry. We expect Atg30 to change its conformation upon binding to

Pex3 and that this is the interaction that activates Atg30 and makes the Atg8 and Atg11 domains sites available to phosphorylation by the kinase.

Rvs167-related

In Chapter 5 of this dissertation, we describe preliminary work on the role of Rvs167, a BAR-protein (14) in pexophagy. We suggest that Rvs167 potentially interacts with Atg30 and plays a role in pexophagy signaling in yeast. Rvs167 has a human homolog, Bif-1, that plays a role in trafficking of Atg9 to the membrane of autophagosomes (15). In addition, there is a predicted genetic interaction of Rvs167 with proteins such as Atg1(16), Atg11 (17), Atg21 (18), Vps21 (19,20) which suggests that Rv167 is part of the same pathway. Atg21 was found to be required for several selective autophagy pathways, including pexophagy (21,22) and required for Atg8 lipidation at the PAS (23). These links to autophagic pathways lead us to a variety of questions about the role of Rvs167: at what step during pexophagy does Rvs167 play a role? Does it affect Atg9 trafficking like Bif-1 does? Does Rvs167 affect Atg8 recruitment or lipidation? Fig. 6-2 depicts a model showing the steps where Rvs157 could be required during autophagic signaling.

There are 63 proteins that were pulled down in wild-type Atg30 and 22 were not found in *pex3m* cells, suggesting a possible role in pexophagy if the process was blocked in these cells. Using the *S. cerevisiae* library in the lab, other protein knockouts should be tested for a block in pexophagy especially if there are candidates that may be related to autophagy.

GABA-related

GABA activates the Tor1 kinase, which then activates Sch9 in yeast to inhibit pexophagy and mitophagy (24), meaning GABA acts on pathways that require their respective receptors, Atg36 (25) and Atg32 (26). We postulate that GABA may act through Tor1 to affect pexophagy via the interactions Atg36 has to promote pexophagy, including Pex3 (25) (Figure 6-3). This regulation may or may not affect the phosphorylation of Atg36, but could potentially affect the expression of the receptor, as Tor regulates expression of Atg32 in *P. pastoris* but does not affect

phosphorylation of the protein (27). Because we know the upstream regulation of the inhibition of pexophagy, it would be interesting to study the chemistry of the receptor proteins themselves during the block of pexophagy. If for example, GABA's downstream affect on Atg36 affected the translation of the protein or the phosphorylation, this would allow us to know the full mechanism of how GABA blocks pexophagy in *S. cerevisiae*.

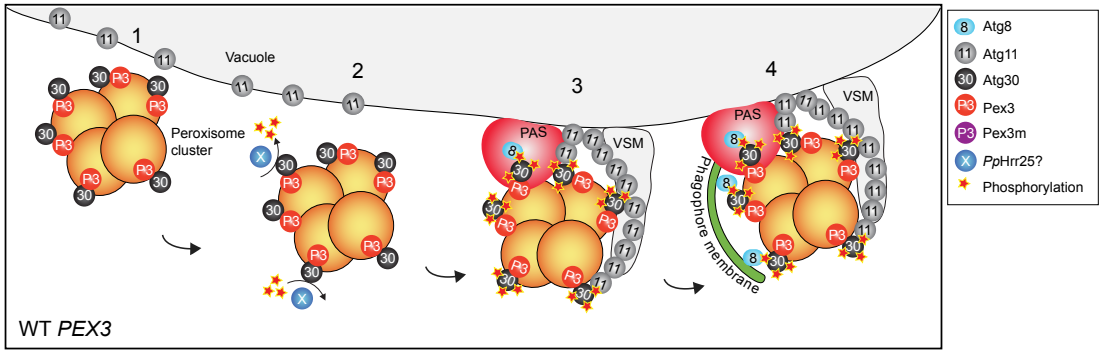

Figure 6-1: Is Hrr25 the kinase for Atg30? Adapted from Chapter 3, here we hypothesize that upon Atg30 targeting to the peroxisome and interacting with Pex3 [1], Atg30 is phosphorylated by PpHrr25 [2]. This phosphorylation recruits Atg11 to the PAS to interact with Atg30 and then Atg11 moves to the vacuole sequestering membranes (VSM) [3]. Atg30-Atg8 interaction also occurs and Atg8 extends into the phagophore membrane (4) to complete pexophagy.

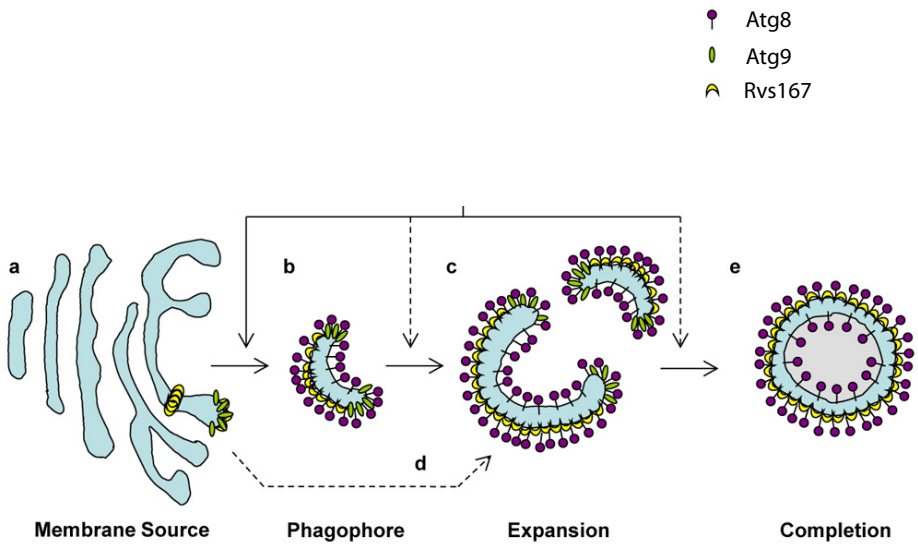

Figure 6-2: At what stage of pexophagy does Rvs167 act and does it co-localize with Atg8? A figure adapted from (28) that shows Rvs167 at various locations in the cell and autophagosome. (a) Rvs167 could co-localize with Atg9 at a membrane source, (b) Rvs167 could co-localize with Atg8 to form the phagophore (d), and/or (c) Rvs167 could expand to and fuse with other membranes to form the autophagosome/pexophagosome and then eventually fuse (e). We currently do not know which stage of pexophagy or if micro- versus macro-pexophagy is affected in *rvs167*Δ cells.

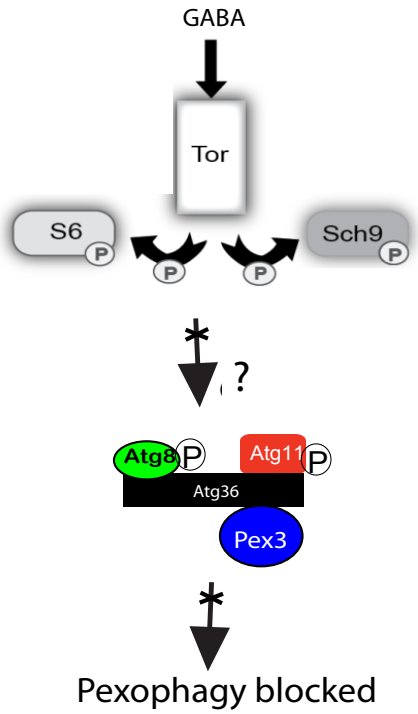

Figure 6-3: Does GABA act through the pexophagy receptor and affect phosphorylation status or protein levels to block pexophagy? Adapted from chapter 1, GABA can activate Tor, which goes on to activate Sch9 and then inhibits pexophagy. However, we don't know if pexophagy is blocked in *S. cerevisiae* because of the protein levels of Atg36 or if the phosphorylation status affects whether Atg8 and Atg11 or Pex3 can interact with it.

References

1. Schmidt, F., Dietrich, D., Eylenstein, R., Groemping, Y., Stehle, T., and Dodt, G. (2012) The role of conserved PEX3 regions in PEX19-binding and peroxisome biogenesis. *Traffic* **9**, 1244-1260

2. Knoblach, B., Sun, X., Coquelle, N., Fagarasanu, A., Poirier, R. L., and Rachubinski, R. A. (2013) An ER-peroxisome tether exerts peroxisome population control in yeast. *EMBO J* **18**, 2439-2453

3. Hattula, K., Hirschberg, D., Kalkkinen, N., Butcher, S. J., and Ora, A. (2014) Association between the Intrinsically Disordered Protein PEX19 and PEX3. *PLoS One* **9**, e103101

4. Sato, Y., Shibata, H., Nakatsu, T., Nakano, H., Kashiwayama, Y., Imanaka, T., and Kato, H. (2010) Structural basis for docking of peroxisomal membrane protein carrier Pex19p onto its receptor Pex3p. *EMBO J* **29**, 4083-4093

5. Schmidt, F., Treiber, N., Zocher, G., Bjelic, S., Steinmetz, M. O., Kalbacher, H., Stehle, T., and Dodt, G. (2010) Insights into peroxisome function from the structure of PEX3 in complex with a soluble fragment of PEX19. *J Biol Chem* **285**, 25410-25417

6. Burnett, S. F., Farré, J. C., Nazarko, T. Y., and Subramani, S. (2015) Peroxisomal Pex3 activates selective autophagy of peroxisomes via interaction with pexophagy receptor, Atg30. *J Biol Chem In press*

7. Farré, J. C., Burkenroad, A., Burnett, S. F., and Subramani, S. (2013) Phosphorylation of mitophagy and pexophagy receptors coordinates their interaction with Atg8 and Atg11. *EMBO Rep* **5**, 441-449

8. Nazarko, T. Y., Ozeki, K., Till, A., Ramakrishnan, G., Lotfi, P., Yan, M., and Subramani, S. (2014) Peroxisomal Atg37 binds Atg30 or palmitoyl-CoA to regulate phagophore formation during pexophagy. *J Cell Biol* **204**, 541-557

9. Farré, J. C., Manjithaya, R., Mathewson, R. D., and Subramani, S. (2008) *Pp*Atg30 tags peroxisomes for turnover by selective autophagy. *Dev Cell* **14**, 365-376

10.Tanaka, C., Tan, L. J., Mochida, K., Kirisako, H., Koizumi, M., Asai, E., Sakoh-Nakatogawa, M., Ohsumi, Y., and Nakatogawa, H. (2014) Hrr25 triggers selective autophagy-related pathways by phosphorylating receptor proteins. *J Cell Biol* **207**, 91-105

11. Mochida, K., Ohsumi, Y., and Nakatogawa, H. (2014) Hrr25 phosphorylates the autophagic receptor Atg34 to promote vacuolar transport of α-mannosidase under nitrogen starvation conditions. *FEBS Lett* **588**, 3862-3869

12. Pfaffenwimmer, T., Reiter, W., Brach, T., Nogellova, V., Papinski, D., Schuschnig, M., Abert, C., Ammerer, G., Martens, S., and Kraft, C. (2014) Hrr25 kinase promotes selective autophagy by phosphorylating the cargo receptor Atg19. *EMBO Rep* **15**, 862-870

13. Kanki, T., Kurihara, Y., Jin, X., Goda, T., Ono, Y., Aihara, M., Hirota, Y., Saigusa, T., Aoki, Y., Uchiumi, T., and Kang, D. (2013) Casein kinase 2 is essential for mitophagy. *EMBO Rep* **14**, 788-794

14. Balguerie, A., Sivadon, P., Bonneu, M., and Aigle, M. (1999) Rvs167p, the budding yeast homolog of amphiphysin, colocalizes with actin patches. *J Cell Sci* **112 (Pt 15)**, 2529-2537

15. Takahashi, Y., Meyerkord, C. L., and Wang, H. G. (2008) BARgaining membranes for autophagosome formation: Regulation of autophagy and tumorigenesis by Bif-1/Endophilin B1. *Autophagy* **4**, 121-124

16. Sharifpoor, S., van Dyk, D., Costanzo, M., Baryshnikova, A., Friesen, H., Douglas, A. C., Youn, J. Y., VanderSluis, B., Myers, C. L., Papp, B., Boone, C., and Andrews, B. J. (2012) Functional wiring of the yeast kinome revealed by global analysis of genetic network motifs. *Genome Res* **22**, 791-801

17. Costanzo, M., Baryshnikova, A., Bellay, J., Kim, Y., Spear, E. D., Sevier, C. S., Ding, H., Koh, J. L., Toufighi, K., Mostafavi, S., Prinz, J., St Onge, R. P., VanderSluis, B., Makhnevych, T., Vizeacoumar, F. J., Alizadeh, S., Bahr, S., Brost, R. L., Chen, Y., Cokol, M., Deshpande, R., Li, Z., Lin, Z. Y., Liang, W., Marback, M., Paw, J., San Luis, B. J., Shuteriqi, E., Tong, A. H., van Dyk, N., Wallace, I. M., Whitney, J. A., Weirauch, M. T., Zhong, G., Zhu, H., Houry, W. A., Brudno, M., Ragibizadeh, S., Papp, B., Pál, C., Roth, F. P., Giaever, G., Nislow, C., Troyanskaya, O. G., Bussey, H., Bader, G. D., Gingras, A. C., Morris, Q. D., Kim, P. M., Kaiser, C. A., Myers, C. L., Andrews, B. J., and Boone, C. (2010) The genetic landscape of a cell. *Science* **327**, 425-431

18. Hoppins, S., Collins, S. R., Cassidy-Stone, A., Hummel, E., Devay, R. M., Lackner, L. L., Westermann, B., Schuldiner, M., Weissman, J. S., and Nunnari, J. (2011) A mitochondrial-focused genetic interaction map reveals a scaffold-like complex required for inner membrane organization in mitochondria. *J Cell Biol* **195**, 323-340

19. Chen, Y., Zhou, F., Zou, S., Yu, S., Li, S., Li, D., Song, J., Li, H., He, Z., Hu, B., Björn, L. O., Lipatova, Z., Liang, Y., Xie, Z., and Segev, N. (2014) A Vps21 endocytic module regulates autophagy. *Mol Biol Cell* **25**, 3166-3177

20. Singer-Krüger, B., and Ferro-Novick, S. (1997) Use of a synthetic lethal screen to identify yeast mutants impaired in endocytosis, vacuolar protein sorting and the organization of the cytoskeleton. *Eur J Cell Biol* **74**, 365-375

21. Strømhaug, P. E., Reggiori, F., Guan, J., Wang, C. W., and Klionsky, D. J. (2004) Atg21 is a phosphoinositide binding protein required for efficient lipidation and localization of Atg8 during uptake of aminopeptidase I by selective autophagy. *Mol Biol Cell* **15**, 3553-3566

22. Tamura, N., Oku, M., and Sakai, Y. (2014) Atg21 regulates pexophagy via its PI(3)P-binding activity in Pichia pastoris. *FEMS Yeast Res* **14**, 435-444

23. Juris, L., Montino, M., Rube, P., Schlotterhose, P., Thumm, M., and Krick, R. (2015) PI3P binding by Atg21 organises Atg8 lipidation. *EMBO J* **34**, 579-688

24. Lakhani, R., Vogel, K. R., Till, A., Liu, J., Burnett, S. F., Gibson, K. M., and Subramani, S. (2014) Defects in GABA metabolism affect selective autophagy pathways and are alleviated by mTOR inhibition. *EMBO Mol Med* **6**, 551-566

25. Motley, A. M., Nuttall, J. M., and Hettema, E. H. (2012) Pex3-anchored Atg36 tags peroxisomes for degradation in *Saccharomyces cerevisiae*. *EMBO J* **13**, 2852-2868

26. Kanki, T., Wang, K., Cao, Y., Baba, M., and Klionsky, D. J. (2009) Atg32 is a mitochondrial protein that confers selectivity during mitophagy. *Dev Cell* **17**, 98-109

27. Aihara, M., Jin, X., Kurihara, Y., Yoshida, Y., Matsushima, Y., Oku, M., Hirota, Y., Saigusa, T., Aoki, Y., Uchiumi, T., Yamamoto, T., Sakai, Y., Kang, D., and Kanki, T. (2014) Tor and the Sin3-

Rpd3 complex regulate expression of the mitophagy receptor protein Atg32 in yeast. *J Cell Sci* **127**, 3184-3196

28. Takahashi, Y., Coppola, D., Matsushita, N., Cualing, H. D., Sun, M., Sato, Y., Liang, C., Jung, J. U., Cheng, J. Q., Mulé, J. J., Pledger, W. J., and Wang, H. G. (2007) Bif-1 interacts with Beclin 1 through UVRAG and regulates autophagy and tumorigenesis. *Nat Cell Biol* **9**, 1142-1151